Bandung Institut of Technology
Lecture, April-May 2013

Volcanoes deformation: measurements and interpretation through modeling

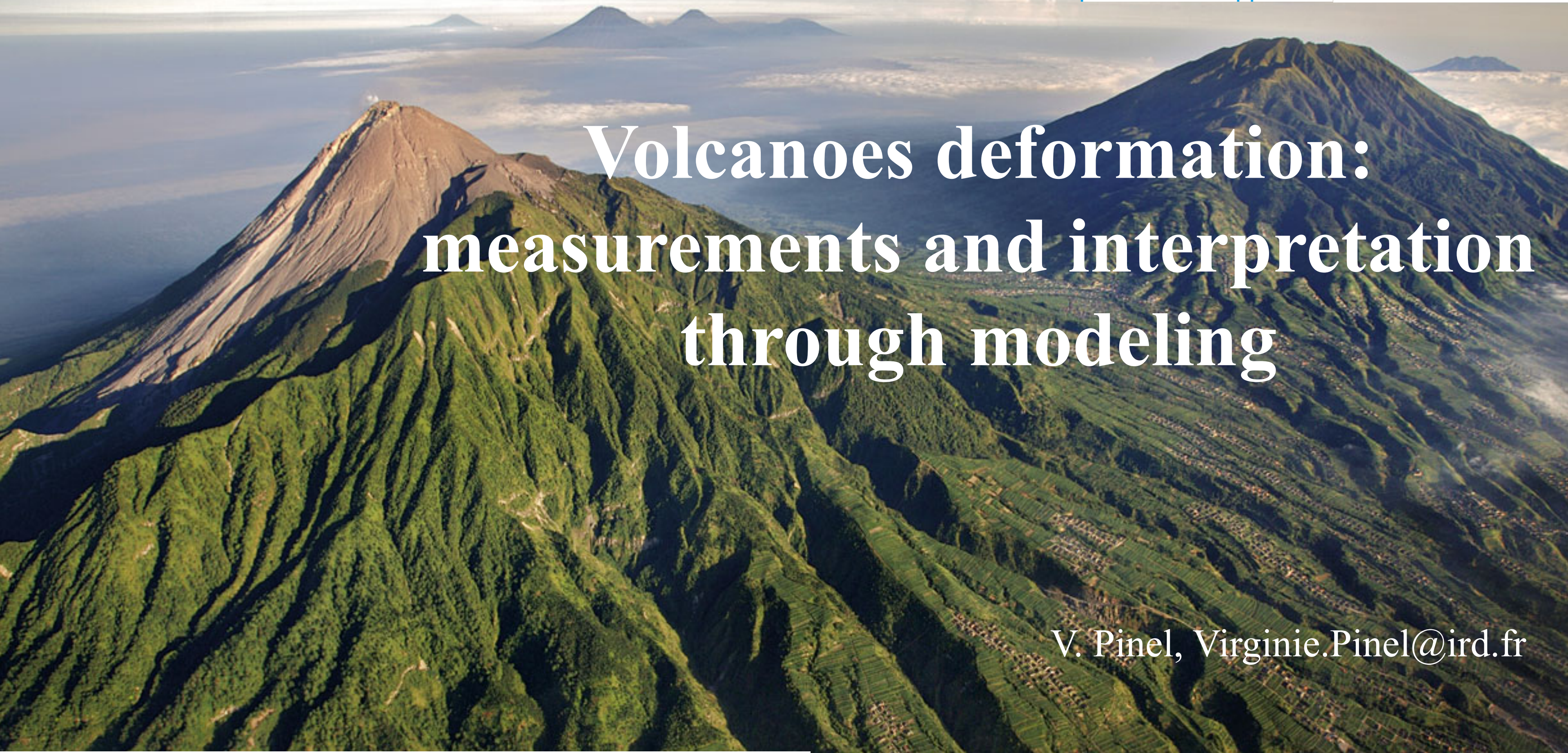

V. Pinel, Virginie.Pinel@ird.fr

Merapi Volcano, Indonesia (2008), from National Geographic

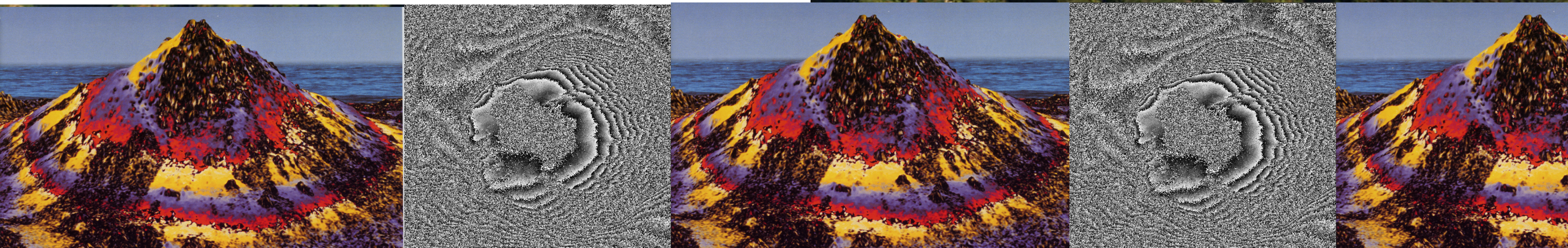

Who I am:

Virginie Pinel: Research Scientist at IRD
Virginie.Pinel@ird.fr

Institut de recherche pour le développement

I work at Chambéry (France)

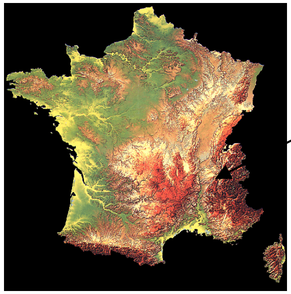

Le Bourget du Lac
photo Antoine Berger

Magma storage and transport through the crust

-Deformation study by InSAR
-Modeling (analytical + numerical) of magmatic plumbing systems beneath volcanoes

You can download this presentation on my web page.
http://isterre.fr/staff-directory/member-web-pages/virginie-pinel/

Outline of the course:

*I Availability of deformation measurements through time SINCE WHEN?
*II Tools used for deformation measurements: HOW?
  -in situ measurements
  -remote sensing: InSAR
*III Various causes of deformation at volcanoes CAUSES?
  -Example of a typical basaltic volcano (Piton de la Fournaise, Reunion Island)
  -Example of a typical andesitic volcano (Montserrat)
*IV Modeling of deformation sources HOW TO USE?
  -Analytical model for volcanoes deformation
  -Numerical models advantages, remaining problems
*V Inversion of deformation data
*VI Why is it important to study volcanoes deformation? WHY?
  - Monitoring for risk assessment.
  - Understanding volcanoes behaviour.
*VII Interest of Complementary measurements
*VIII Two exemples of numerical models.

Optional: Practical works
-Analytic models (Matlab)
-Numerical models (COMSOL software)

Eruption precursors
Volcanoes monitoring

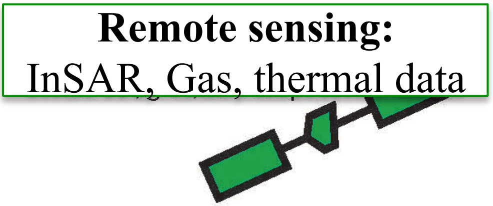

When an eruption will start?

In case a shallow storage is detected, is it possible to know when magma will start its ascent towards the surface?

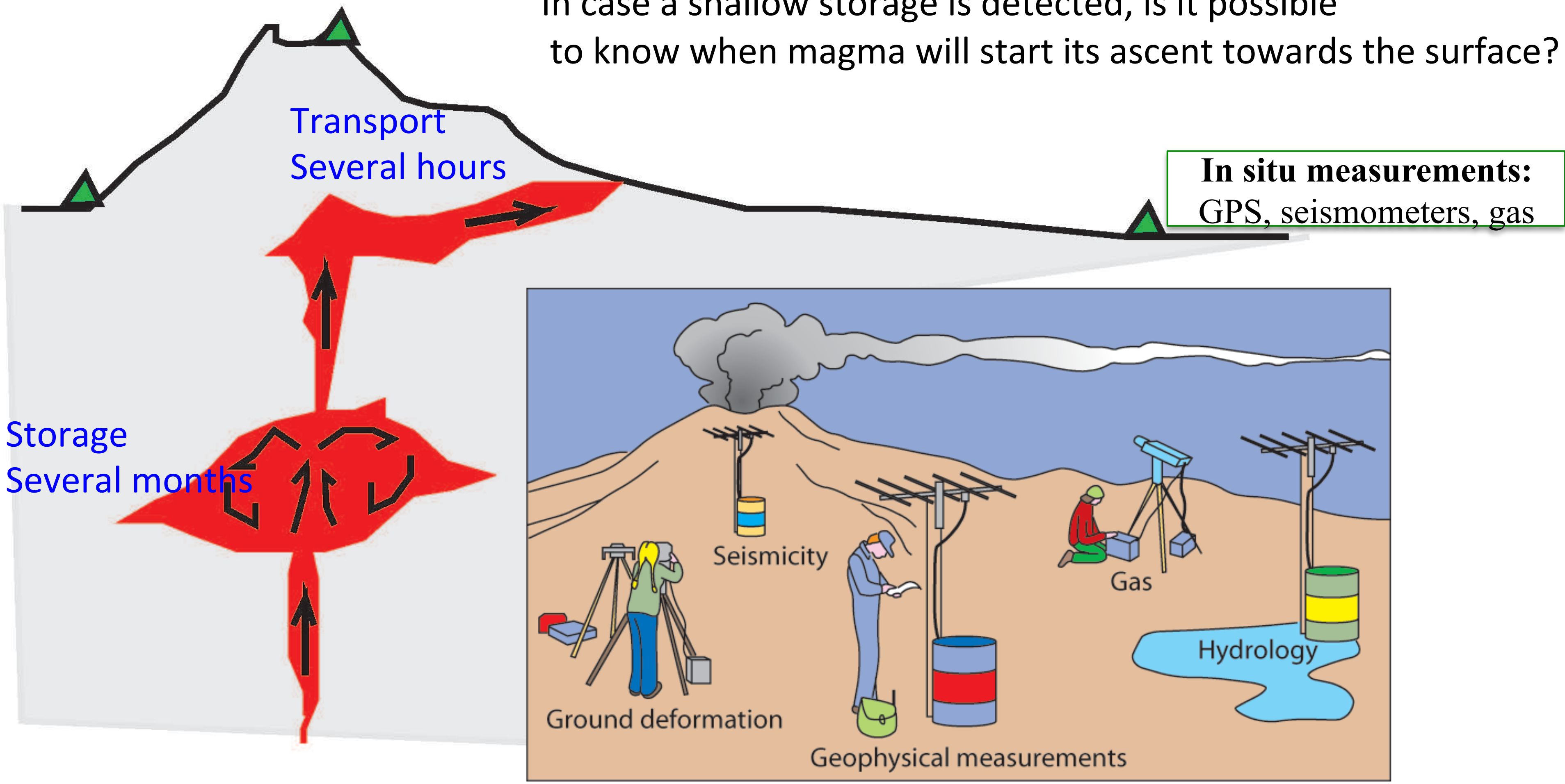

Measurements of surface deformation available at volcanoes

Temporal series are available over more than 100 years.

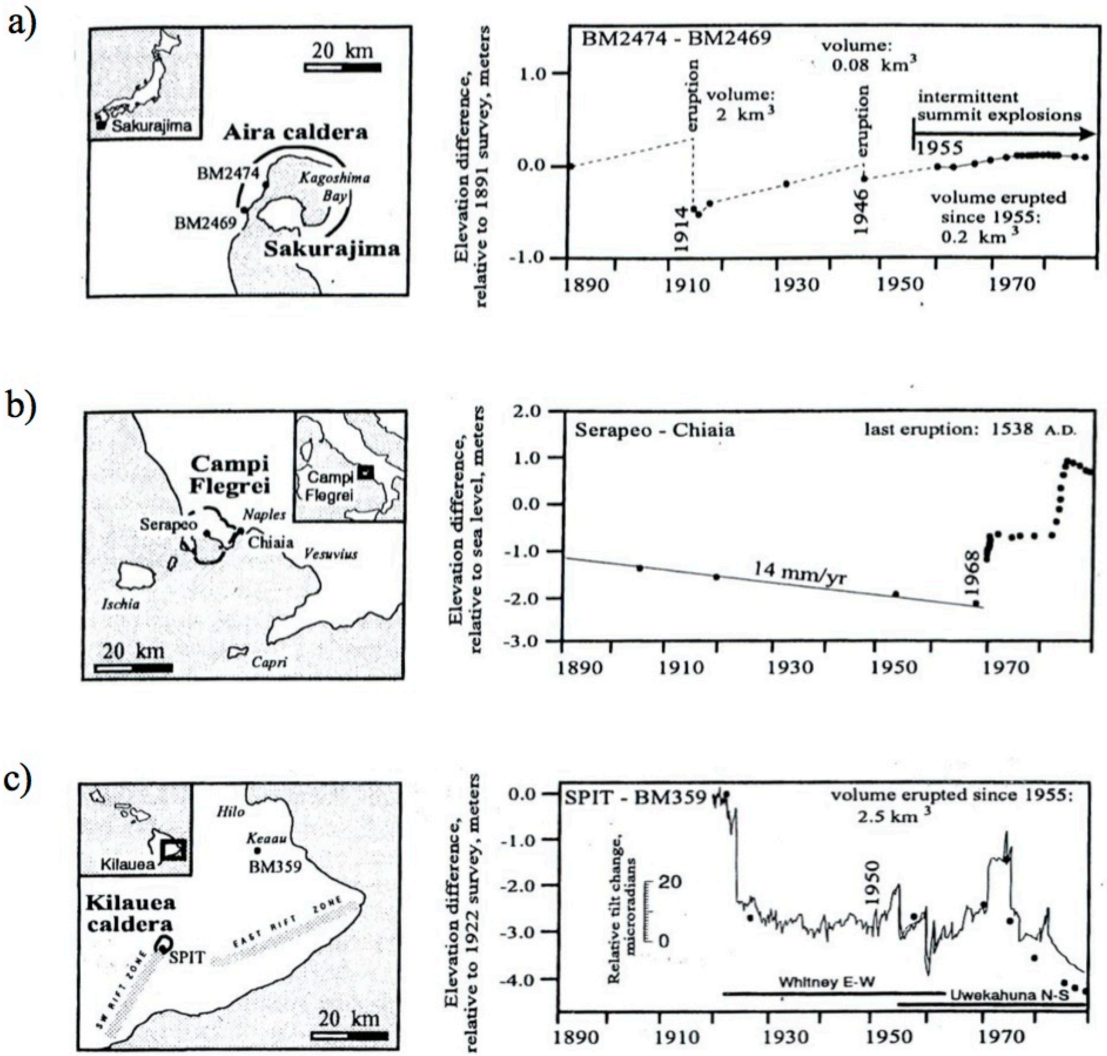

For a few well-studied volcanoes.

With a low frequency of measurements.

Observatorio Vesuviano since 1845

Hawaiian Volcano Observatory since 1912

From Dvorak et Dzurisin, 1997

Some long term information also exists over 10,000 years

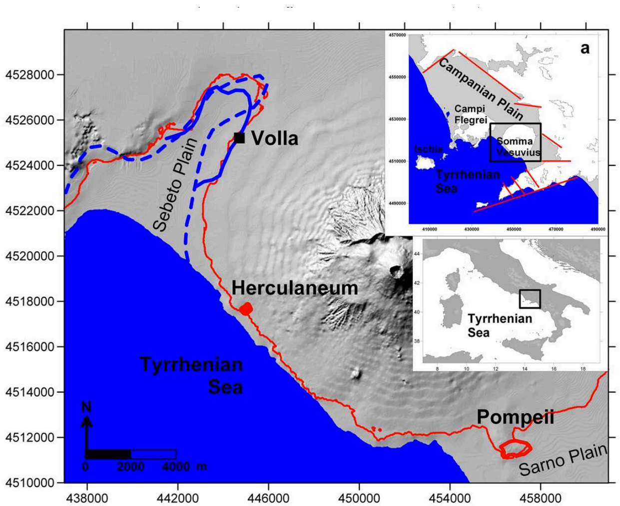

Vesuvius, Italy

Using paleoecology

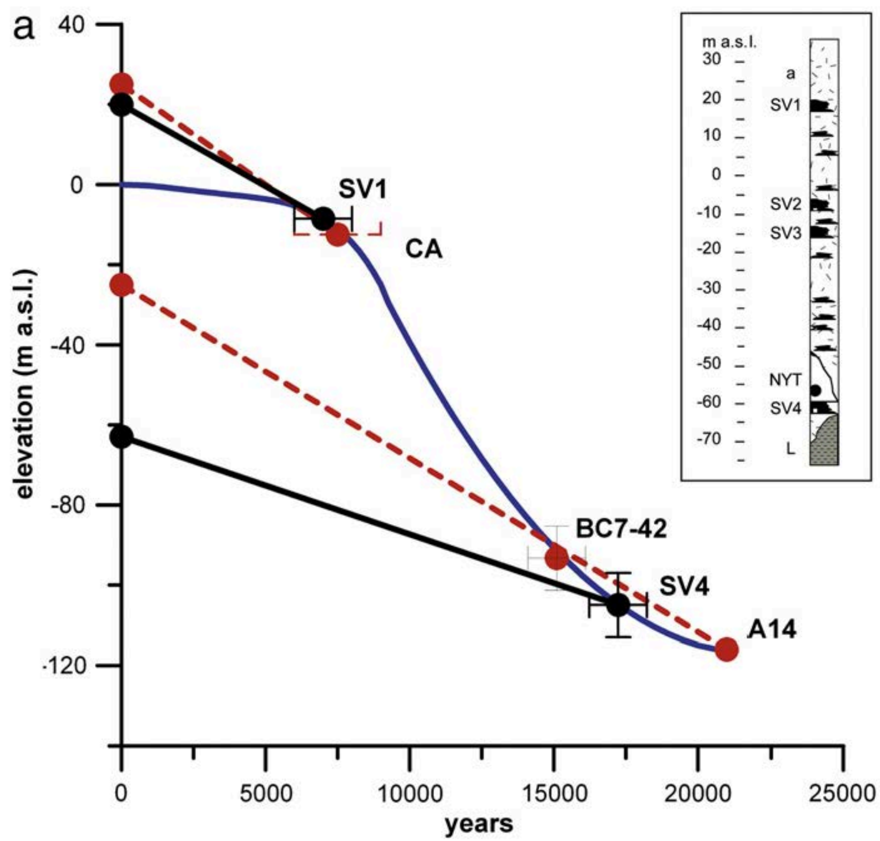

From Marturano et al, 2012

Some long term information also exists over 10,000 years.

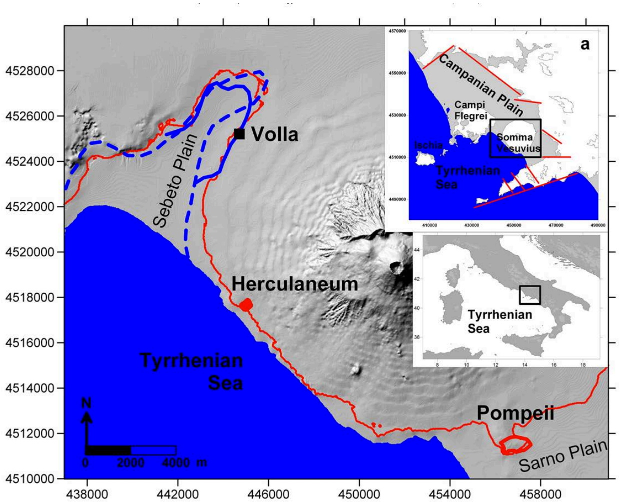

Vesuvius, Italy

Using paleoecology

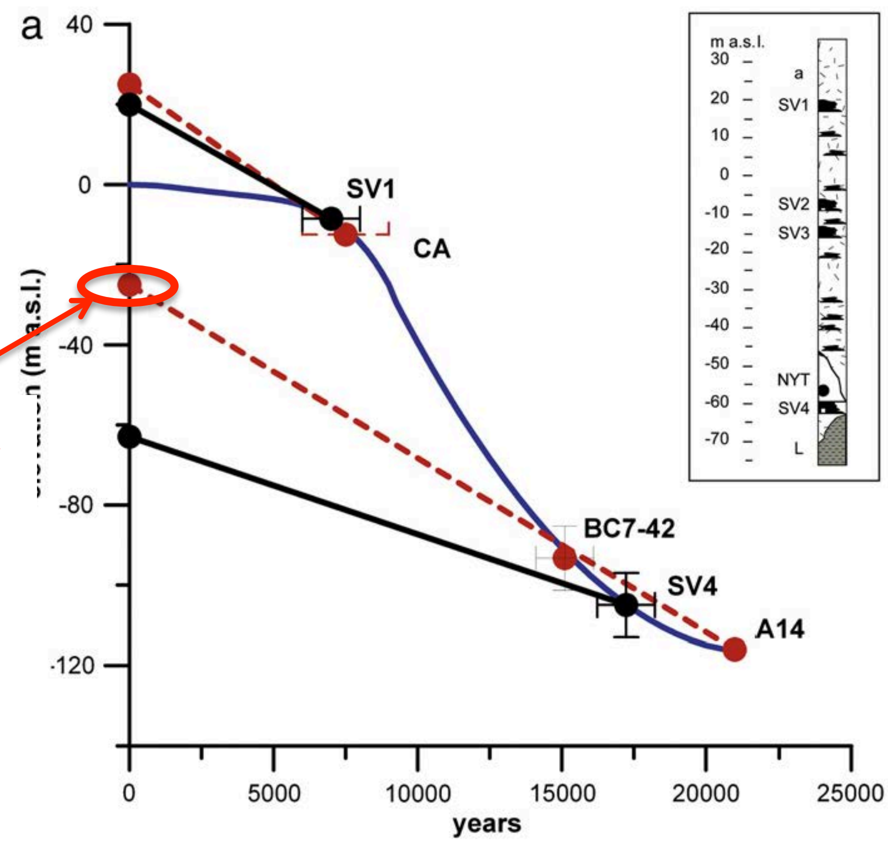

Position at present time

From Marturano et al, 2012

Some long term information also exists over 10,000 years.

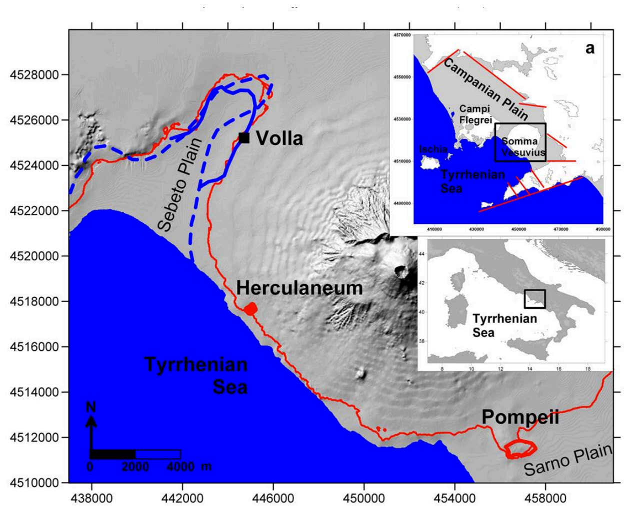

Vesuvius, Italy

Using paleoecology

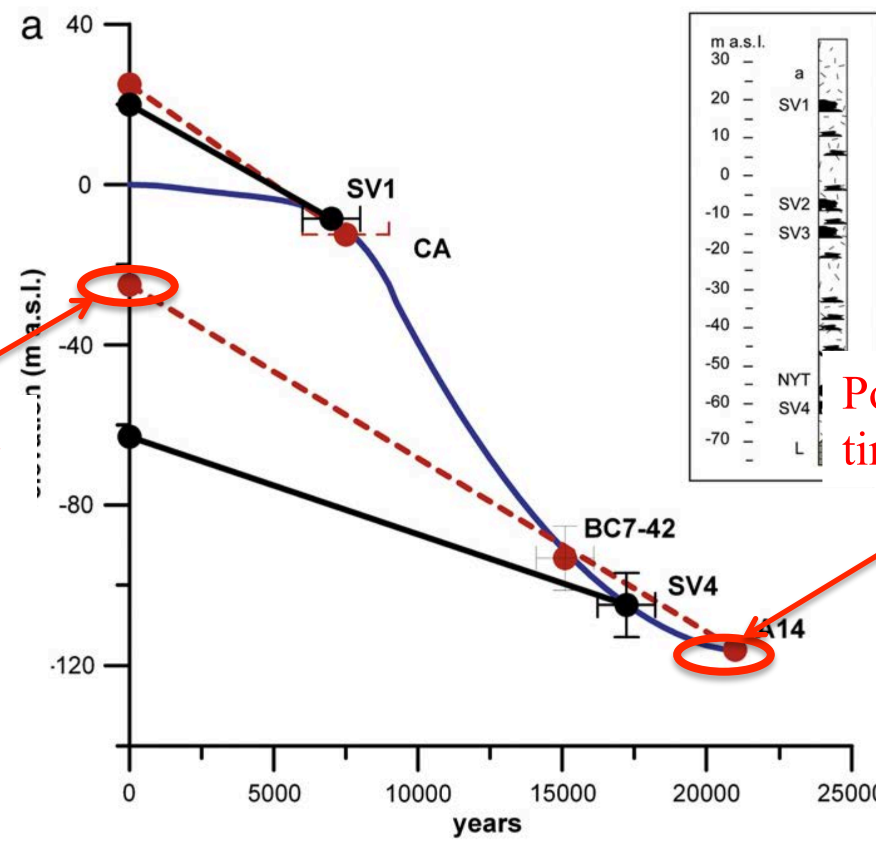

Position at present time

Position at time of deposit

From Marturano et al, 2012

Some long term information also exists over 10,000 years.

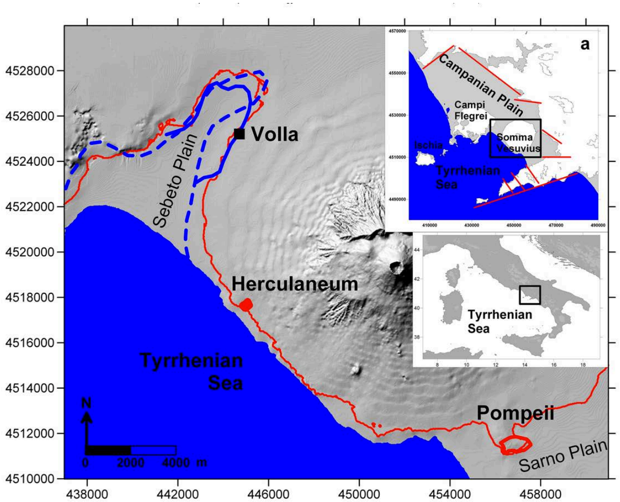

Vesuvius, Italy

Using paleoecology

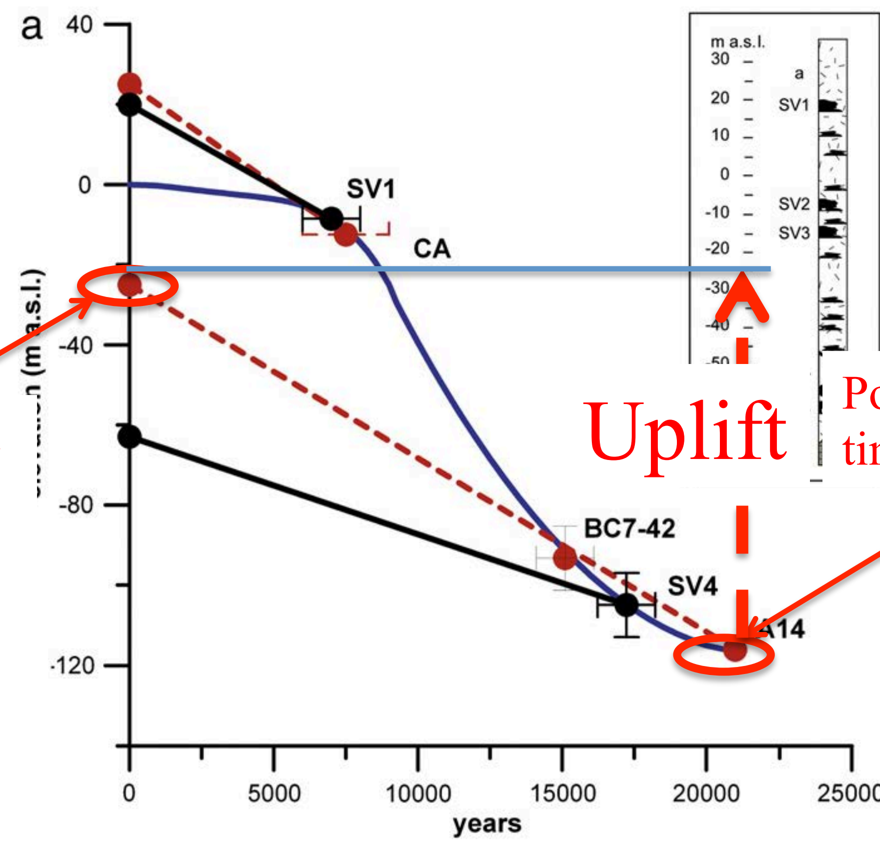

Position at present time

Position at time of deposit

From Marturano et al, 2012

First interpretation of volcano deformation : Hawaii

1958 : Mogi model

+ Triangulation
● Levelling + triangulation

DT> 5 ans

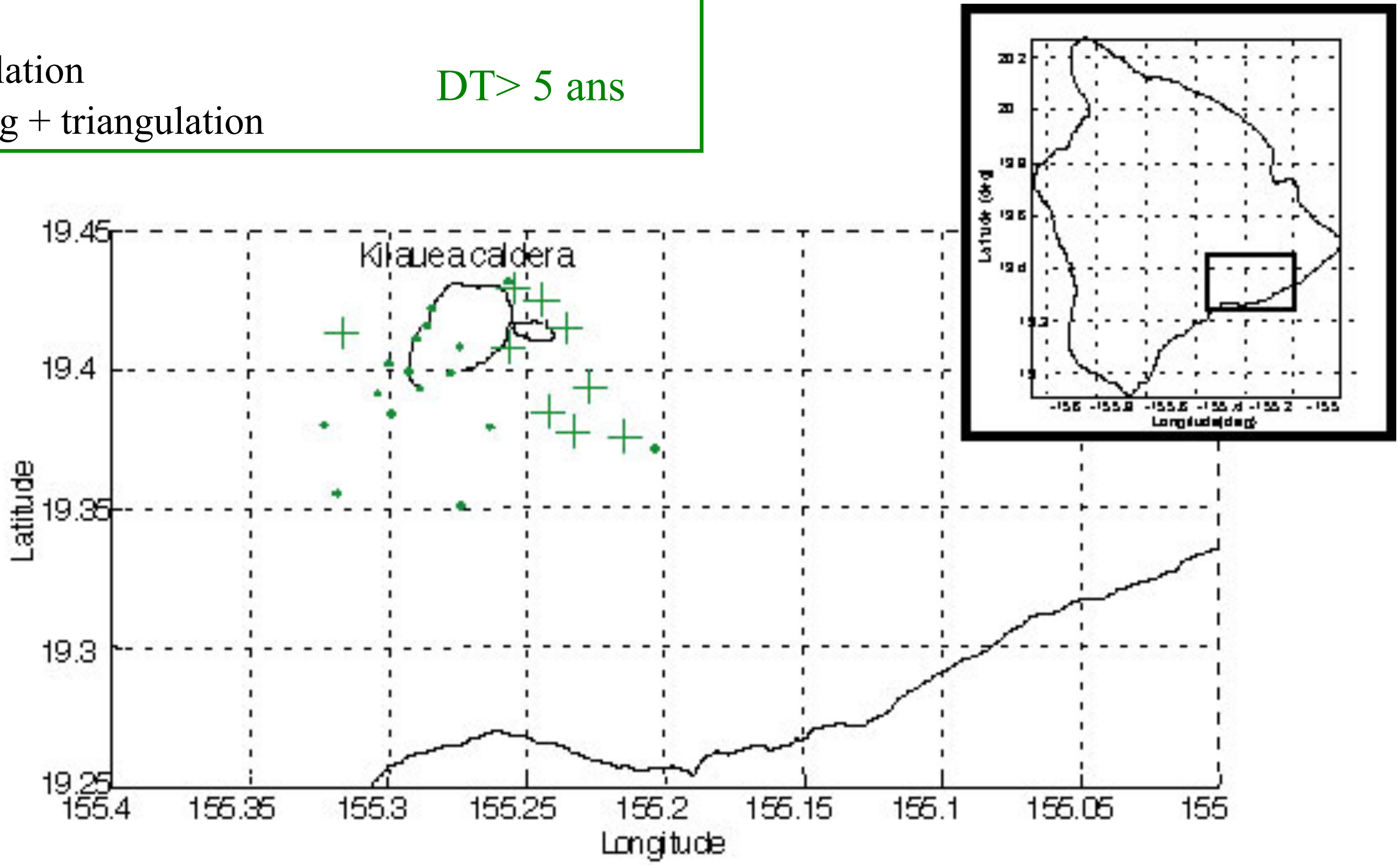

Recently: a significant improvment of the spatial and temporal resolution of deformation measurements : Hawaii

1958 : Mogi model

Triangulation
Levelling + triangulation

ΔT> 5 ans

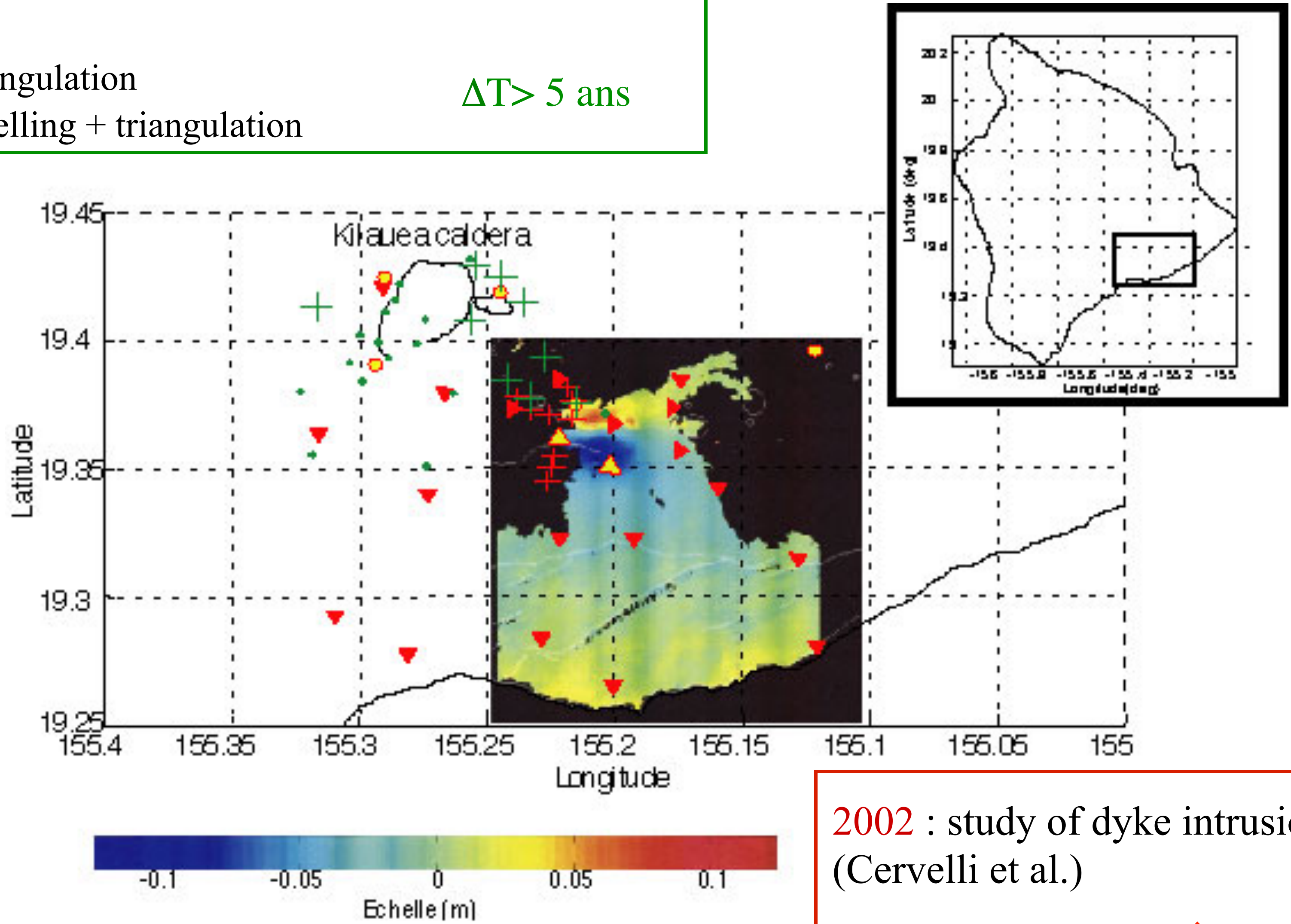

2002 : study of dyke intrusion (Cervelli et al.)

Remote sensing data : GPS + INSAR

2 main progress:

Continuus measurements
(GPS, tiltmeters, EDM…)

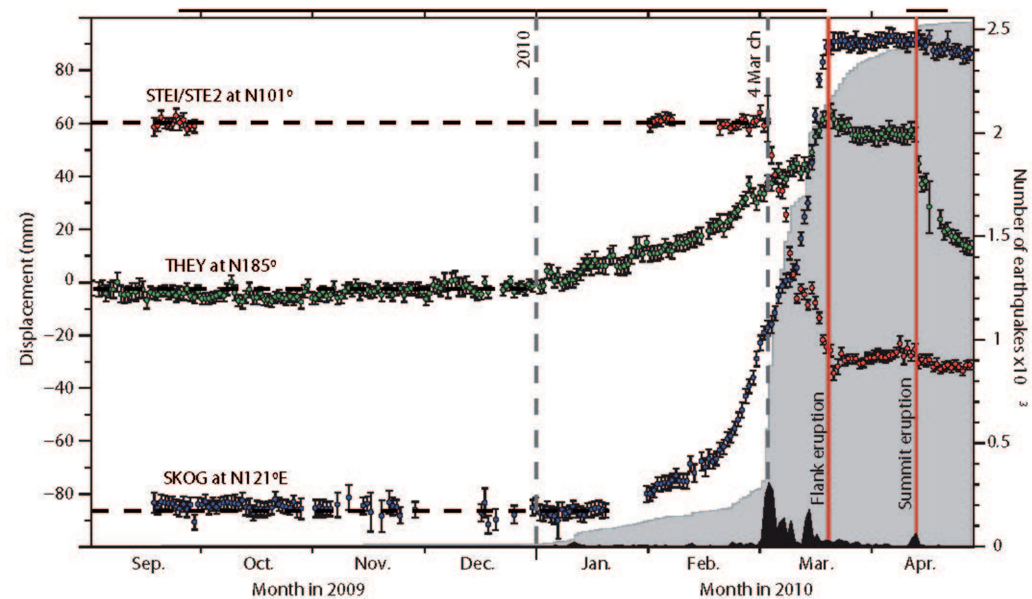

InSAR→
Map of surface
of displacement

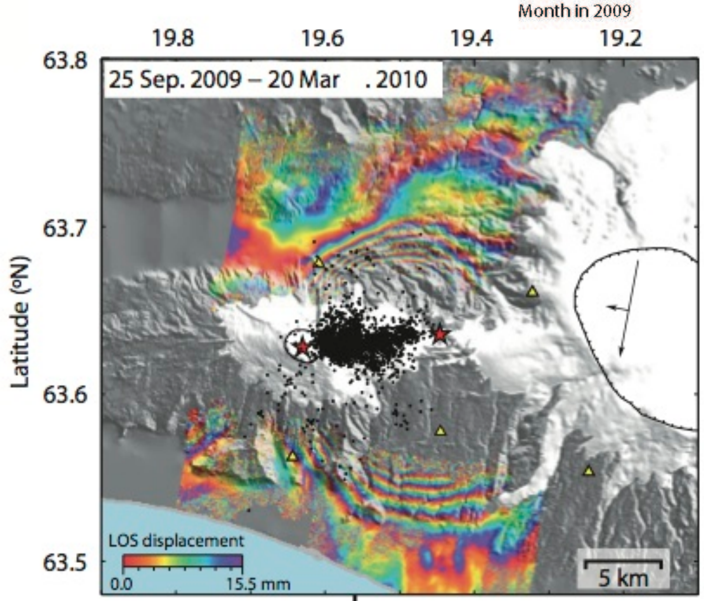

From Sigmundsson et al. Nature, 2010

Tools for surface deformation measurements:

-in situ measurements → Continuous sensors

→ Repeat surveys

-InSAR → Repeat surveys

Tools for surface deformation measurements:

-in situ measurements → Continuous sensors

-InSAR → Repeat surveys

Most often used on volcanoes:

-GPS
-EDM measurements
-levelling
-photogrammetry

In situ measurements require benchmarks

Levelling surveys:

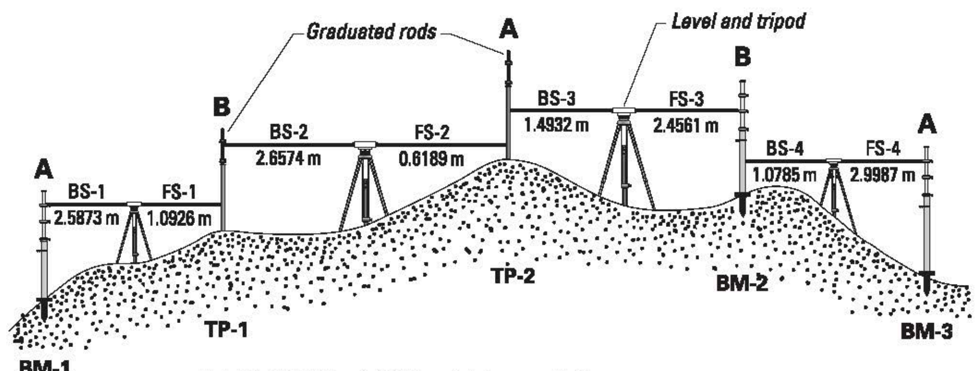

Height (BM-1) = 0.0000 m (datum point)
Height (TP-1) = 0.0000 m – (1.0926 m – 2.5873 m) = 1.4947 m
Height (TP-2) = 1.4947 m – (0.6189 m – 2.6574 m) = 3.5332 m
Height (BM-2) = 3.5332 m – (2.4561 m – 1.4932 m) = 2.5703 m
Height (BM-3) = 2.5707 m – (2.9987 m – 1.0785 m) = 0.6501 m

From Dzurizin, 2007

Tools for surface deformation measurements:

-in situ measurements → Continuous sensors

-InSAR → Repeat surveys

Most often used on volcanoes:

-tiltmeters
-strainmeters
-GPS
-EDM measurements

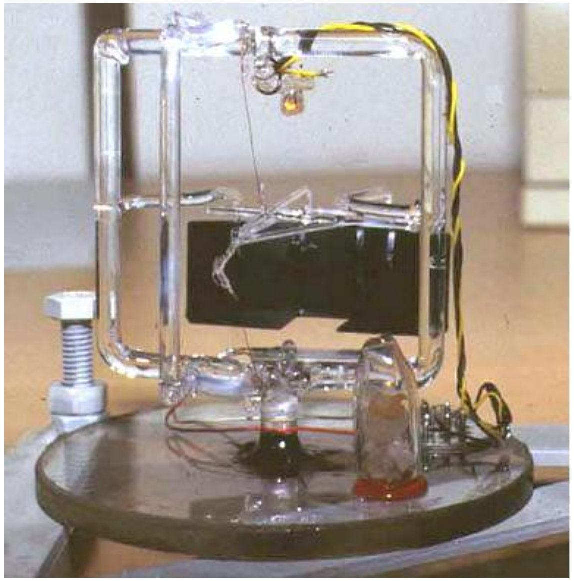

Tiltmeters:

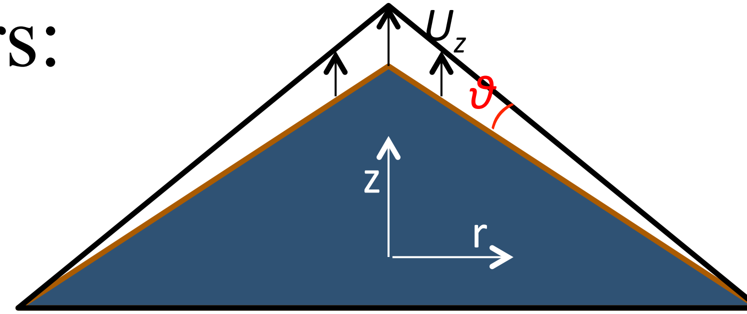

$$\underline{\theta} = \begin{pmatrix} \theta_x \\ \theta_y \end{pmatrix} = \begin{pmatrix} \frac{\partial U_x}{\partial z} \\ \frac{\partial U_y}{\partial z} \end{pmatrix} = \begin{pmatrix} -\frac{\partial U_z}{\partial x} \\ -\frac{\partial U_z}{\partial y} \end{pmatrix}$$

$$\theta_r = \frac{\partial U_r}{\partial z} = -\frac{\partial U_z}{\partial r}$$

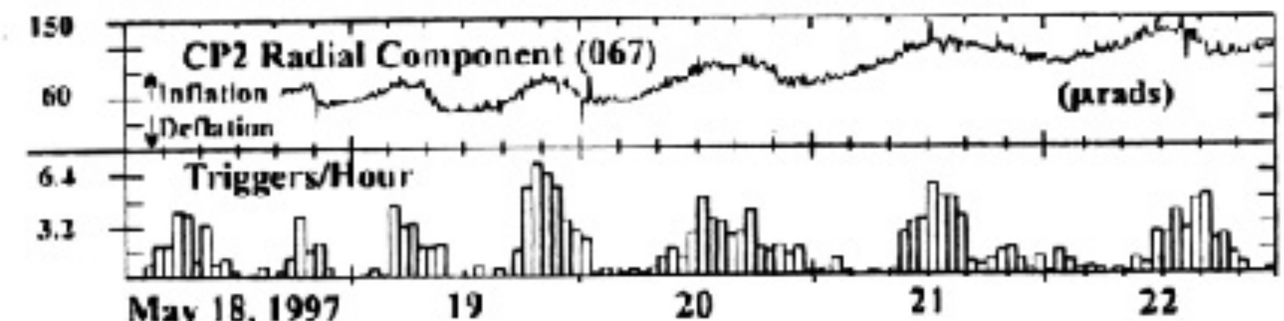

(Voight et al., Science 1999)

Simple bubble tiltmeters : precision around 1 μrad. (a few 1000$)
Borehole long-base tiltmeters: precision around 1nrad (10^{-9} rad) (more expensive)

Extensometers:

Normal, tangential and vertical displacement along a fault
U_n, U_t, U_v

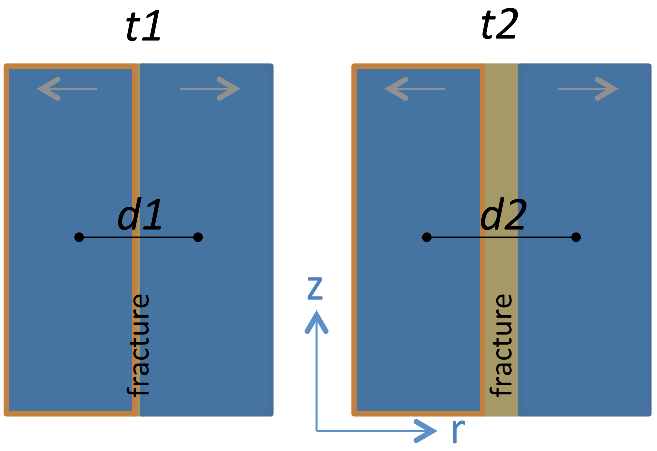

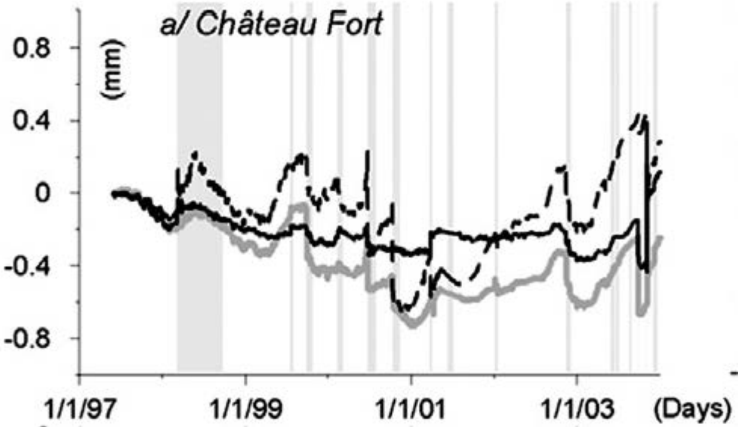

From Peltier et al, 2006

Strainmeters:

Measure the strain (ε_{xx},ε_{yy},ε_{zz})
Volumetric strainmeters measure $\Delta V/V=\varepsilon_{xx}+\varepsilon_{yy}+\varepsilon_{zz}$
Often placed in boreholes
Sampling frequency 1Hz to 100Hz
Precision around 10^{-12}, can detect strain around $5*10^{-8}$ over months
Price around 10000$

GPS

Ux, Uy (precision around mm)
Uz (precision around cm)

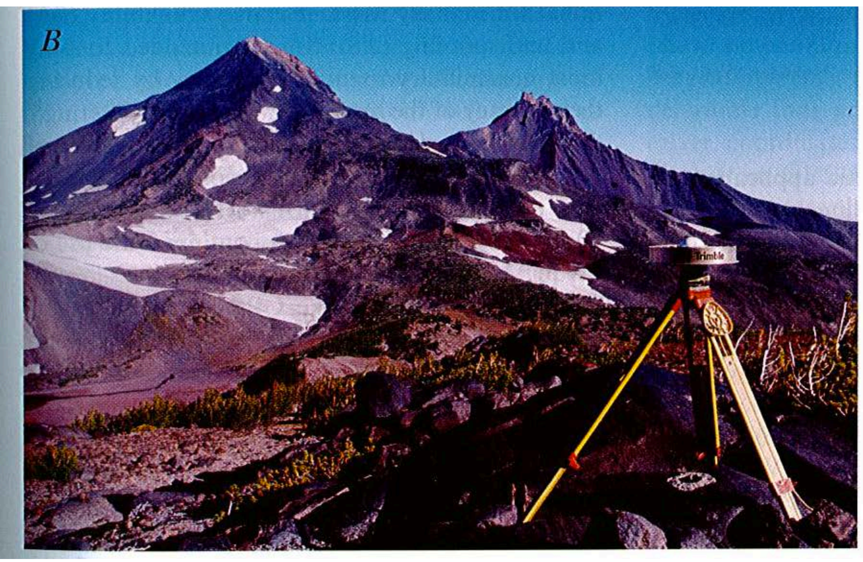

From Dzurisin, 2007

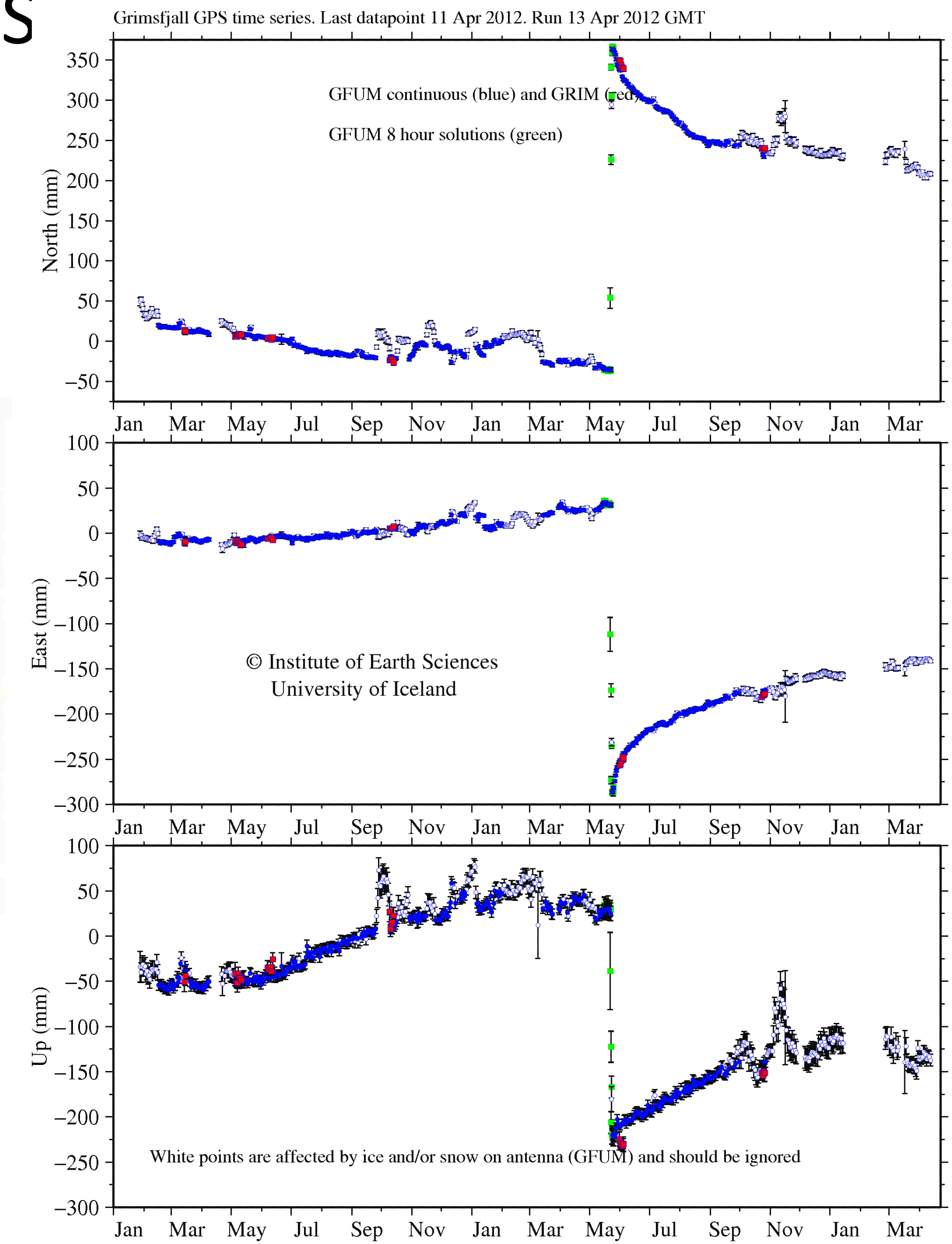

EDM measurements:

Distance between two points

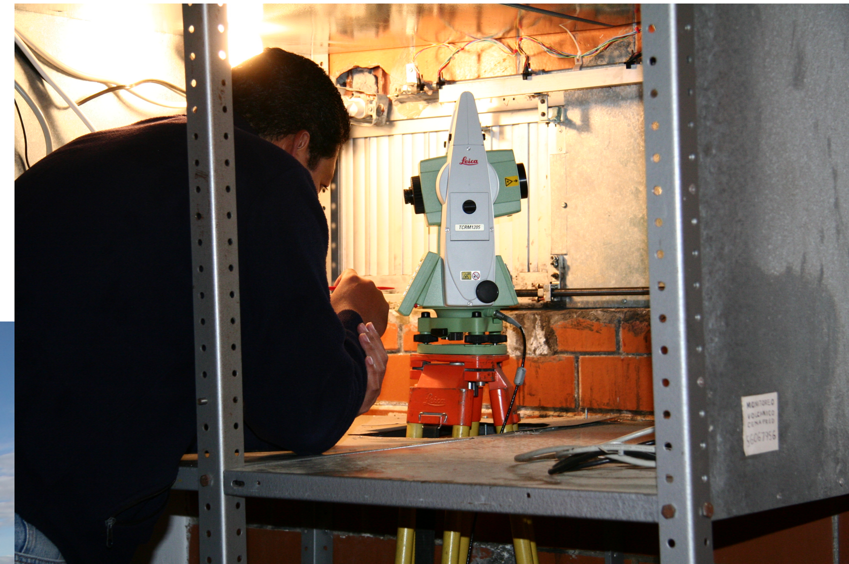

Photogrammetry:

Use of photographs or videos to measure surface displacements.

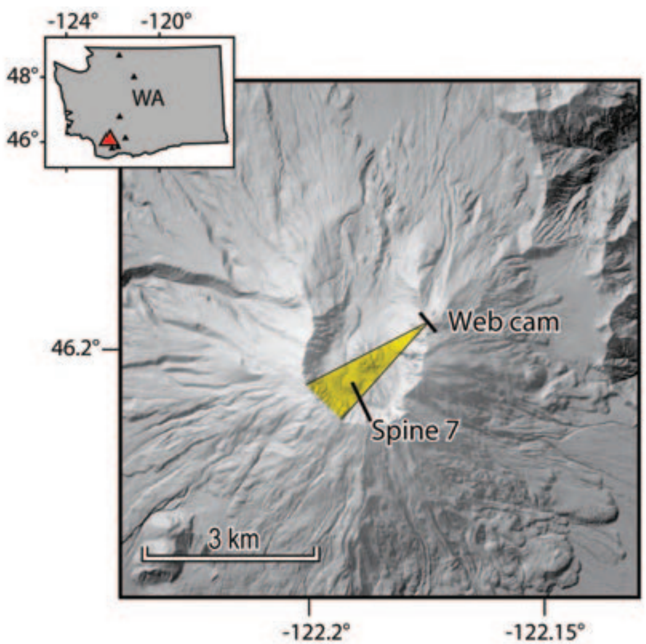

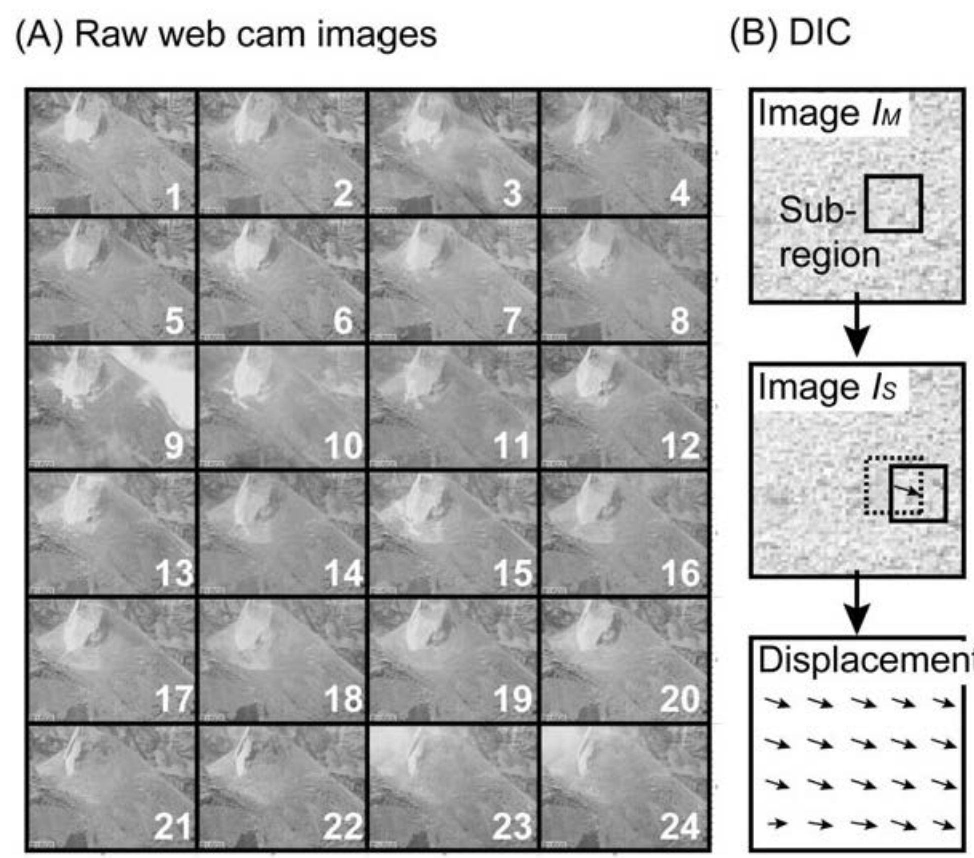

From Walter, GJInt, 2011

Tools for surface deformation measurements:

-in situ measurements → Continuous sensors
-InSAR → Repeat surveys

InSAR

Massonnet et al, 1995

Principle:

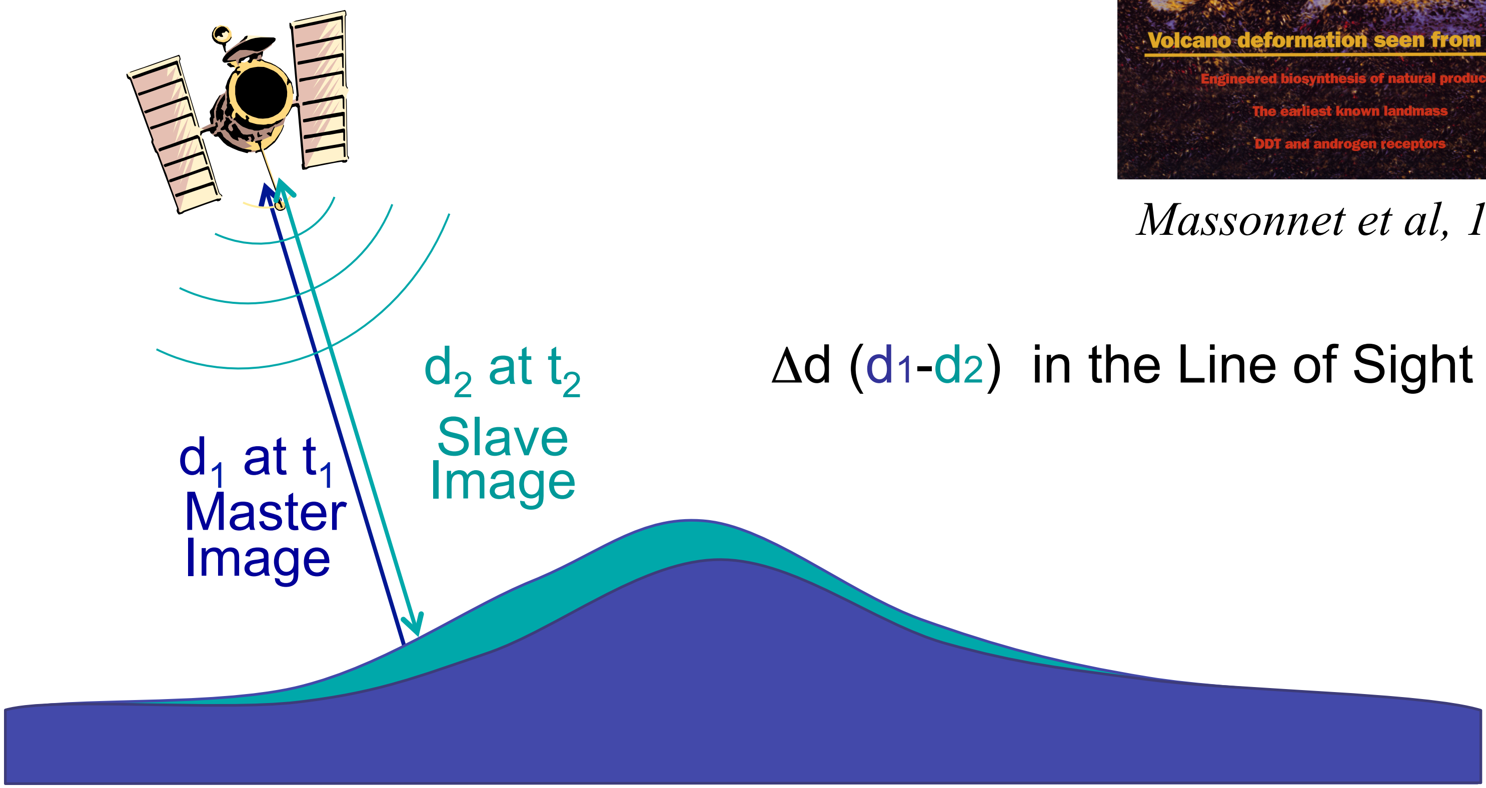

Map of displacement in a given direction.

Wavelength used by SAR imagery

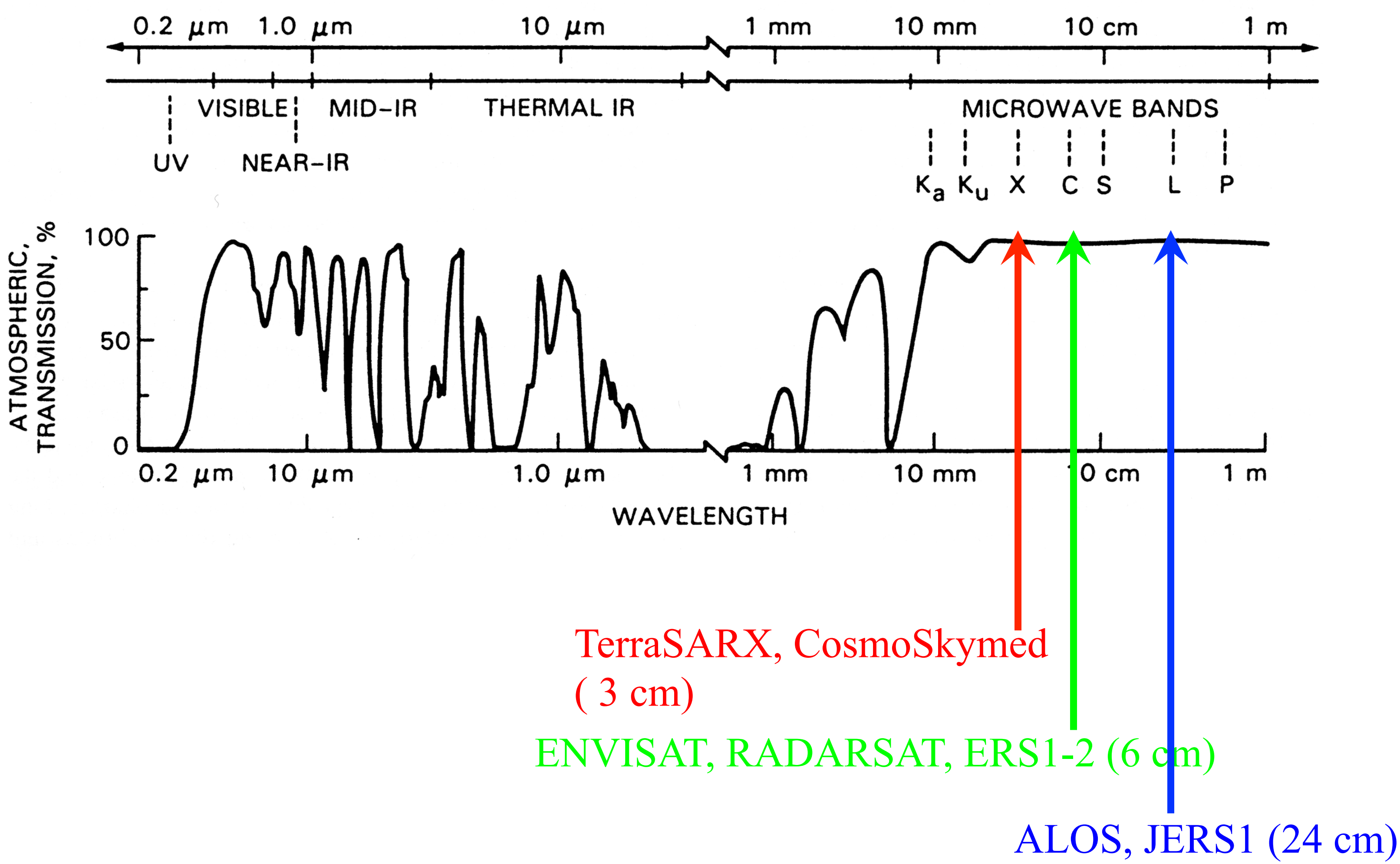

Satellite providing SAR data

Satellite	Period	Revisit time (days)	Altitude (km)	Frequency (GHz)	Band	Incidence Angle (deg)	Swath (km)
ERS-1	1991-1996	35	790	5.3	C	23	100
ERS-2	1995-2011	35	790	5.3	C	23	100
JERS-1	1992-1998	44	568	1.275	L	39	85
Radarsat	1995-	24	792	5.3	C	20-49	10-500
ENVISAT	2001-	35	800	5.3	C	20-50	100-500
ALOS	2002-2011	45	700	1.27	L	8-60	40-350
Radarsat 2	2007-	24	798	5.3	C	20-60	20-500
TerraSAR-X (2)	2007-	11	514	9.65	X	20-55	10-100
Cosmo-Skymed (4)	2007-	16	619.61	9.6	X	40-50	10-200
ALOS2	2013-	14	628	1.2	L	8-70	25-350
Sentinel1 (2)	2013- ?	12	6935	5.4	C	>25	>250

Satellites

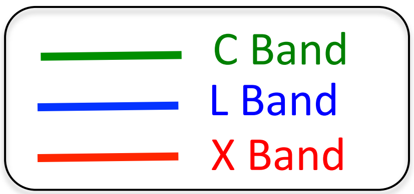

Spatial and temporal resolution is improving

A large amount of data is expected around 2015 with Sentinel 1

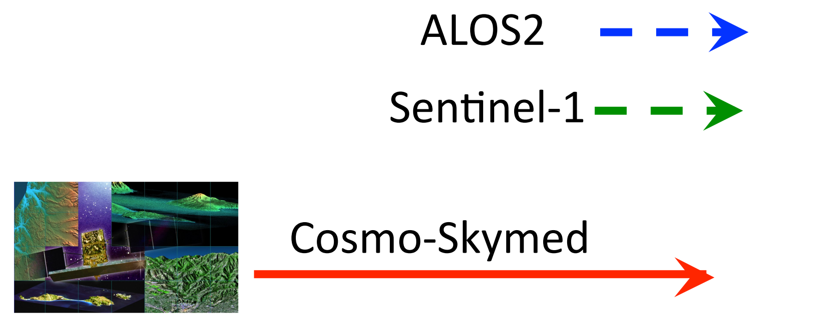

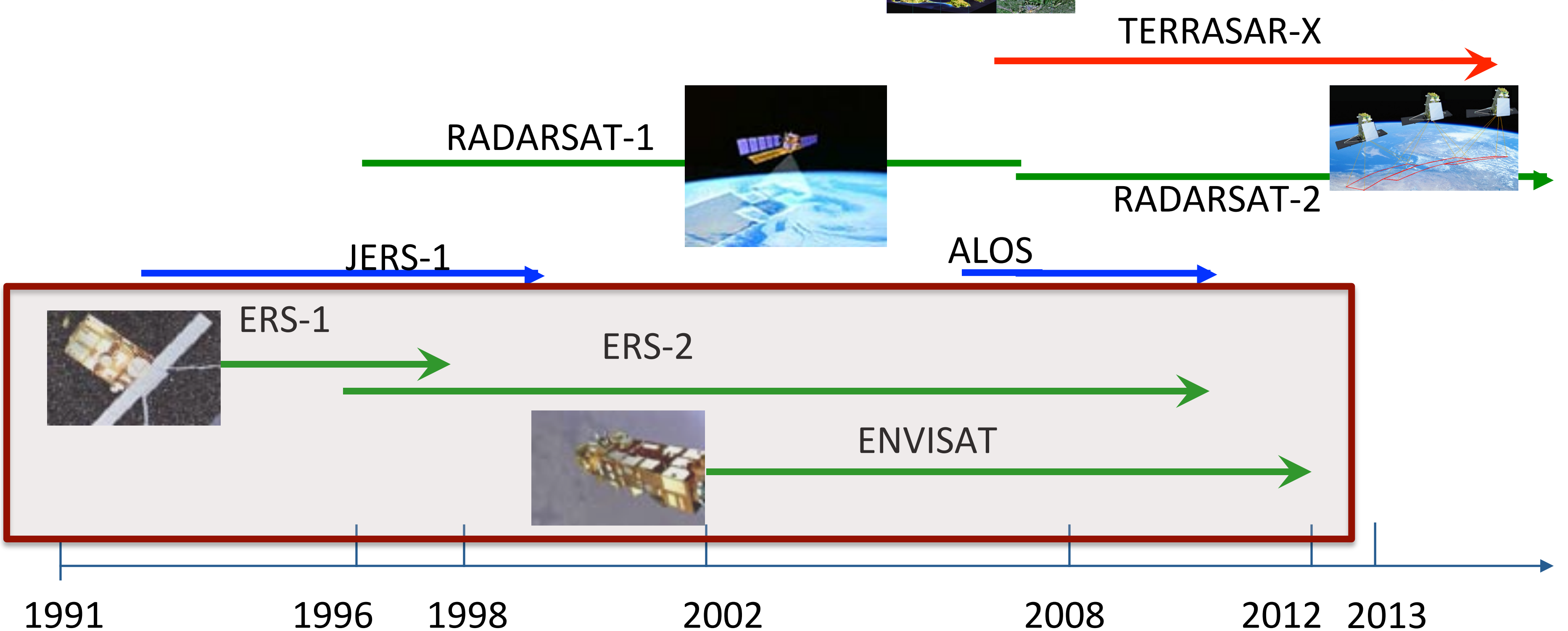

Principle of SAR (Synthetic Aperture Radar)

Resolution in azimuth is given by Rλ/L→ 5km for ERS

This resolution is improved par Synthetic Aperture processing:

-Using Doppler effect in azimuth =azimuth compression

-Using frequency modulation of the signal in range=range compression

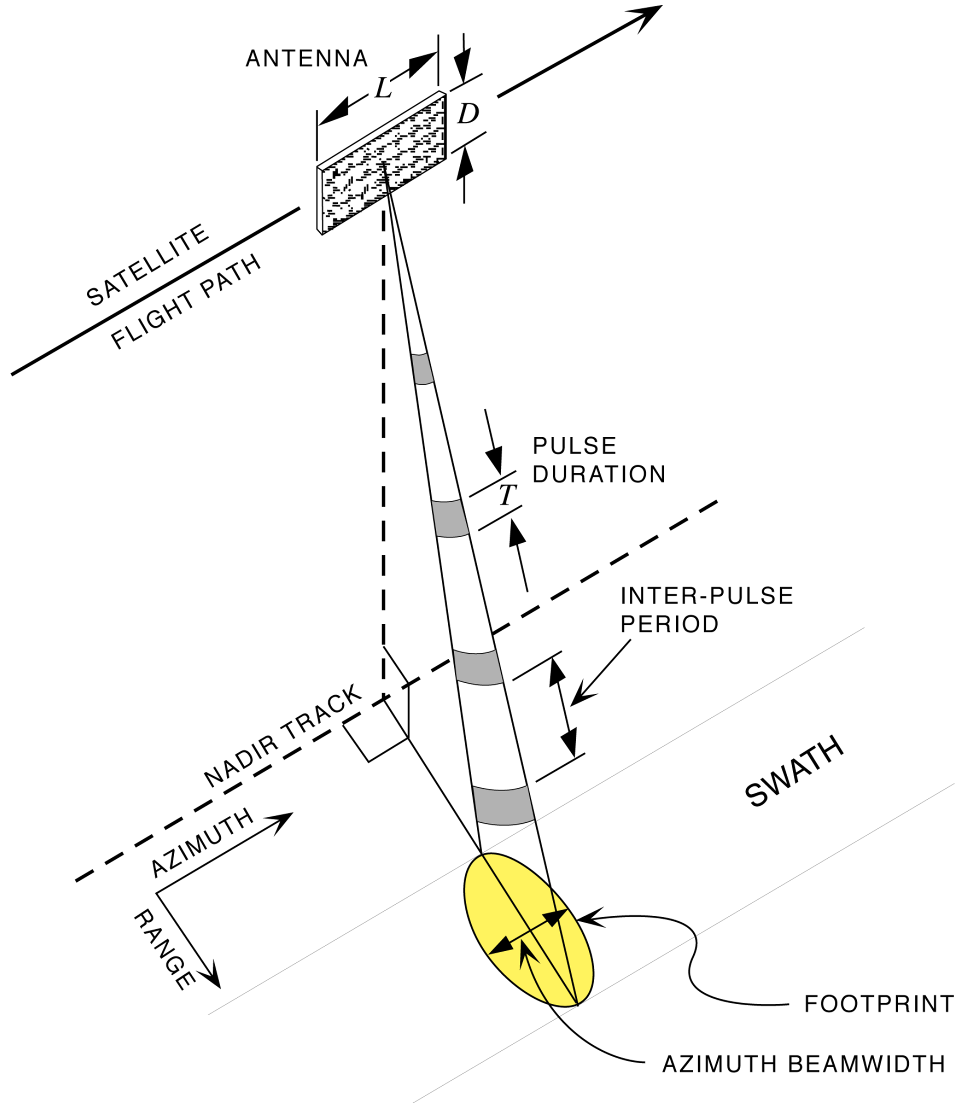

Images SAR

SAR Synthesis

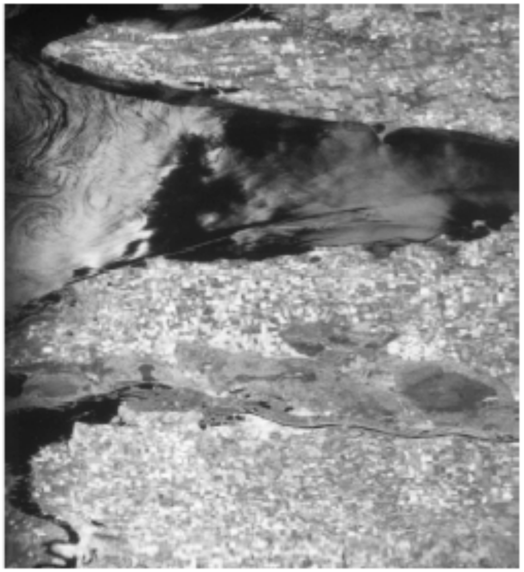

ERS scene
100*100km
140 millions of pixels

Raw data
Resolution
5km in azimuth
14km in range
For ERS

Single look complex (SLC) Image
=focused image
Resolution
5 m in azimuth
20 m in range

(Massonnet et al., 1998)

High Resolution SAR imagery

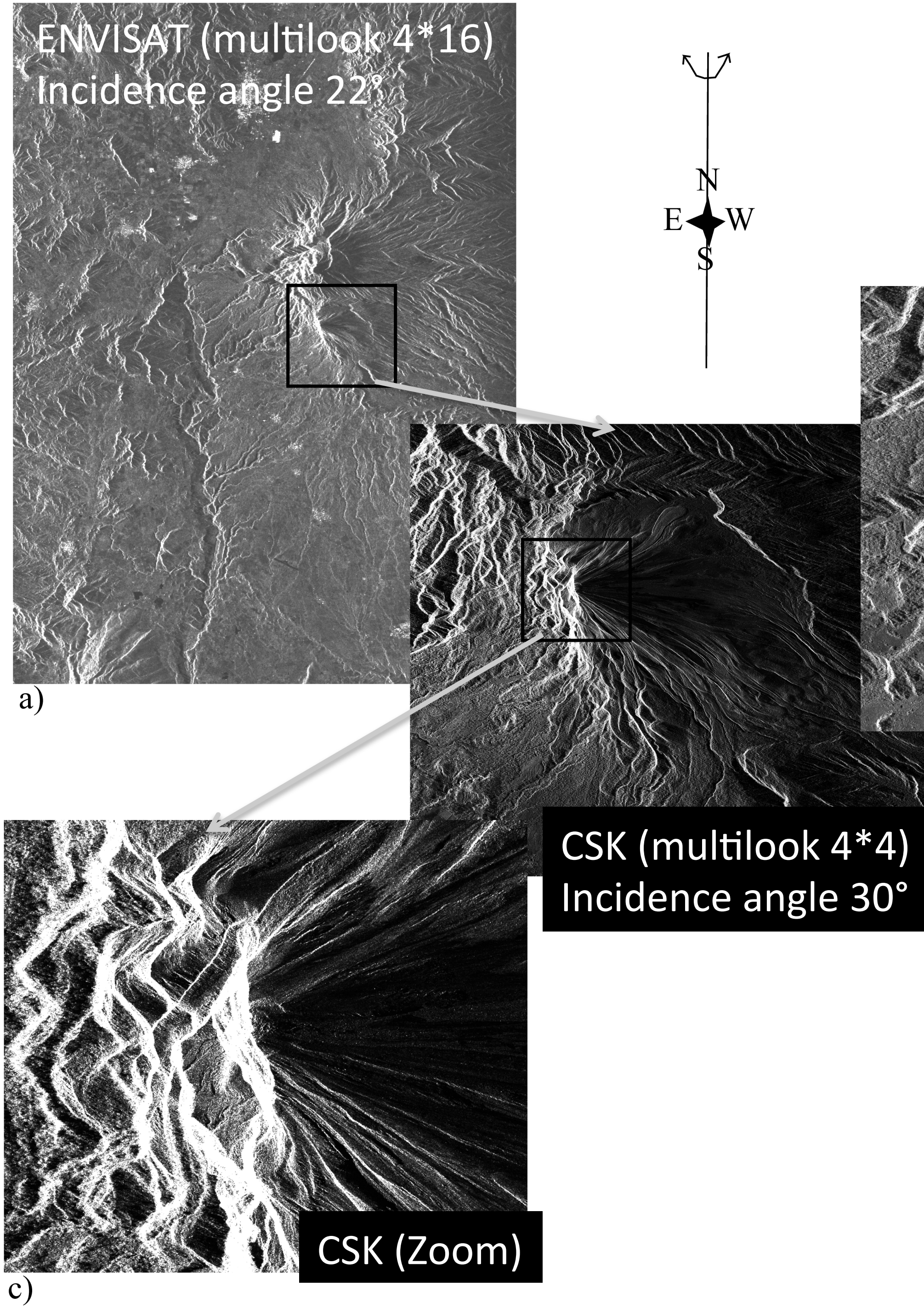

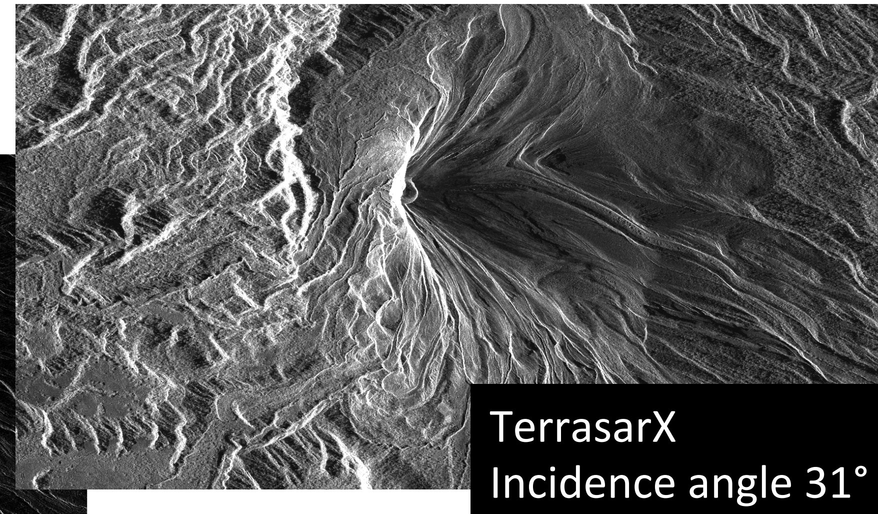

Colima volcano, Mexico

Cosmo-Skymed or TerraSAR-X data
1*1m in Spotlight mode

Synthetic Aperture Radar (SAR) imagery

Remote sensing
All weather and day/night observations
A given target is defined by its distance from the satellite.

A complex signal: $y_M=|y_M|e^{if_M}$

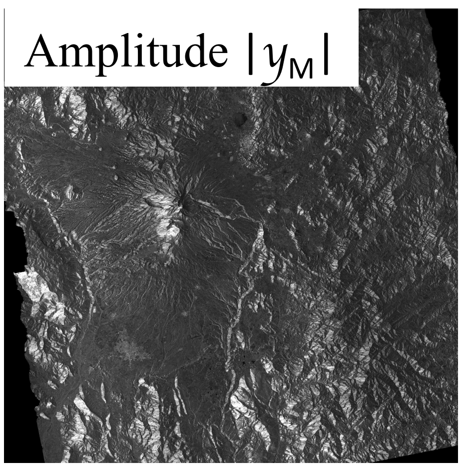

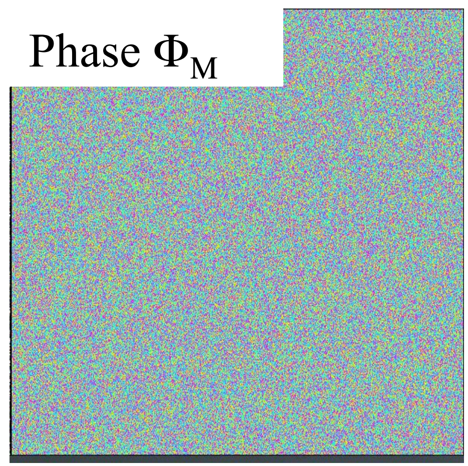

Random signal

SAR geometry

- **Foreshortening**

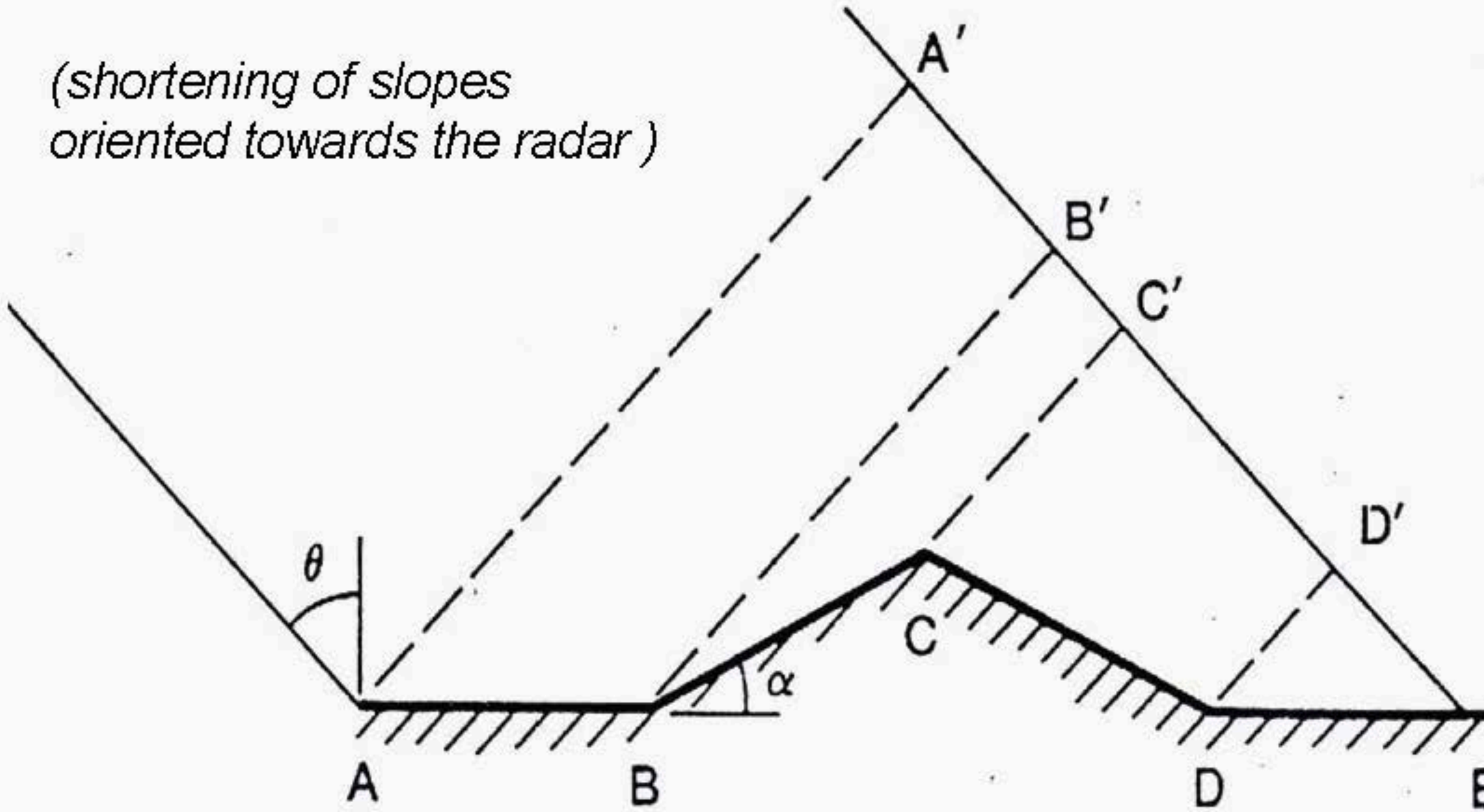

$$A'B' = AB \sin\theta,\ B'C' = BC \sin(\theta - \alpha),\ C'D' = CD \sin(\theta + \alpha)$$

Image quality: geometry

➔ foreshortening et layover effect

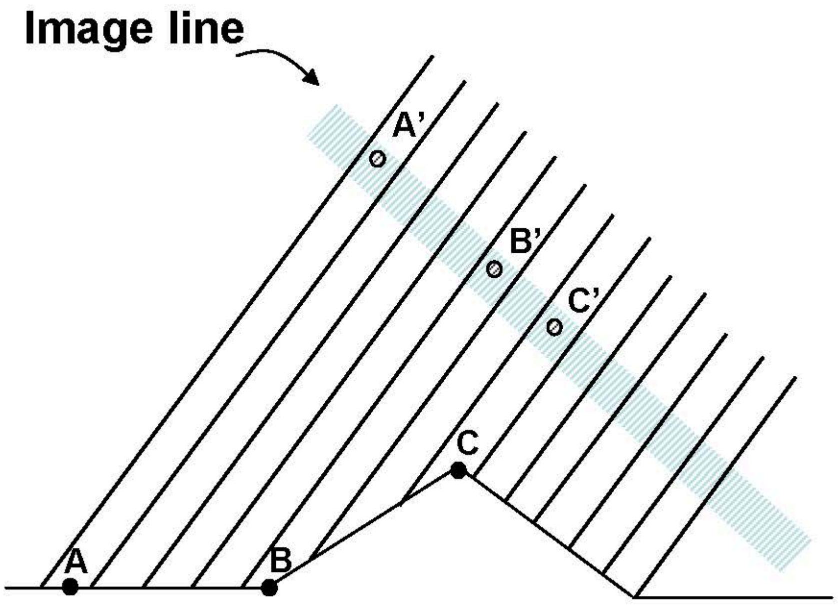

Foreshortening

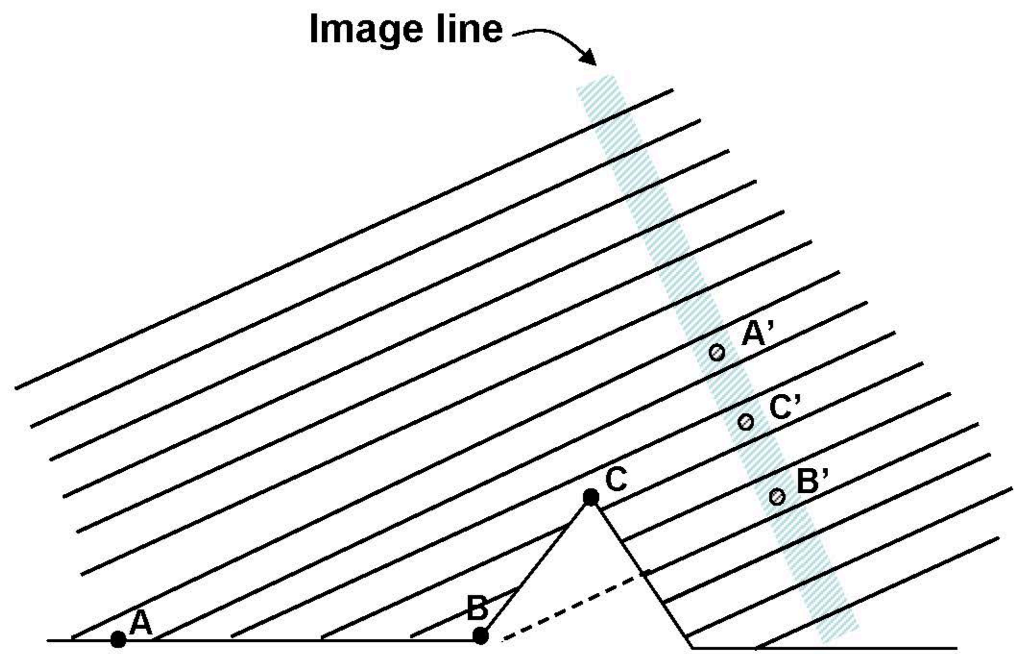

Layover

Image quality: geometry

➔ example of layover effect

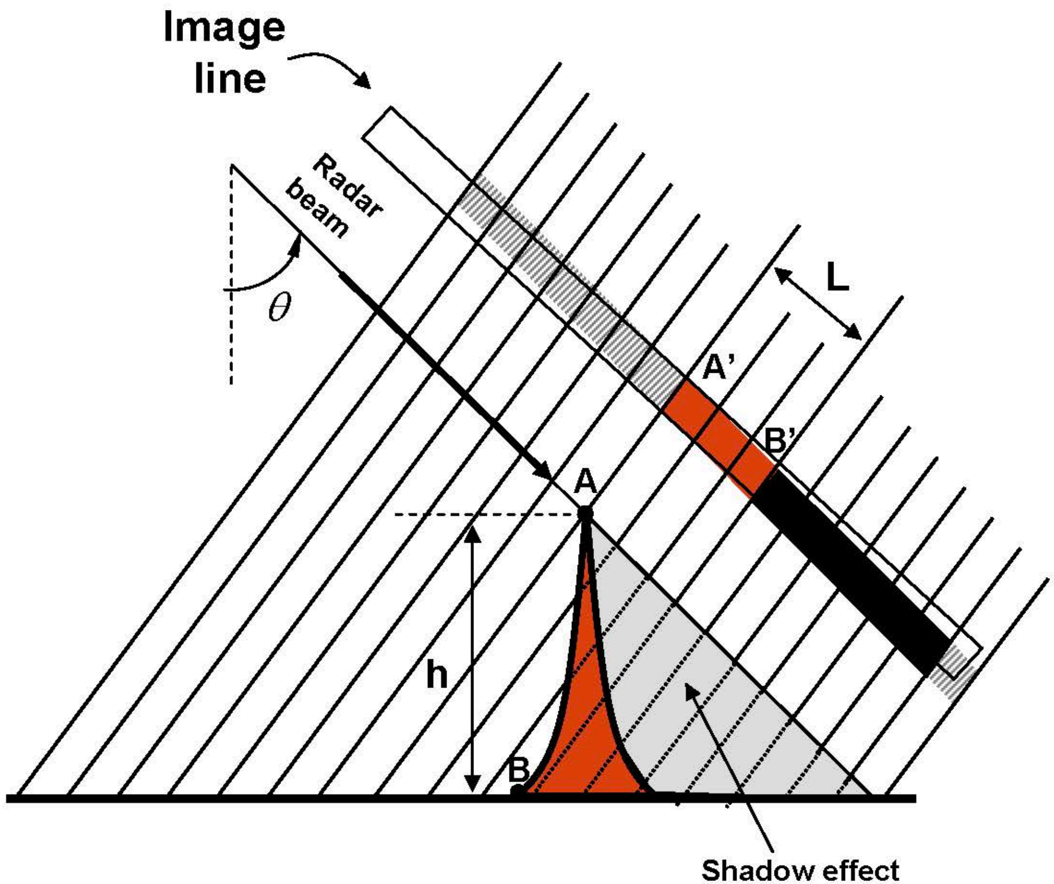

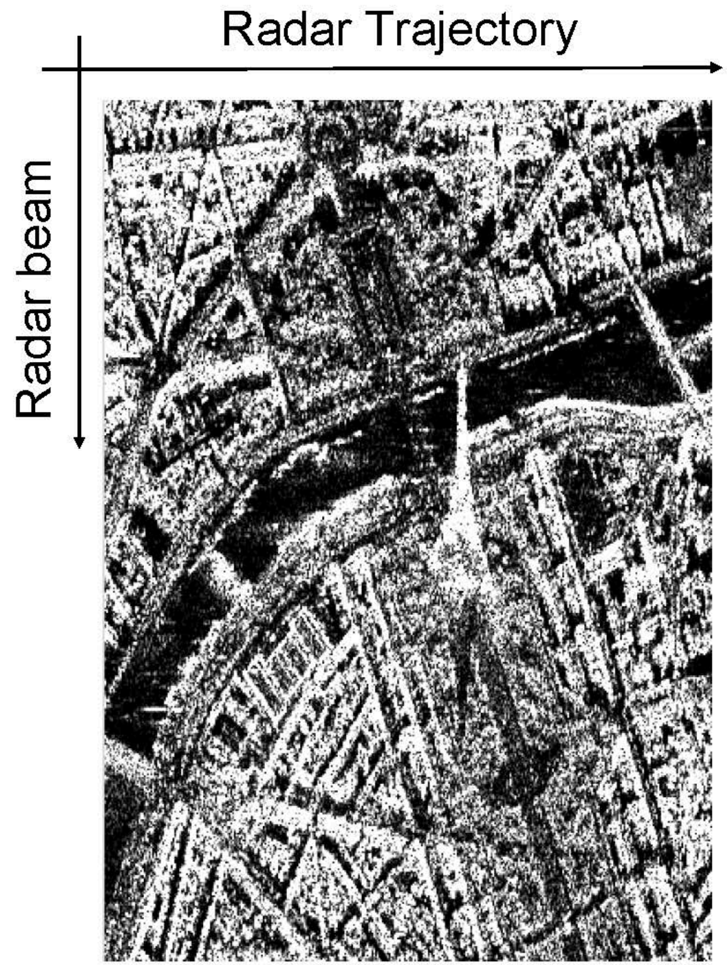

Difficulty: There are some « holes » in the signal.

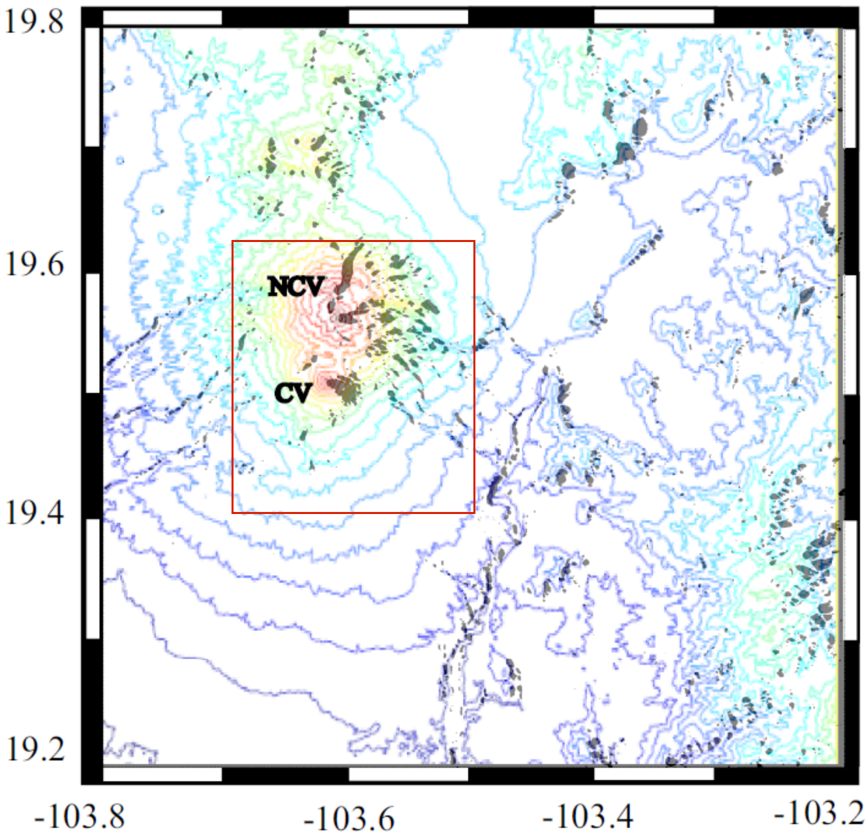

Descending (3.6 % of image)
7%

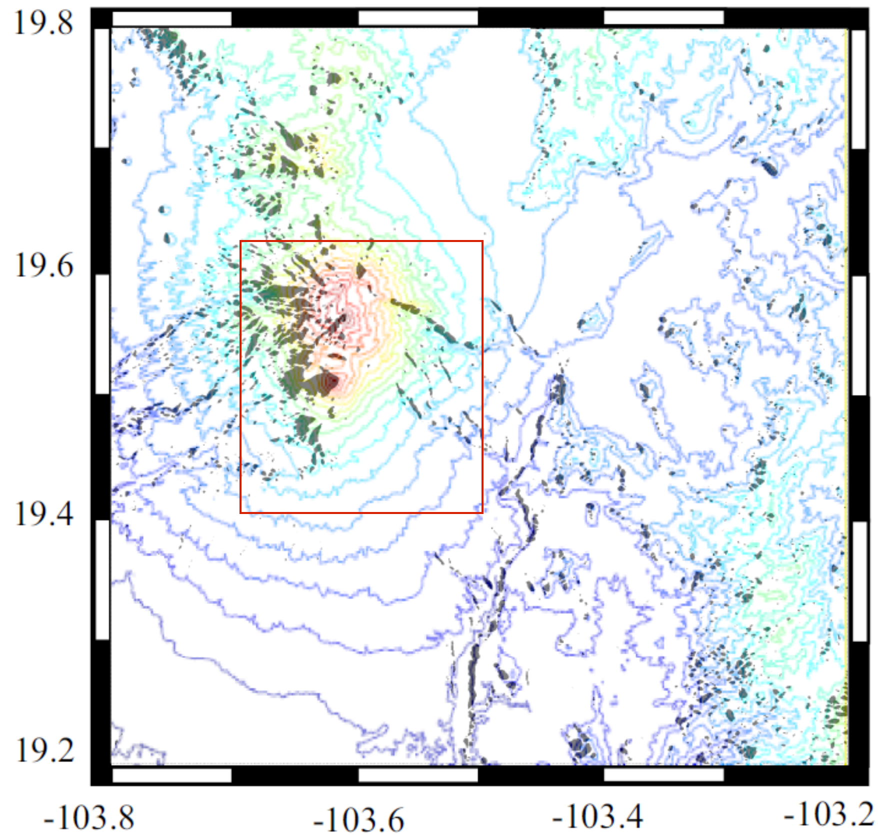

Ascending (4.9 % of image)
12%

InSAR: Interferometry between 2 images

2 dates of acquisitions → Master image (M)
→ Slave image (S)

- Temporal baseline(ΔT) : time difference between 2 images

-Spatial baseline (B$\perp$) : distance between the 2 satellites position

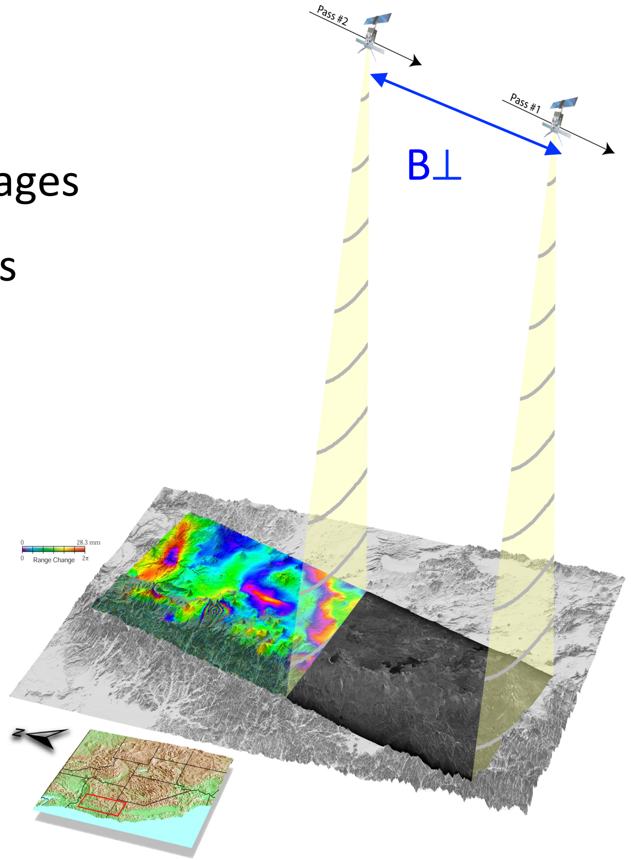

InSAR provides maps of surface displacement in Line of Sight

Exemple ENVISAT images on Colima volcano

2 acquisitions radar: $\rightarrow$ Master Image (M)

$\searrow$ Slave Image (S)

Couple of images characterized by: $B\perp$, ΔT

$$Int = y_M y_S^* = |y_M||y_S| exp(j(\phi_M - \phi_S))$$

$$\Phi_M - \Phi_S = \Delta\Phi = \Delta\Phi_{spatial}(B_{perp}, z) + \Delta\Phi_{atmo} + (4\pi/\lambda)\,\boxed{d} + \Delta\Phi_{noise}$$

1 fringe corresponds to a displacement of $\lambda/2$ in the Line of Sight
Precision around 1 cm

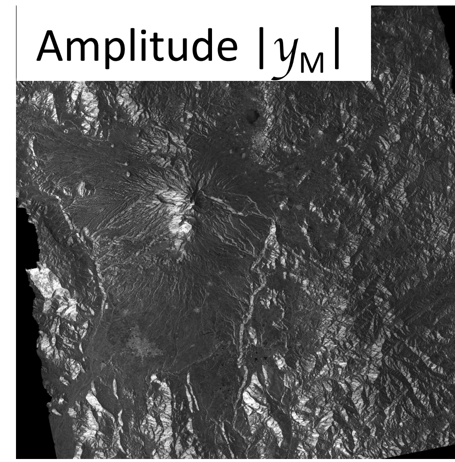

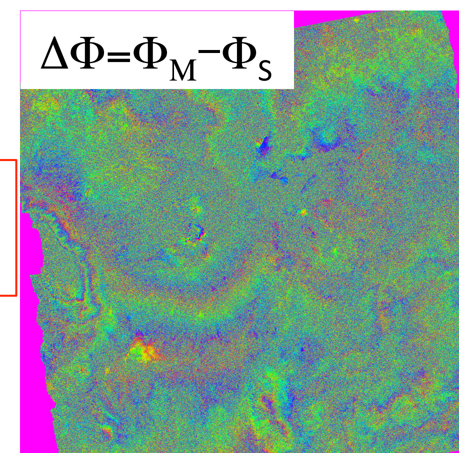

Displacement in Line of Sight

Example of unit vector for a descending track:

[0,442; -0,117; 0,889]

East North Up

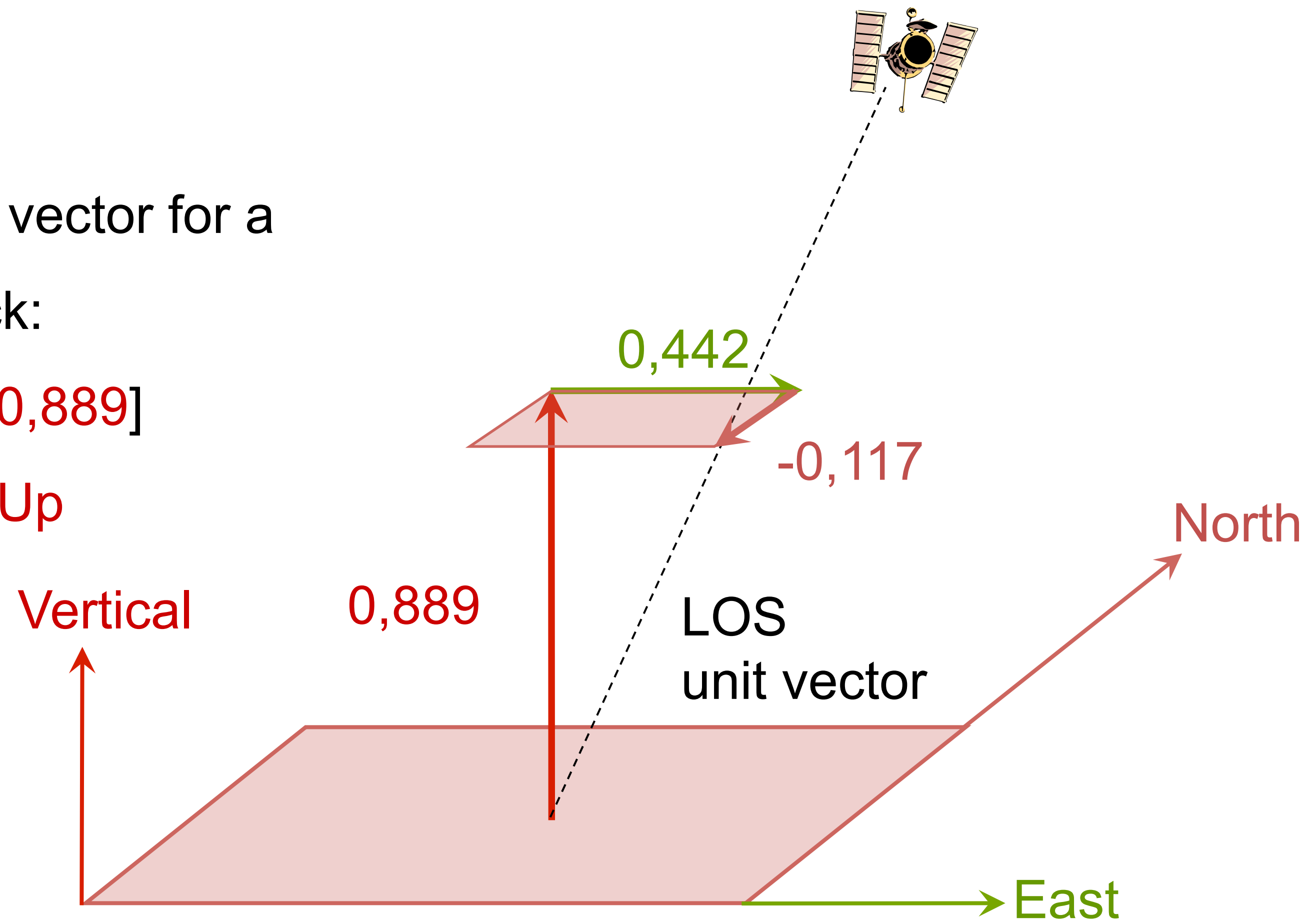

Enable to measure vertical and E-W displacements.

Ambiguity of phase information

$\Delta\Phi$ is known with an ambiguity of 2π

Phase unwraping is required to obtained displacement with regards to a reference point

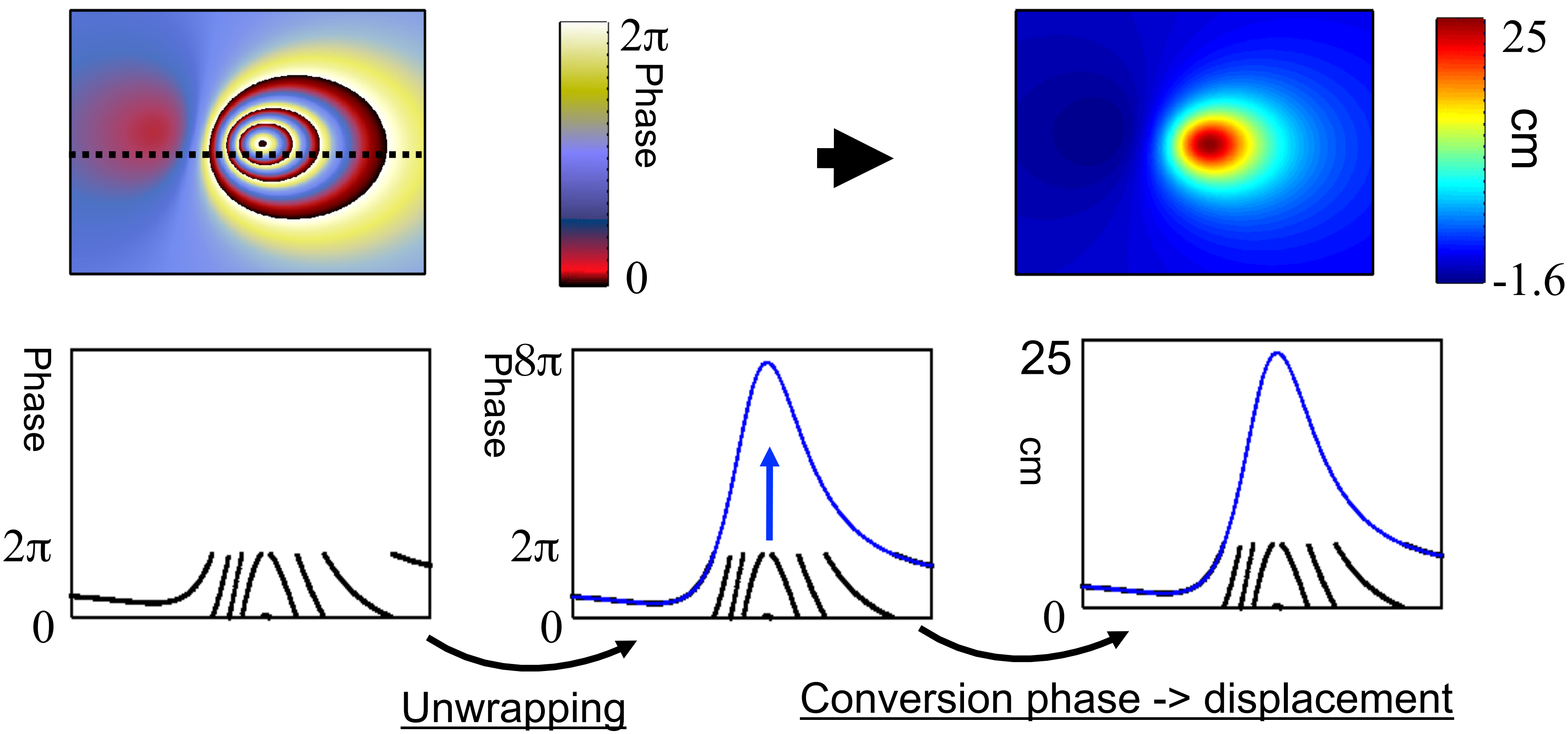

Coherence

$$coherence = \gamma = \frac{\left|\sum M_i . E_i^*\right|}{\sqrt{\sum \left|M_i\right|^2 . \sum \left|E_i\right|^2}} \quad ; \quad 0 \leq \gamma \leq 1$$

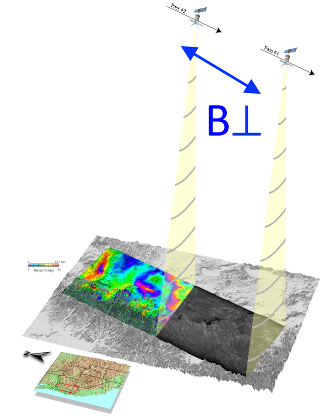

Spatial Resolution : 40 m * 40 m

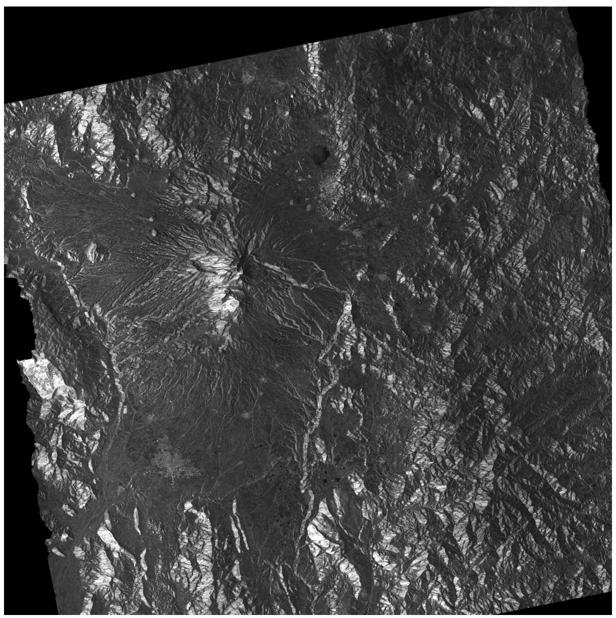

Mean Amplitude

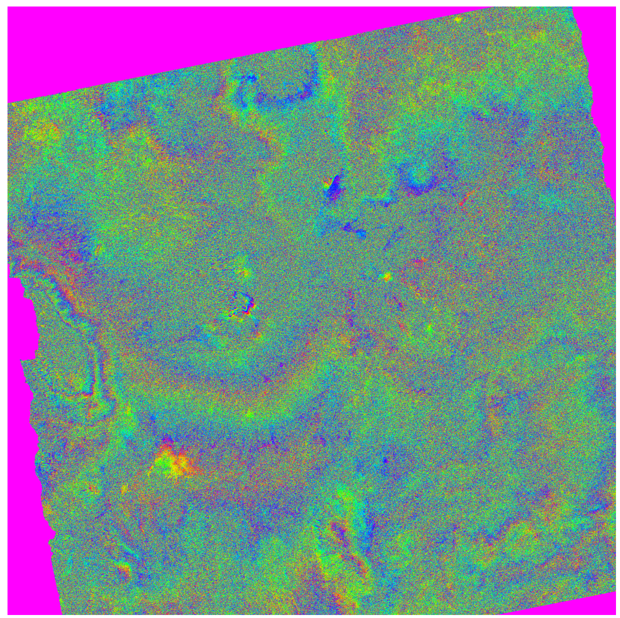

Phase difference $\Delta\phi$

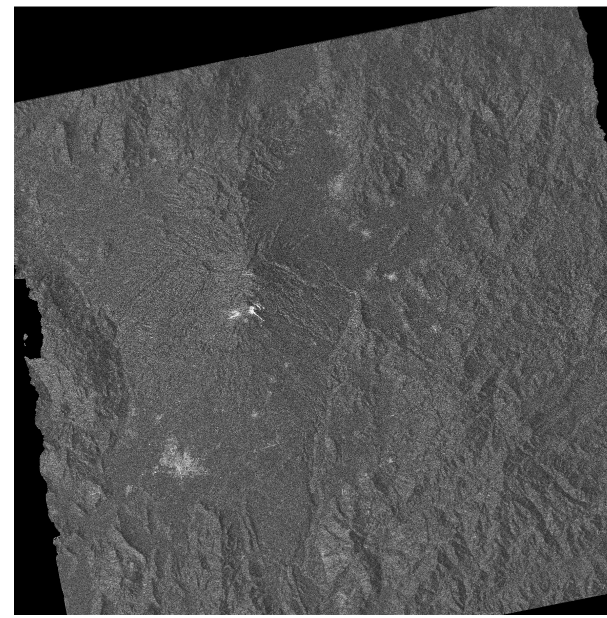

Coherence

Coherence

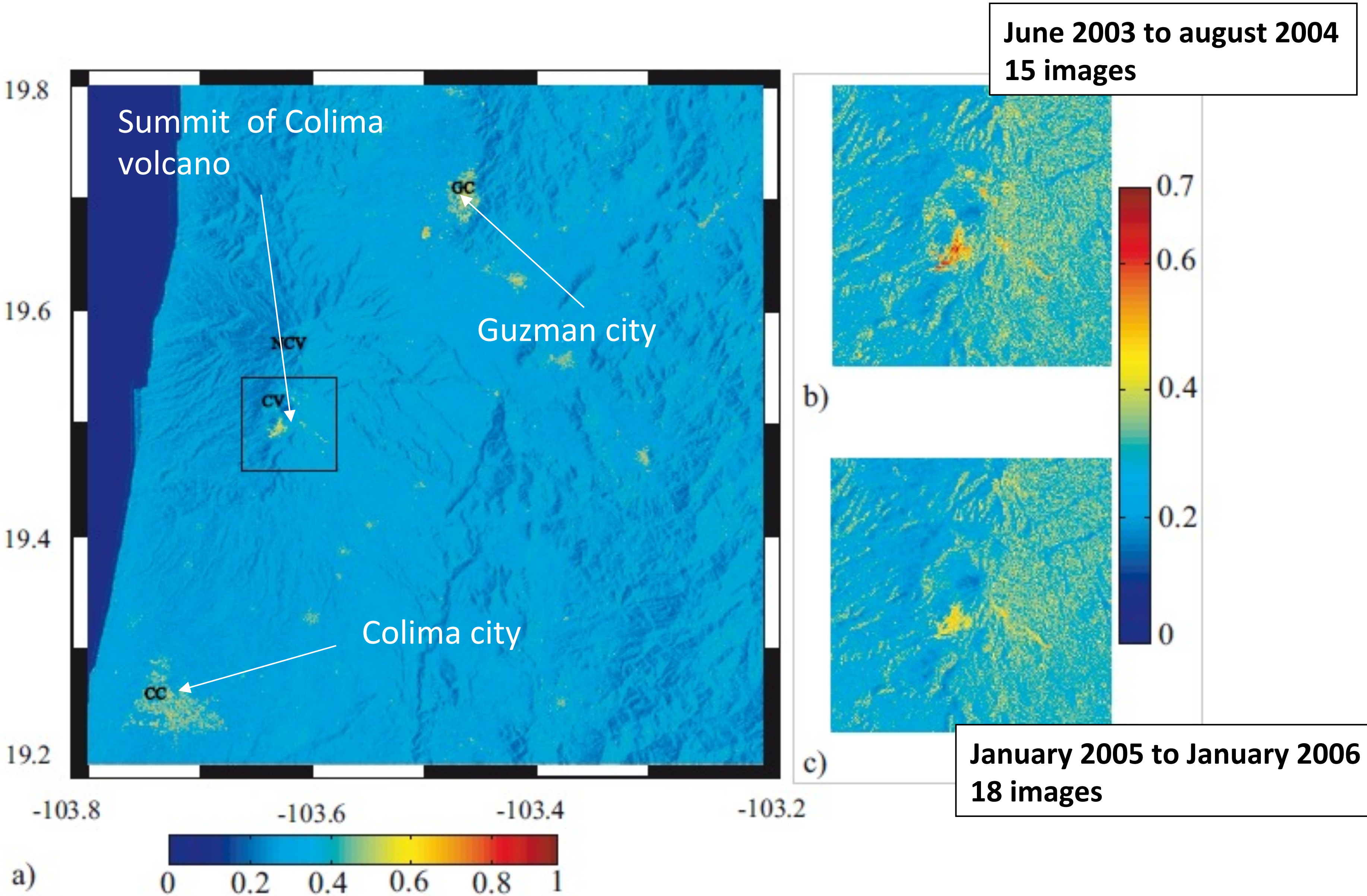
June 2003 to august 2004
15 images
Summit of Colima volcano
Guzman city
Colima city
GC
NCV
CV
CC
19.8
19.6
19.4
19.2
-103.8
-103.6
-103.4
-103.2
a)
0
0.2
0.4
0.6
0.8
1
b)
c)
0.7
0.6
0.4
0.2
0
January 2005 to January 2006
18 images

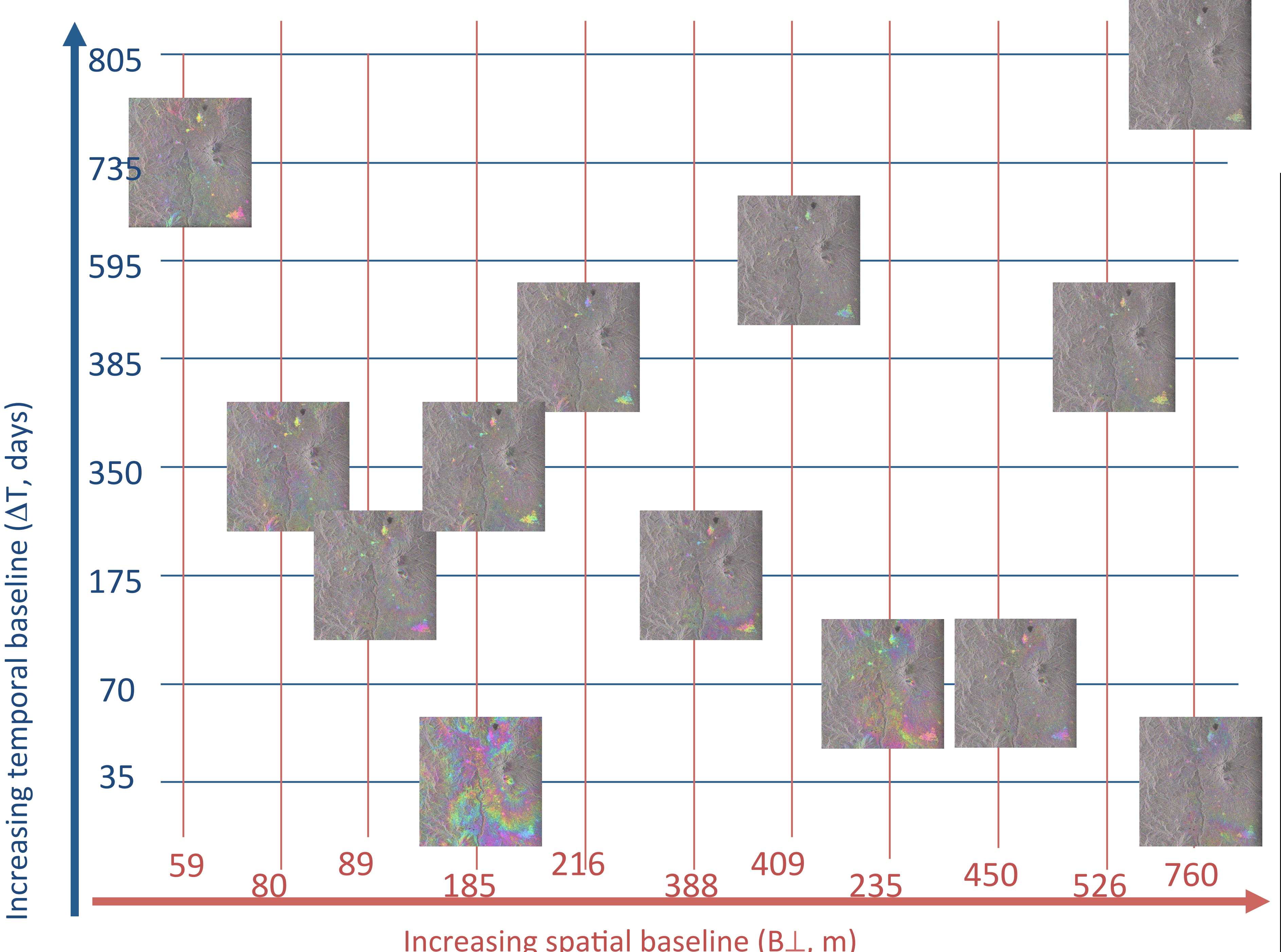

Increasing temporal baseline (ΔT, days)
805
735
595
385
350
175
70
35
59
80
89
185
216
388
409
235
450
526
760
Increasing spatial baseline (B⊥, m)

Coherence is better with L-band over vegetated areas

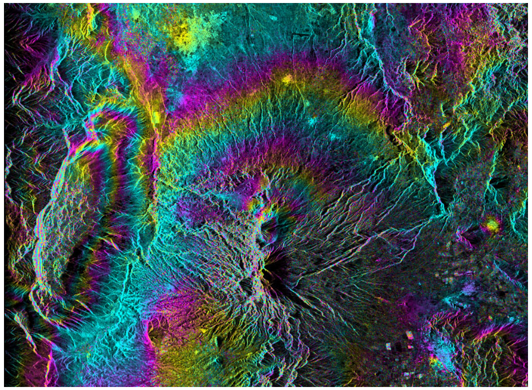

ENVISAT: ΔT=385 jours
B⊥=5m

C-band

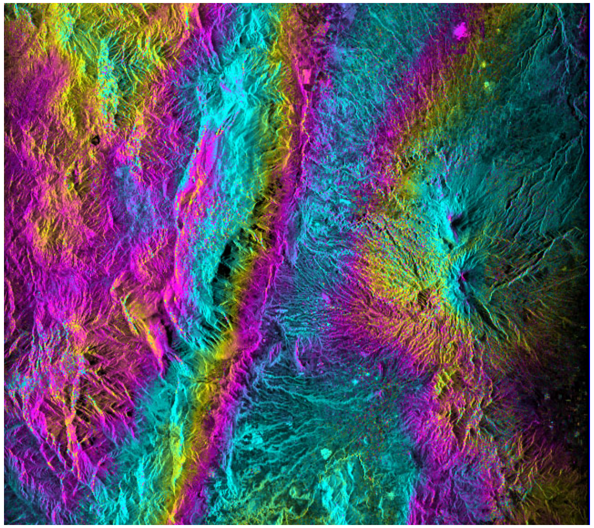

ALOS: ΔT=873 jours
B⊥=177m

L-band

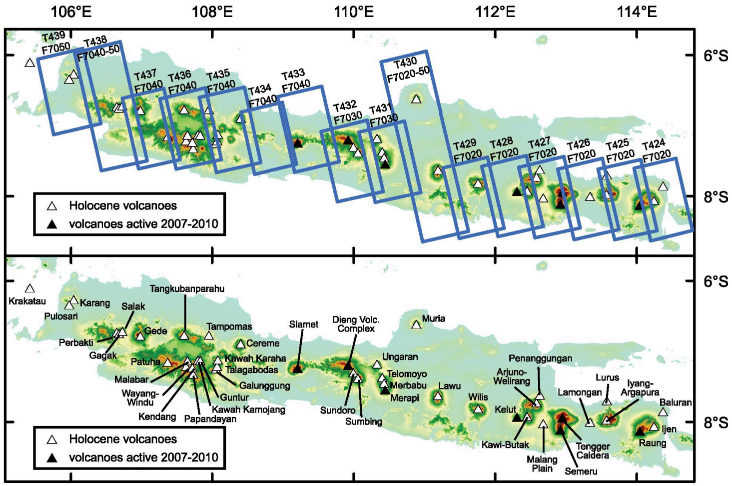

Coherence with L-band over Java

From Philibosian & Simons , 2011

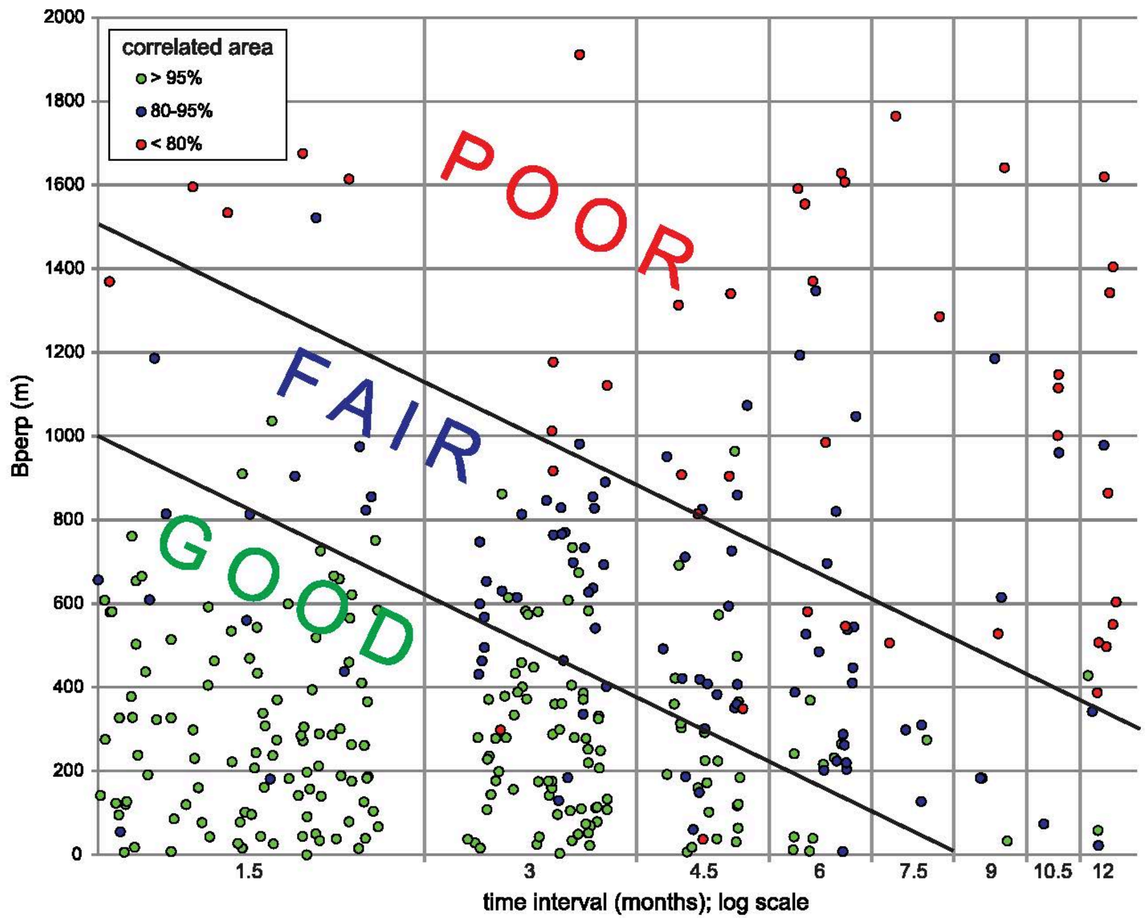

Processing chains
Conventional InSAR

- DIAPASON developed by CNES (Massonnet)
- ROI_PAC (Jet Propulsion Lab. & Caltech) http://www.roipac.org/
with mdx to visualize
- NEST (Next ESA SAR Toolbox) http://nest.array.ca/web/nest

- Also some useful tools written in C can be found here:
http://www.efidir.fr/

Processing chain (ROIPAC example).

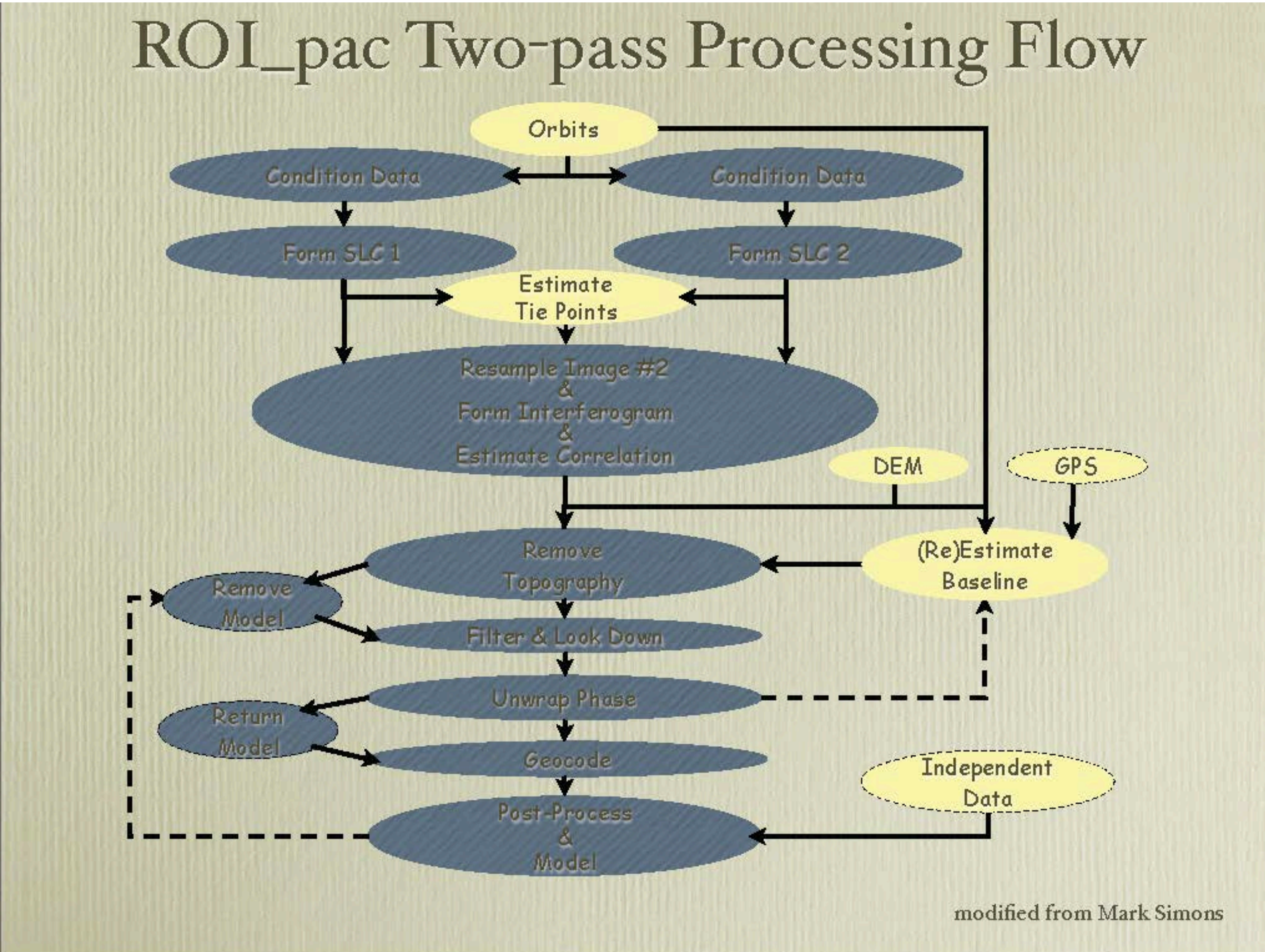

Processing chain (ROIPAC example).

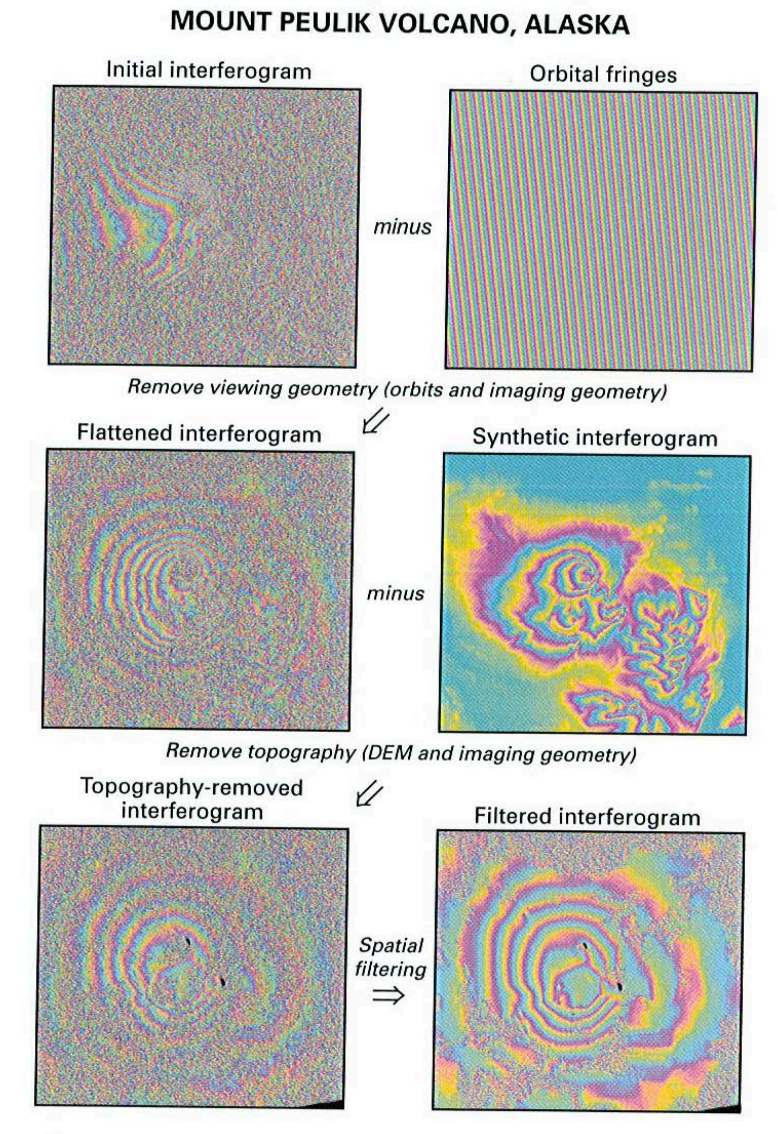

From Dzurizin, 2007

Processing chain (ROIPAC example).

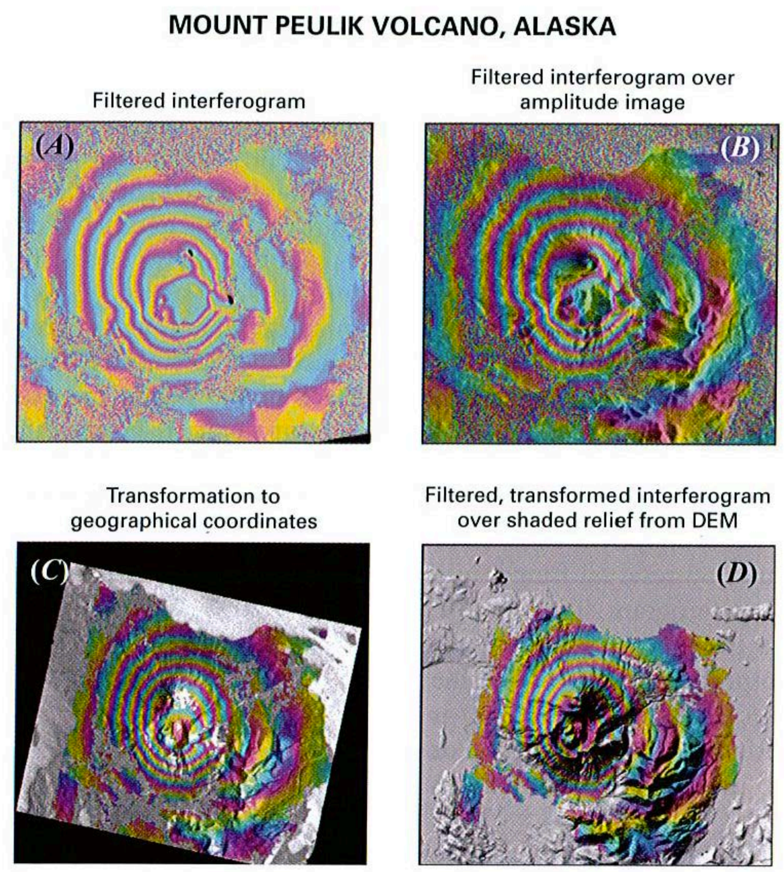

From Dzurizin, 2007

An example of interferogram

Piton de la Fournaise, Reunion Island
Eruption on the 23rd of August 2003

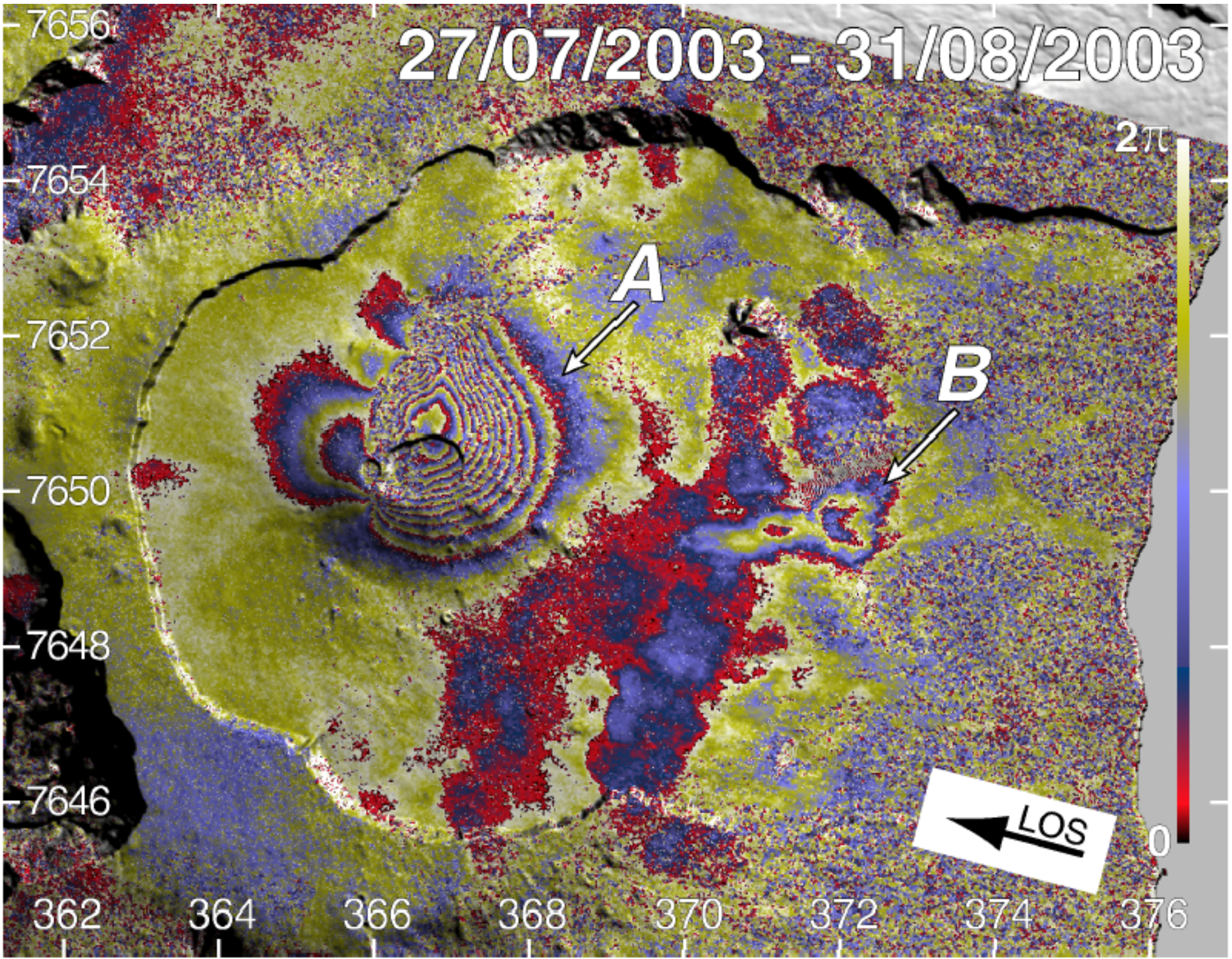

From Froger et al, 2004

Signal is not always so obvious

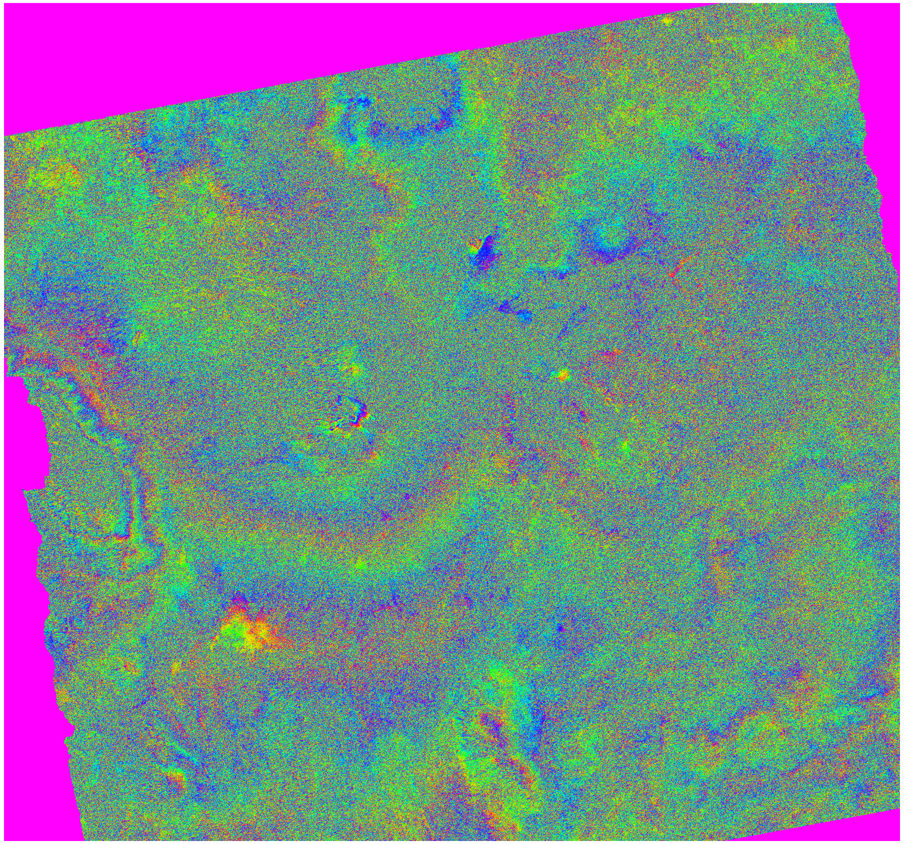

Atmospheric, orbit and DEM errors

Errors can become larger than the signal for low strain and short time intervals

SAR Time series analysis: a way to improve signal/noise

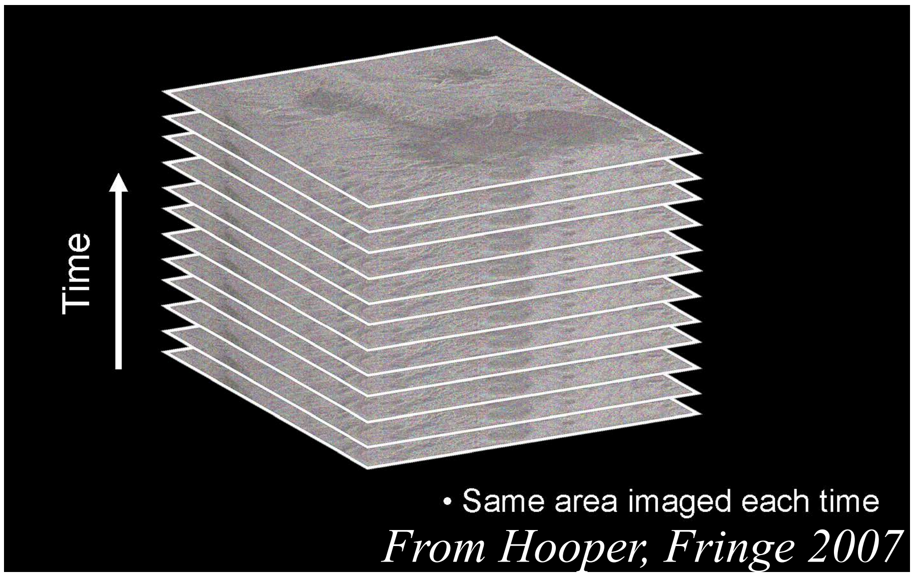

Allow picking of coherent pixels.
DEM estimation error is possible
Other errors are reduced by filtering in time.

Any InSAR method using multiple images of the same area acquired at different time.

Two families of Time series studies

(see Hooper et al, Tectonophysics, 2012)

*<u>Persistent Scatterer methods</u>

optimized for pixels dominated by a single scatterer

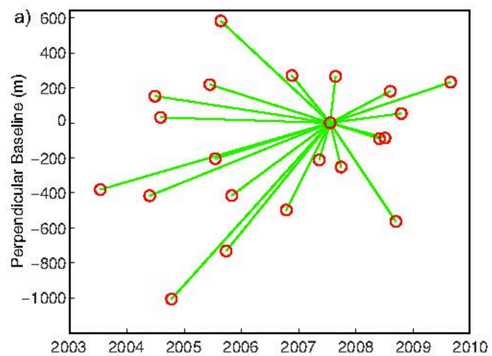

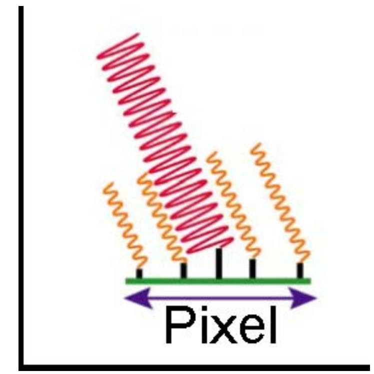

*<u>Small Baseline methods</u>:

optimized for pixels with a Gaussian distribution of scatterers

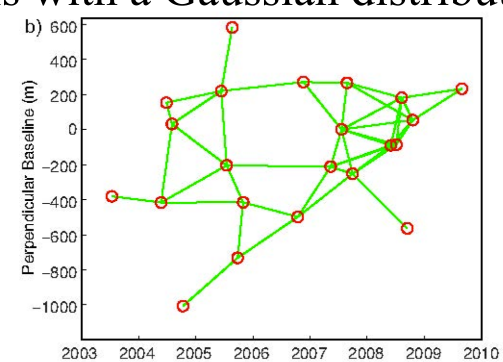

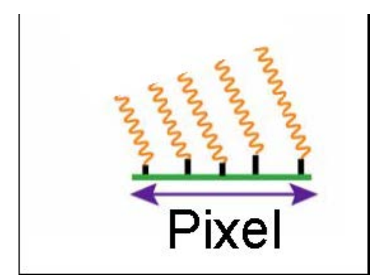

Processing chains
SAR time series

- StaMPS Andy Hooper

http://radar.tudelft.nl/~ahooper/stamps/index.html

- NSBAS Marie-Pierre Doin and EFIDIR team

http://www.efidir.fr/

Example of Small Baseline Approach

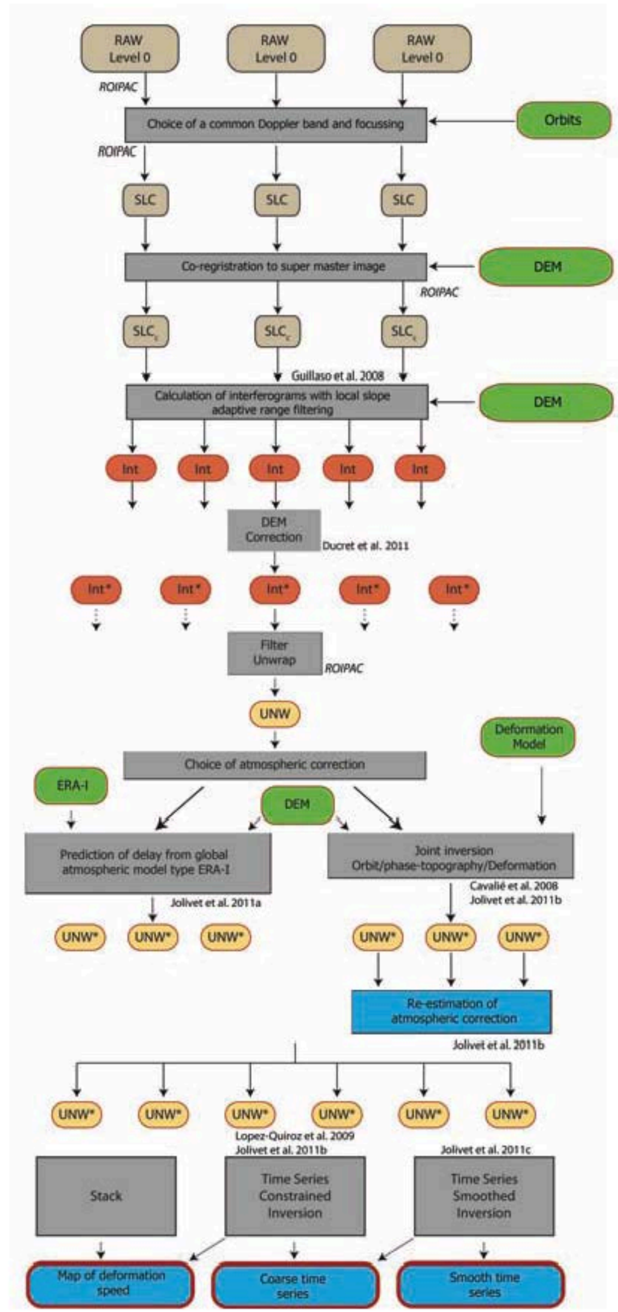

From Doin et al, 2011

Main improvements due to InSAR

Detection of deformation in remoted areas/ Regional studies

Detection of deep storage zones.

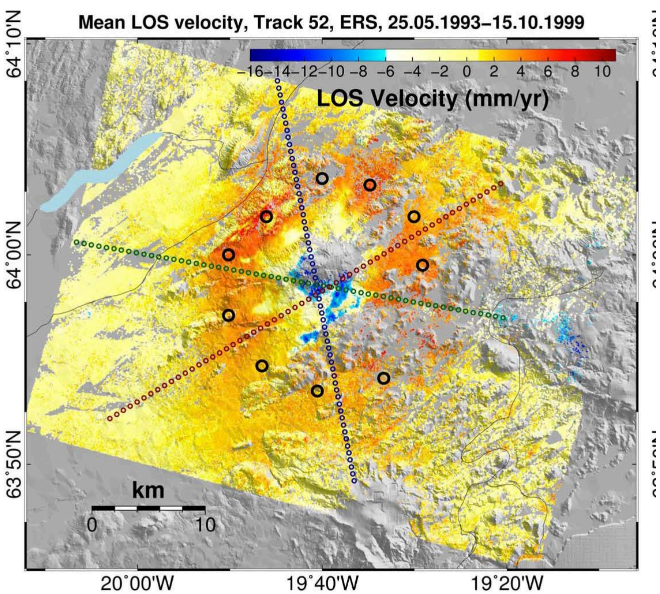

Ofeigsson, et al. 2011

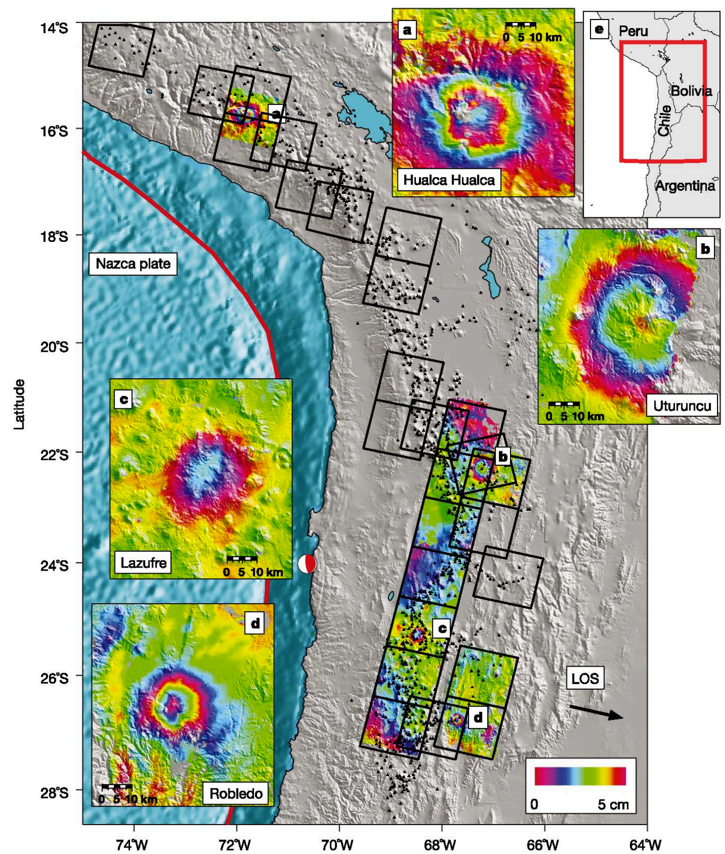

Better imagery of deformation sources

Pritchard & Simons, 2002

Main InSAR limitations

*Poor temporal resolution (35 days reduced sometimes to 1 day)

*Atmospheric artefacts:

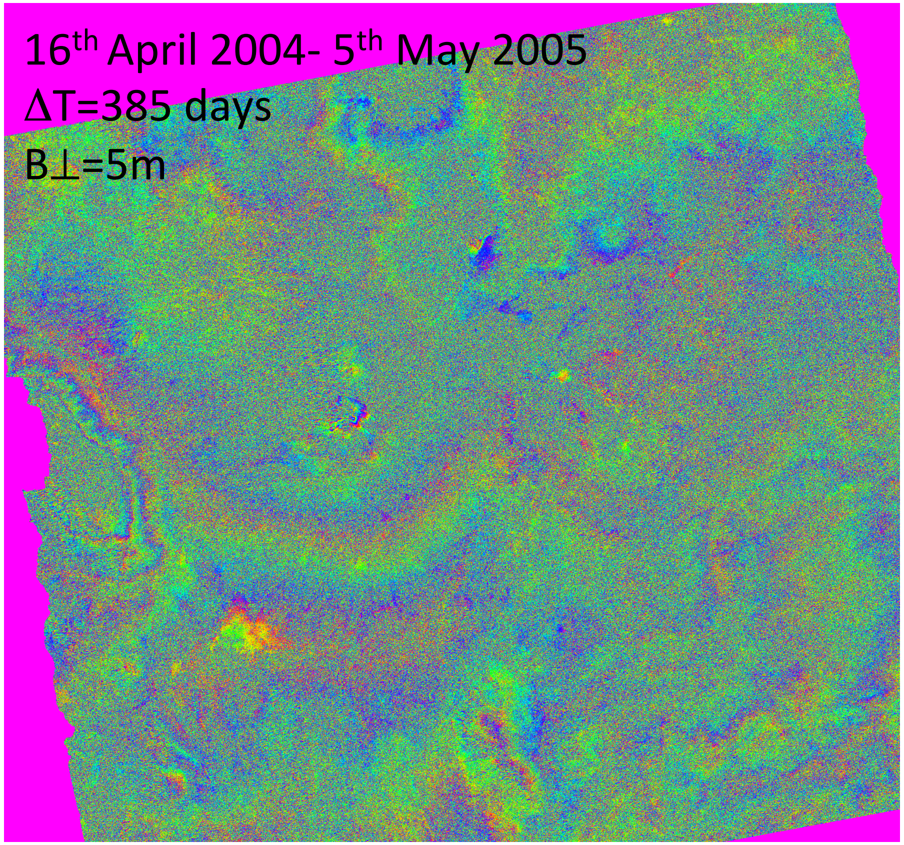

DEM-SRTM

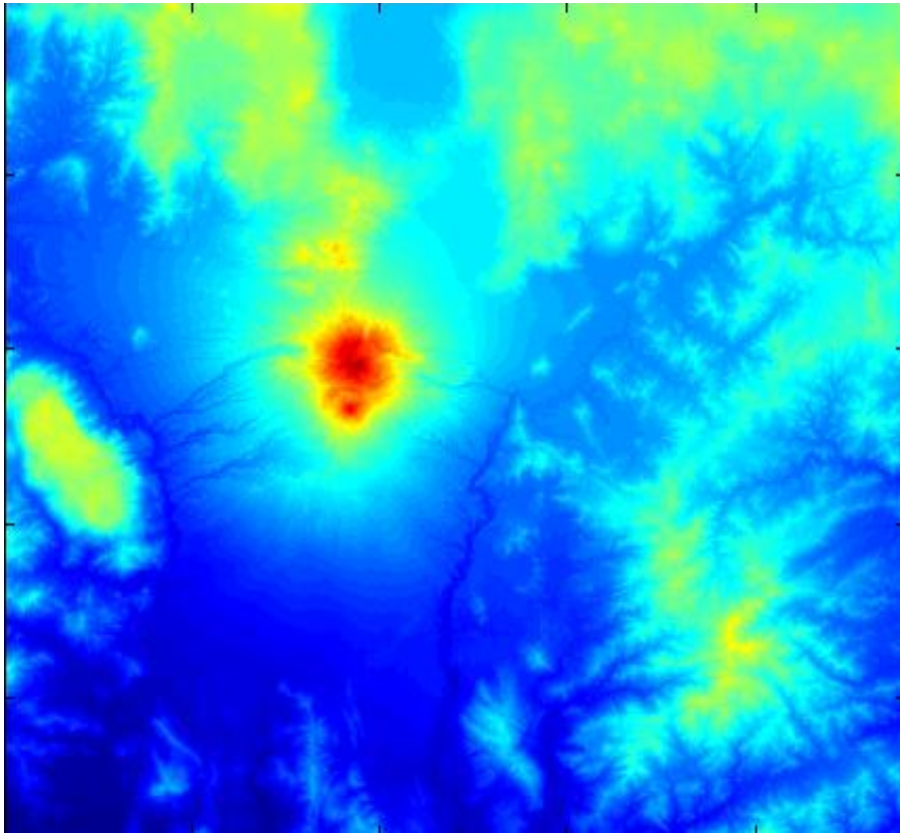

Under sea measurements

Pressure at the seafloor is measure and converted to depth:

- **bottom pressure recorders (BPRs)**

Continuous record, useful to measure sudden deformation event.

- **mobile pressure recorder (MPR)** connected to a remotely operated vehicle (ROV).

Several survey with MPRs deployment onto an array of seafloor benchmarks to make campaign-style pressure measurements, allows to quantify long term deformation.

<u>Application: seamounts deformation quantification, also used to quantify tsunamis</u>

Under sea measurements

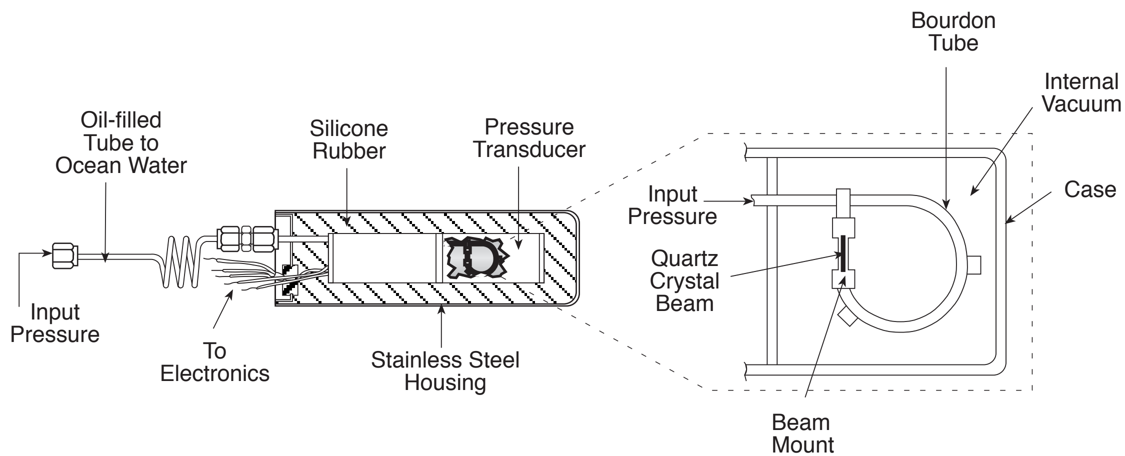

Sketch of a bottom pressure recorder

Summary

Instrument	Information	Spatial sampling	Temporal sampling	Available since…	Precision
EDM	Distance variations	Punctual	Days to years	A few 100 years	mm
Theodolite	Angle variations	Punctual	Months to years	A few 100 years	mgr
Extensometers	Fault opening	Punctual	A few seconds	Around 30 years	10µm
Volumetric strainmeter	Volume variation	Punctual	A few seconds		
Tiltmeter	Tilt variations	Punctual	A few seconds	Around 100 years (around 40 years for continuous)	nrad
GPS	3D displacement	Punctual	A few seconds	20 years	mm for horizontal cm for vertical
SAR SAR time series	1D displacement	Maps (100 km^2)	Around 10 days	Since 1995 20 years	cm mm

Summary

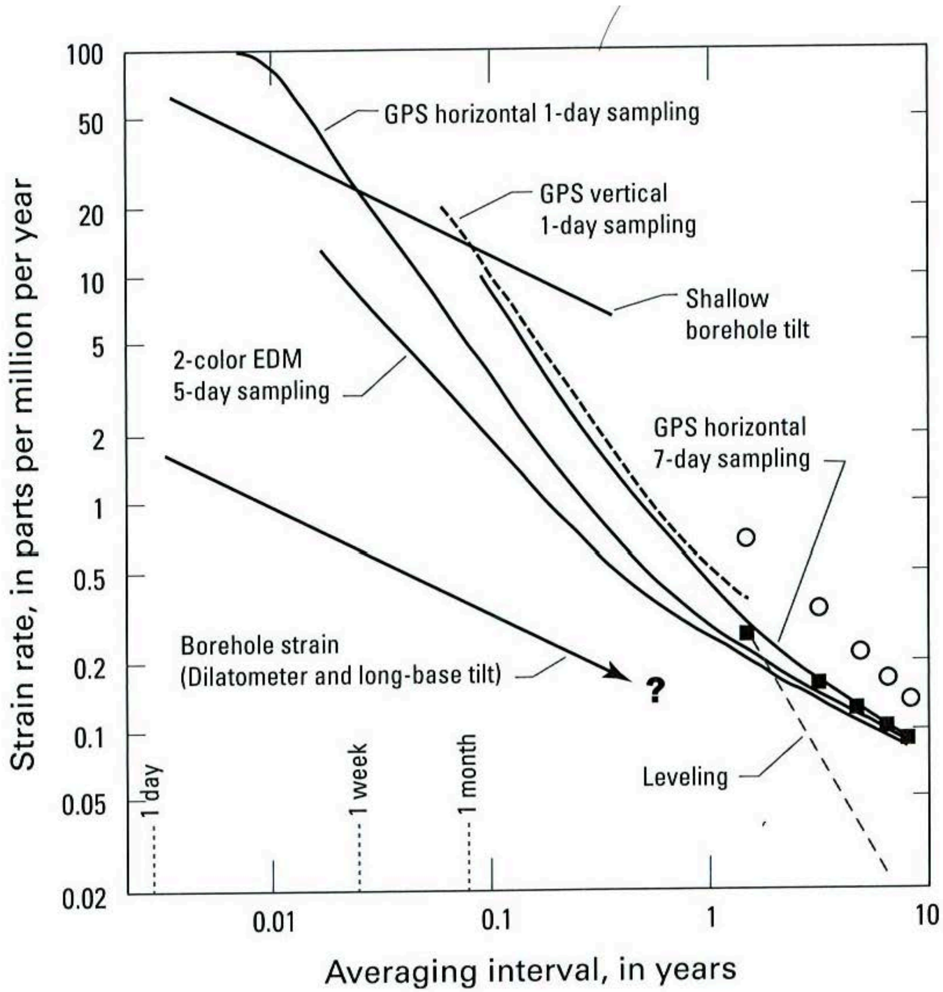

From Dzurizin, 2007

Various types of measurements

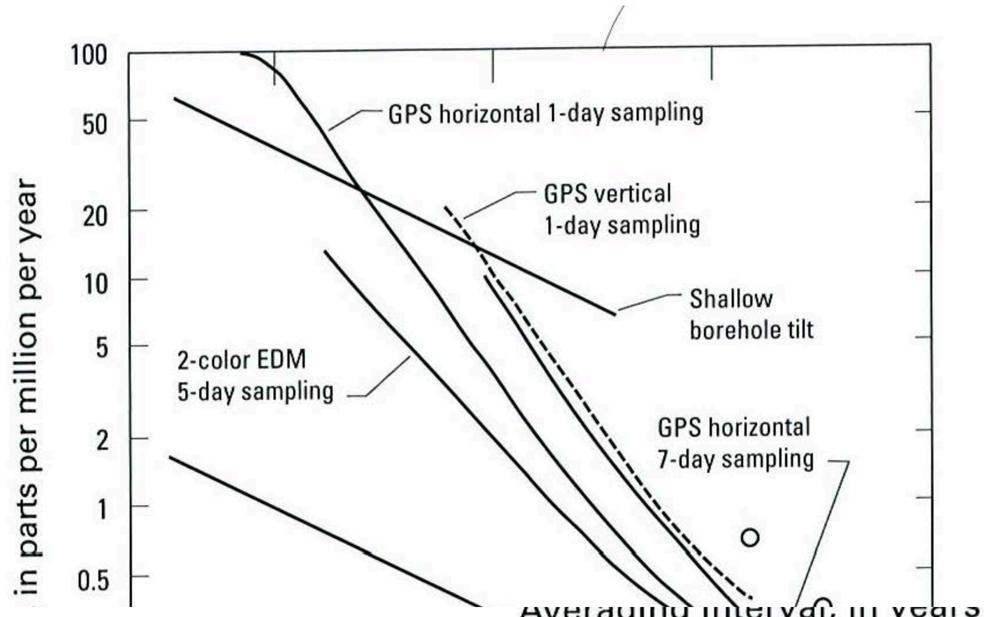

Figure 1.23. Strain rate detection threshold for various deformation-monitoring techniques as a function of the interval over which repeated measurements are averaged (J. Langbein, USGS, written commun., 1998). An 8-km baseline was assumed for GPS and EDM. Open circles and solid squares represent annual GPS measurements and annual two-color EDM measurements, respectively. Most geodetic measurements are subject to both random-walk noise (e.g., monument drift) and white noise (e.g., atmospheric effects, instrument noise). Using a high sampling rate and averaging a large number of samples can sometimes mitigate the effect of white noise; in such cases, random-walk noise becomes a limiting factor. Borehole strainmeters and long-base tiltmeters provide the most accurate information over timescales of minutes to days, while repeated leveling or GPS surveys are best over periods of months to years.

Averaging interval, in years

Complementary measurements are useful

because the type of signal, which can be recorded and quantified, strongly depends on the instrument and on the network geometry

Various causes of deformation at volcanoes

Ex: temporal evolution of surface displacement recorded at Grimsvötn

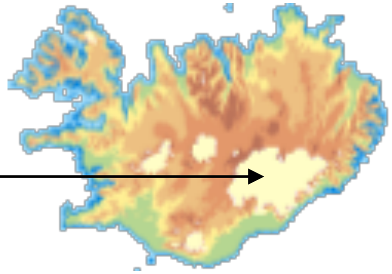

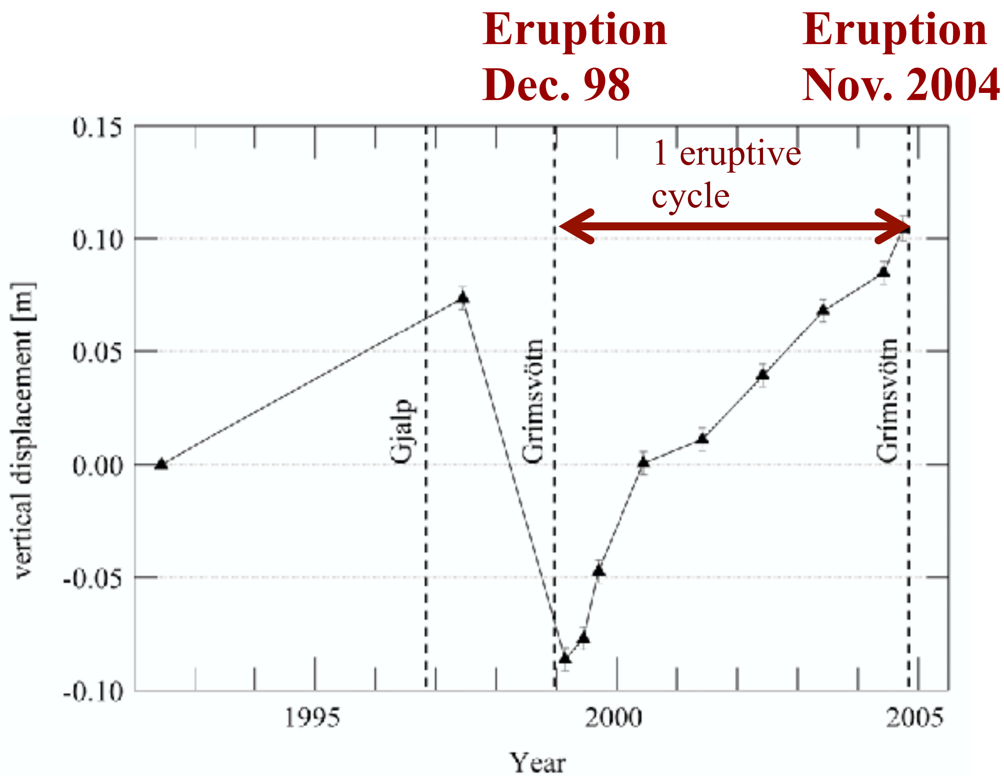

(from Sturkell et al., JVGR, 2006)

GPS campaigns

Ex: temporal evolution of surface displacement recorded at Grimsvötn

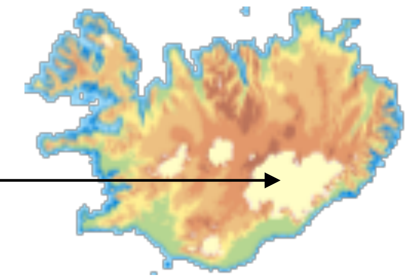

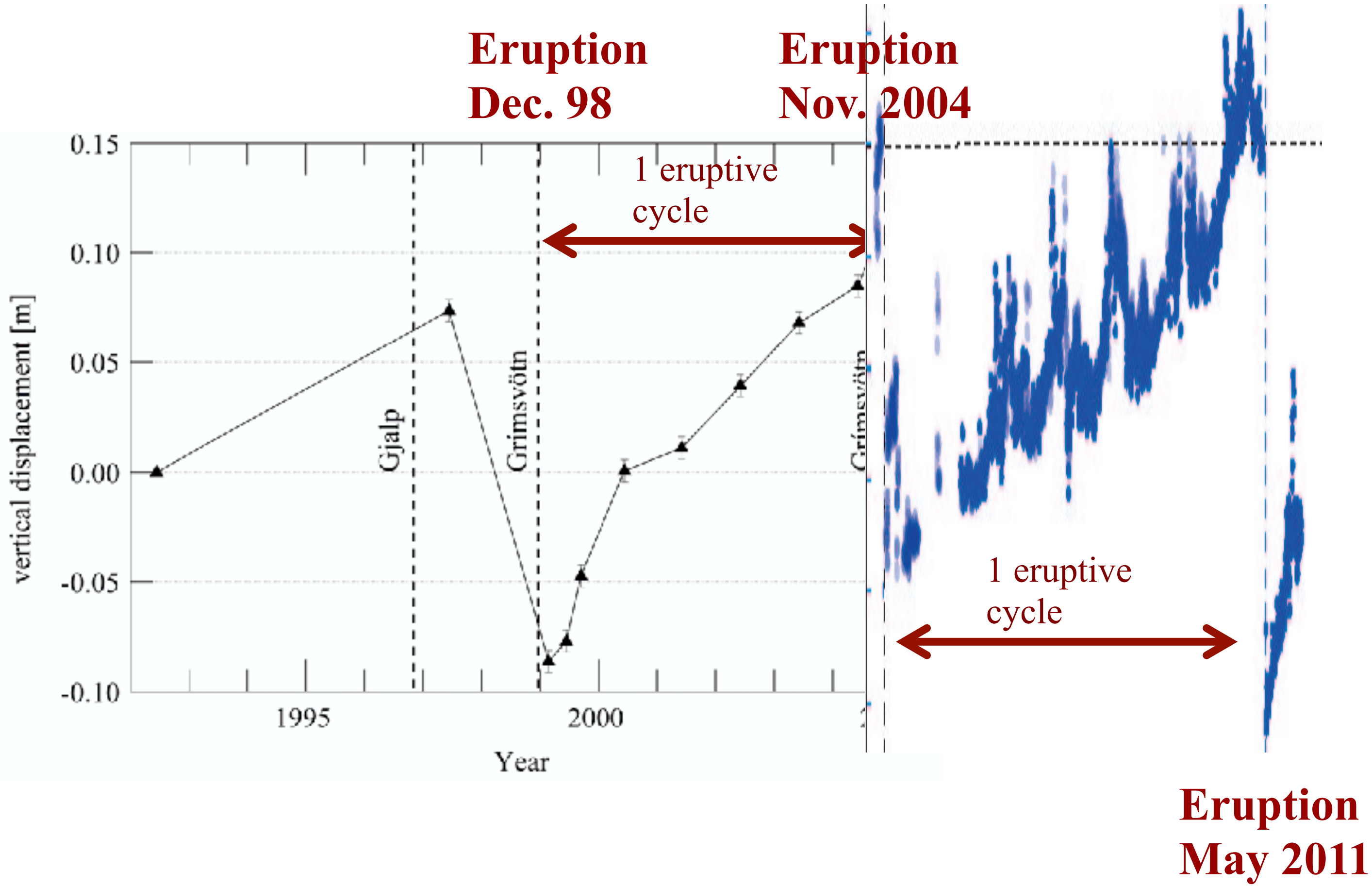

GPS campaigns + CGPS

Interpretation: magma storage at shallow depth

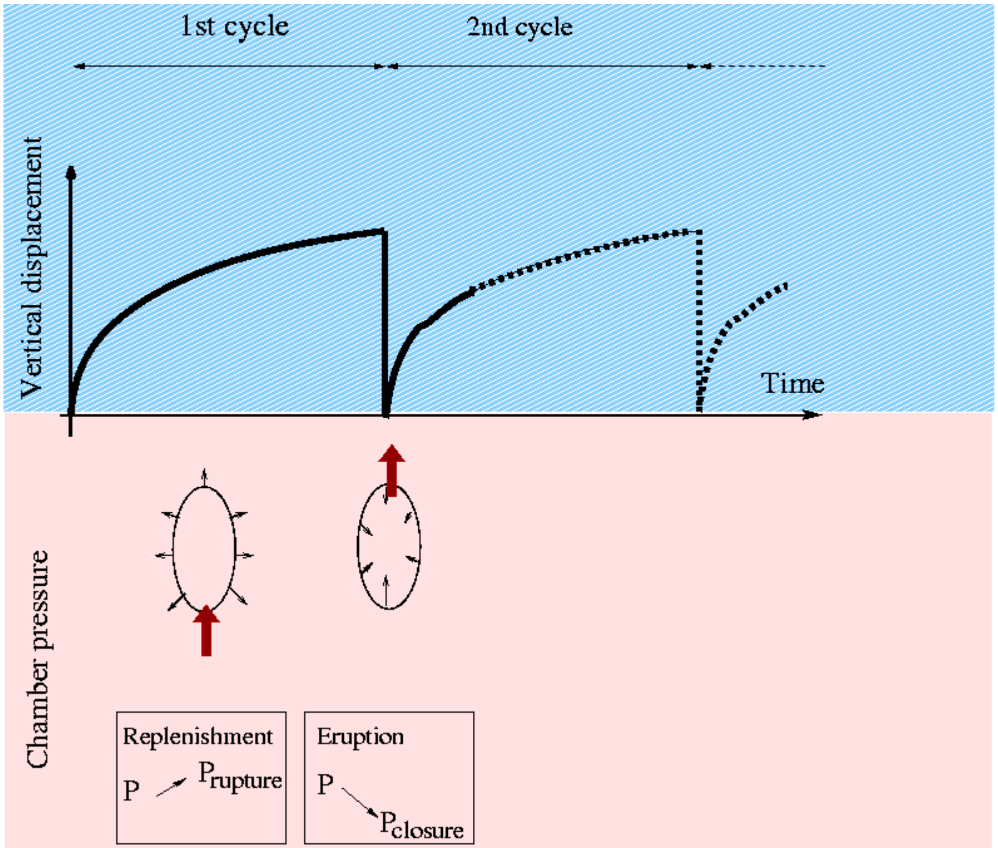

Inflation by magma accumulation in a storage zone during inter-eruptive periods.
Deflation by magma withdrawal during eruptions.

Magmatic intrusion during an eruptive event

Piton de la Fournaise, Reunion Island
Eruption on the 23rd of August 2003

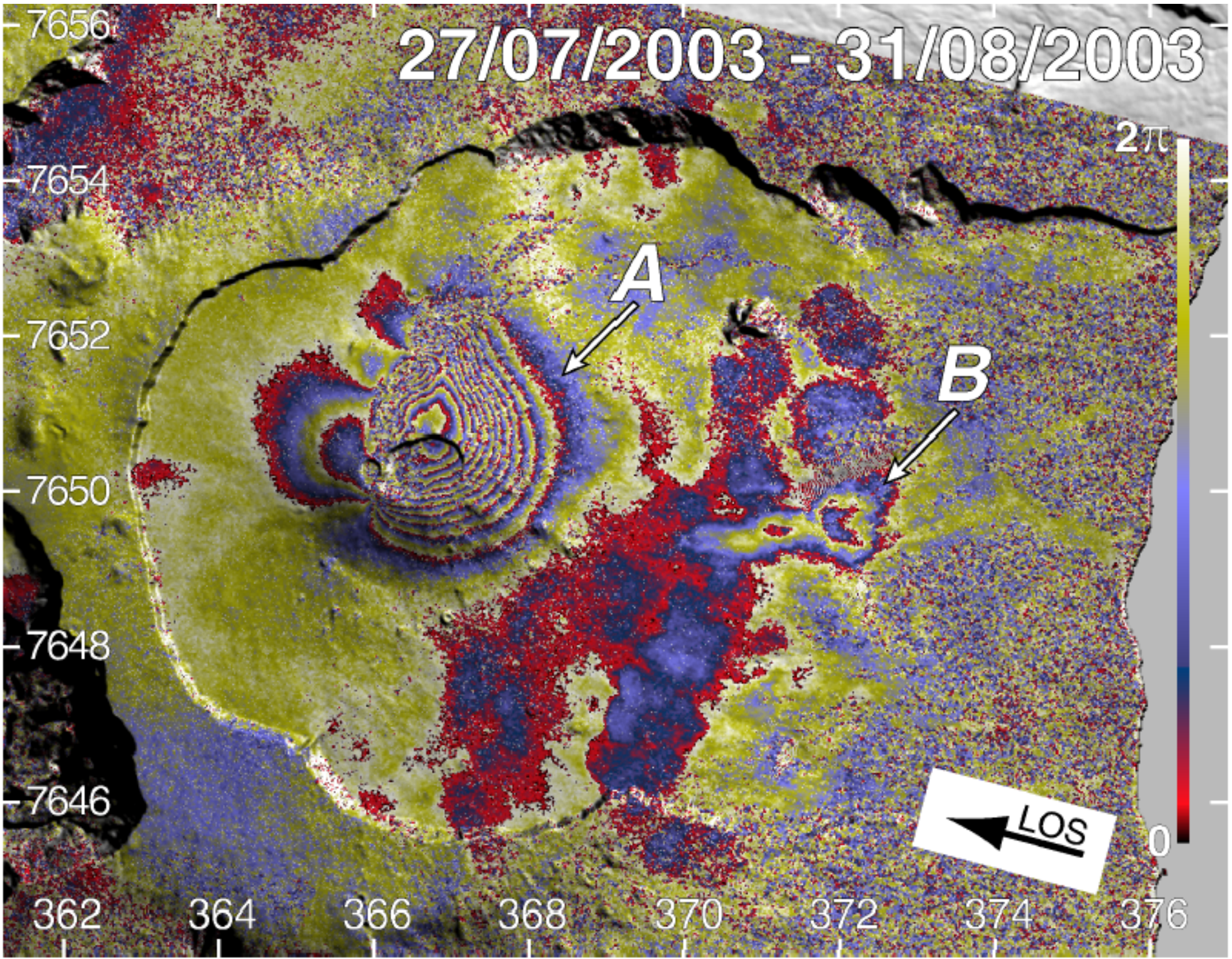

From Froger et al, 2004

Magma flow within a conduit

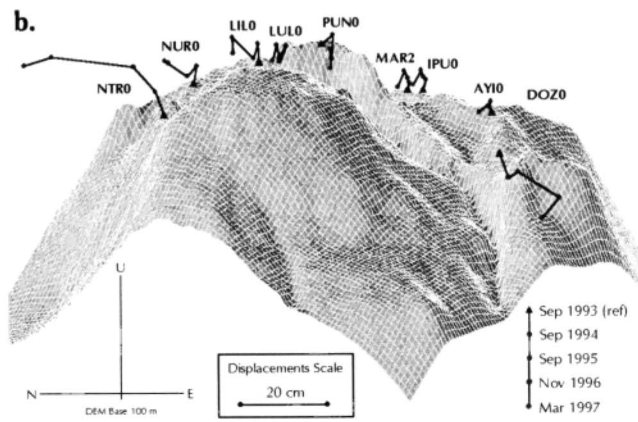

Cumulative displacements at GPS benchmarks
from 1993 to 1997 in a vertical plan (azimuth N145°E).
Merapi volcano summit area.

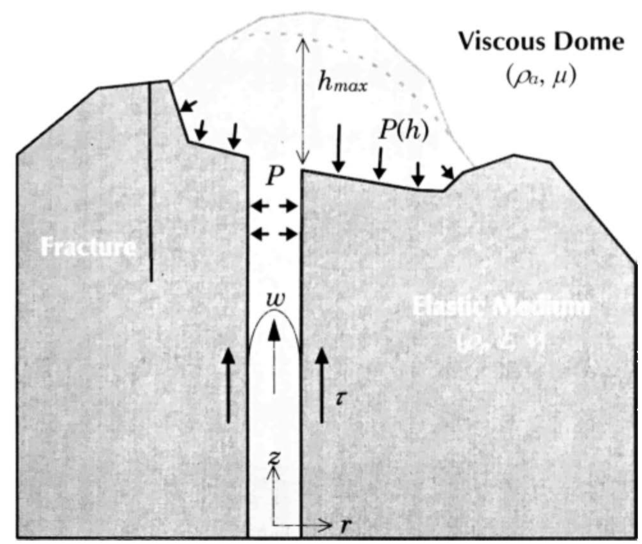

From Beauducel et al, 2000

Uplift around Katla volcano, Iceland

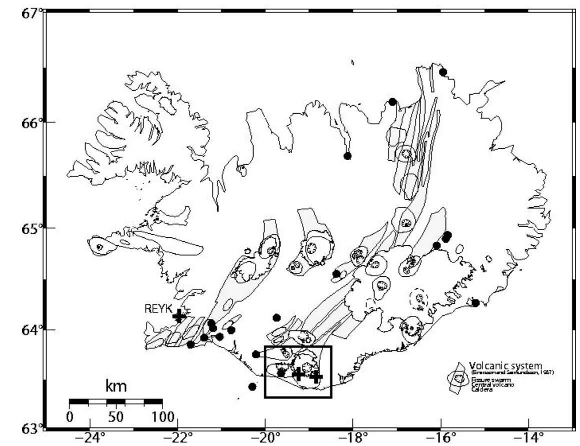

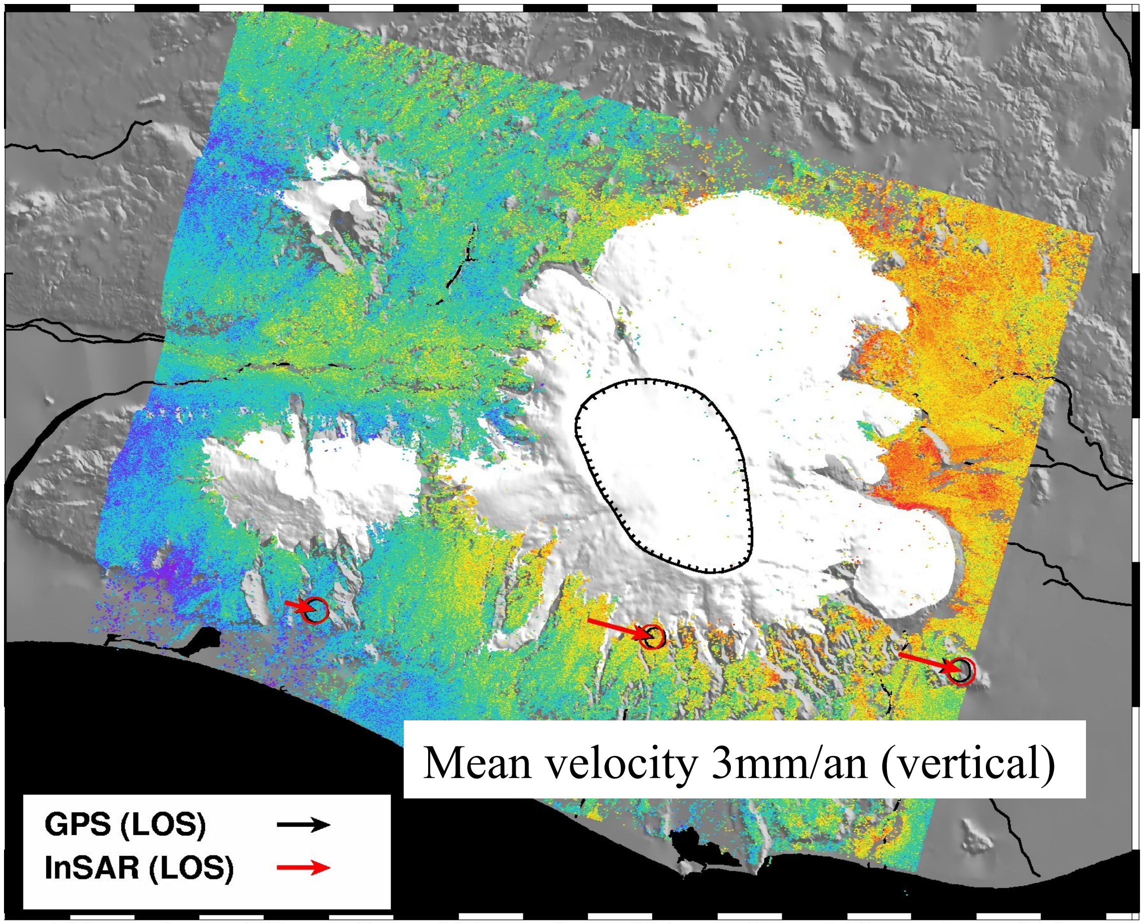

Uplift around Katla volcano, Iceland

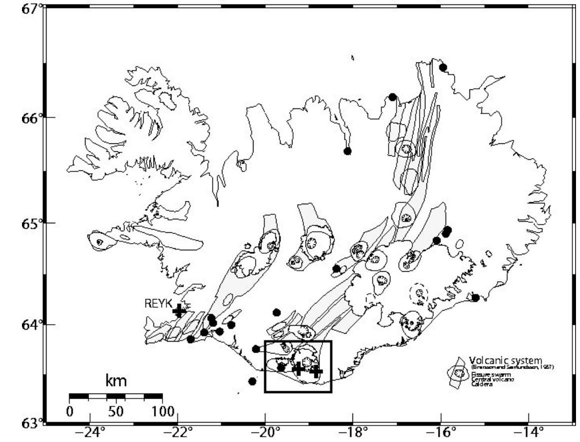

- Uplift measured by GPS

(Sturkell et al, 2008)

June 2001-June 2004

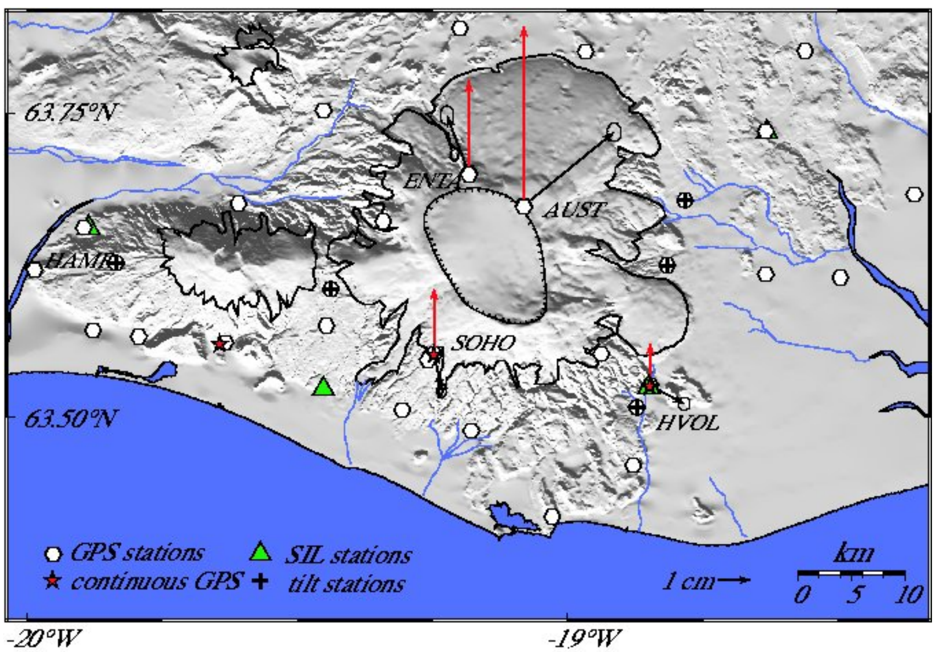

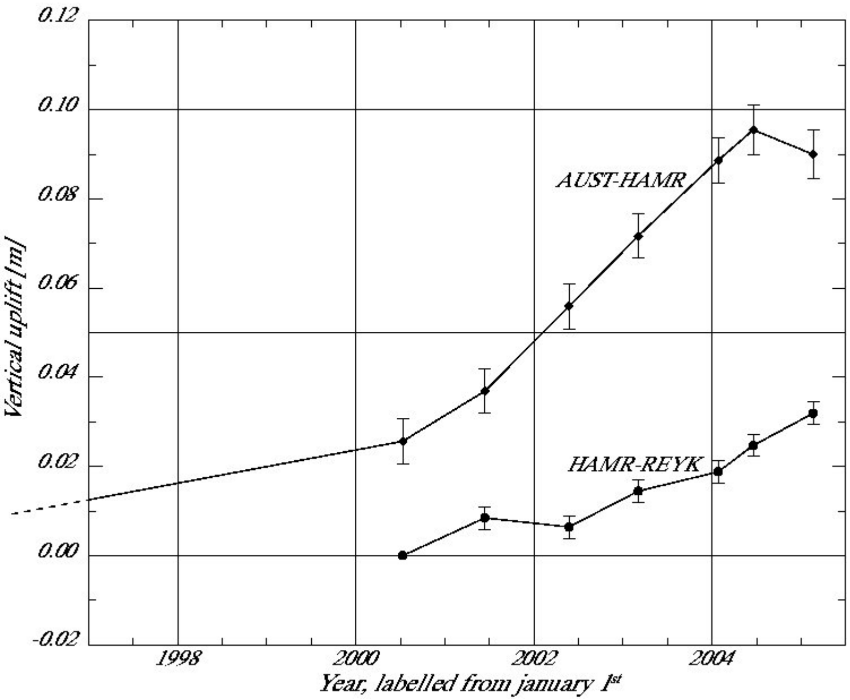

Uplift around Katla volcano, Iceland

2 possible sources :

- an input of magma beneath Katla volcano

- the unloading effect induced by the retreat of the glacier

A peripheric long term decrease:

Ablation of ice ($\rho = 900$ kg/m^3) mainly occurs from May to September.

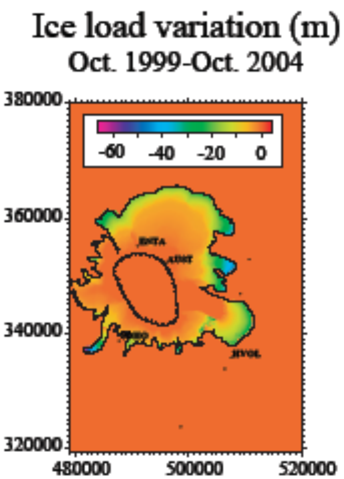

Fig.3

Subsidence induced by the load of eruptive deposits.

*Colima volcano (Mexico): a summit subsidence (more than 2 cm/an) mostly localized on lava flows.

Descending track 384

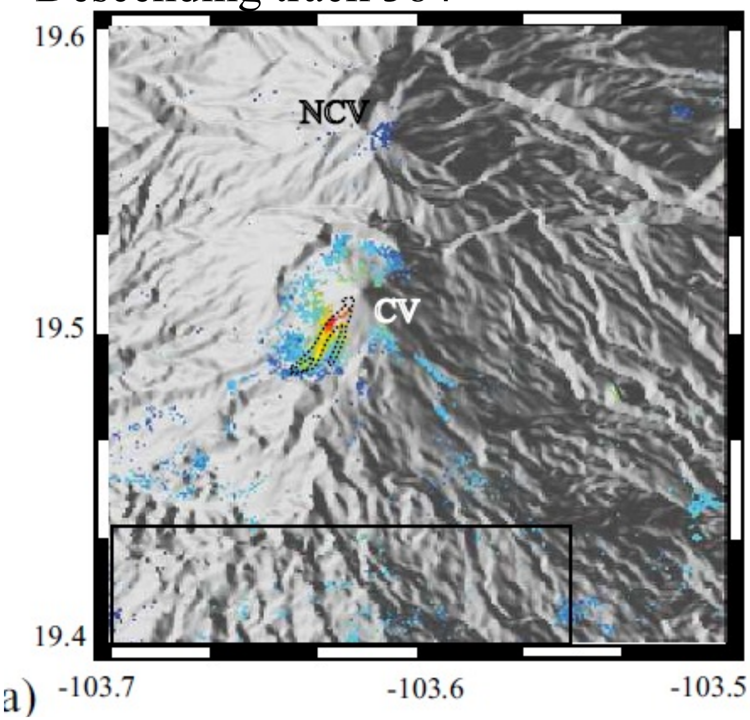

Mean velocity LOS (mm/y)

(Navarro-Ochoa et al., JVGR, 2002)

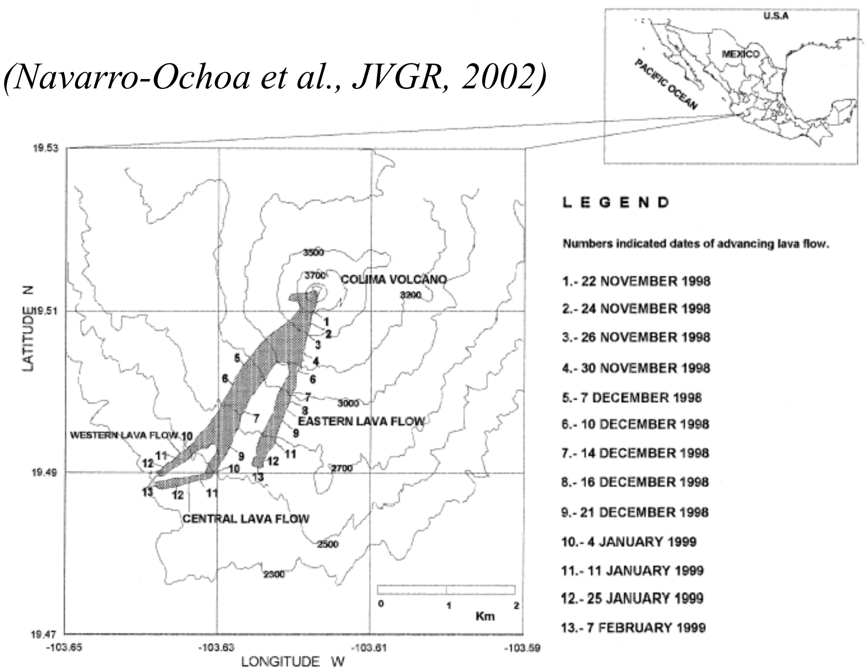

From Pinel et al, 2011

Subsidence induced by the load of eruptive deposits.

Volcano	Lava composition	Age (yr)	Max. flow thickness (m)	Max. subsidence rate (cm/yr)	References
Krafla (1975–1984)	Basaltic	17–20	50	0.6	Sigmundsson et al. (1997)
Tolbachik (1975–1976)	Basaltic	16–28	80	~ 2	Pritchard and Simons (2004) and Fedotov et al. (1980)
Okmok (1945–1958)	Basaltic	35–38	20–30	~ 1.5	Lu et al. (2005b)
Okmok (1997)	Basaltic	0.1	50	83	Lu et al. (2005b)
Okmok (1997)	Basaltic	3	50	4	Lu et al. (2005b)
Colima (1998–1999)	Andesitic	3–8	30 (flow fronts)	1.5	Pinel et al. (2011), Navarro-Ochoa et al. (2002) and Zobin (2002)
Santiaguito (2004–2005)	Dacitic	4–6	120	6	This work
Paricutin (1943–1953)	Basaltic–andesite	54–65	> 70	4–4.5	Fournier et al. (2010)
Reventador (2005)	Andesitic	3–4	–	1–2	Mothes et al. (2008)
Sierra Negra (1979)	Basaltic	13–19	–	3	Amelung and Day (2002)
Lonquimay (1988–1989)	Andesitic	13–21	55	2	Fournier et al. (2010); Naranjo et al. (1992)
Nyamuragira (1991–1993)	Basaltic	6–11	–	1–4	Colclough (2006)
Nyamuragira (1991–1993)	Basaltic	13–18	–	0.9	G. Wadge, personal communication, 2012
Nyamuragira (2004)	Basaltic	2–5	–	1	G. Wadge, personal communication, 2012
Etna (1983)	Basaltic	10–14	55	0.8	Stevens et al. (1999)
Etna (1989)	Basaltic	3–4	10	3.5	Briole et al. (1997)
Etna (1991–1993)	Basaltic	1–2	96	25.6	Briole et al. (1997)

From Ebmeier et al, 2012

Volcanic edifice instabilities
Large flank displacements

Etna, Italy, active

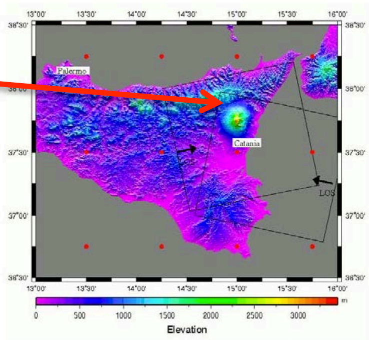

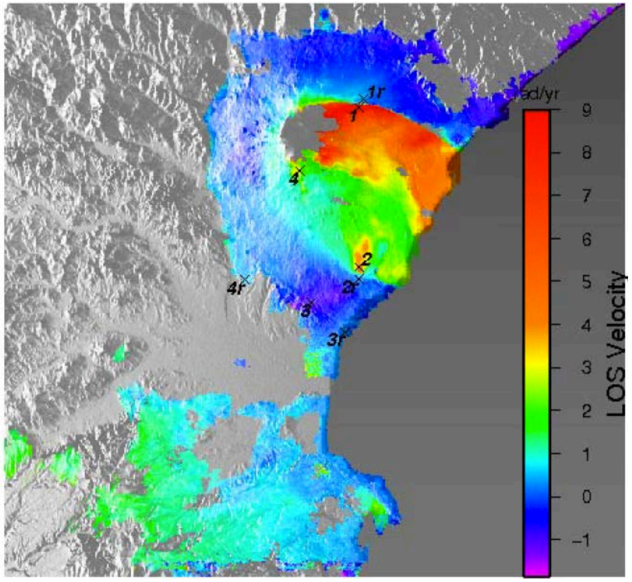

From Doin et al, 2011

Damavand, Iran, inactive

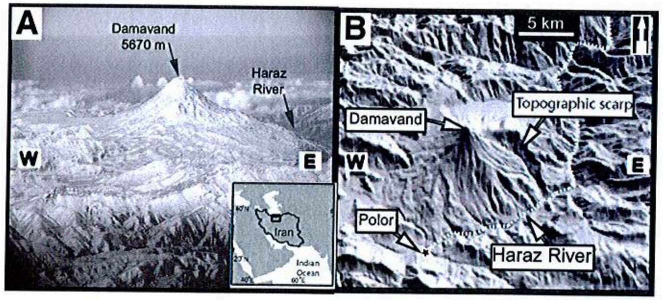

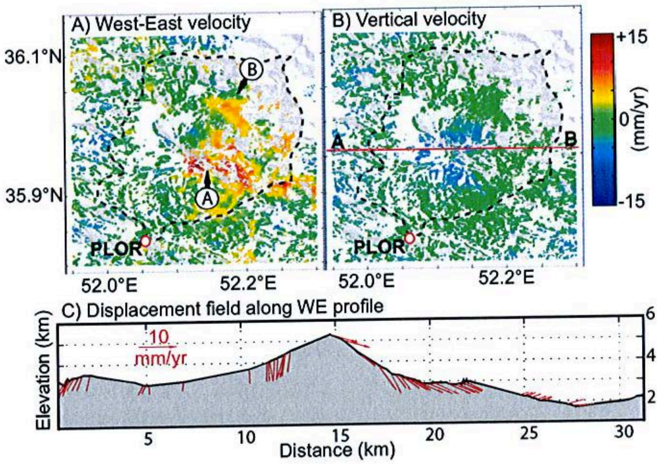

From Shirzaei et al, 2011

Hydrothermal systems

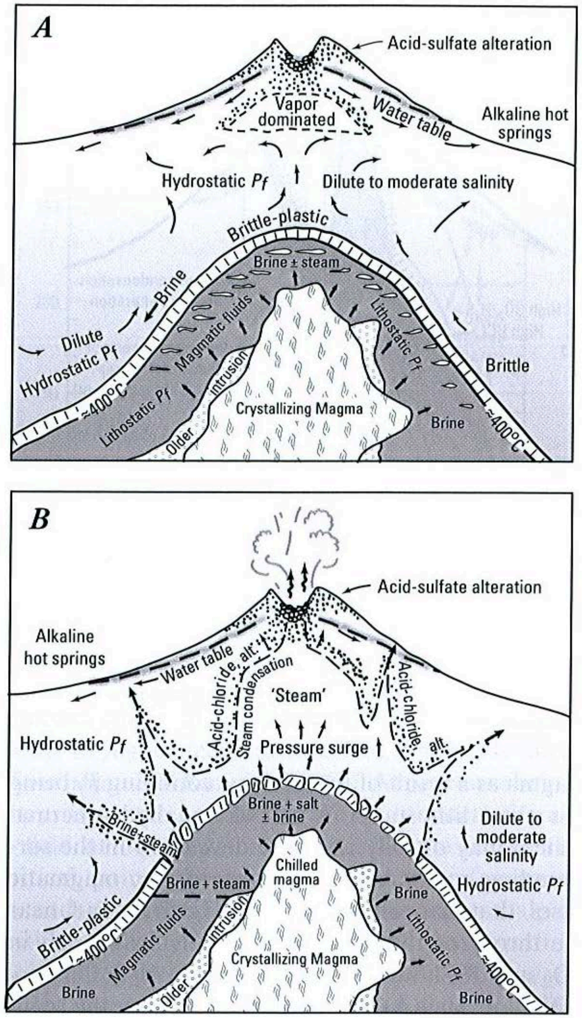

Figure 10.9. Schematic model of the transition from magmatic to epithermal conditions in a sub-volcanic environment where the tops of intruded plutons are at depths in the range 1 to 3 km. (A) The brittle-to-plastic transition occurs at about 370° to 400°C and dilute, dominantly meteoric water circulates at hydrostatic pressure in brittle rock, while highly saline, dominantly magmatic fluid at lithostatic pressure accumulates in plastic rock. (B) Episodic and temporary breaching of a normally self-sealed zone allows magmatic fluid to escape into the overlying hydrothermal system. See text for discussion.

From Dzurizin, 2007

Various causes of deformation at volcanoes

-Storage of magma in a shallow reservoir/ withdrawal of a shallow reservoir.
-Emplacement of magmatic intrusion at shallow depth.
-Magma conduit flow.
-Movements induced by surface load changes, compaction/contraction of eruptive deposits.
-Flank instabilities.
-Hydrothermal systems

Not always related to magmatic activity

For instance: Katla (Iceland), Damavand volcano (Iran)

Deformation observed on a typical basaltic volcano

Ex Piton de la Fournaise, Reunion Island

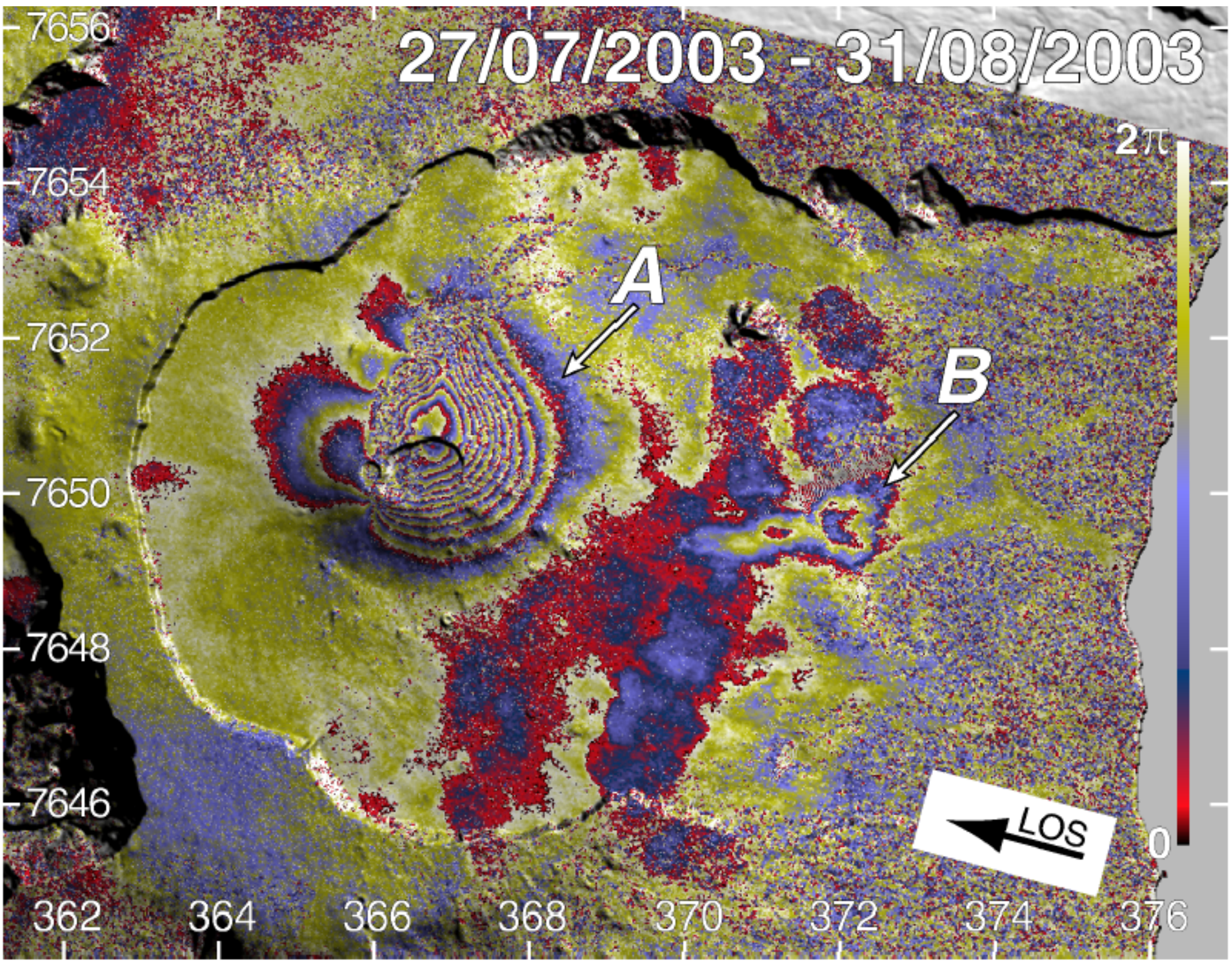

Eruption in August 2003
0.8 * 10^6 m^3

From Froger et al, 2004

Deformation observed on a typical basaltic volcano

Ex Piton de la Fournaise, Reunion Island

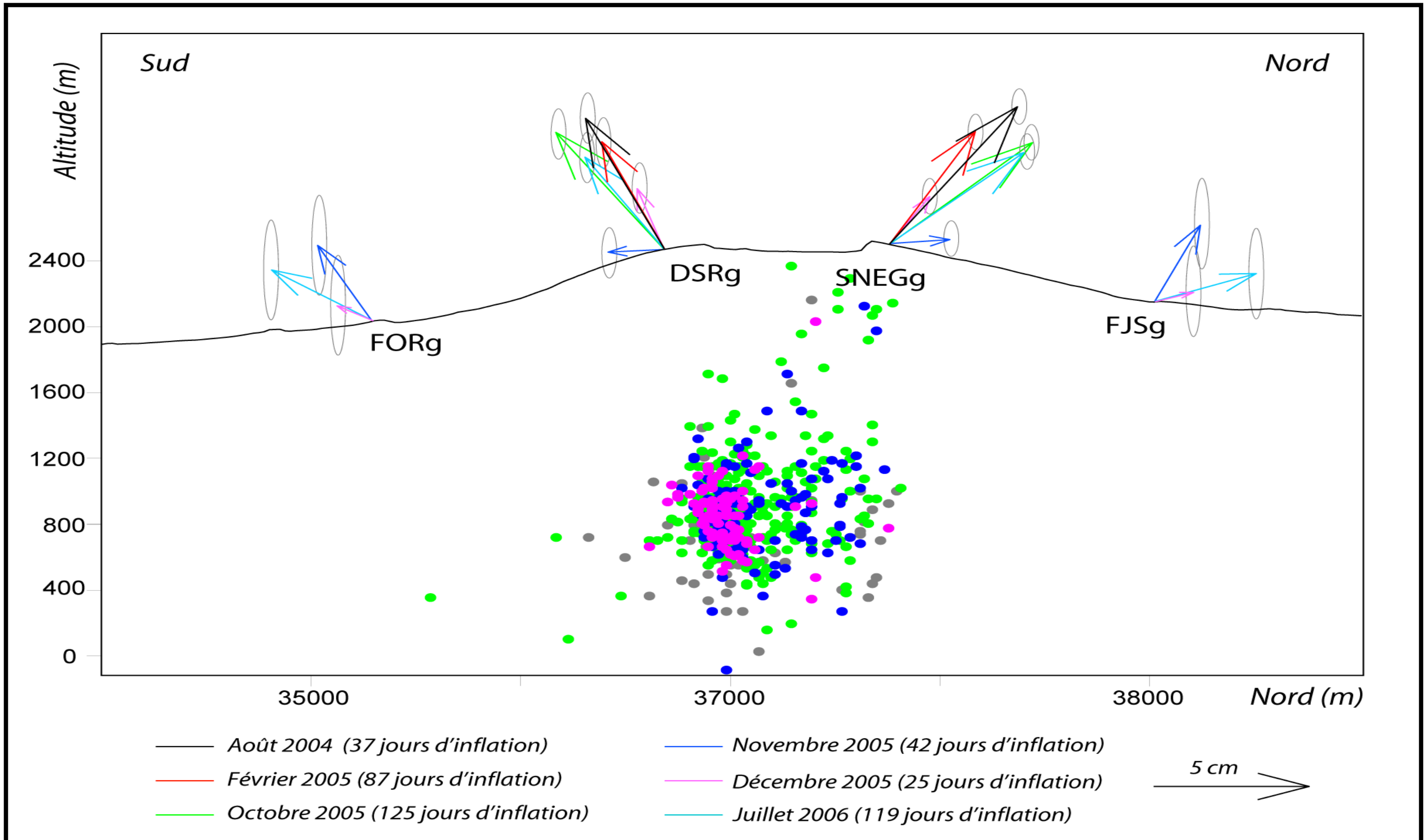

Peltier, seminar in Grenoble, 2009

Deformation observed on a typical basaltic volcano

Ex Piton de la Fournaise, Reunion Island

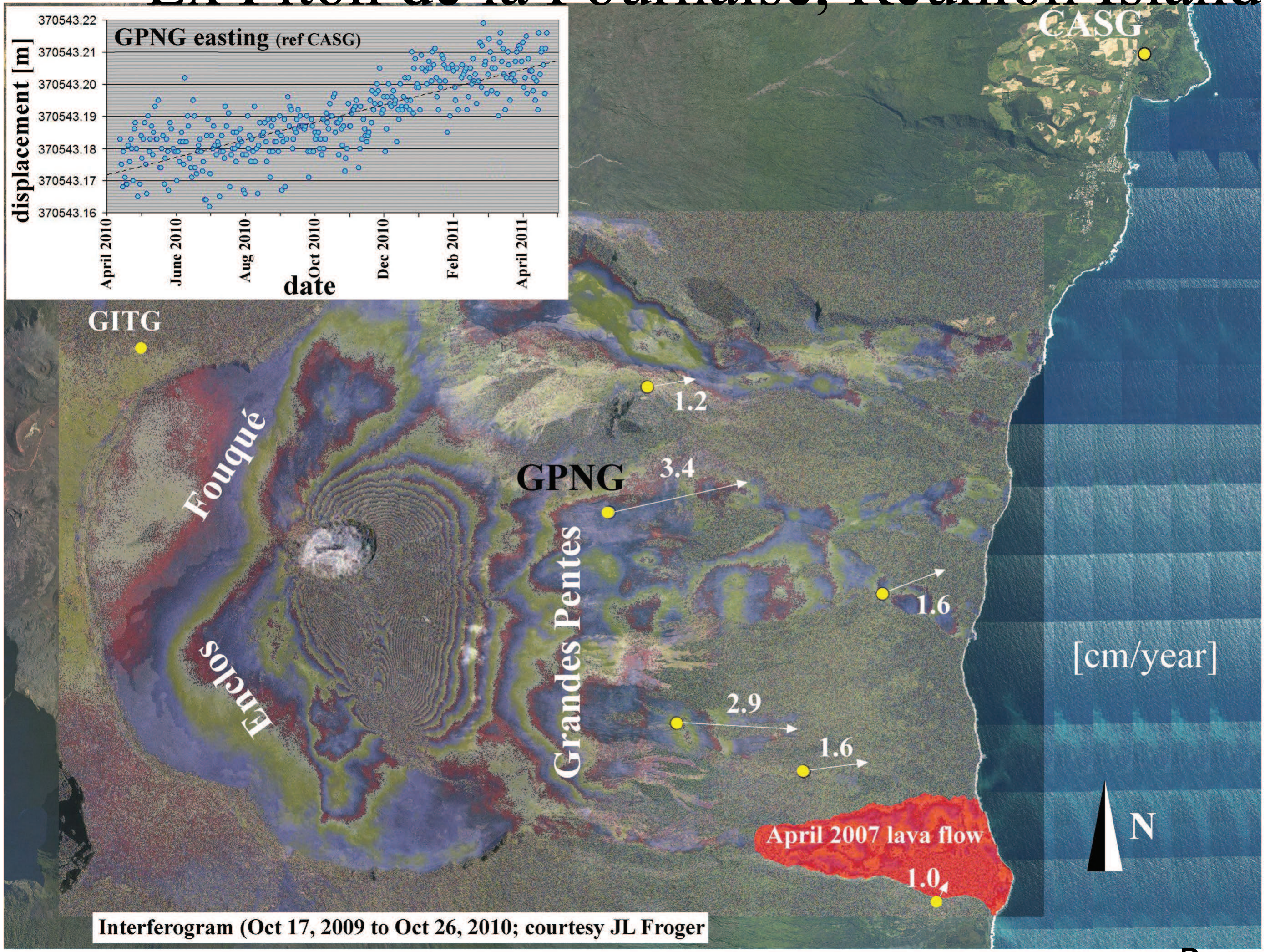

Brenguier et al. ,2012

Deformation observed on a typical andesitic volcano

Ex: Montserrat

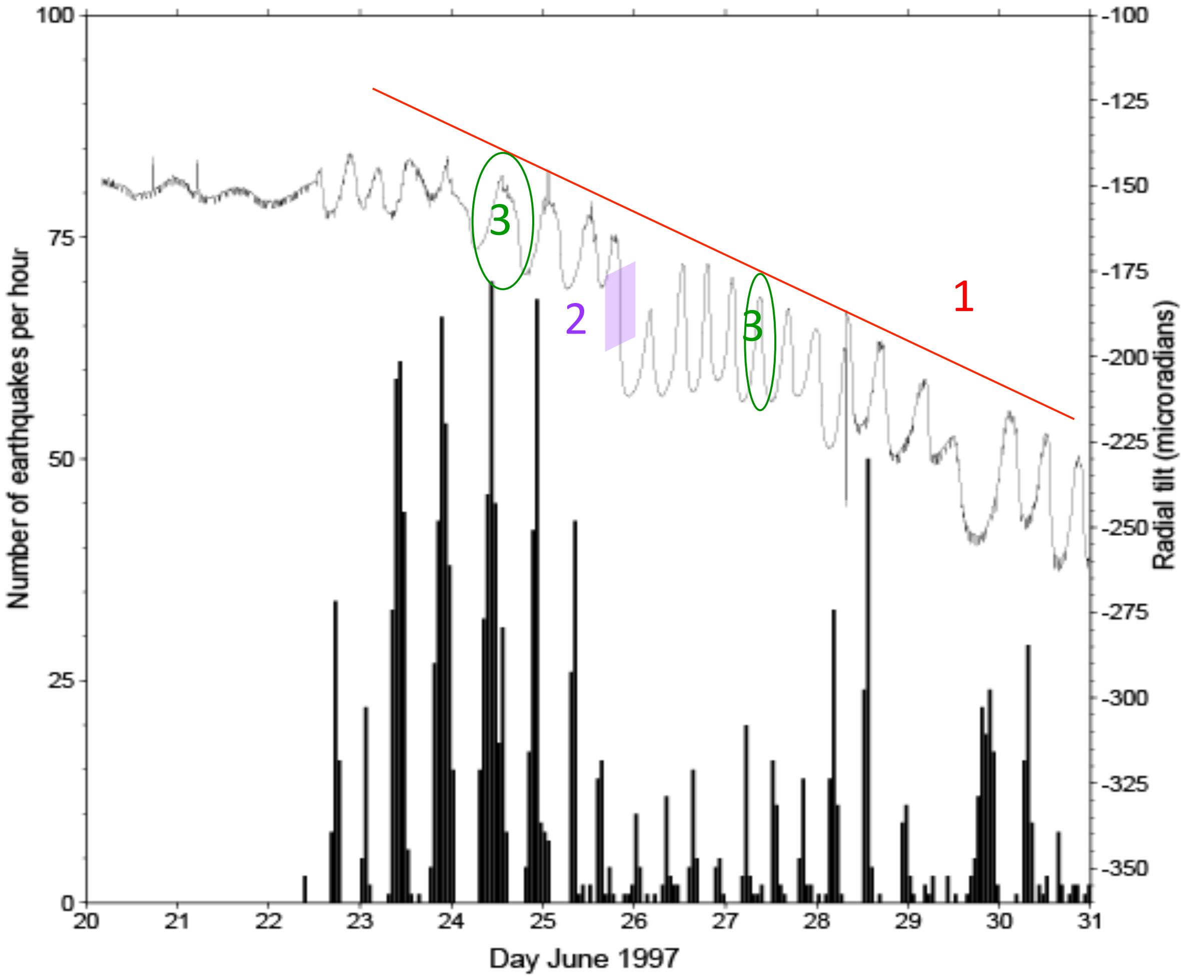

from Sparks (2003)

Mechanisms

(1) Pressure variation within the magma reservoir.

(2) Dome collapse

(3) Magma flow within the conduit.

Deformation observed on a typical andesitic volcano

Ex: Montserrat

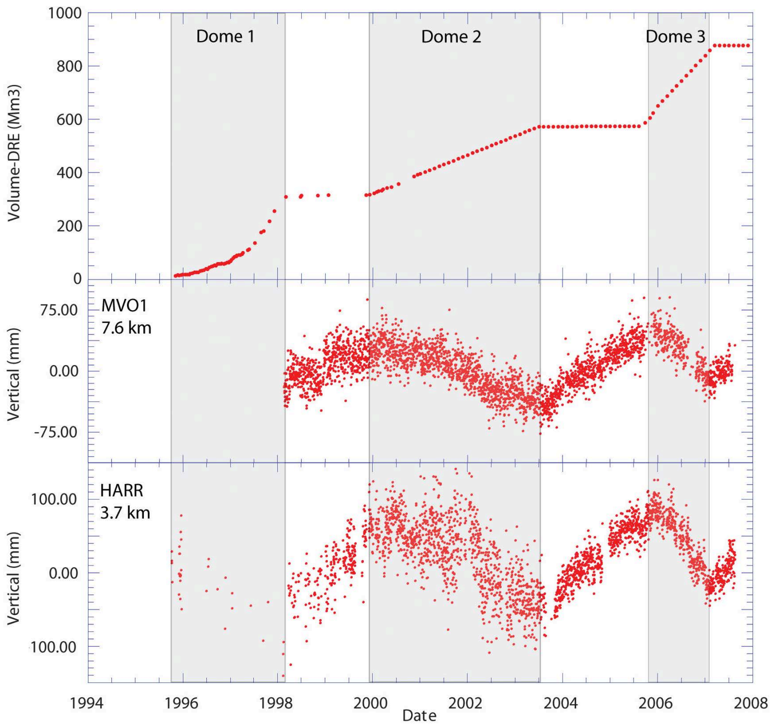

From Elsworth et al. (2008)

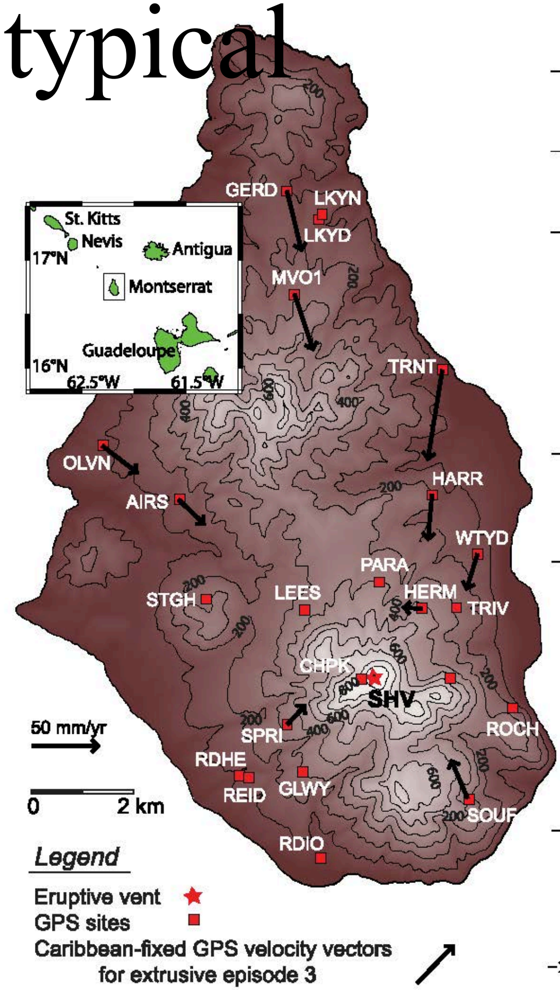

Apparent depth of the magmatic source
Increases with the distance crater-GPS station
→ 2 sources (5 and 17 km)
Foroozan et al, 2010,2011

Summary: Types of deformation

	Basaltic volcanoes	Andesitic volcanoes
Reservoir	*	*
Intrusions	*	
Conduit		*
Load	*	*
Destabilisation	*	*

Modeling of deformation sources

Observed displacements are due to stress perturbations

$$\underline{\underline{\sigma}} = \begin{pmatrix} \sigma_{xx} & \sigma_{xy} & \sigma_{xz} \\ \sigma_{yx} & \sigma_{yy} & \sigma_{yz} \\ \sigma_{zx} & \sigma_{zy} & \sigma_{zz} \end{pmatrix} \xrightarrow{\text{Rheology}} \underline{\underline{\epsilon}} = \begin{pmatrix} \epsilon_{rr} & \epsilon_{r\theta} & \epsilon_{rz} \\ \epsilon_{r\theta} & \epsilon_{\theta\theta} & \epsilon_{\theta z} \\ \epsilon_{rz} & \epsilon_{\theta z} & \epsilon_{zz} \end{pmatrix}$$

Stress tensor

Strain tensor

$$\underline{\underline{\varepsilon}} = \frac{1}{2}(\overrightarrow{grad}\,\underline{u} + \overrightarrow{grad}^{T}\,\underline{u})$$

Forces

$$\underline{U} = \begin{pmatrix} U_x \\ U_y \\ U_z \end{pmatrix}$$

Observed displacements are due to stress perturbations

$$\underline{\underline{\sigma}} = \begin{pmatrix} \sigma_{xx} & \sigma_{xy} & \sigma_{xz} \\ \sigma_{yx} & \sigma_{yy} & \sigma_{yz} \\ \sigma_{zx} & \sigma_{zy} & \sigma_{zz} \end{pmatrix} \xrightarrow{\text{Rheology}} \underline{\underline{\epsilon}} = \begin{pmatrix} \epsilon_{rr} & \epsilon_{r\theta} & \epsilon_{rz} \\ \epsilon_{r\theta} & \epsilon_{\theta\theta} & \epsilon_{\theta z} \\ \epsilon_{rz} & \epsilon_{\theta z} & \epsilon_{zz} \end{pmatrix}$$

Stress tensor

Strain tensor

Forces

$$\underline{U} = \begin{pmatrix} U_x \\ U_y \\ U_z \end{pmatrix}$$

What we measure

Observed displacements are due to stress perturbations

$$\underline{\underline{\sigma}} = \begin{pmatrix} \sigma_{xx} & \sigma_{xy} & \sigma_{xz} \\ \sigma_{yx} & \sigma_{yy} & \sigma_{yz} \\ \sigma_{zx} & \sigma_{zy} & \sigma_{zz} \end{pmatrix} \xrightarrow{\text{Rheology}} \underline{\underline{\epsilon}} = \begin{pmatrix} \epsilon_{rr} & \epsilon_{r\theta} & \epsilon_{rz} \\ \epsilon_{r\theta} & \epsilon_{\theta\theta} & \epsilon_{\theta z} \\ \epsilon_{rz} & \epsilon_{\theta z} & \epsilon_{zz} \end{pmatrix}$$

Stress tensor

Strain tensor

Forces

$$\underline{U} = \begin{pmatrix} U_x \\ U_y \\ U_z \end{pmatrix}$$

What we want to know

What we measure

Observed displacements are due to stress perturbations

$$\underline{\underline{\sigma}} = \begin{pmatrix} \sigma_{xx} & \sigma_{xy} & \sigma_{xz} \\ \sigma_{yx} & \sigma_{yy} & \sigma_{yz} \\ \sigma_{zx} & \sigma_{zy} & \sigma_{zz} \end{pmatrix} \xrightarrow{\text{Rheology}} \underline{\underline{\epsilon}} = \begin{pmatrix} \epsilon_{rr} & \epsilon_{r\theta} & \epsilon_{rz} \\ \epsilon_{r\theta} & \epsilon_{\theta\theta} & \epsilon_{\theta z} \\ \epsilon_{rz} & \epsilon_{\theta z} & \epsilon_{zz} \end{pmatrix}$$

Stress tensor

Strain tensor

Elasticity

$$\boxed{\boldsymbol{\varepsilon} = \frac{1}{E}((1+\nu)\boldsymbol{\sigma} - \nu \mathrm{Tr}(\boldsymbol{\sigma})\mathbf{I})}$$

Forces

$$\underline{U} = \begin{pmatrix} U_x \\ U_y \\ U_z \end{pmatrix}$$

What we want to know

What we measure

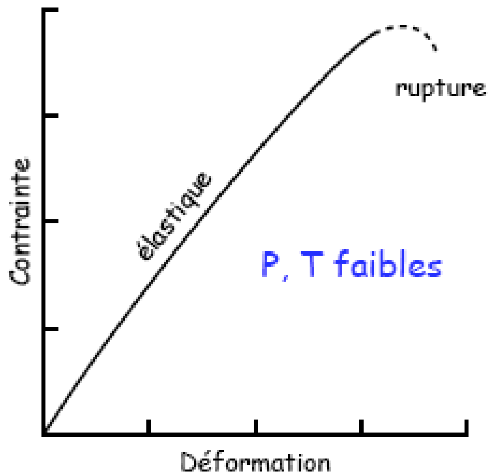

Elastique → Fragile
rupture cassante

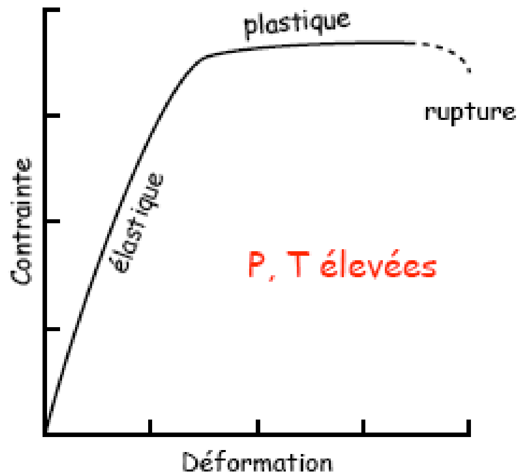

Elastique → Plastique
déformation ductile

Strain and displacement…

Displacement vector defined at each point:

$$\underline{U} = \begin{pmatrix} U_x \\ U_y \\ U_z \end{pmatrix}$$

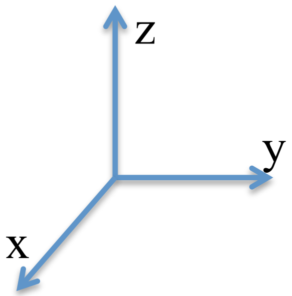

For "small" displacements, strain tensor is given by:

$$\underline{\underline{\epsilon}} = \begin{pmatrix} \epsilon_{xx} & \epsilon_{xy} & \epsilon_{xz} \\ \epsilon_{xy} & \epsilon_{yy} & \epsilon_{yz} \\ \epsilon_{xz} & \epsilon_{yz} & \epsilon_{zz} \end{pmatrix}$$

with

$$\epsilon_{xx} = \frac{\partial U_x}{\partial x} \qquad \epsilon_{xy} = \frac{1}{2}(\frac{\partial U_x}{\partial y} + \frac{\partial U_y}{\partial x})$$

$$\epsilon_{yy} = \frac{\partial U_y}{\partial y} \qquad \epsilon_{xz} = \frac{1}{2}(\frac{\partial U_x}{\partial z} + \frac{\partial U_z}{\partial x})$$

$$\epsilon_{zz} = \frac{\partial U_z}{\partial z} \qquad \epsilon_{yz} = \frac{1}{2}(\frac{\partial U_z}{\partial y} + \frac{\partial U_y}{\partial z})$$

Strain and displacement…

Cylindrical coordinates

Displacement vector defined
at each point:

$$\underline{U} = \begin{pmatrix} U_r \\ U_\theta \\ U_z \end{pmatrix}$$

$$x = r \cos \theta$$

$$y = r \sin \theta$$

$$z = z$$

$$dV = r\, dr\, d\theta\, dz$$

$$ds^2 = dr^2 + r^2\, d\theta^2 + dz^2$$

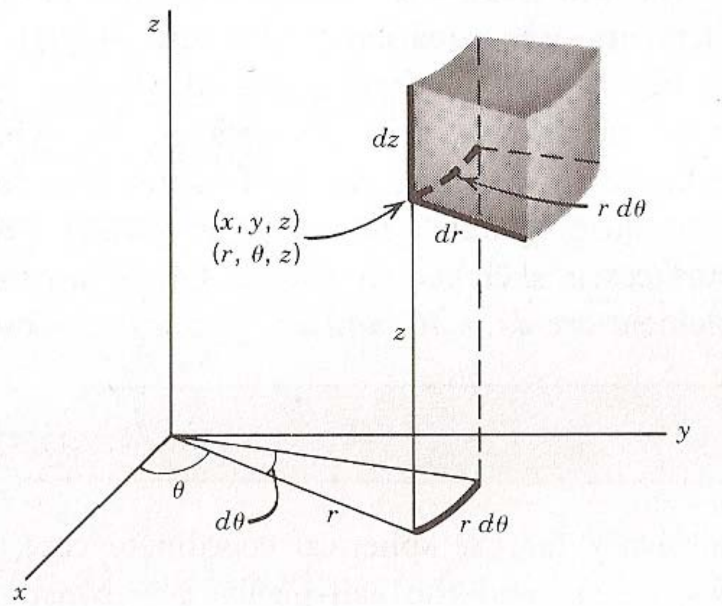

For "small" displacements, strain tensor is given by:

$$\underline{\underline{\epsilon}} = \begin{pmatrix} \epsilon_{rr} & \epsilon_{r\theta} & \epsilon_{rz} \\ \epsilon_{r\theta} & \epsilon_{\theta\theta} & \epsilon_{\theta z} \\ \epsilon_{rz} & \epsilon_{\theta z} & \epsilon_{zz} \end{pmatrix}$$

with

$$\epsilon_{rr} = \frac{\partial U_r}{\partial r}$$

$$\epsilon_{\theta\theta} = \frac{1}{r}\frac{\partial U_\theta}{\partial \theta} + \frac{U_r}{r}$$

$$\epsilon_{zz} = \frac{\partial U_z}{\partial z}$$

$$\epsilon_{r\theta} = \frac{1}{2}(\frac{1}{r}\frac{\partial U_r}{\partial \theta} + \frac{\partial U_\theta}{\partial r} - \frac{U_\theta}{r})$$

$$\epsilon_{rz} = \frac{1}{2}(\frac{\partial U_r}{\partial z} + \frac{\partial U_z}{\partial r})$$

$$\epsilon_{\theta z} = \frac{1}{2}(\frac{1}{r}\frac{\partial U_z}{\partial \theta} + \frac{\partial U_\theta}{\partial z})$$

Strain and displacement…

Spherical coordinates

$$x = r \sin\theta \cos\phi$$

$$y = r \sin\theta \sin\phi$$

$$z = r \cos\theta$$

$$dV = r^2 \sin\theta \, dr \, d\theta \, d\phi$$

$$ds^2 = dr^2 + r^2 \, d\theta^2 + r^2 \sin^2\theta \, d\phi^2$$

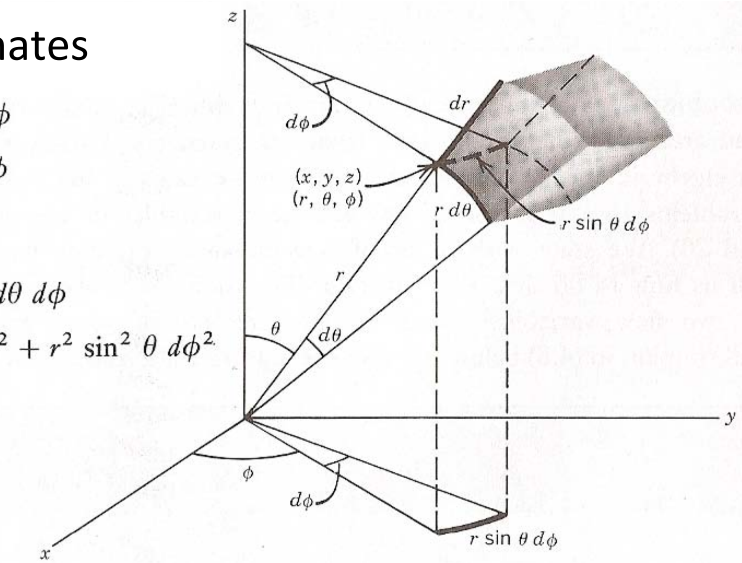

Displacement vector defined
at each point:

$$\underline{U} = \begin{pmatrix} U_r \\ U_\theta \\ U_\phi \end{pmatrix}$$

For "small" displacements, strain tensor is given by:

$$\underline{\underline{\epsilon}} = \begin{pmatrix} \epsilon_{rr} & \epsilon_{r\theta} & \epsilon_{r\phi} \\ \epsilon_{r\theta} & \epsilon_{\theta\theta} & \epsilon_{\theta\phi} \\ \epsilon_{r\phi} & \epsilon_{\theta\phi} & \epsilon_{\phi\phi} \end{pmatrix}$$

with

$$\epsilon_{rr} = \frac{\partial U_r}{\partial r}$$

$$\epsilon_{\theta\theta} = \frac{1}{r}\frac{\partial U_\theta}{\partial \theta} + \frac{U_r}{r}$$

$$\epsilon_{\phi\phi} = \frac{1}{r\sin\theta}\frac{\partial U_\phi}{\partial \phi} + \frac{U_r}{r} + \frac{U_\theta \mathrm{cotan}}{r}$$

$$\epsilon_{r\theta} = \frac{1}{2}(\frac{1}{r}\frac{\partial U_r}{\partial \theta} + \frac{\partial U_\theta}{\partial r} - \frac{U_\theta}{r})$$

$$\epsilon_{r\phi} = \frac{1}{2}(\frac{1}{r\sin\theta}\frac{\partial U_r}{\partial \phi} + \frac{\partial U_\phi}{\partial r} - \frac{U_\phi}{r})$$

$$\epsilon_{\theta\phi} = \frac{1}{2}(\frac{1}{r\sin\theta}\frac{\partial U_\theta}{\partial \phi} + \frac{1}{r}\frac{\partial U_\phi}{\partial \theta} - \frac{U_\phi \mathrm{cotan}\theta}{r})$$

What is a model ?

A model is a theoretical representation of reality
which aims at better knowing and better understanding this reality.

A model is a framework which allows:
- to interpret various observations (surface displacements, heat flux, self-potential, seismicity, gravity…)
- to constrain our knowledge (on crustal rheologies, stress field, initial state…)

The model: A chalenging tool

Knowing that:

"All is simple is false.
All is complicated is useless" Paul Valéry.

The degree of complexity has to be related to the numbers of available observations.

The model: Classical steps

You have to choose:

- The physics

The model: Classical steps

You have to **choose**:

- The physics

- Medium properties

The model: Classical steps

<u>You have to **choose**:</u>

- The physics

- Medium properties

- The geometry

The model: Classical steps

You have to **choose**:

- The physics

- Medium properties

- The geometry

- The boundary conditions

The model: Classical steps

You have to **choose**:

- The physics

- Medium properties

- The geometry

- The boundary conditions

- The initial state

The model: Classical steps

You have to **choose**:

- The physics

- Medium properties

- The geometry

- The boundary conditions

- The initial state

- Perturbation considered

The model: Classical steps

<u>You have to **choose**:</u>

- The physics

- Medium properties

- The geometry

- The boundary conditions

- The initial state

- Perturbation considered

And eventually to perform a **dimensionless study**

Various methods for modeling

Analytical modeling

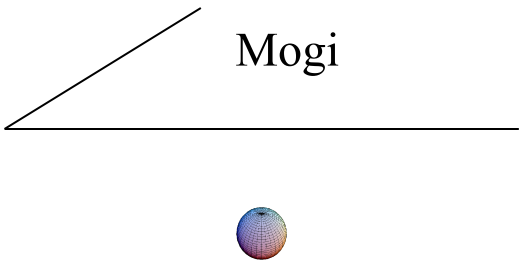

Numerical modeling

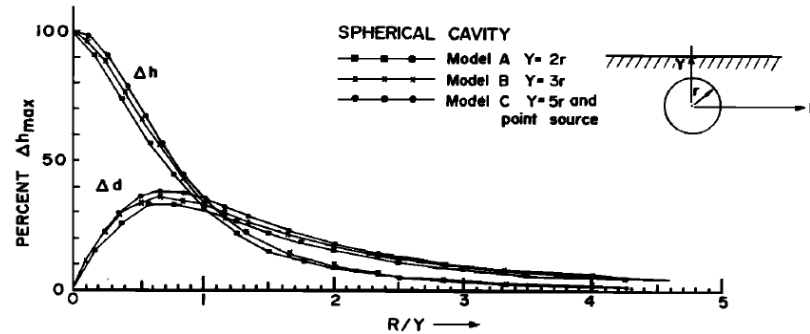

From Dieterich and Decker, JGR, 1975

Analogue modeling

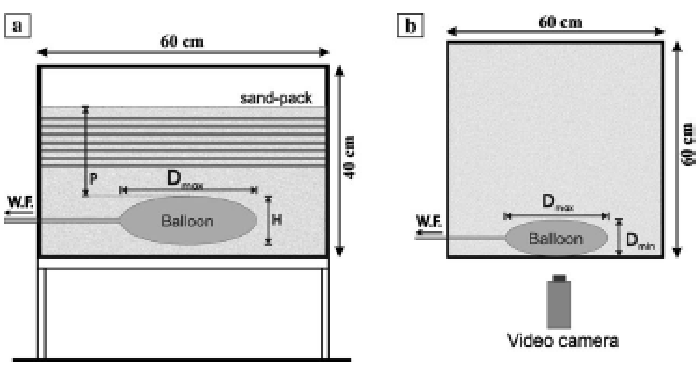

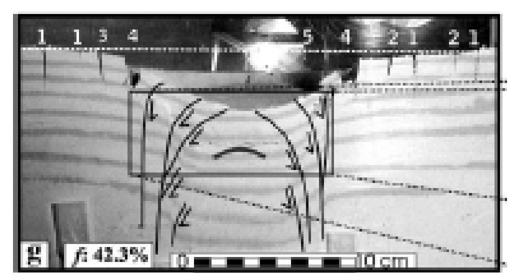

Importance of scaling

From Geyer et al, JVGR, 2006

Various methods for modeling

Analytical modeling

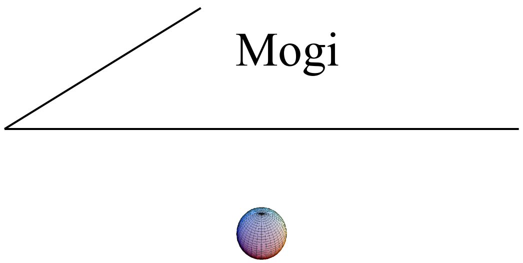

Numerical modeling

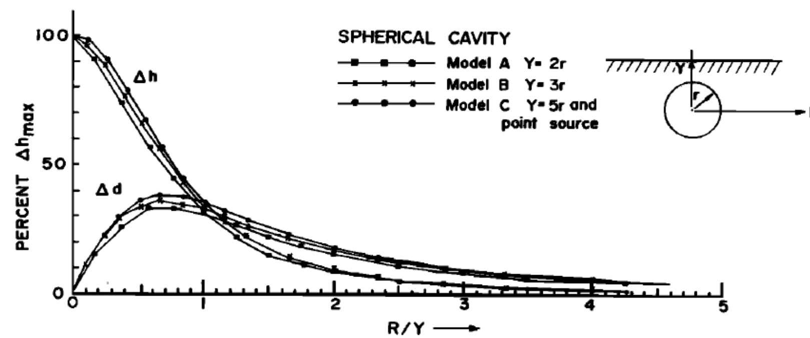

From Dieterich and Decker, JGR, 1975

Analogue modeling

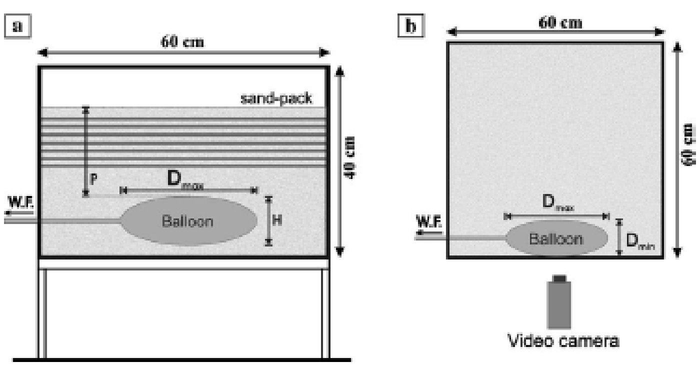

Importance of scaling

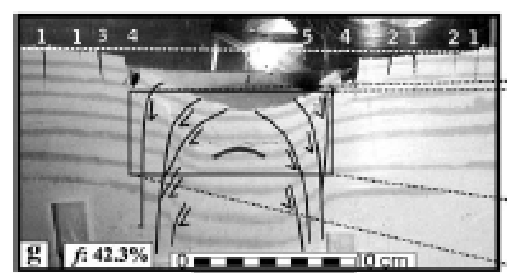

From Geyer et al, JVGR, 2006

Modeling of deformation sources
1- Analytical models for volcanoes deformation

Assumptions

Crust is considered as an isotropic, homogeneous, half-space

with an <u>elastic behaviour</u>:

Hooke's law:

$$\boldsymbol{\varepsilon} = \frac{1}{E}\left((1+\nu)\boldsymbol{\sigma} - \nu \mathrm{Tr}(\boldsymbol{\sigma})\mathbf{I}\right)$$

$$\boldsymbol{\sigma} = \frac{E}{1+\nu}\left(\boldsymbol{\varepsilon} + \frac{\nu}{1-2\nu}\mathrm{Tr}\left(\boldsymbol{\varepsilon}\right)\mathbf{I}\right)$$

E: Young's modulus
ν: Poisson's ratio

G: Modulus of rigidity is also used
G=E/(2*(1+ν))

Young's modulus

From seismic data: a dynamic value

$$\nu = \frac{(V_p/V_s)^2 - 2}{2(V_p/V_s)^2 - 2}, \qquad E = 2\rho_r V_s^2(1+\nu)$$

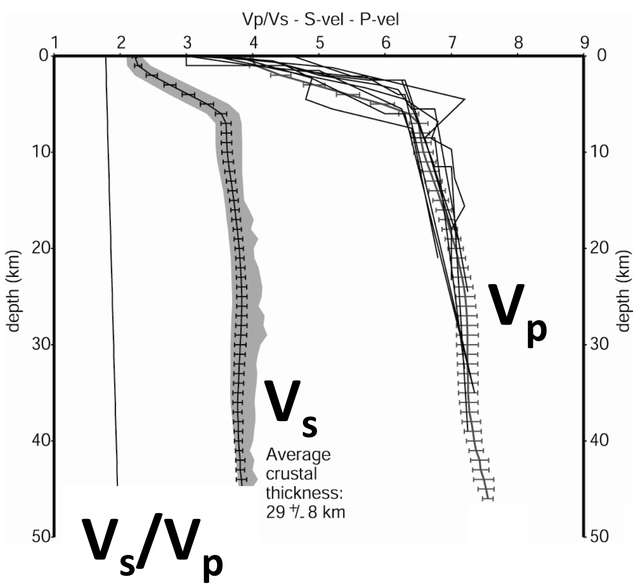

Poisson's ratio: 0.27 - 0.33

(Allen et al., 2002)

The « Mogi » model (1958)

(Bull. Of the Earthq. Res. Inst. Vol 36, 1958)

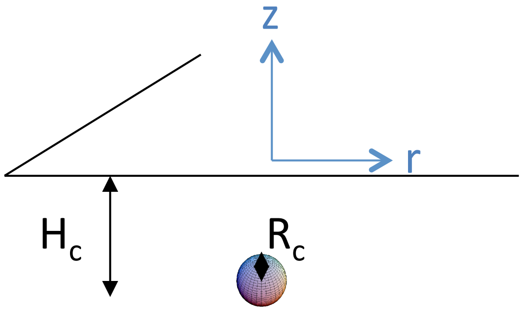

Four parameters: position, depth, strength

- The physics Continuum mechanics, solid, linear elasticity (Hooke's law)

  No distant force $\boxed{\text{div } \sigma = 0}$
- Medium properties Homogeneous E, ν
- The geometry Half-space (H_c, R_c) with R_c/H_c<<0
- The boundary conditions Free upper surface, zero displacements at infinity
- The initial state Equilibrium, no initial stress field
- Perturbation considered Punctual pressure source (ΔP)

- The dimensionless study For a given ν, only one solution when scaling all distances by chamber depth H_c and displacement by $(\Delta P R_c^{3)}/(E H_c^{2})$

$$u_v=2(1-\nu^2)/(1+r^2)^{3/2},\ u_r=2(1-\nu^2)*r/(1+r^2)^{3/2}$$

Mogi Model

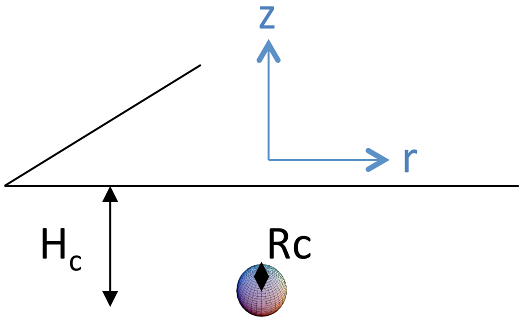

Most simple analytical model=
Point source model in an homogeneous elastic half-space:
« Mogi model » (1958) (4 parameters)

Vertical displacement:

$$U_z(z=0,r) = 2(1-\upsilon^2)\frac{\Delta P_c R_c^3}{E}\frac{H_c}{(H_c{}^2+r^2)^{3/2}}$$

$$U_{zmax}(z=0) = 2(1-\upsilon^2)\frac{\Delta P_c R_c^3}{E H_c^2}$$

$$\boxed{U_z = U_r * H_c / r}$$

Horizontal displacement:

$$U_r(z=0,r) = 2(1-\upsilon^2)\frac{\Delta P_c R_c^3}{E}\frac{r}{(H_c{}^2+r^2)^{3/2}}$$

Tilt: $$\theta_r(r) = 6(1-\upsilon^2)\frac{\Delta P_c R_c^3 H_c}{E}\frac{r}{(H_c{}^2+r^2)^{5/2}}$$

Vertical displacement

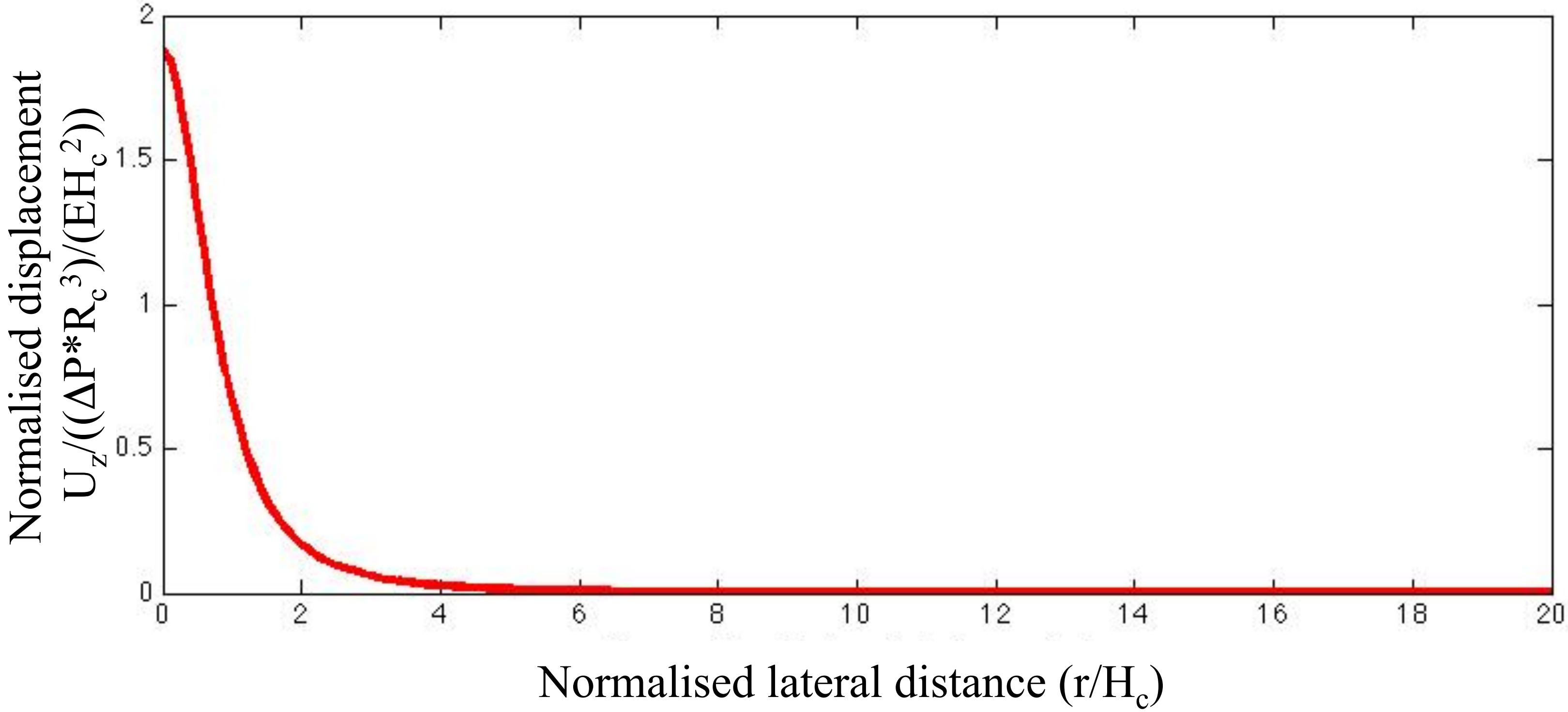

With ν=0.25

Horizontal displacement

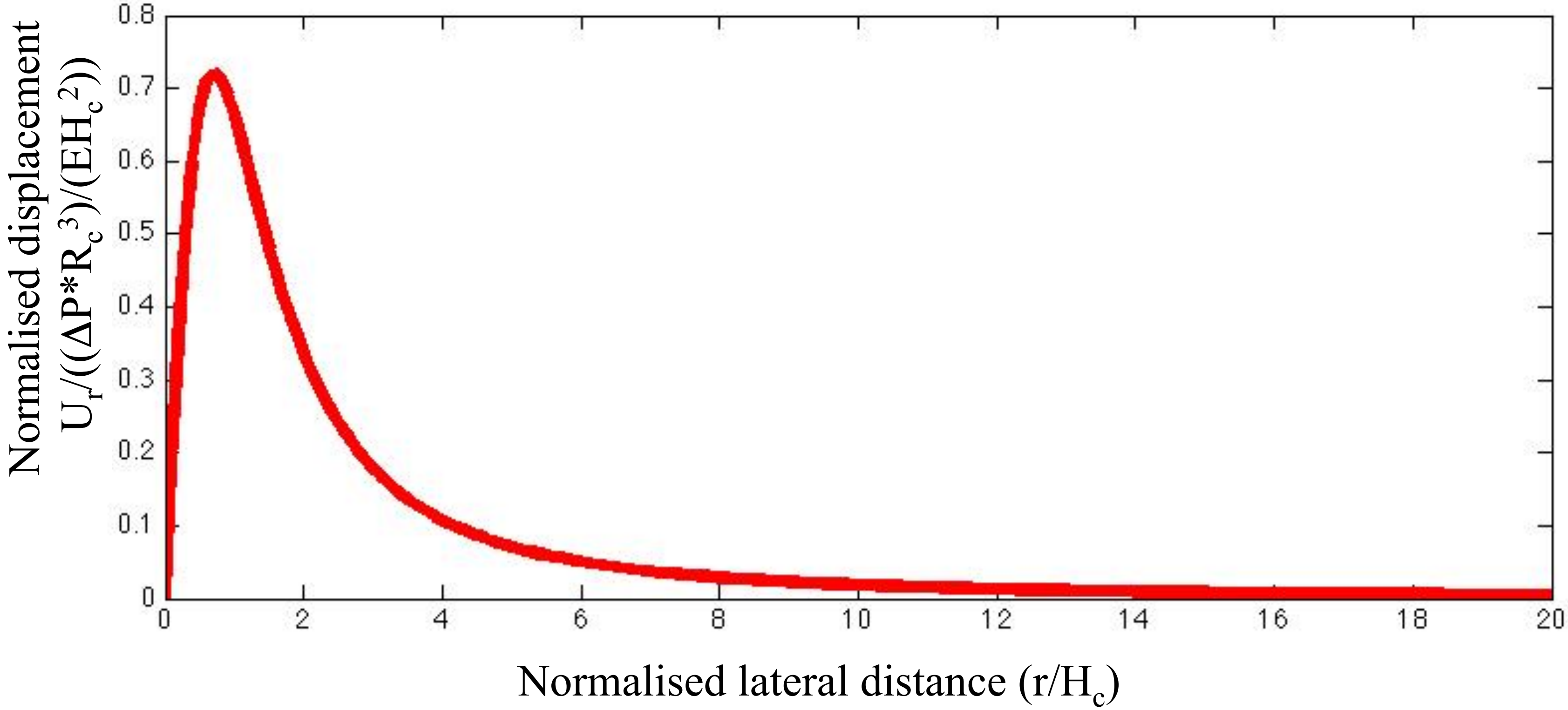

With ν=0.25

Tilt

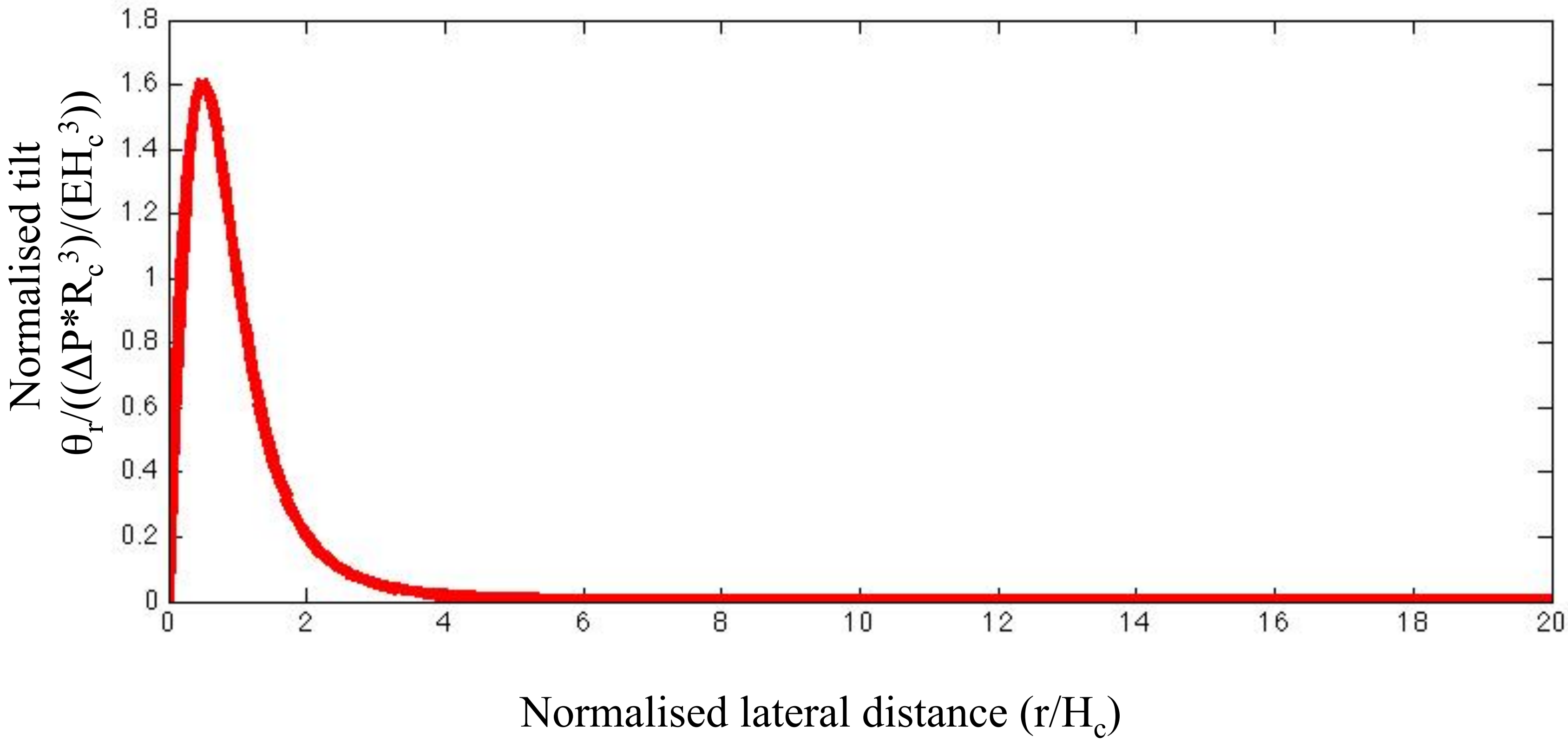

With our convention, inflation induces a positive tilt

With ν=0.25

Mc Tigue's formulation for a finite sphere

Mogi model is a point source model, valid only in case $R_c << H$
Only give $\Delta P R_c^3/E$: no information on the source size.
McTigue (*JGR, 1987*) propose a better analytical approximation depending on R_c:

Vertical displacement:

$$U_z(z=0,r) = 2(1-\upsilon^2)\frac{\Delta P_c R_c^3}{E}\left[\frac{H_c}{({H_c}^2+r^2)^{3/2}} - \frac{(1+\nu)}{2(7-5\nu)}\frac{1}{{H_c}^2}\frac{R_c^3}{({H_c}^2+r^2)^{3/2}} + \frac{15(2-\nu)}{4(7-5\nu)}\frac{R_c^3}{({H_c}^2+r^2)^{5/2}}\right]$$

Horizontal displacement:

$$U_r(z=0,r) = 2(1-\upsilon^2)\frac{\Delta P_c R_c^3}{E}\left[\frac{r}{({H_c}^2+r^2)^{3/2}} - \frac{(1+\nu)}{2(7-5\nu)}\frac{1}{{H_c}^3}\frac{rR_c^3}{({H_c}^2+r^2)^{3/2}} + \frac{15(2-\nu)}{4(7-5\nu)}\frac{1}{H_c}\frac{rR_c^3}{({H_c}^2+r^2)^{5/2}}\right]$$

Tilt:

$$\theta_r(r) = 6(1-\upsilon^2)\frac{\Delta P_c R_c^3}{E}\left[\frac{H_c r}{({H_c}^2+r^2)^{5/2}} - \frac{(1+\nu)}{2(7-5\nu)}\frac{1}{{H_c}^2}\frac{rR_c^3}{({H_c}^2+r^2)^{5/2}} + \frac{25(2-\nu)}{4(7-5\nu)}\frac{rR_c^3}{({H_c}^2+r^2)^{7/2}}\right]$$

Vertical displacement

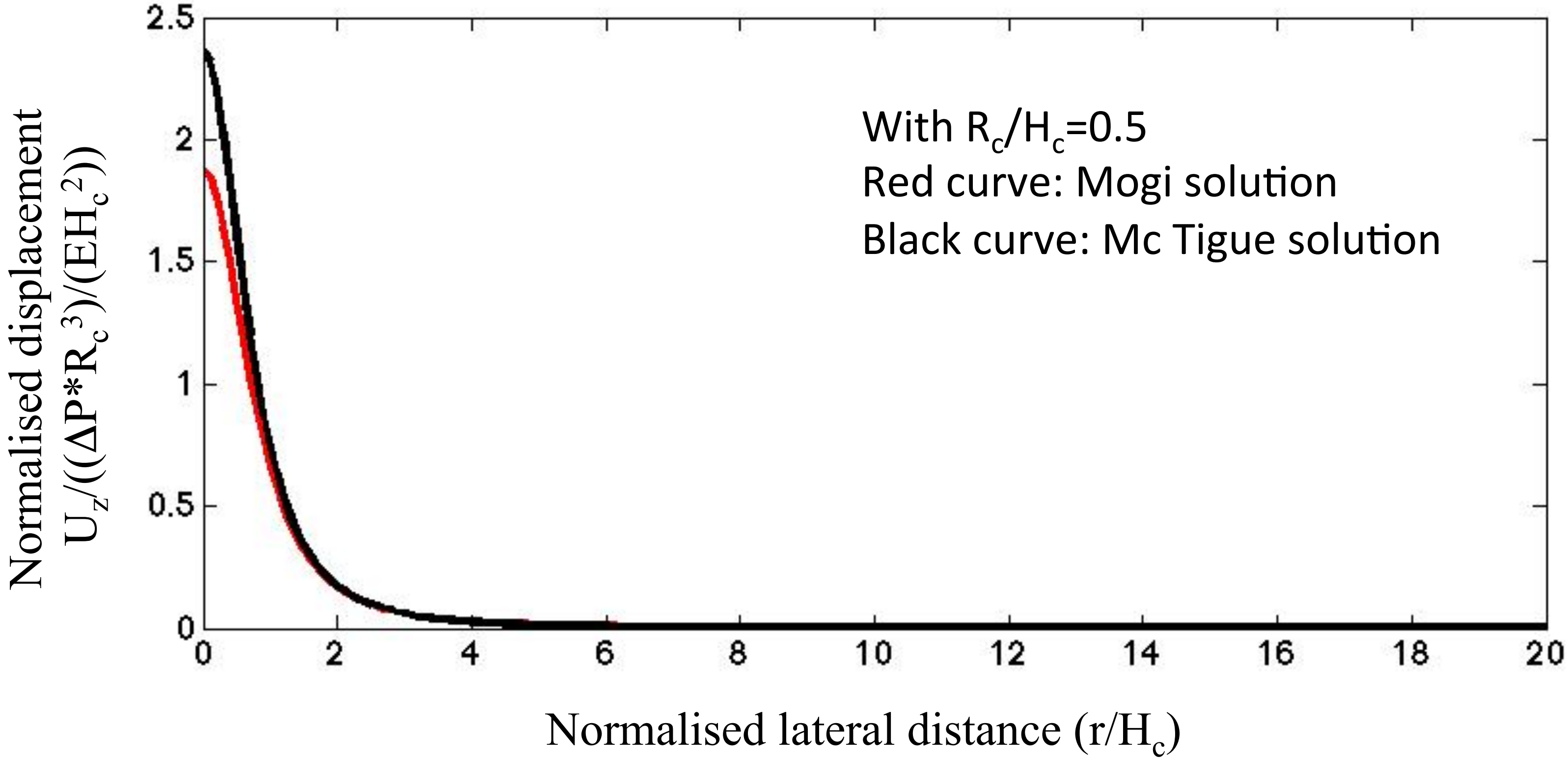

With ν=0.25

Horizontal displacement

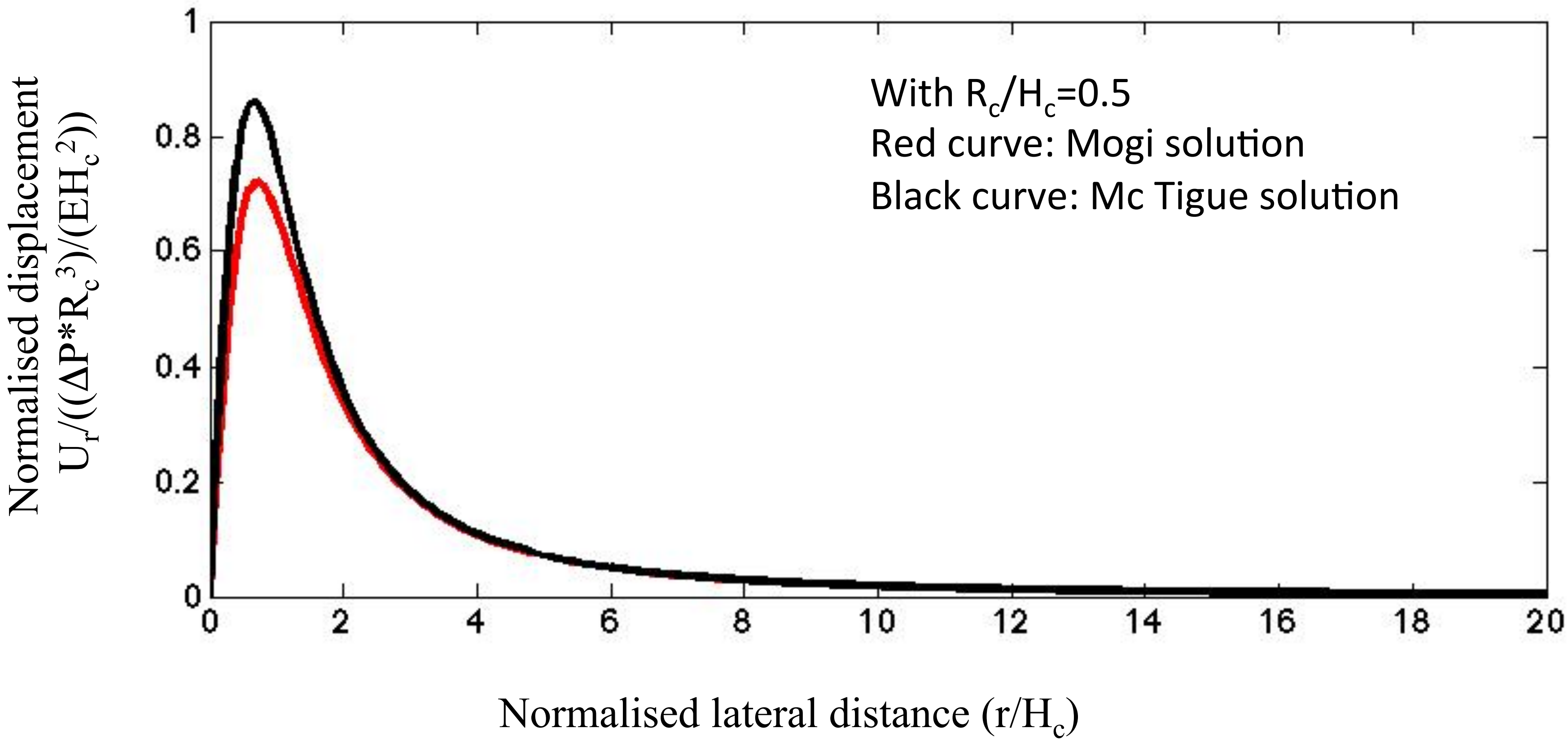

With ν=0.25

Tilt

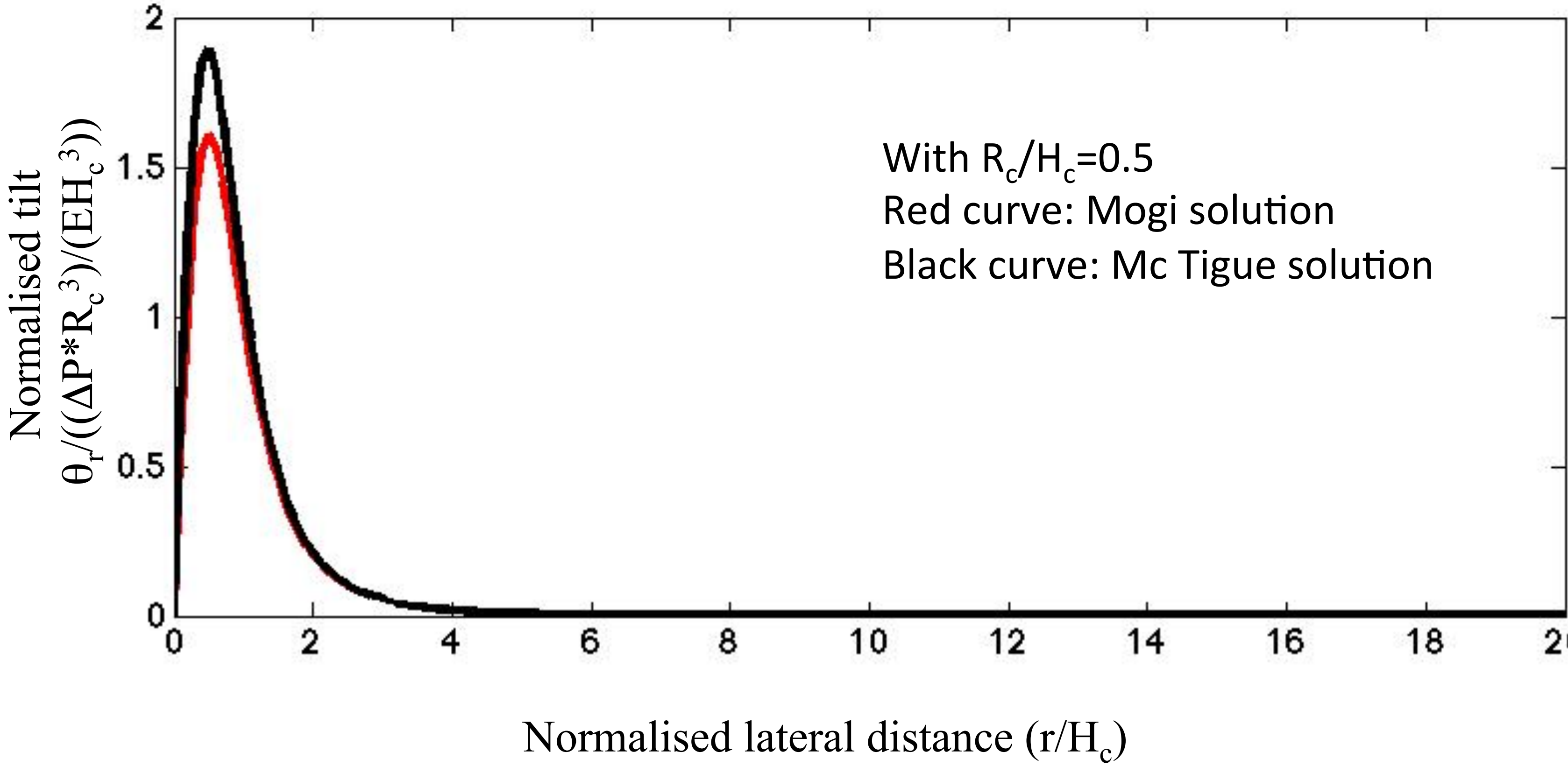

With our convention, inflation induces a positive tilt

With ν=0.25

It is difficult to have an information on magma reservoir size from surface deformation

Ex: Wesdhal, Alaska (Lu et al., 2000) :
Inflation of 16 cm from sept. 93 to oct. 98 due to a storage zone at 9 km depth

Case 1 : R_c=1000 m
ΔP= 200 bars

Case 2 : R_c=1600 m
ΔP= 50 bars

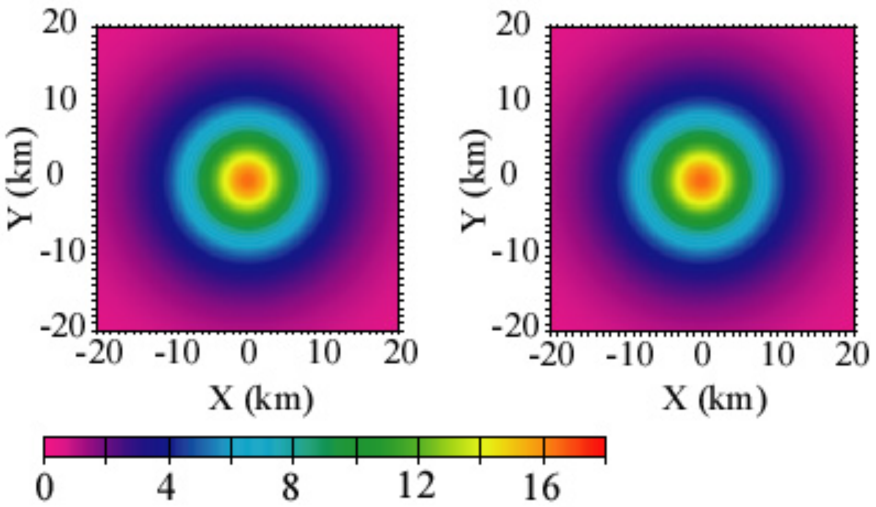

Vertical displacement (cm)

Difference of vertical displacement at surface < mm.

Contrains on reservoir size from temporal evolution of surface displacement

For basaltic volcanoes a simple model coupling crustal deformation and magma flow :

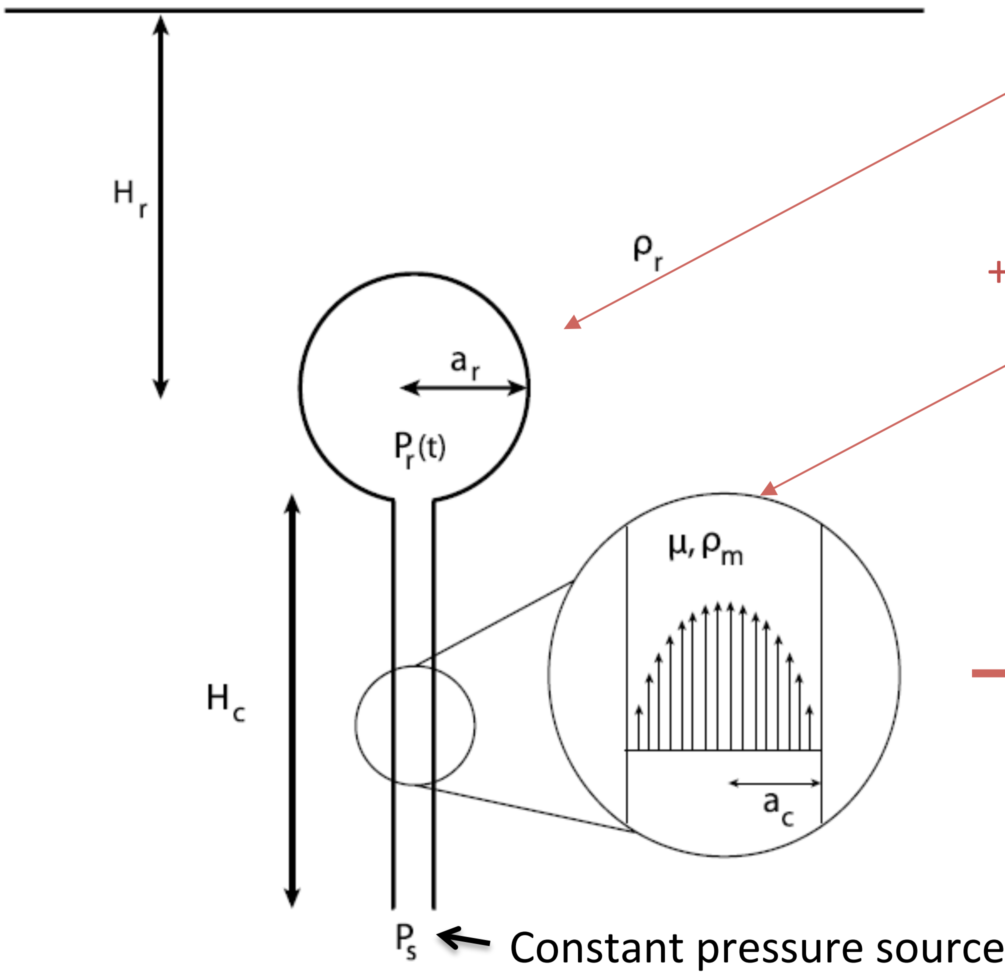

Elastic deformation (Mogi)

$$\Delta V_{in}(t) = \Delta P(t)\,\frac{\pi a_r^3}{G}$$

+

Poiseuille flow

$$Q(t) = \frac{\pi a_c^4}{8\mu H_c}\left[\Delta P_s - \Delta P_r(t) + (\rho_r - \rho_m) g H_c\right]$$

$$\boxed{\Delta P(t) = P\left(1 - \exp\left(\frac{-t}{\tau}\right)\right)}$$

$$\boxed{\tau = \frac{8\mu H_c a_r^3}{G a_c^4}}$$

Contrains on reservoir size from temporal evolution of surface displacement

With a smaller reservoir the Displacement rate is larger at the beginning.

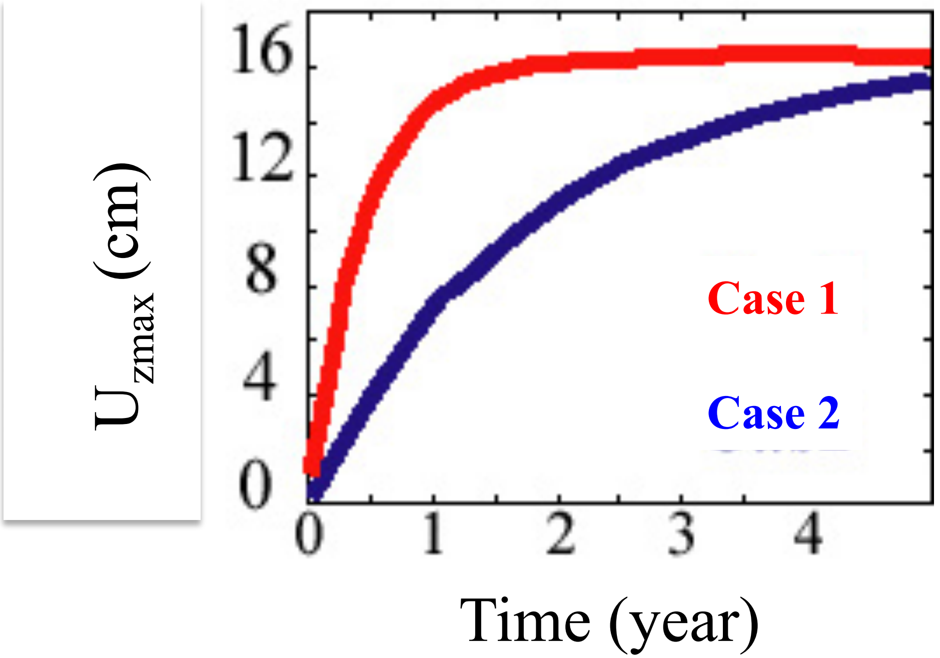

Exponential decay of surface displacement is observed.

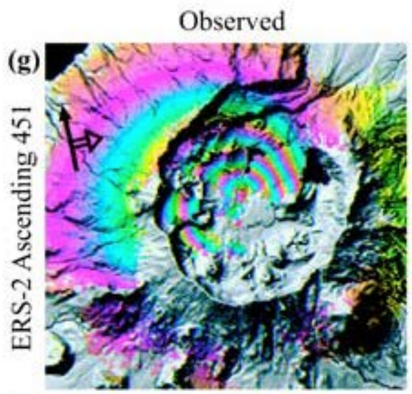

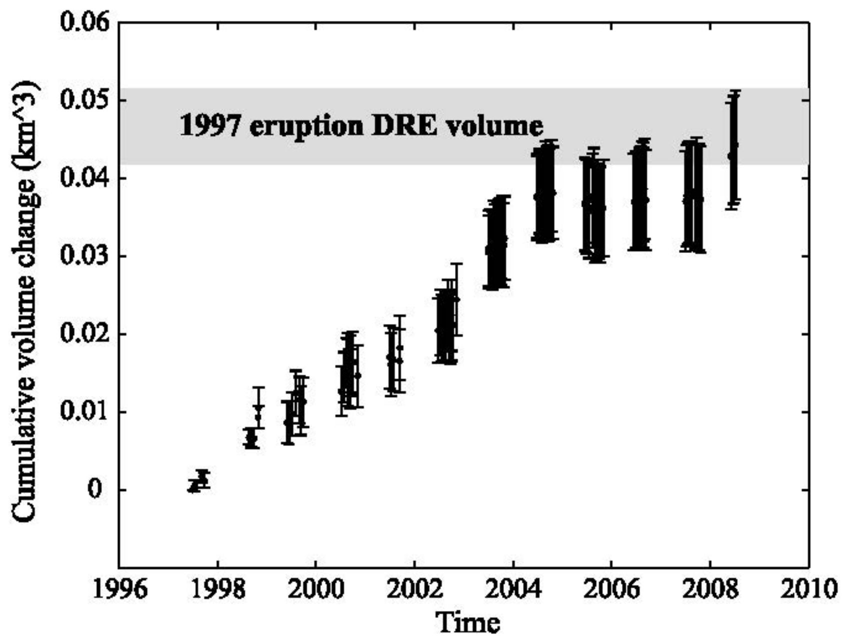

Lu et al, JGR, 2010

Influence of surface slope

Analytical solutions:
Small slope influence can be estimated

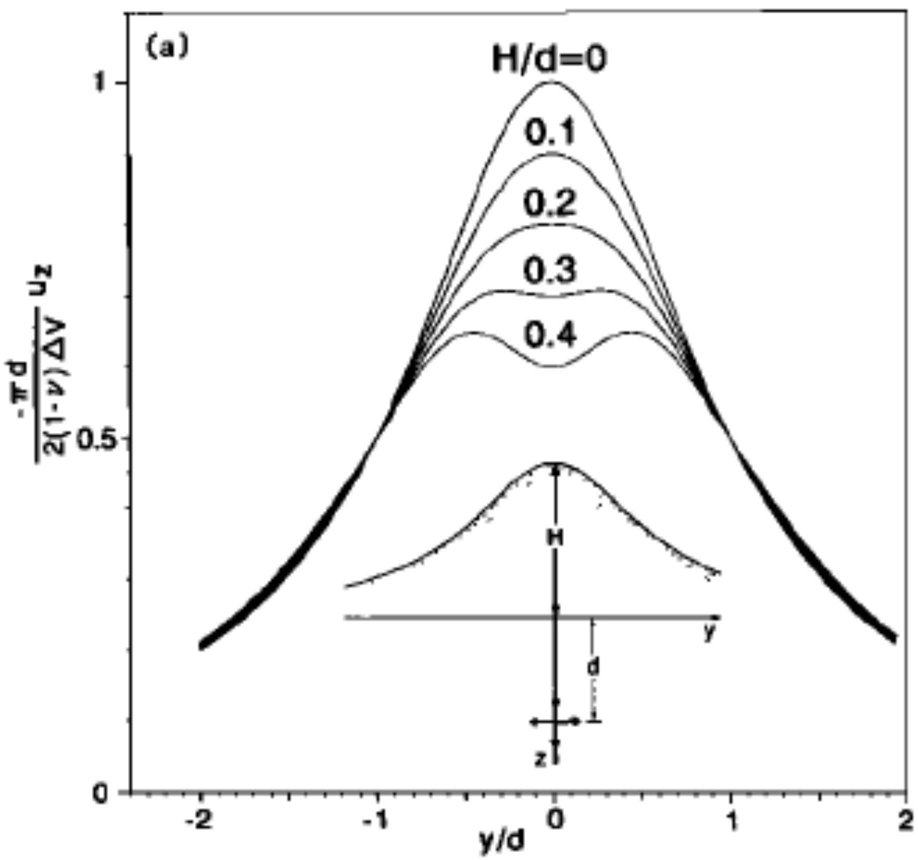

(McTigue & Segall,GRL, 1988)

Influence of reservoir geometry

Ellipsoïdal source
Yang et al, JGR 88

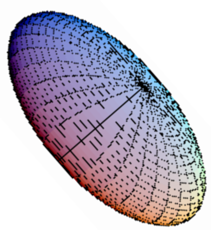

Sill
Fialko et al, 2001

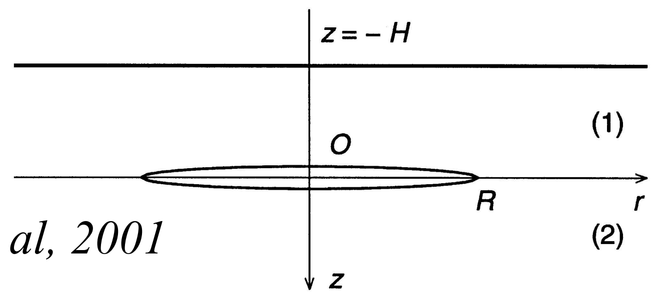

Influence of reservoir geometry

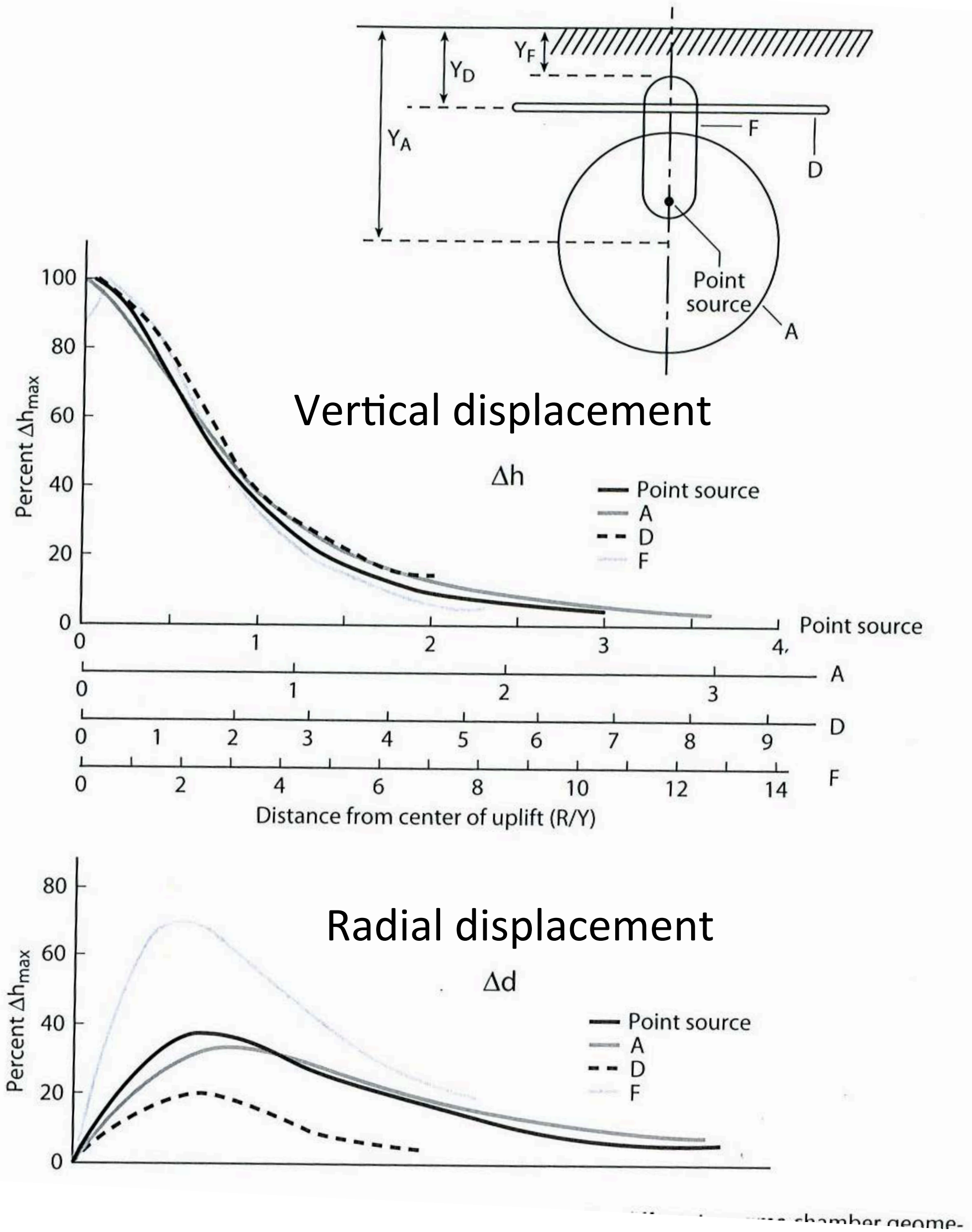

From Segall, 2010

Oblate ellipsoid

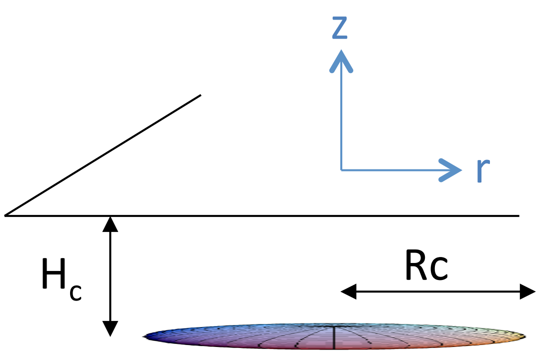

Vertical displacement:

$$U_z(z = 0, r) = 2(1 - v^2)\frac{\Delta P_c R_c^3}{E}\frac{4H_c^3}{\pi\,({H_c}^2 + r^2)^{5/2}}$$

Horizontal displacement:

$$U_r(z = 0, r) = 2(1 - v^2)\frac{\Delta P_c R_c^3}{E}\frac{4H_c^2 r}{\pi({H_c}^2 + r^2)^{5/2}}$$

$$\boxed{U_z = U_r * H_c / r}$$

Influence of a viscous halo around the reservoir

Analytical solutions:

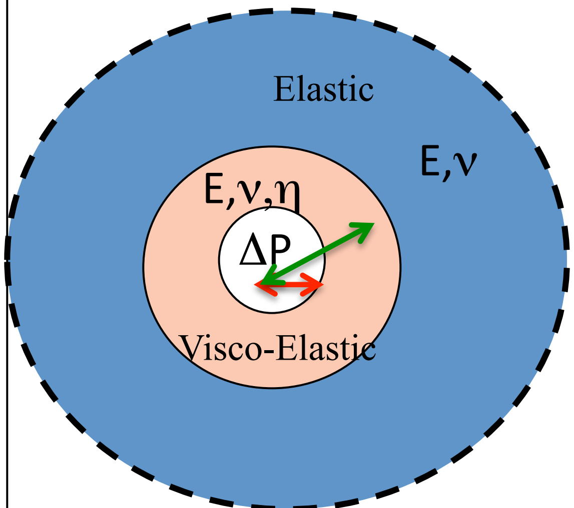

Dragoni and Magnanensi, PEPI, 1989

ΔP(t) Heaviside function (step function)

ΔP(t)=0 for t<0

= ΔP for t≥0

$$t_r = \frac{6\,\eta\,(1-\nu)R_{c2}^3}{E\,R_{c1}^3}$$

$$U_r(r,t) = \frac{(1+\nu)\Delta P R_{c1}^3}{2E}\left[e^{-\frac{t}{t_r}} + \frac{R_{c2}^3}{R_{c1}^3}\left(1-e^{-\frac{t}{t_r}}\right)\right]$$

R_{c1}: internal radius

R_{c2}: external radius

Influence of a viscous halo around the reservoir

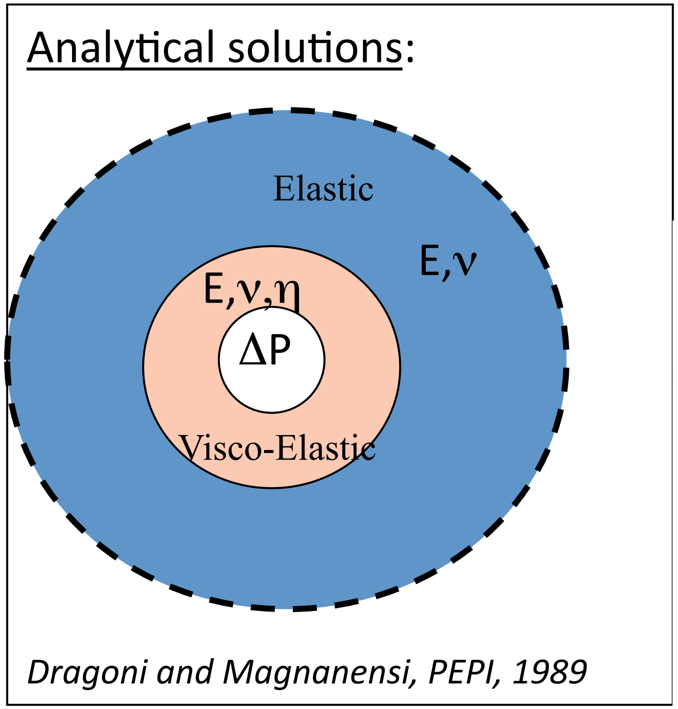

ΔP(t) Heaviside function
ΔP(t)=0 for t<0
= ΔP for t≥0

$$t_r = \frac{6\,\eta\,(1-\nu)R_{c2}^3}{E\,R_{c1}^3}$$

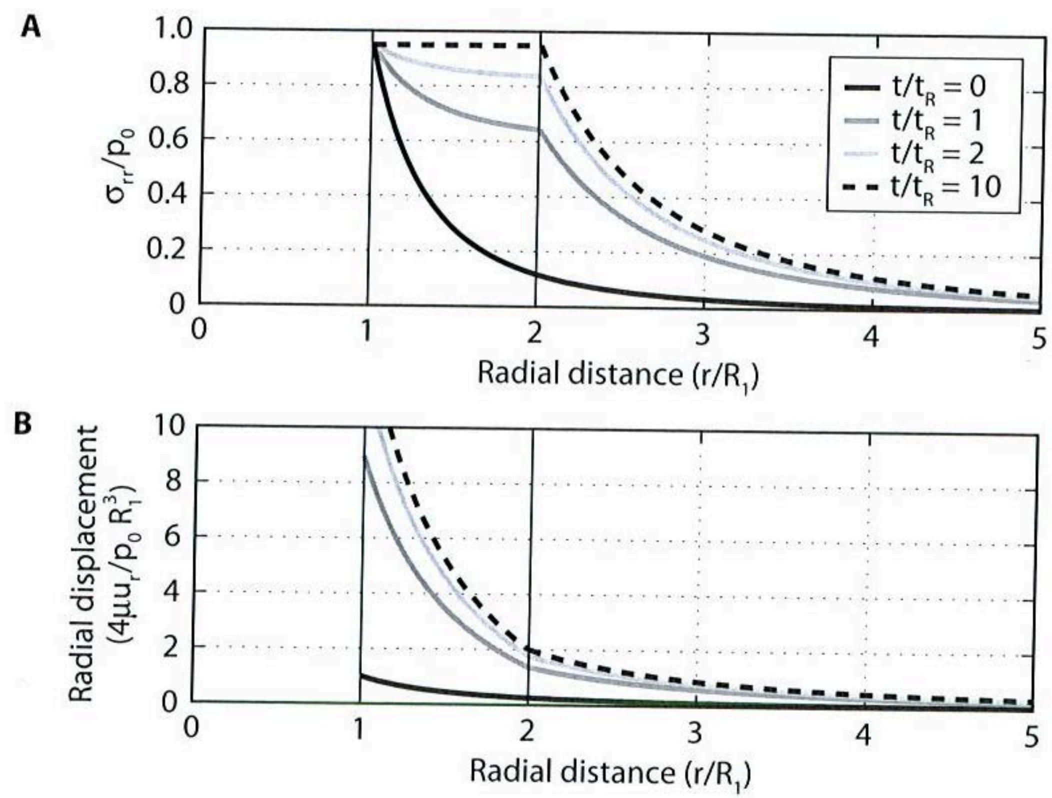

From Segall, 2010

Case $R_{2c}=2R_{c1}$

Influence of a viscous halo around the reservoir

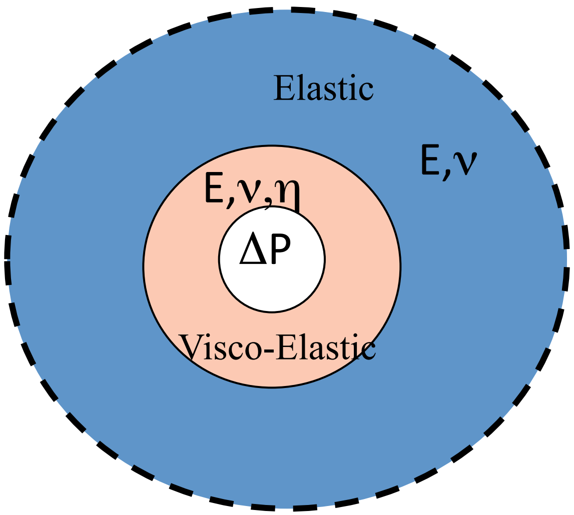

In an elastic half-space (*Segall, 2010*)

R_{c1}: radius of the chamber
R_{c2}: radius of the chamber+ the viscous shell

$\Delta P(t)$ Heaviside function
$\Delta P(t)=0$ for $t<0$
$= \Delta P$ for $t \geq 0$

$$t_r = \frac{6\,\eta\,(1-\nu) R_{c2}^3}{E\,R_{c1}^3}$$

$$U_z(z=0,r,t) = 2(1-\nu^2)\frac{\Delta P_c R_c^3}{E}\frac{H_c}{({H_c}^2+r^2)^{3/2}}\left[e^{-\frac{t}{t_r}} + \frac{R_{c2}^3}{R_{c1}^3}\left(1-e^{-\frac{t}{t_r}}\right)\right]$$

Influence of a viscous halo around the reservoir

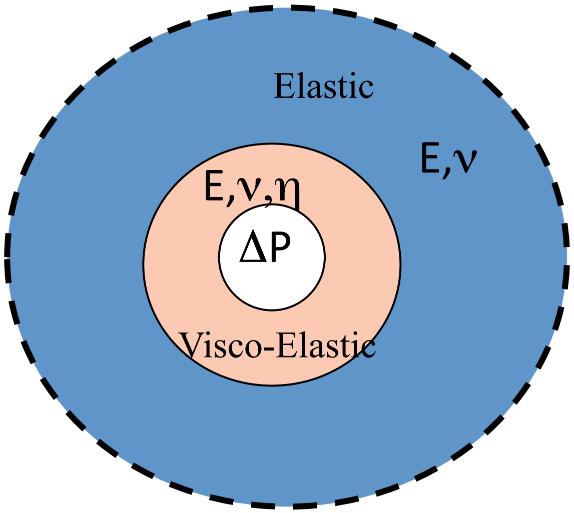

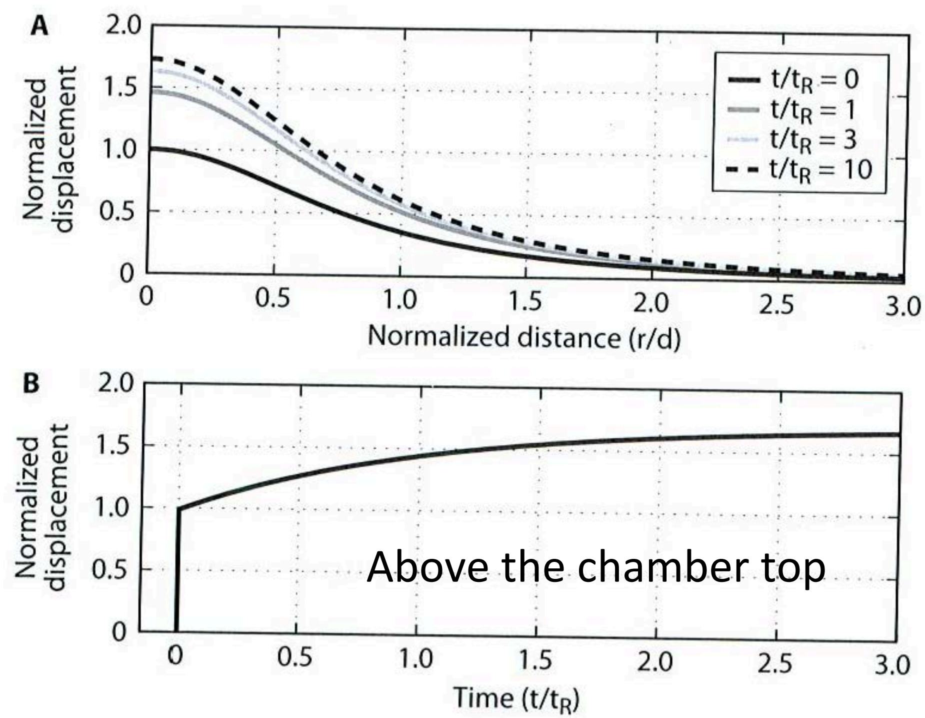

$$U_z(z=0,r,t) = 2(1-\upsilon^2)\frac{\Delta P_c R_c^3}{E}\frac{H_c}{({H_c}^2+r^2)^{3/2}}\left[e^{-\frac{t}{t_r}} + \frac{R_{c2}^3}{R_{c1}^3}\left(1-e^{-\frac{t}{t_r}}\right)\right]$$

From Segall, 2010

The « Okada » model (1985)

Dislocation in an homogeneous elastic half-space.
10 parameters: Latitude, Longitude, Depth, Width, Length, Strike, Dip, Rake, Displacement vector (tangential+normal).

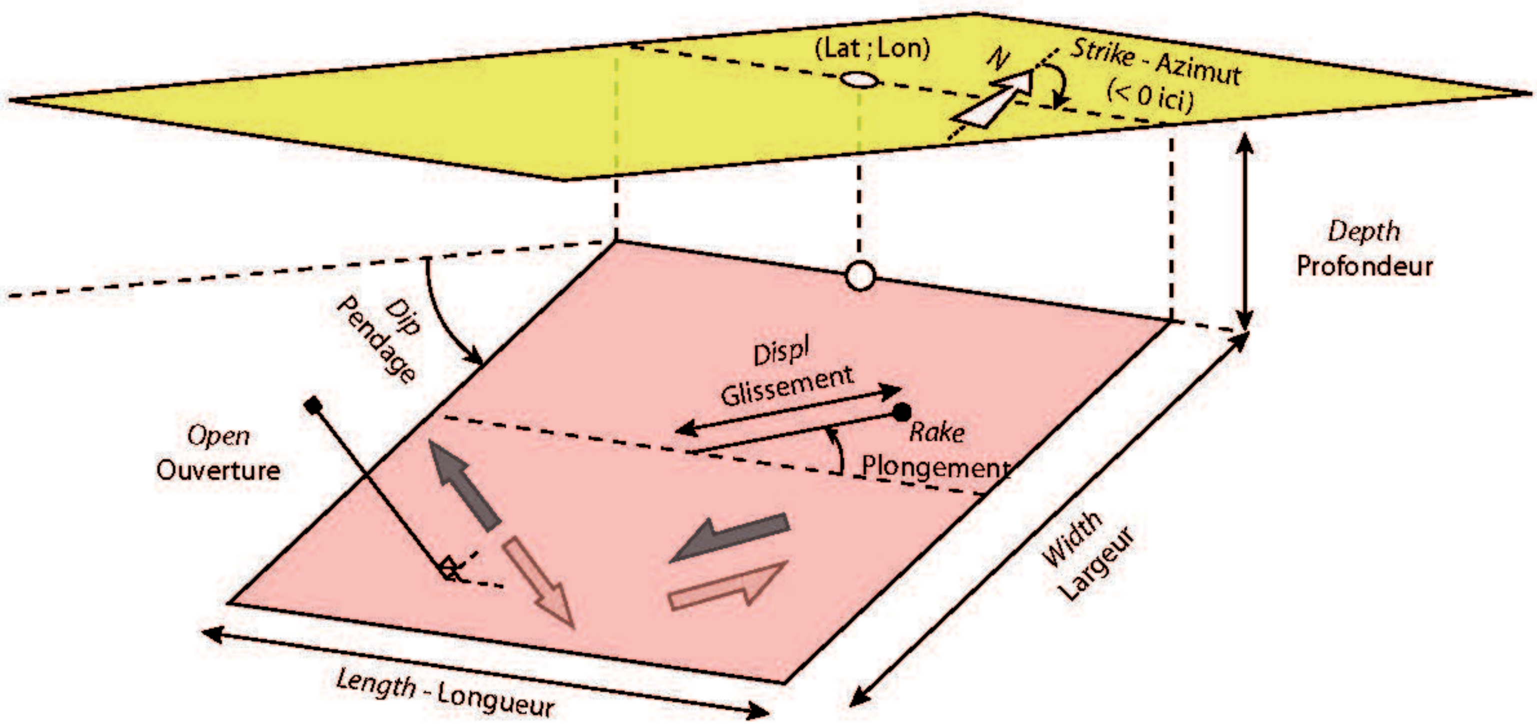

Useful to model dykes or sills, the normal component of the displacement vector (opening) dominates.

The « Okada » model (1985)

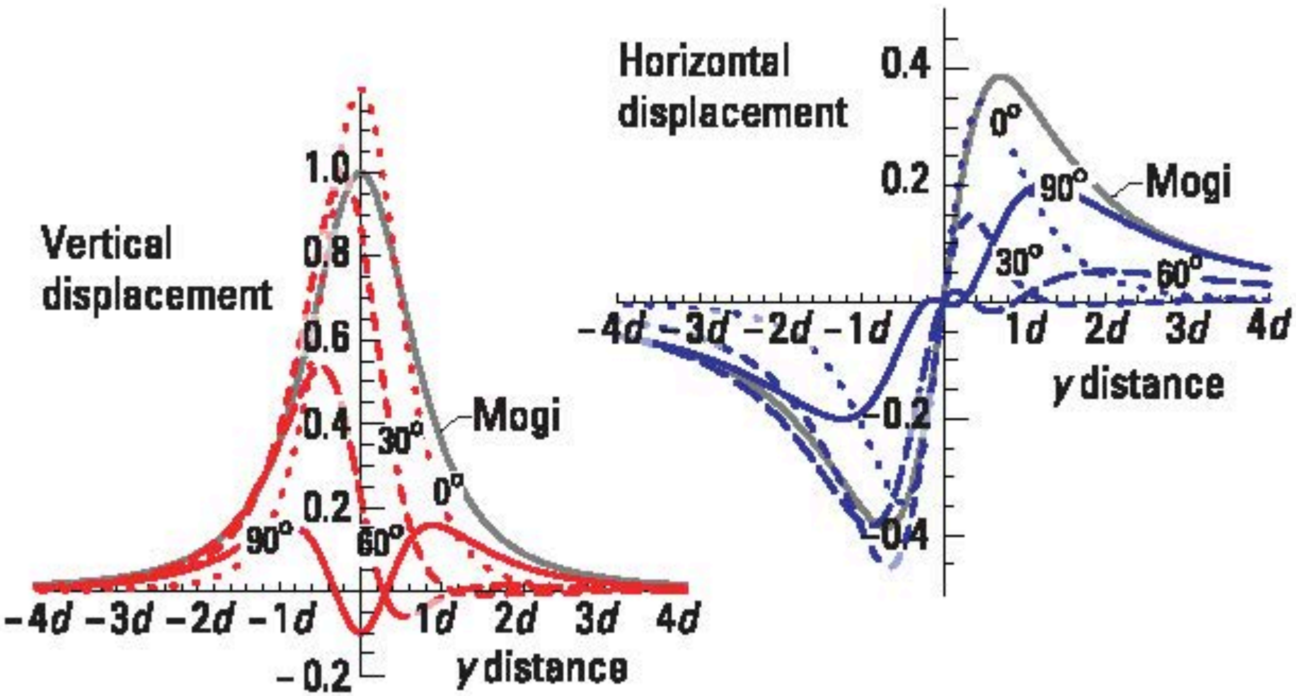

Figure 8.33. Profiles of normalized vertical (*left*) and horizontal (*right*) displacements across a point tension crack with dips of 0°, 30°, 60°, and 90°. The distance is in source depths. A profile for a point source with equivalent moment is shown in gray for comparison.

From Dzurisin, 2007

The « Okada » model (1985)

The eruptive fissure can be discretized in a large number of small elements with a given displacement vector.

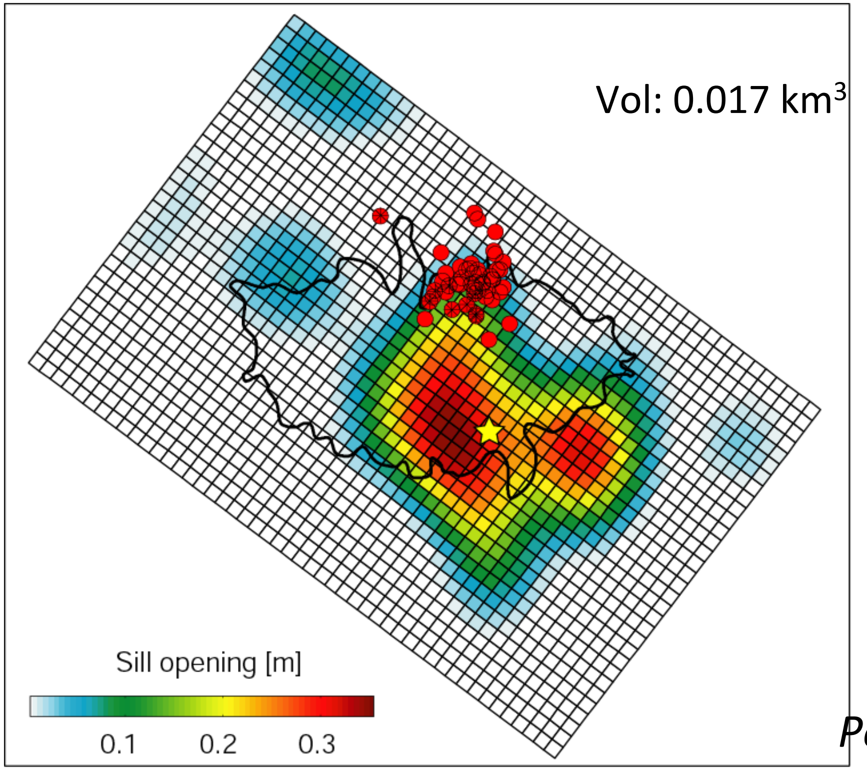

Intrusion depth:

4.5-6.0 km

Pedersen & Sigmundsson, 2004

Disadvantage: we get an opening distribution however we would like a pressure distribution.

Magma flow within a conduit

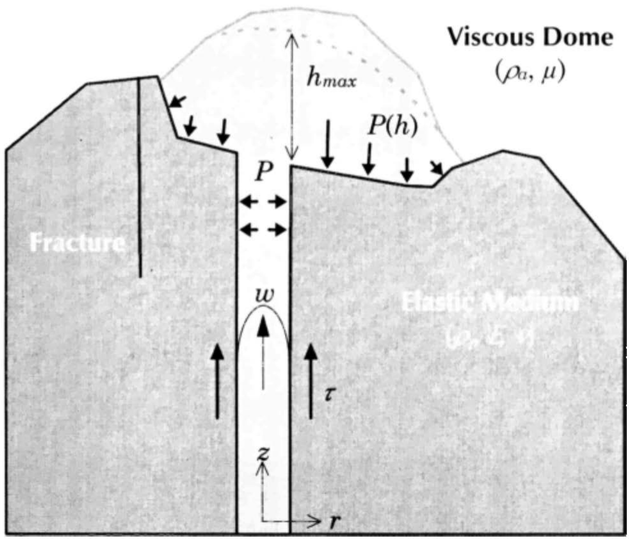

a_c

Beauducel, 2000

Overpressurized conduit (Love 1987):

$$U_r = \frac{a_c^2 P_c}{2rG},$$

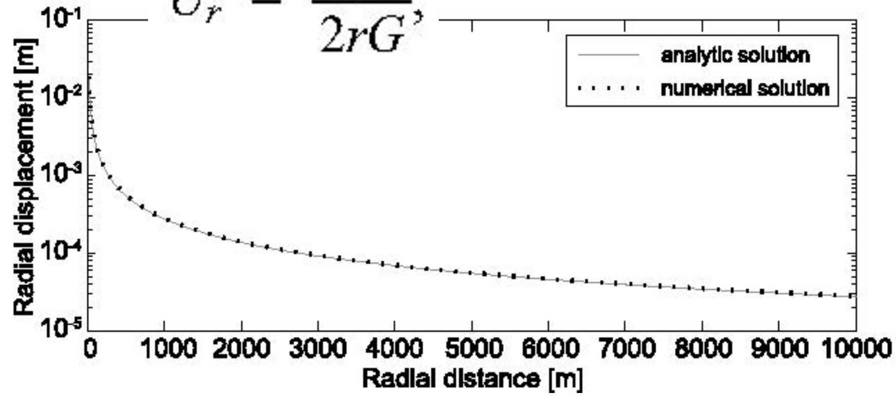

Shear along the conduit walll (Anderson, 2010):

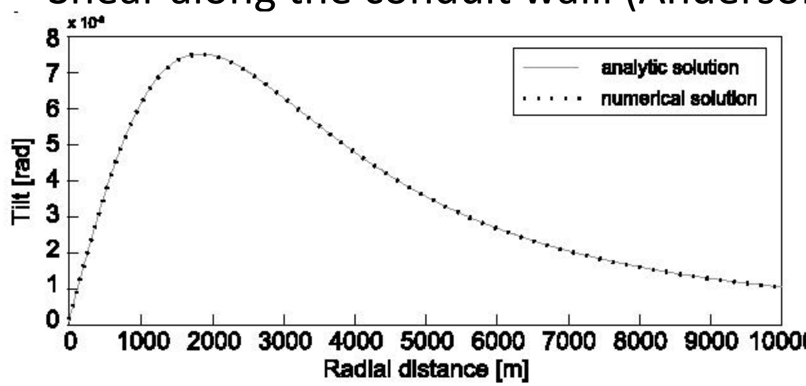

L=5km, a_c=15m,G=0.8GPa, ν=0.25, P=10MPa, τ=3kPa

Displacement induced by the surface load

Displacement induced by a point source load **on a elastic half-space**:

$$U_{r\,G^{\infty}}(r) = -\frac{g}{2\pi}\frac{(1+\nu)(1-2\nu)}{E}\frac{1}{r}$$

$$U_{z\,G^{\infty}}(r) = \frac{g}{\pi}\frac{1-\nu^2}{E}\frac{1}{r}$$

Integrating, we have the solution for any surface load distribution

$$U_z^{\infty}(\vec{r}) = \int_R U_{z\,G^{\infty}}(\vec{r}-\vec{r'})\rho(\vec{r'})h(\vec{r'})\,dS(\vec{r'})$$

Pinel et al, GJInt, 2007

Displacement induced by the surface load

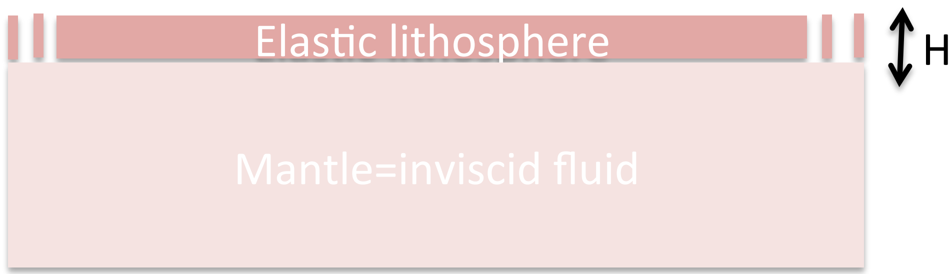

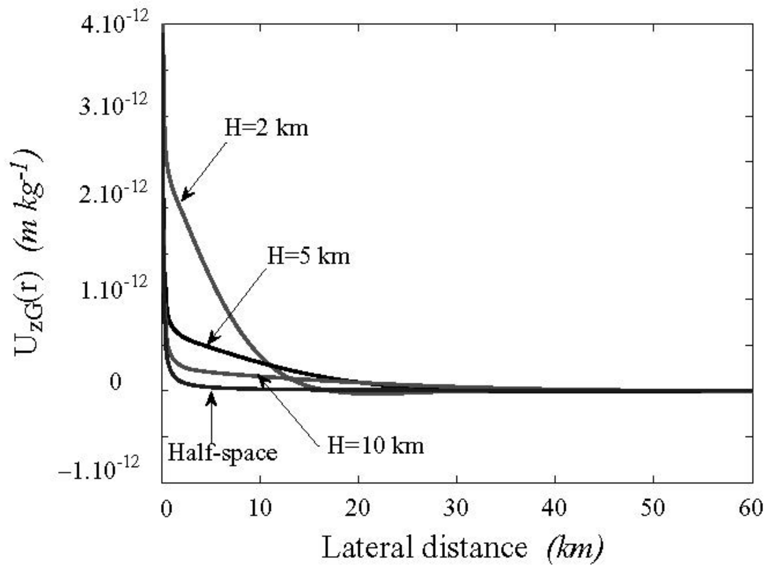

Figure 1. Vertical displacement as a function of lateral distance. Curves represent the value of $U_{zG\infty}$ (half-space case) and U_{zGH} with $H = 2$, 5 and 10 km (thick plate case). Calculations are done with $\nu = 0.25$ and $E =$ 15 GPa. The curve representing U_{zGH} for $H = 50$ km overlaps with the curve for the half-space.

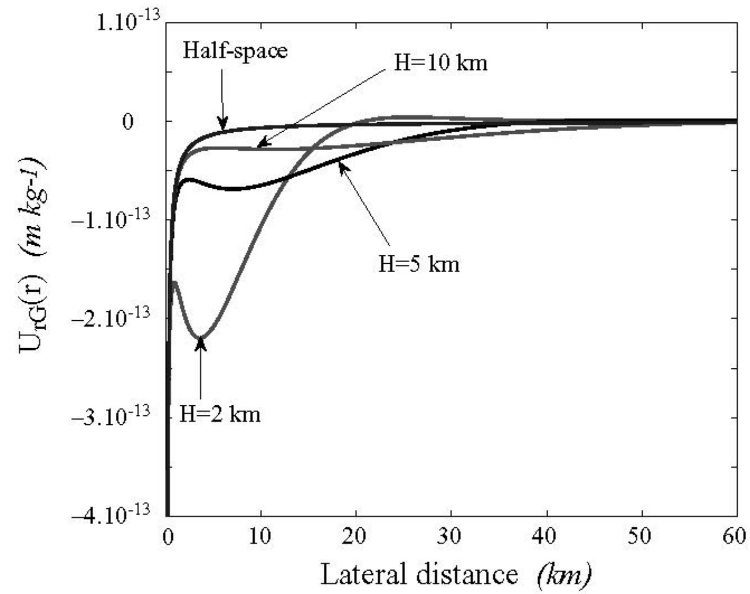

Figure 2. Radial displacement as a function of lateral distance. Curves represent the value of $U_{rG\infty}$ (half-space case) and U_{rGH} with $H = 2$, 5 and 10 km (thick plate case). Calculations are done with $\nu = 0.25$ and $E = 15$ GPa. The curve representing U_{rGH} for $H = 50$ km overlaps with the curve for the half-space.

Pinel et al, GJInt, 2007

Displacement induced by the surface load

Model :

Spatial integration of Green's function :

For an elastic half-space

U_{inf}

Parameters: Young's modulus E, ν

Instantaneous response

Seasonal effect

For a thick plate overlying an inviscid fluid

U_H

Parameters: Young's modulus E, ν
Plate thickness H, Mantle density ρ_M

Fully relaxed response

$$U(r,t)=(U_{inf}(r)-U_H(r))e^{-t/t_R}+U_H(r)$$

with t_R depending on mantle viscosity (μ) estimated using a disk load on an elastic plate lying above a viscous medium

Long term effect

Volcanic edifice instability

Displacement occurs when

$\sigma_t > So + \tan\phi\ (\sigma_n - P_f)$
with ϕ the angle of internal friction
P_f: fluid pressure
σ_t : tangential stress
σ_n :normal stress

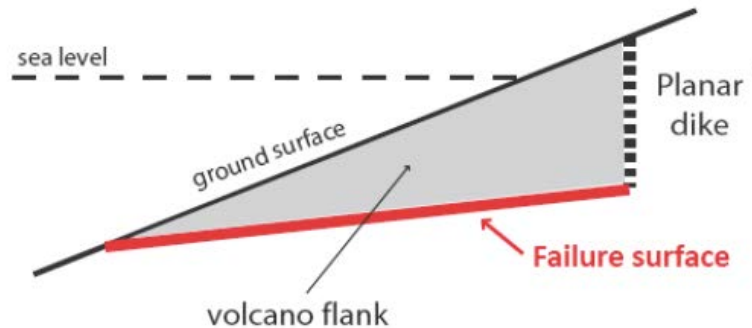

Elsworth &Voight, 1995

Modeling of deformation sources

2- Numerical models

-Advantages

-Remaining problems

NUMERICAL MODELING: spatial and temporal discretization

An added step: The meshing

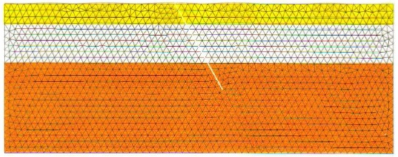

Various methods:

*Based on continuum physics

The physics is approximately solved for each element at each time step.

-Finite difference

-Finite Element

-Boundary element

*Discrete Element methods:

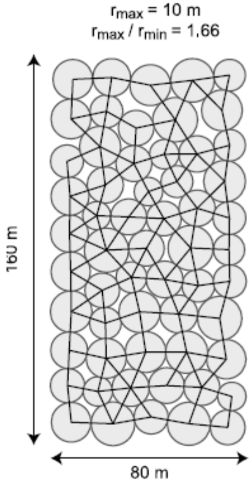

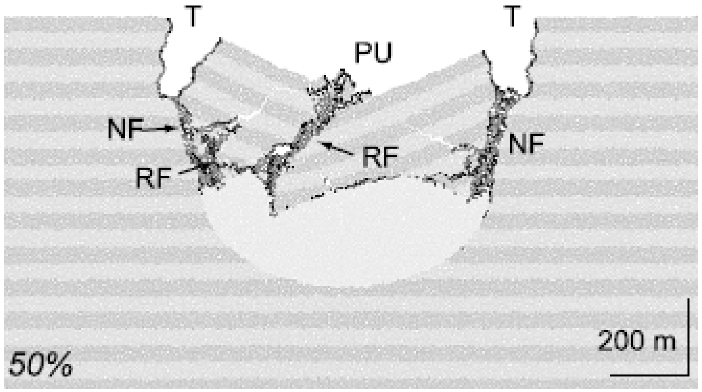

From Holohan et al, JGR, 2011

More complexe geometry: real topography

Analytical solutions:
Small slope influence can be estimated

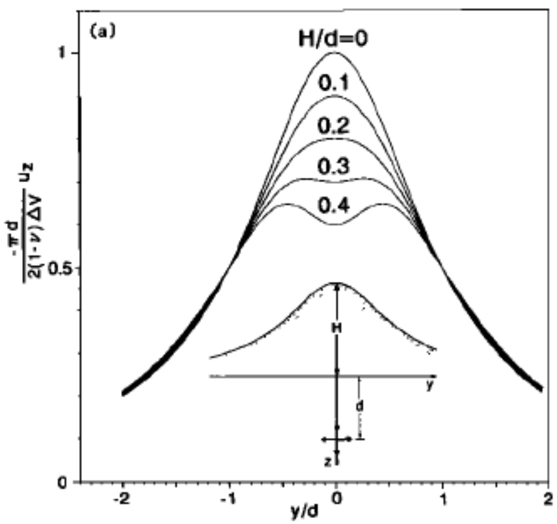

(McTigue & Segall,GRL, 1988)

Numerical models: real DEM

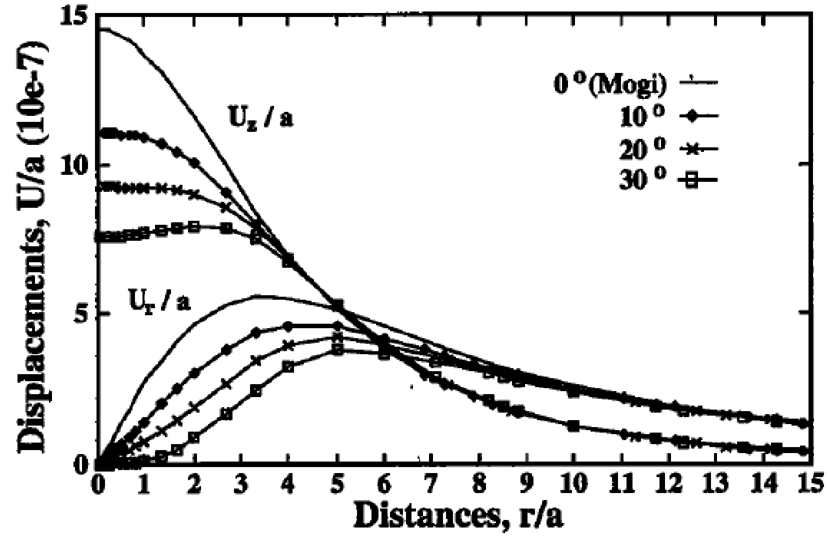

From Cayol et Cornet, GRL, 98

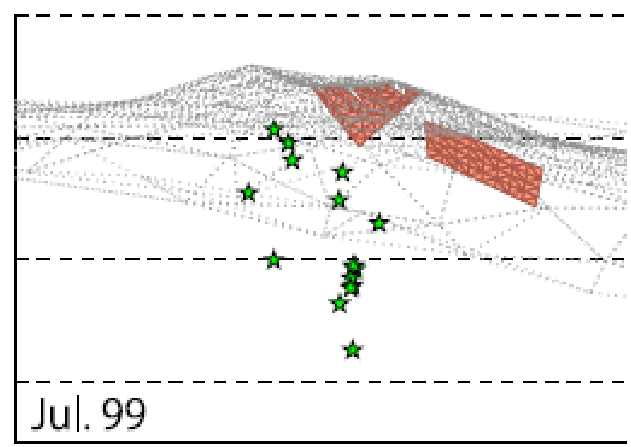

From Fukushima et al, JGR, 2010

More complexe geometry: reservoir shapes

<u>Analytical solutions:</u>

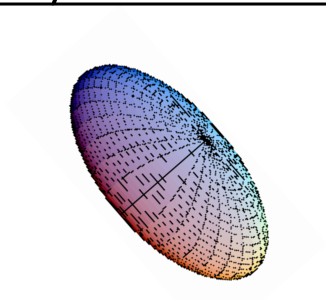

Ellipsoidal shape

(Yang et al,JGR, 1988)

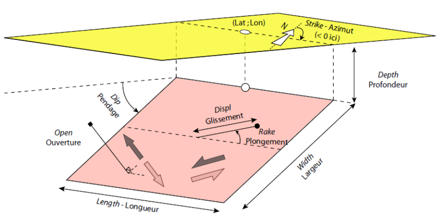

Dislocations

(Okada, 1985)

<u>Numerical models</u>:

Completely free ….

even if most often simple shape are tested mainly because of the lack of information on real shapes

Heterogeneous medium

<u>Analytical solutions</u>:
Only homogeneous or layered medium.

<u>Numerical models</u>:

Results from tomography can be used….

Chiarabba et al., 2006

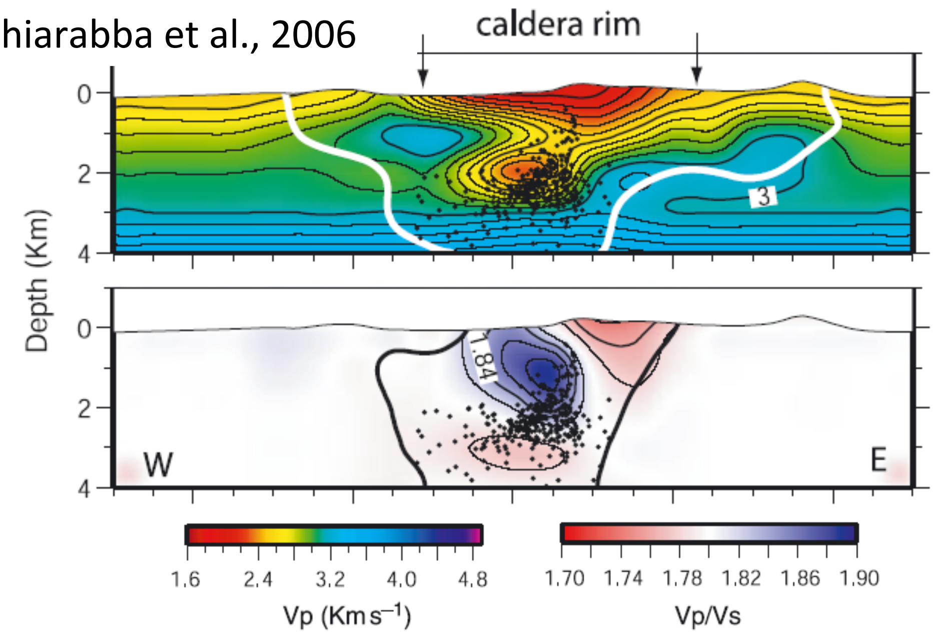

…in order to define spatial distribution of elastic parameters

$$E = 5/6 \rho V_p^2$$

$$\nu = [(V_p / V_s)^2 - 2]/[2(V_p / V_s)^2 - 2]$$

More complex rheology

Analytical solutions:

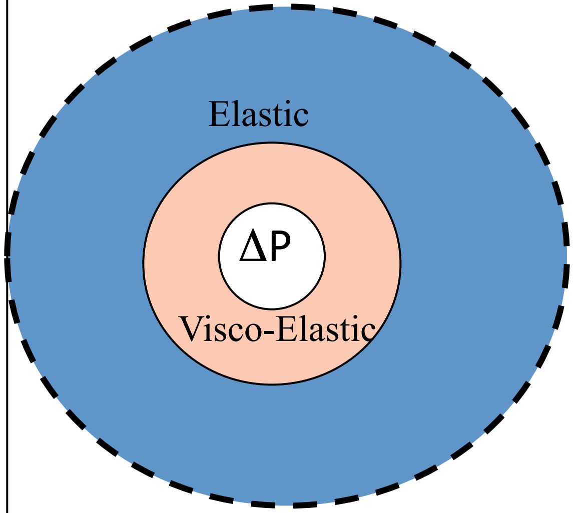

Dragoni and Magnanensi, PEPI, 1989

Numerical models:

-Visco-elasticity (Pearse et al,*JGR* 2010, *Del Negro et al, PEPI, 2009*…)

-Elasto-plasticity *(Currenti et al, JGR 2010)*

More realistic initial state

Analytical solutions:
Isotropic initial stress field

Numerical models:

*Lithostatic:
- Isotropic (*Mc Garr, 1988)*

- $$\sigma_{xx} = \sigma_{yy} = \frac{\nu}{1-\nu}\sigma_{zz}$$

(Jaeger and Cook, 1979)

*Close to failure and water saturated
(Townend and Zoback, 2000)

$$\sigma_{xx} = \sigma_{yy} = [\frac{\sqrt{1+\mu^2}-\mu}{\sqrt{1+\mu^2}+\mu} + 2\frac{\rho_w}{\rho_r}\frac{\mu}{\sqrt{1+\mu^2}+\mu}]\sigma_{zz}$$

More realistic initial state

<u>Analytical solutions</u>:
Isotropic initial stress field

<u>Numerical models:</u>

Isotropic stress field

Stress field in extension

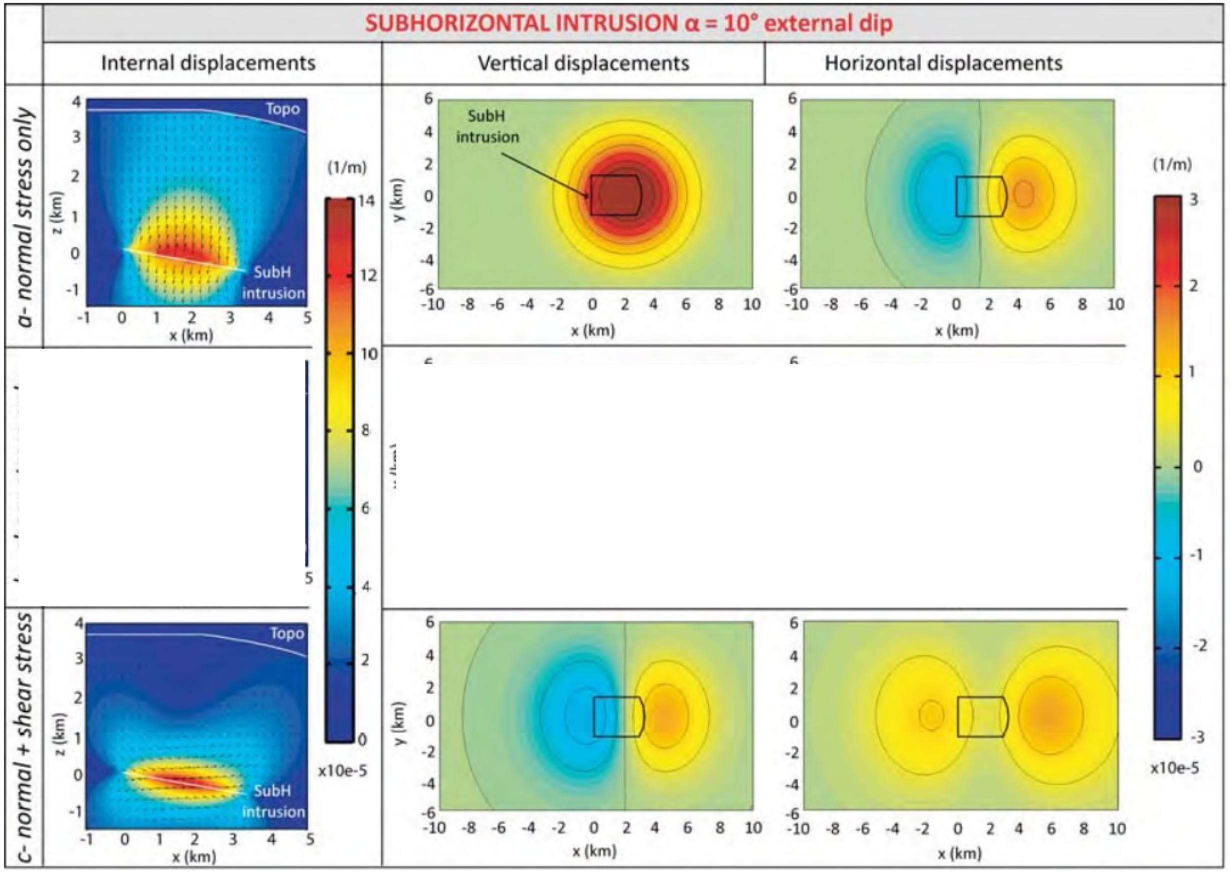

From Catry, PhD Thesis 2011

Coupling various physics

Analytical solution:
One problem at once

Numerical models:

Coupled model

Heat conduction equation
⇩
Temperature profile

Viscoelastic model
⇩
Numerical solution of deformation field

Thermal boundary condition

$$T(z) = T_s + \left(\frac{q_m z}{k}\right) + \left(\frac{A_s b^2}{k}\right)\left(1 - e^{-z/b}\right)$$

$$\eta = A_D exp\left(\frac{E}{RT}\right)$$

Thermal parameters	
Ts	273 K
qm	0.03 mWm^{-2}
k	4 Wm^{-1}K^{-1}
As	2.47 10^{-6} Wm^{-3}
b	14.170 km
Mechanical parameters	
A_D	10^9 Pas
E	120 kJ/(mol)
K	8.314 J/(mol K)

Temperature and viscosity profile

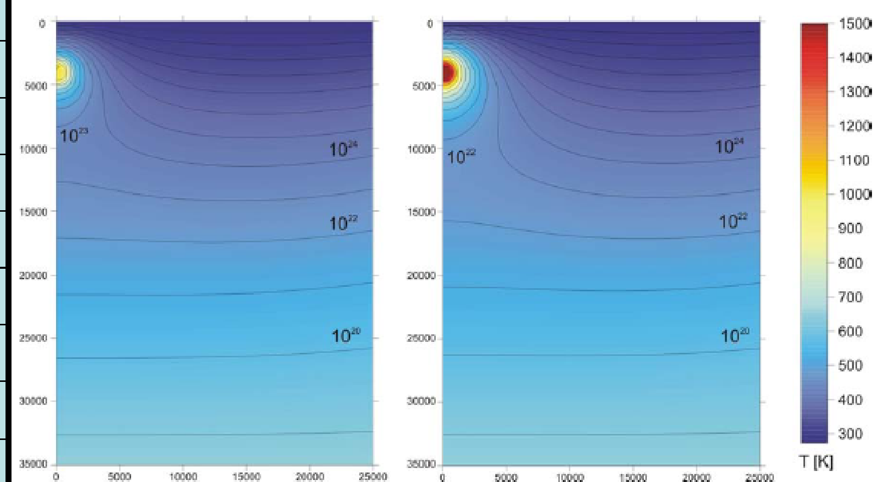

From Del Negro et al, PEPI, 2009

Hydrothermal systems modeling

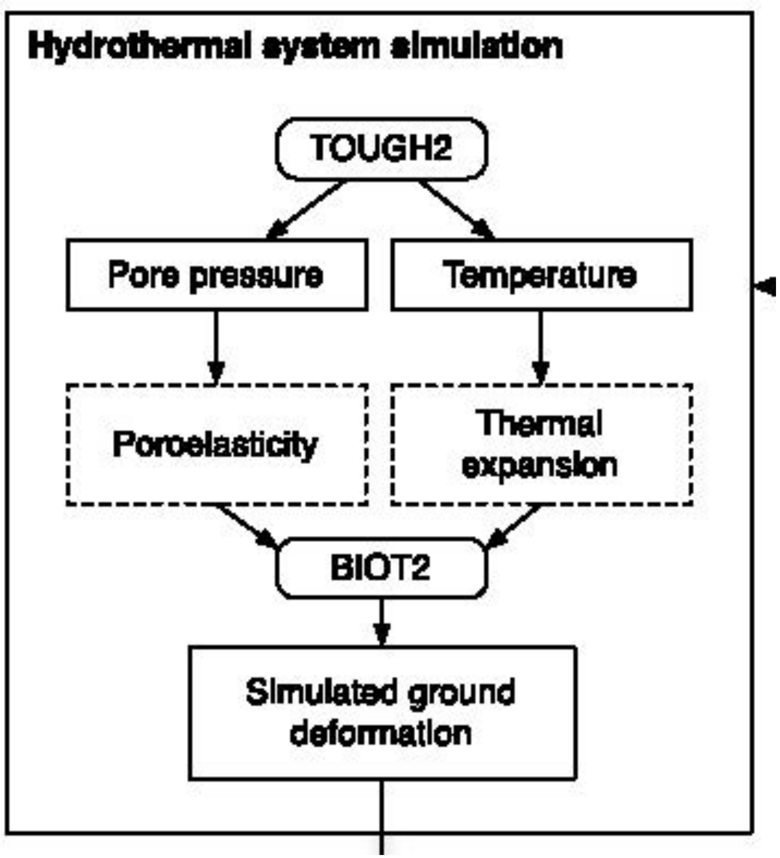

From Fournier & Chardot , 2012

Hydrothermal systems modeling

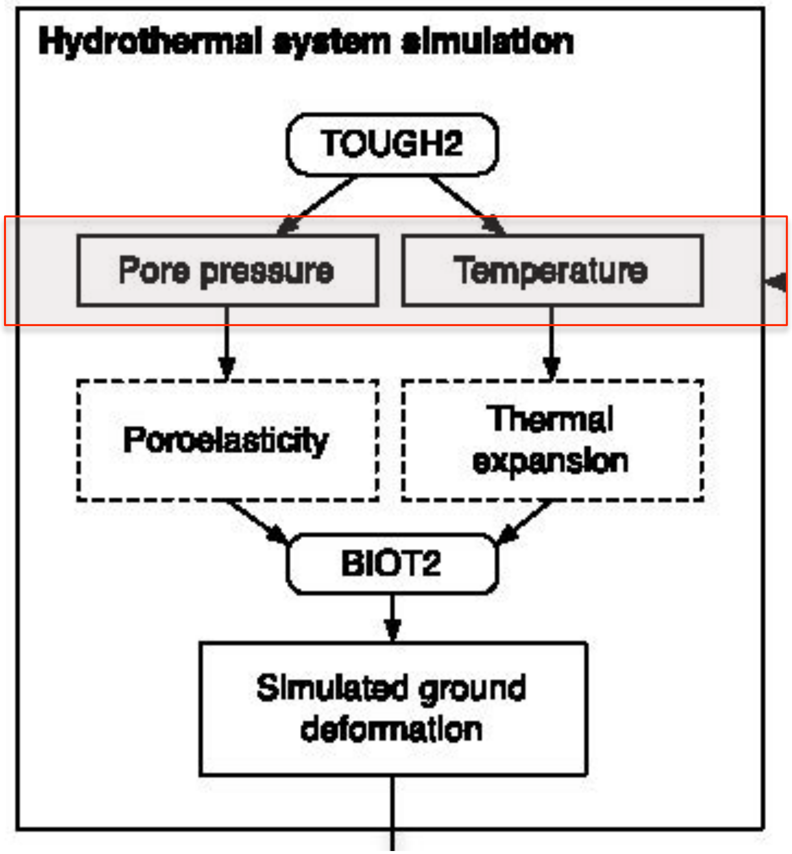

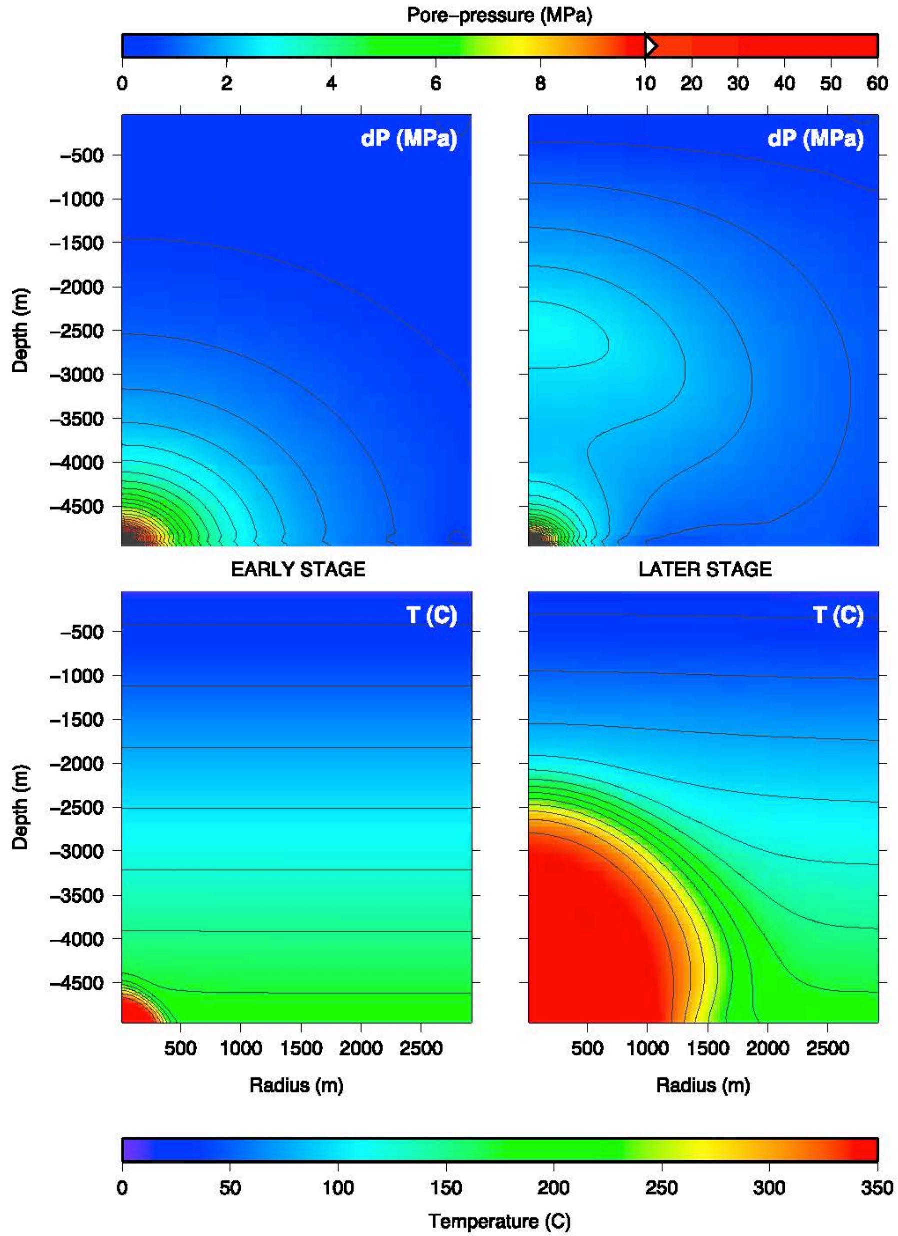

From Fournier & Chardot , 2012

Hydrothermal systems modeling

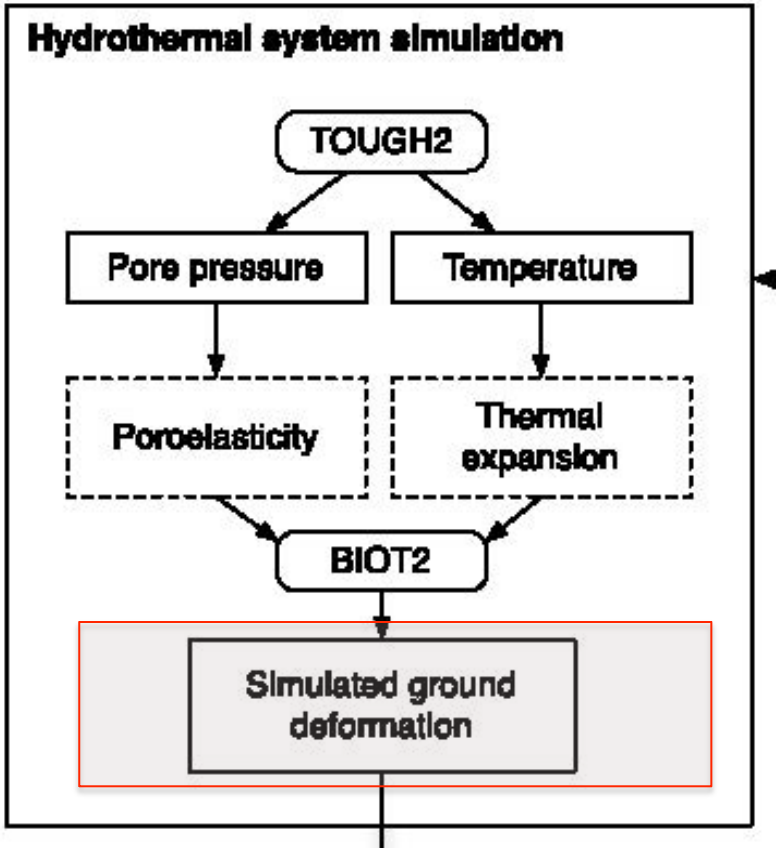

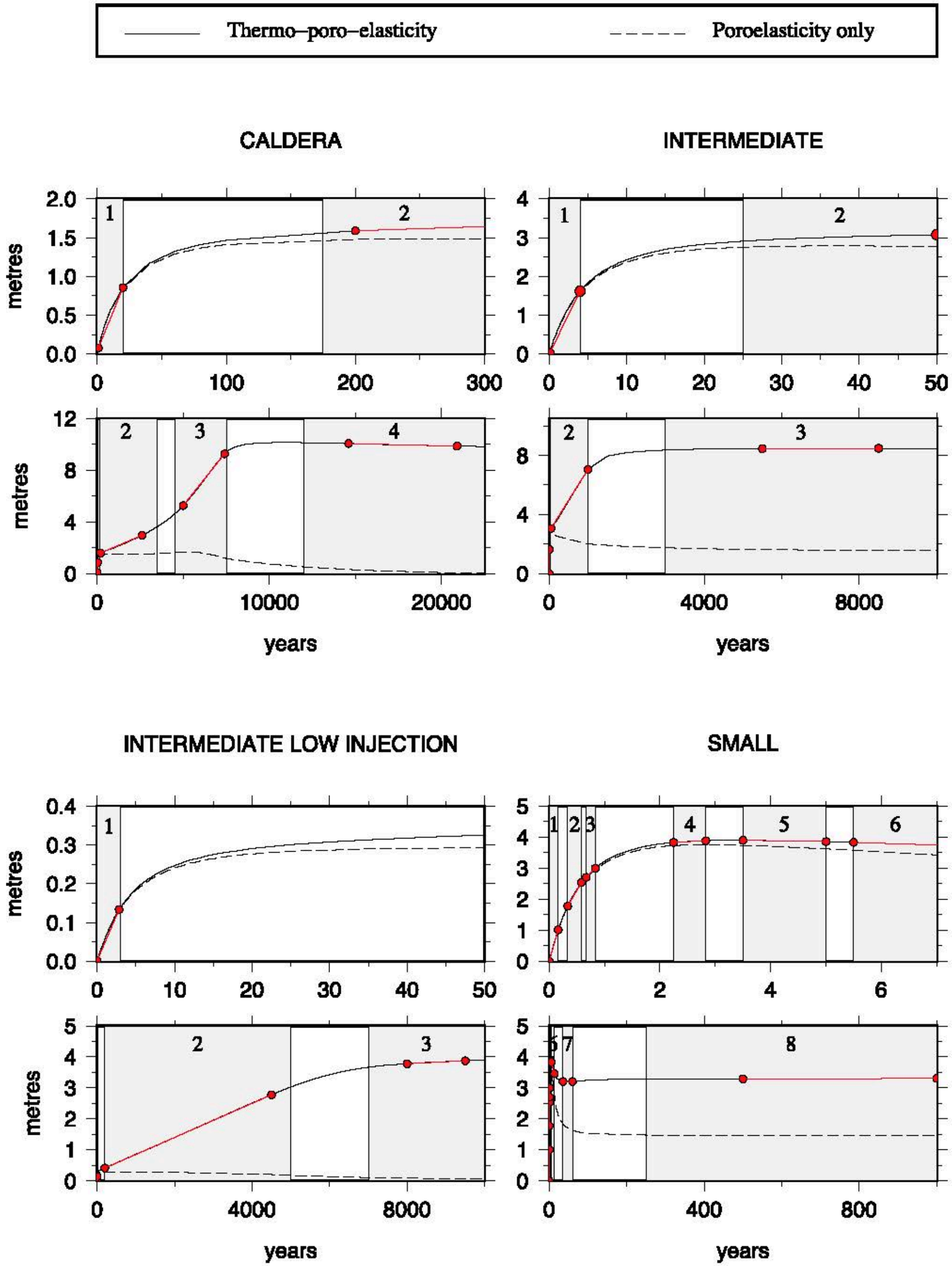

From Fournier & Chardot , 2012

Hydrothermal systems modeling

Table 1. TOUGH2 Models Parameters: Domain Dimensions, Injection Depths, Durations and Rates, and Fluid Temperature[a]

Model	Radius (km)	Inject. Depth (km)	Duration (kyr)	Inject. Temperature (°C)	Inject. Rate H_2O ($t\ d^{-1}$)	Inject. Rate CO_2 ($t\ d^{-1}$)
1 Large caldera	50	5	22.5	350	10×10^3	500
2 Intermediate	5	1.7	10	350	10×10^3	500
3 Intermediate	5	1.7	10	350	1×10^3	50
4 Small	5	0.5	10	250	10×10^3	500

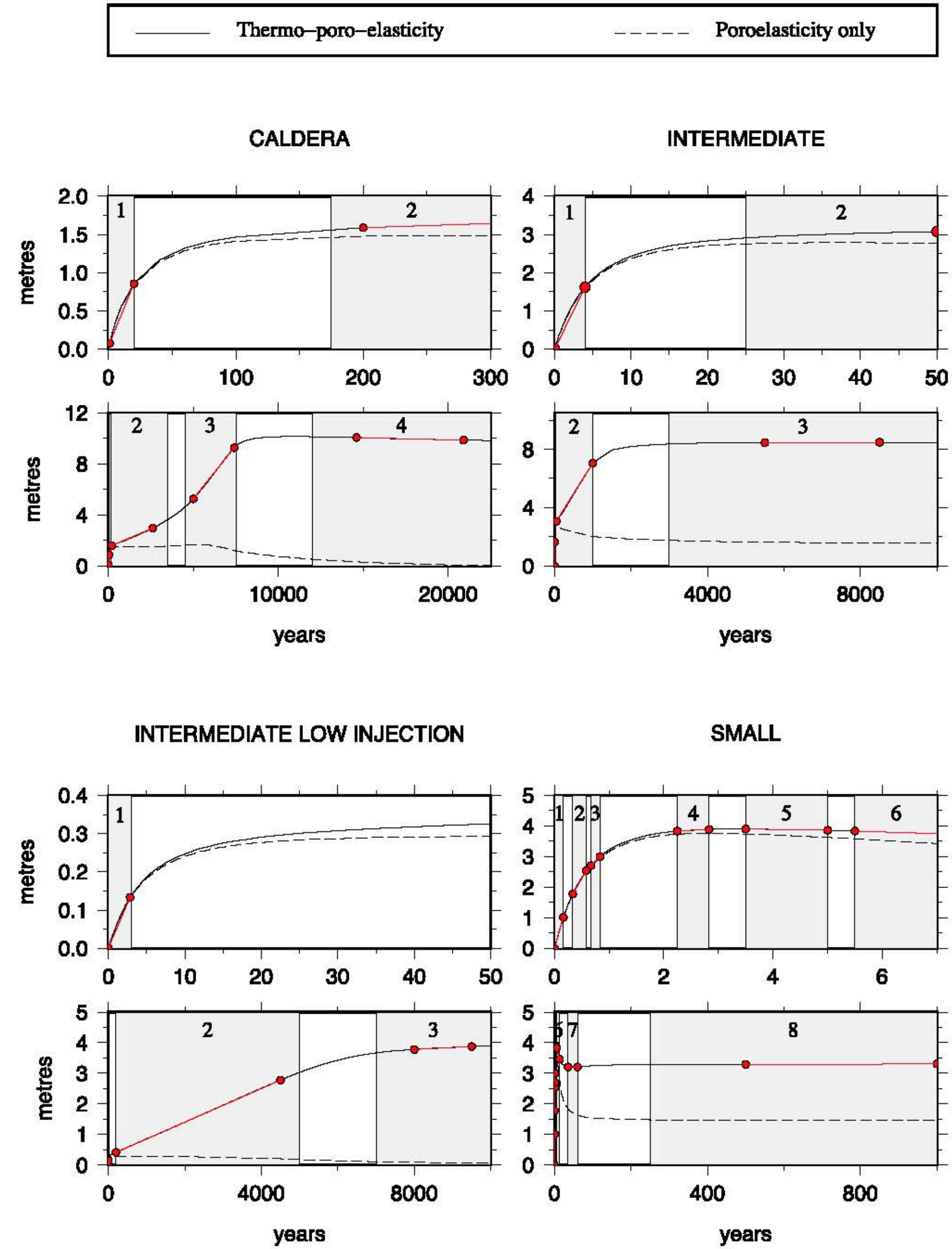

From Fournier & Chardot , 2012

Fluid-structure interaction

Analytical solution:
Usually one medium is considered

<u>Numerical models:</u>

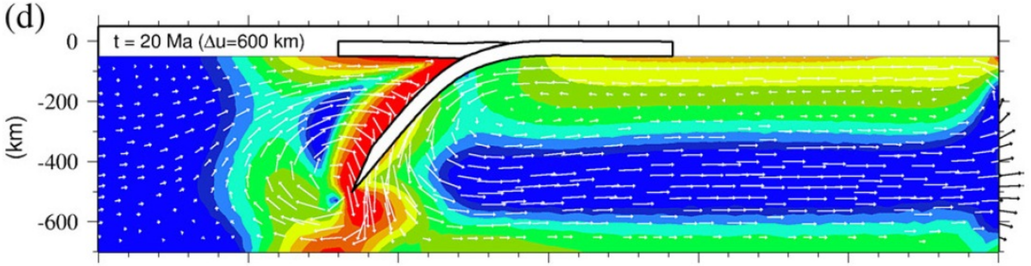

From Bonnardot et al, EPSL, 2008

<u>At the fluid surface interface:</u>

- same velocity for the fluid and the solid
- Continuity of the stress vector applied at the surface

Fluid-structure interaction
A key problem in volcanology

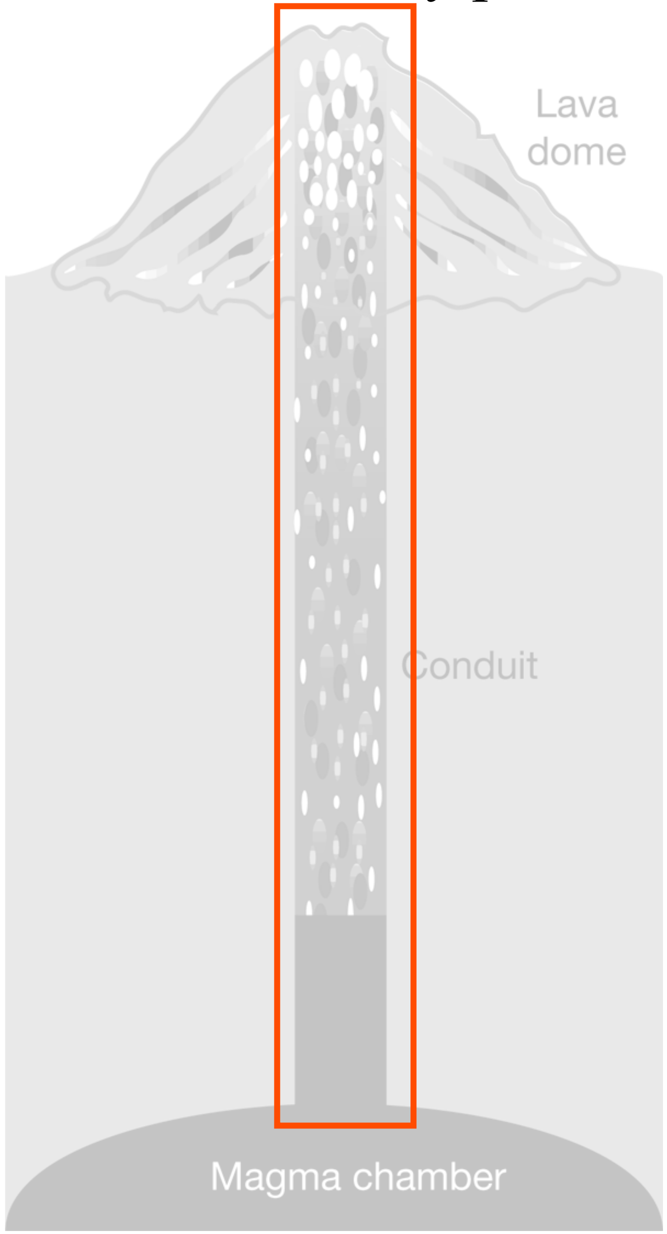

Models of fluid flow in a rigid conduit
-including crystallization, degassing…,
-aiming at understanding
effusive/explosive transitions, flux rate variations
Sparks, 1997, Melnik & Sparks 1999, Barmin et al., 2002

Plug formation is expected.

Not often linked to geophysical observations

Fluid-structure interaction
A key problem in volcanology

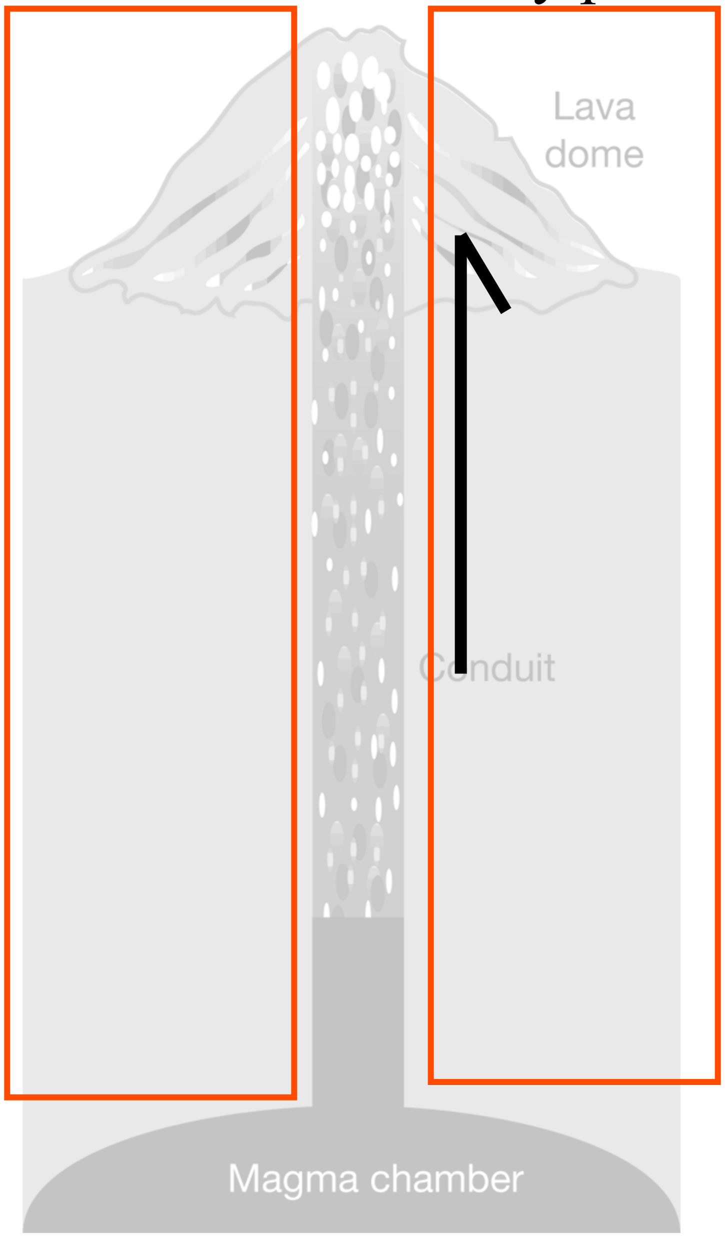

Models used to interpret geophysical observations

(Beauducel et al, 2000, Green et al, 2006, Anderson et al, 2011…)

Not often related to the physics of magma flow

Fluid-structure interaction
A key problem in volcanology

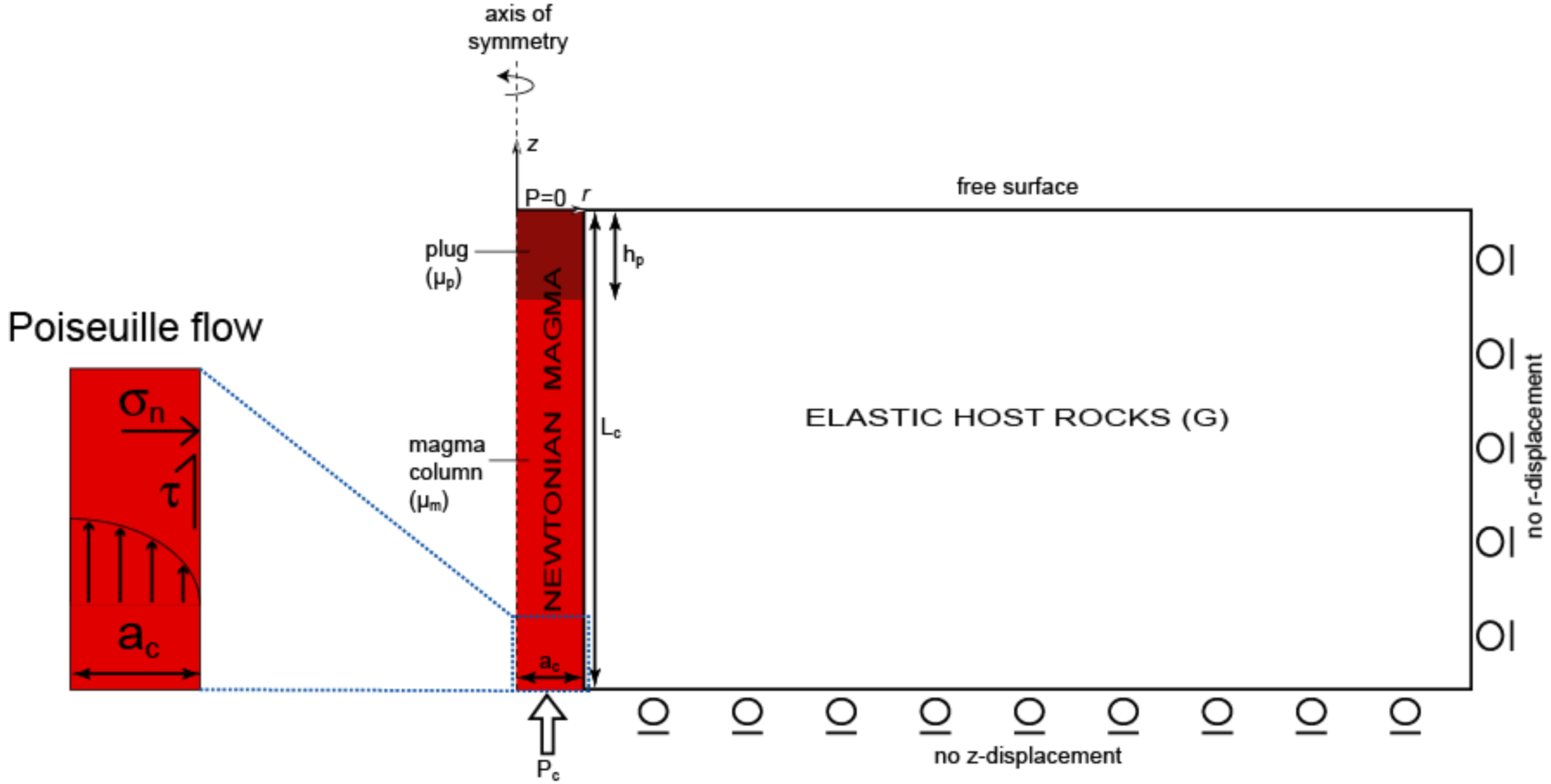

- Axial symmetry
- Stress continuity at the solid-fluid interface
- Full coupling considering the conduit deformation

→Quantification of deformation induced by plug formation

(Albino et al, GJInt, 2011)

NUMERICAL MODELS VALIDATION: A REQUIRED STEP

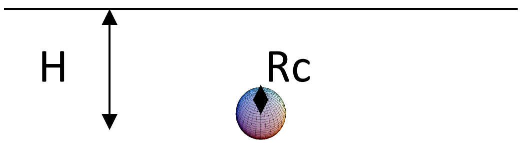

Case Rc/H=0.1

Radial displacement

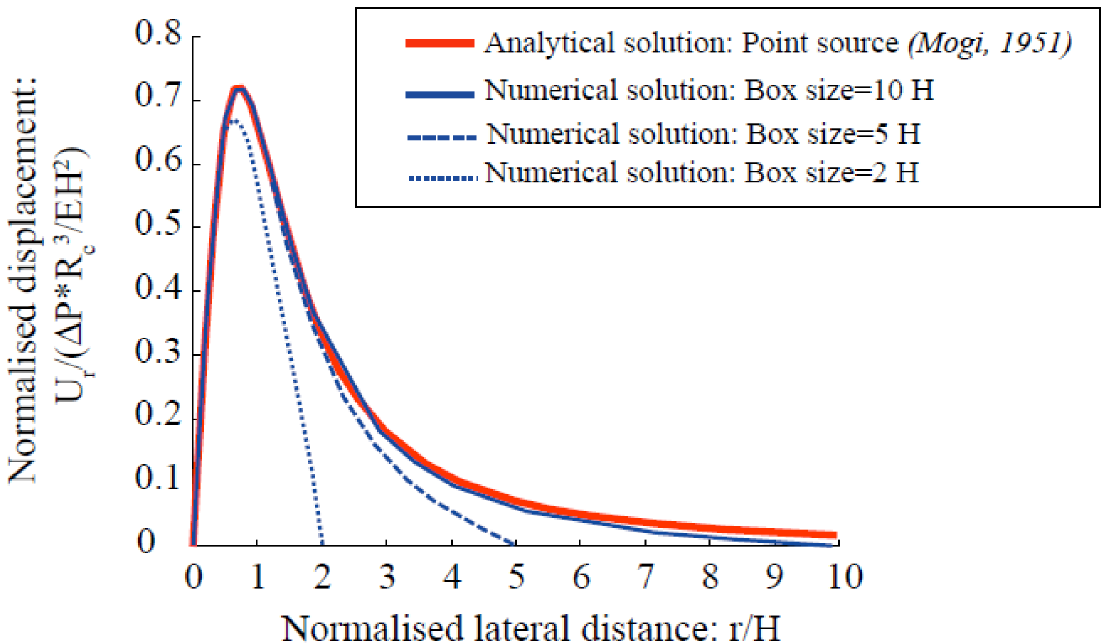

NUMERICAL MODELS VALIDATION: A REQUIRED STEP

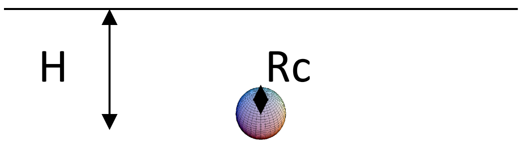

Box size is 10H.

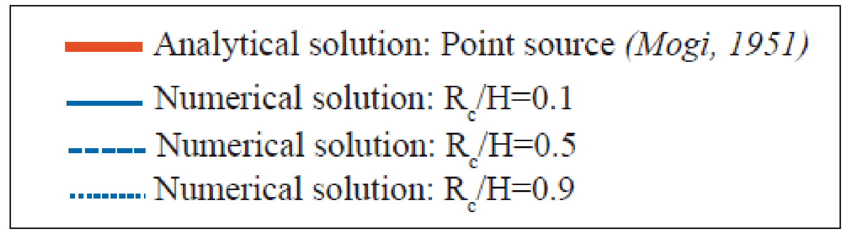

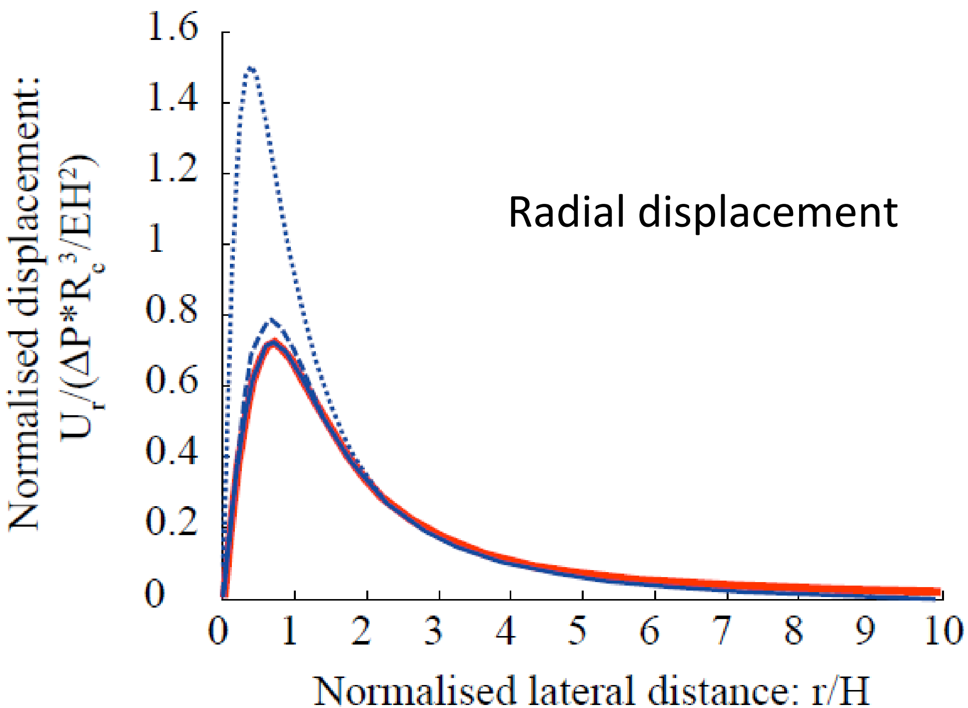

Sub-surface properties are not well-constrained

For instance, close to the surface, static elastic parameters might be different from the dynamic ones:

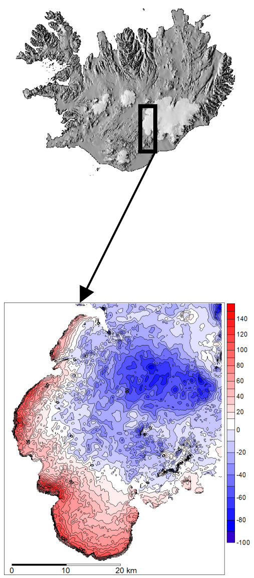

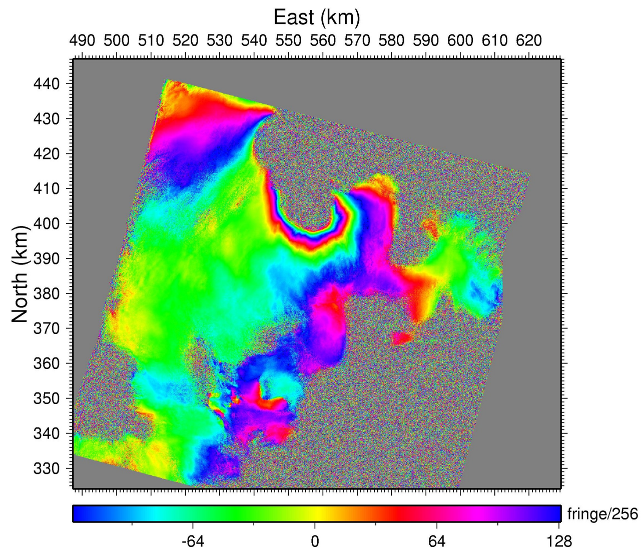

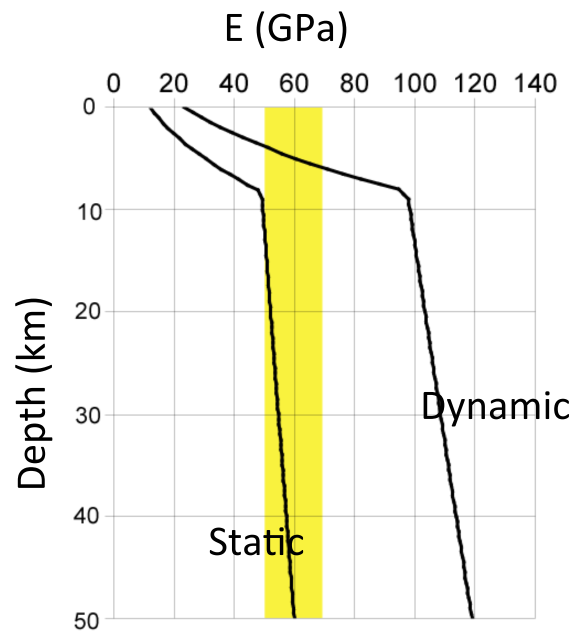

Large possibilities however few constrains.
Choices have to be made.

Same problem of definition of the physics as for analytical models

For instance another key problem in volcanology is to define a **fracturation criterium**

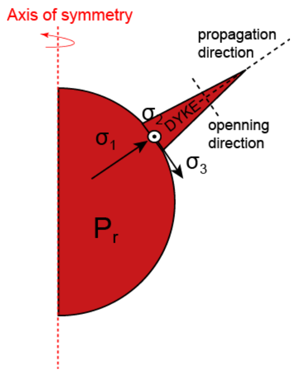

1

Minimum stress must exceed Tensile strength

$$\sigma_3 < -T_s$$

ΔP increases with depth
ΔP>70MPa for z>3km

When independent estimations give ΔP~3-15MPa

2

Coulomb criterium

$$\sigma_t > S_o + \tan\phi_f(\sigma_n - P_f),$$

However rupture has to be in tension

3

Minimum deviatoric stress must exceed Tensile strength

$$\frac{2\sigma_3 - \sigma_1 - \sigma_2}{2} \leq -T_s$$

ΔP constant with depth

Compatible with dyke propagation theory

Inversion of deformation data

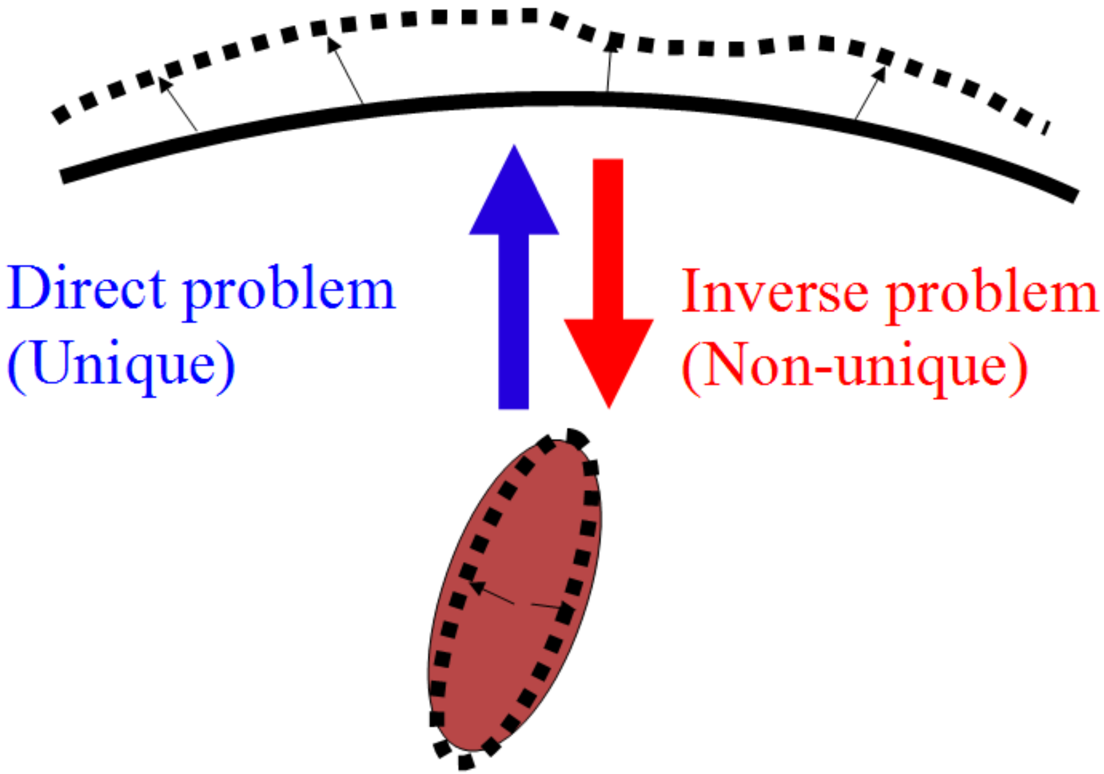

Inversion of deformation data

Mechanical model

Source of displacement
For instance pressure source

Surface displacement

(parameters ϕ, rheology)

Inversion

Expression du Misfit

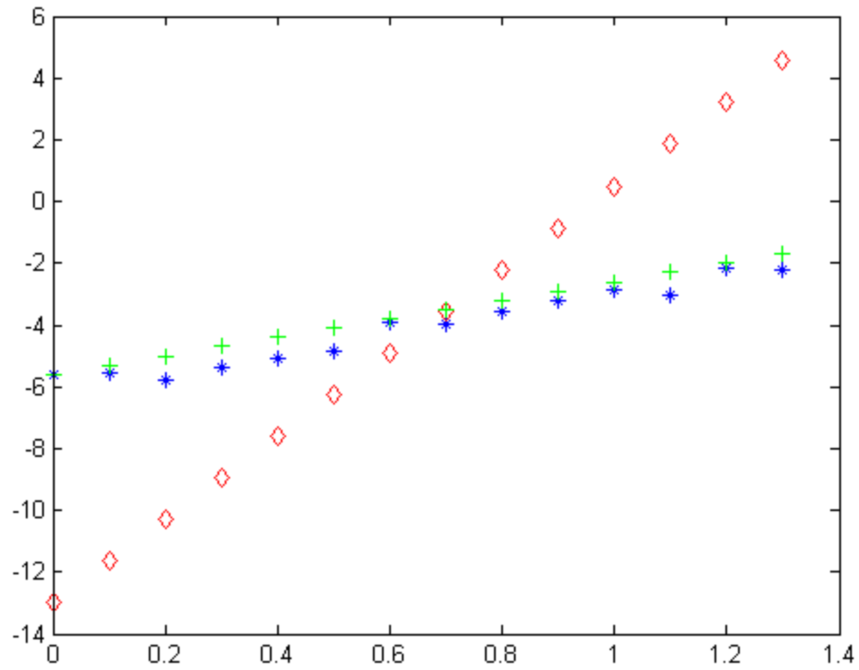

$$\sum_{i=1}^{n}\left(x_{mod,i}-x_{obs,i}\right)=1.940 \qquad \sum_{i=1}^{n}\left(x_{mod,i}-x_{obs,i}\right)=6.10$$

Expression du Misfit

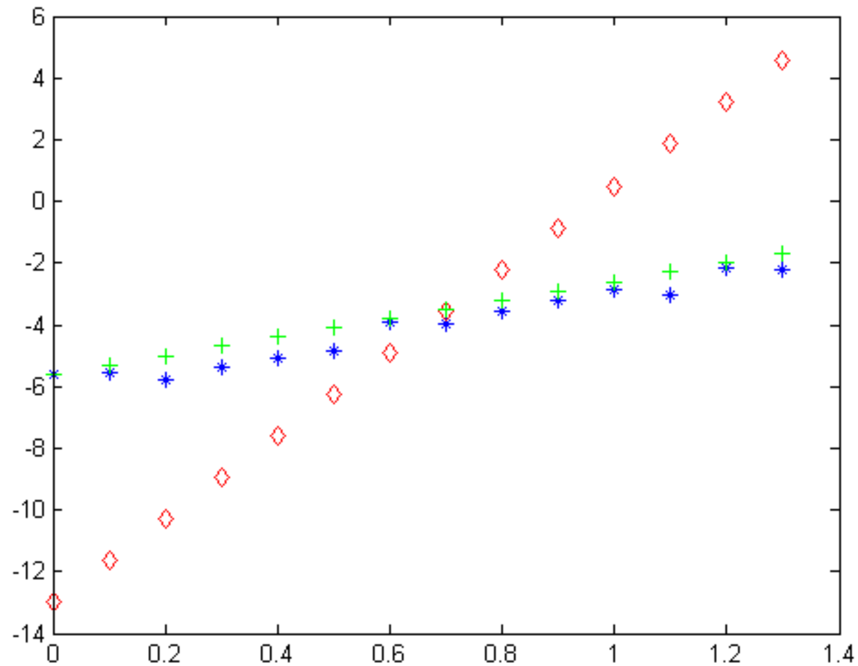

$$\sum_{i=1}^{n}\left(x_{mod,i}-x_{obs,i}\right)=1.940$$

$$\sum_{i=1}^{n}\left(x_{mod,i}-x_{obs,i}\right)=6.10$$

$$\sum_{i=1}^{n}\left|x_{mod,i}-x_{obs,i}\right|=50.94$$

$$\sum_{i=1}^{n}\left|x_{mod,i}-x_{obs,i}\right|=6.10$$

Choice of Misfit expression

L1 : $\sum_{i=1}^{n} \left| x_{mod,i} - x_{obs,i} \right|$

Same weight for each difference.

L2 :

$$\sum_{i=1}^{n} (x_{mod,i} - x_{obs,i})^2$$

Largeur differences have larger effect

Normalised Misfit (%)

$$\frac{\sum_{i=1}^{n} \left| x_{mod,i} - x_{obs,i} \right|}{\sum_{i=1}^{n} \left| x_{obs,i} \right|} * 100$$

Inversion of deformation data

- Choice of a forward model (analytical or numerical)
- Data downsampling (ex: quadtree, Jonsson 2002)
- Data weighting (covariance)
- Estimation of a cost function using the forward

$$\chi^2(\mathbf{m}) = (\mathbf{u}_o - \mathbf{u}_m)^T C_d^{-1} (\mathbf{u}_o - \mathbf{u}_m),$$

- Exploration of space parameters
- Sometimes smoothing is required
- Estimation of results fiability

(residuals, root mean square error (RMSE), density distributions)

Still difficult to use numerical models to invert data

Mainly because of computational cost

Possible ways to proceed :

-use analytical solutions together with correction functions determined with numerical modeling (*Manconi et al, JGR, 2010*)

-use of summation of Green's function *(Masterlark 2007)*

-use of synthetic tests

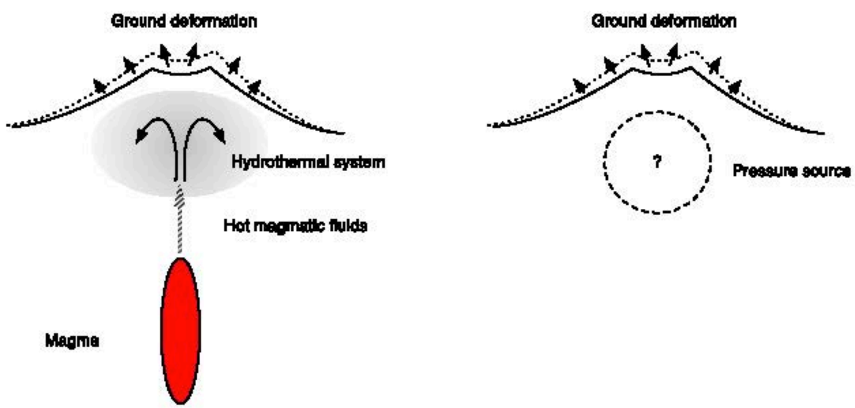

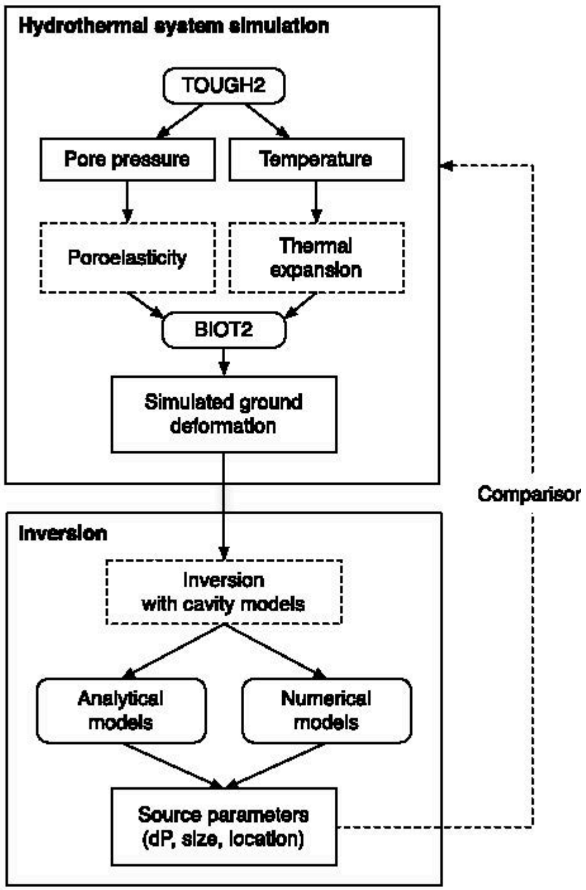

From Fournier & Chardot, 2012

Why studing deformation at volcanoes?

*1 Monitoring for risk assessment.
*2 Understanding volcanoes behaviour.

Detection of magma storage

Detection of long term precursors (months or years before an eruption).

InSAR:
Useful for remote areas.

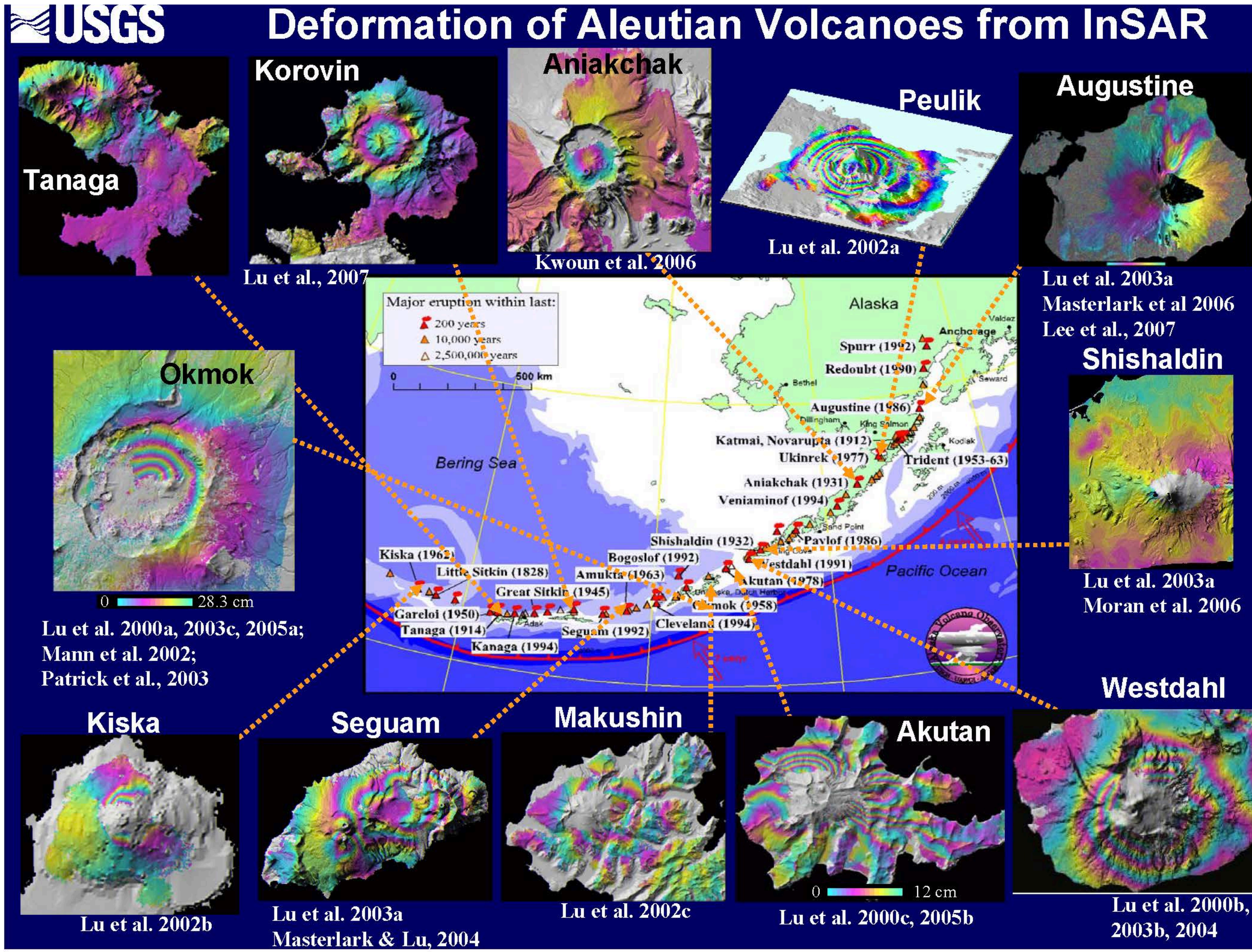

From Lu et al, 2008

Detection of deformation in remoted areas

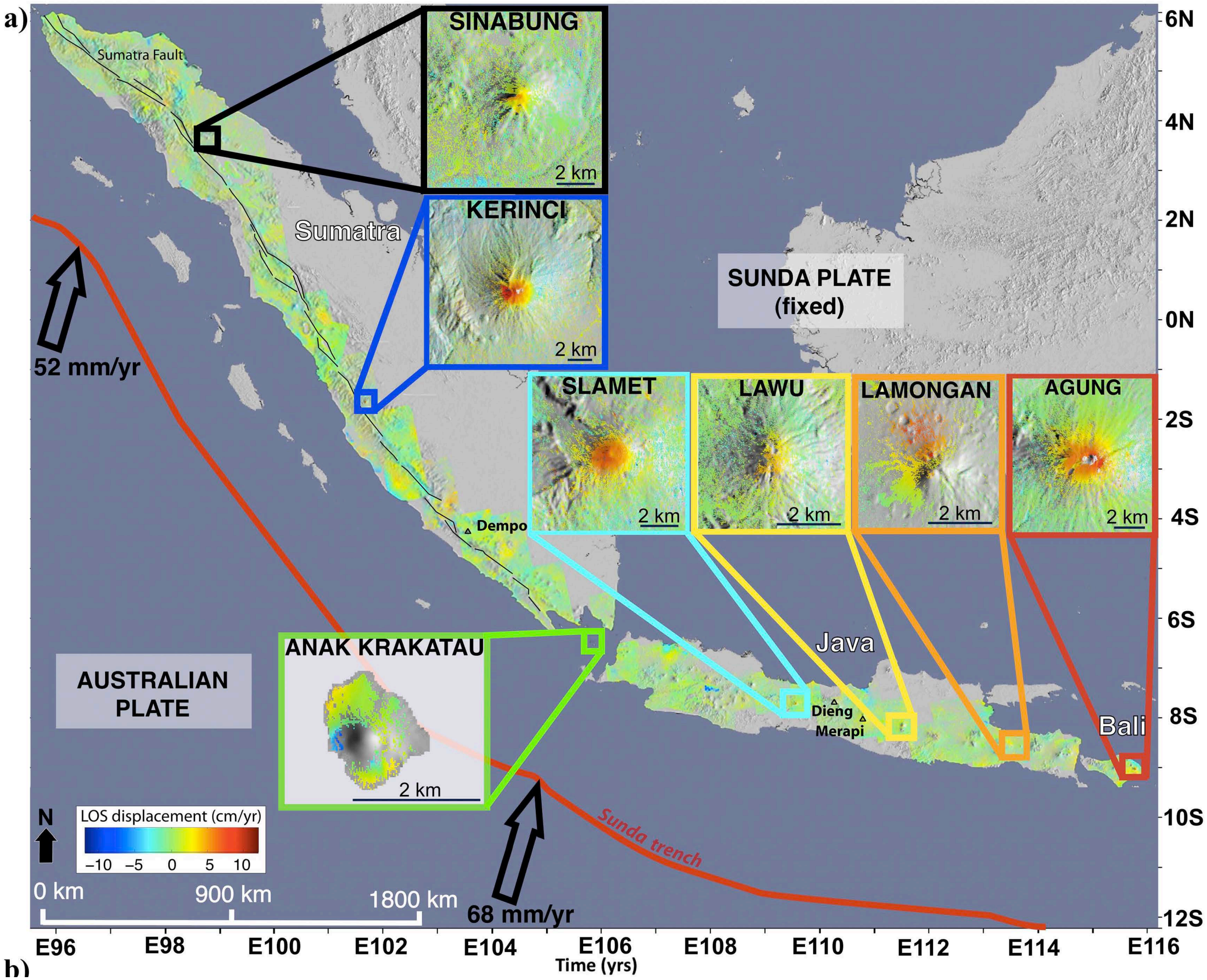

Using time series analysis

Chaussard and Amelung, 2012

Detection of deformation in remoted areas

- A tool to decide where to put in-situ instruments
- A tool to performed regional studies and establish correlation

between magma reservoir depth and the tectonic context (Chaussard and Amelung, 2012)

However no systematic correlation between eruption and deformation signal (especially for andesitic stratovolcanoes)

Ex: temporal evolution of surface displacement recorded at Grimsvötn

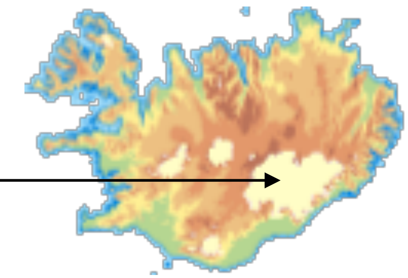

Eruption Dec. 98

Eruption Nov. 2004

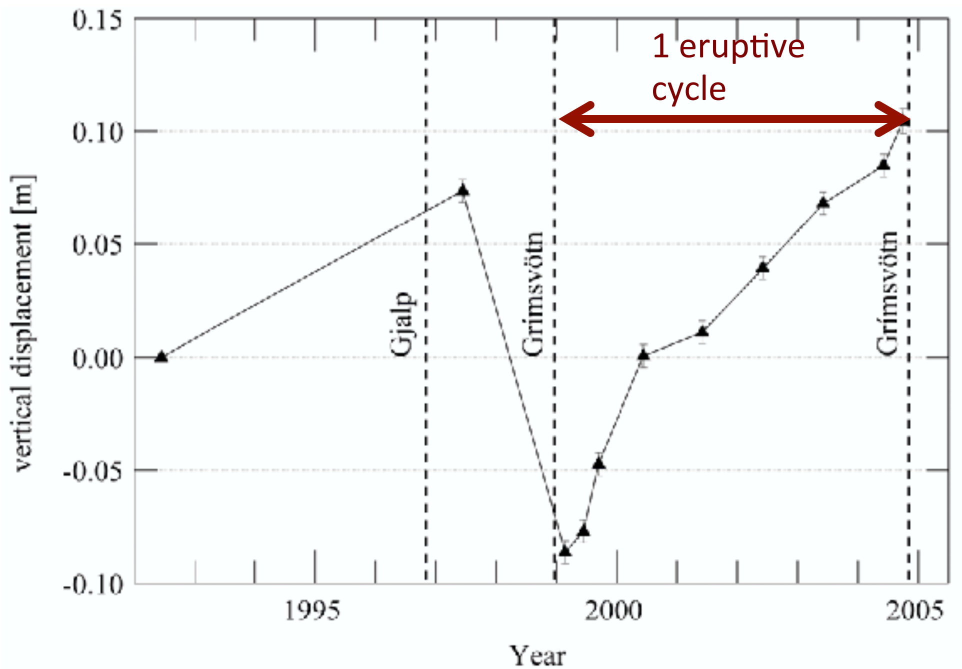

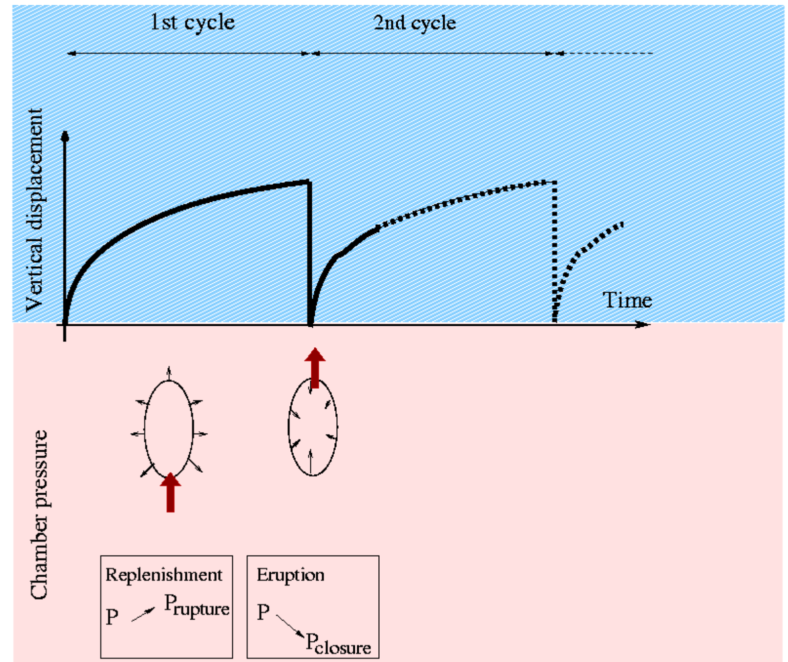

(from Sturkell et al., JVGR, 2006)

Displacement → $(\Delta P_c * R_c^3)/E$

Magmatic Overpressure at eruption onset
From displacement data

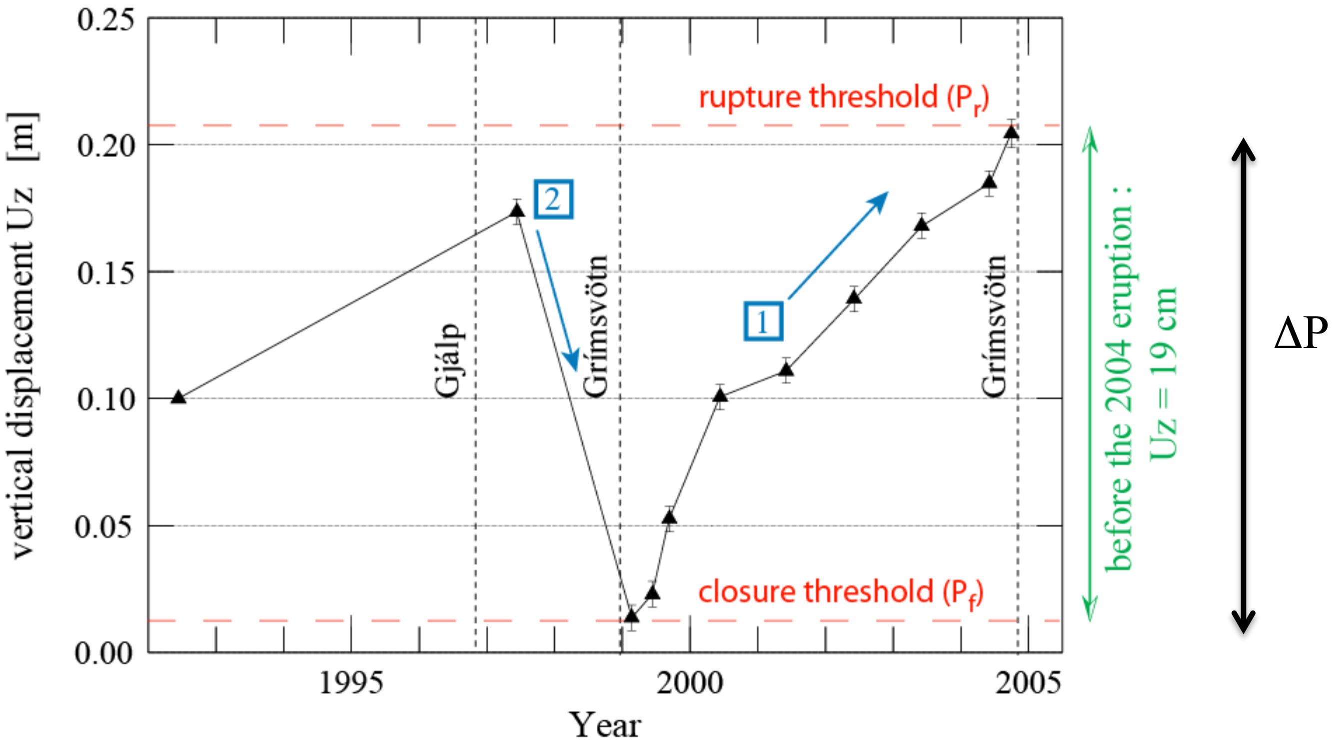

1 reservoir replenishement (P_c ↗ until P_r)

2 reservoir withdrawal (P_c ↘ until P_f)

With E=30GPa, ν=0.25, H_c=3km

ΔP=24MPa for a spherical chamber (R_c=1.5km)

ΔP=5.5MPa for an oblate chamber (a=2.5km,b=0.5km)

A realistic rupture criterion

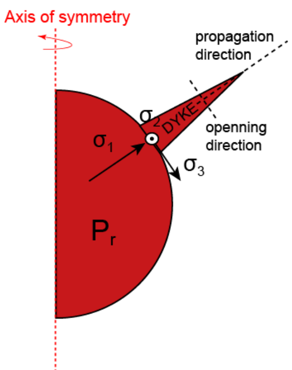

Objective: - To know when the magma will leave a storage zone.

~~1~~

Minimum stress must exceed Tensile strength

$$\sigma_3 < -T_s$$

ΔP increases with depth
ΔP>70MPa for z>3km

When independent estimations give ΔP~1-15MPa

~~2~~

Coulomb criterium

$$\sigma_t > S_o + \tan\phi_f(\sigma_n - P_f),$$

However rupture has to be in tension

3

Deviatoric component of the minimum stress must exceed Tensile strength

$$\frac{2\sigma_3 - \sigma_1 - \sigma_2}{2} \leq -T_s$$

$$\rightarrow \quad \Delta P \geq 2T_s$$

ΔP constant with depth

Consistent with dyke propagation theory

What does it practically mean?

Knowing -the chamber size, position and shape
-the surrounding stress field
-the crustal tensile strength

We can quantify the magma pressure required for chamber wall rupture.

Magmatic Overpressure at eruption onset From displacement data

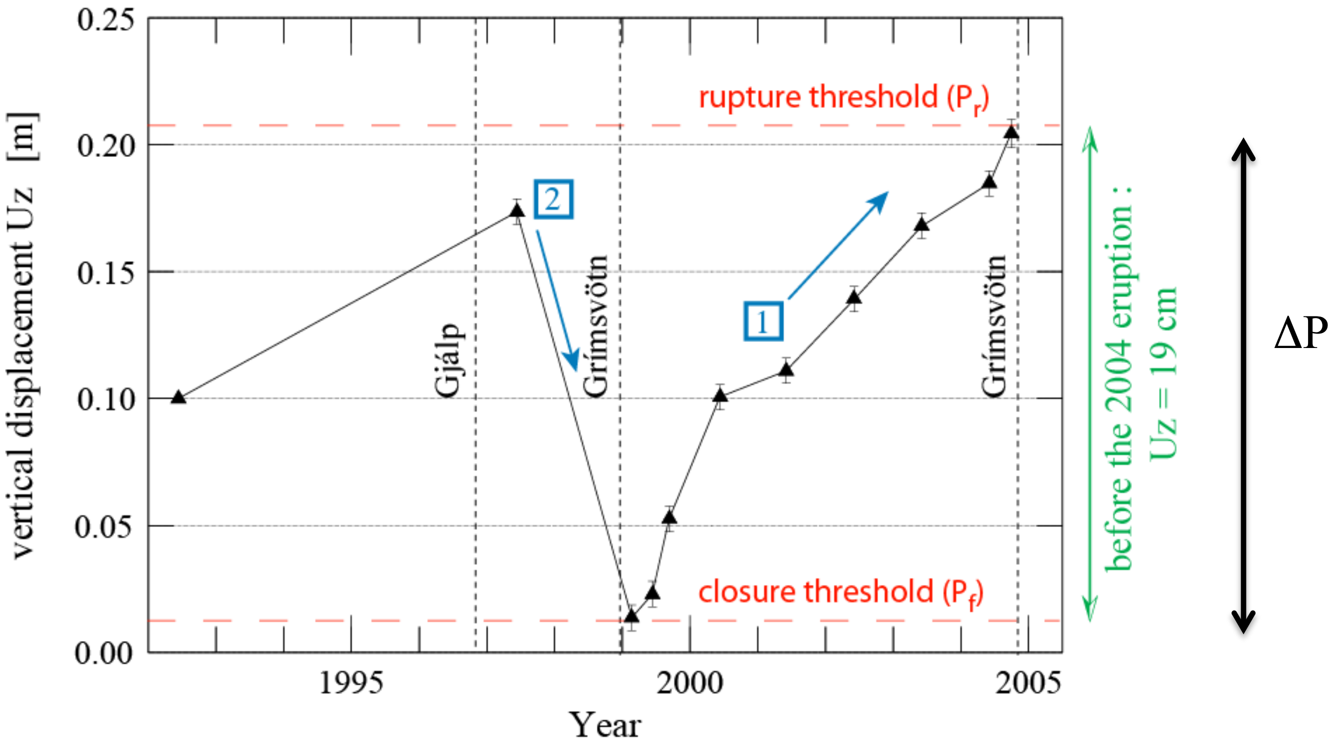

1 reservoir replenishement (P_c ↗ until P_r)

2 reservoir withdrawal (P_c ↘ until P_f)

With E=30GPa, ν=0.25, H_c=3km
for an oblate chamber (a=2.5km,b=0.5km)

ΔP=5.5MPa

T_s= 22MPa

Detection of edifice destabilization

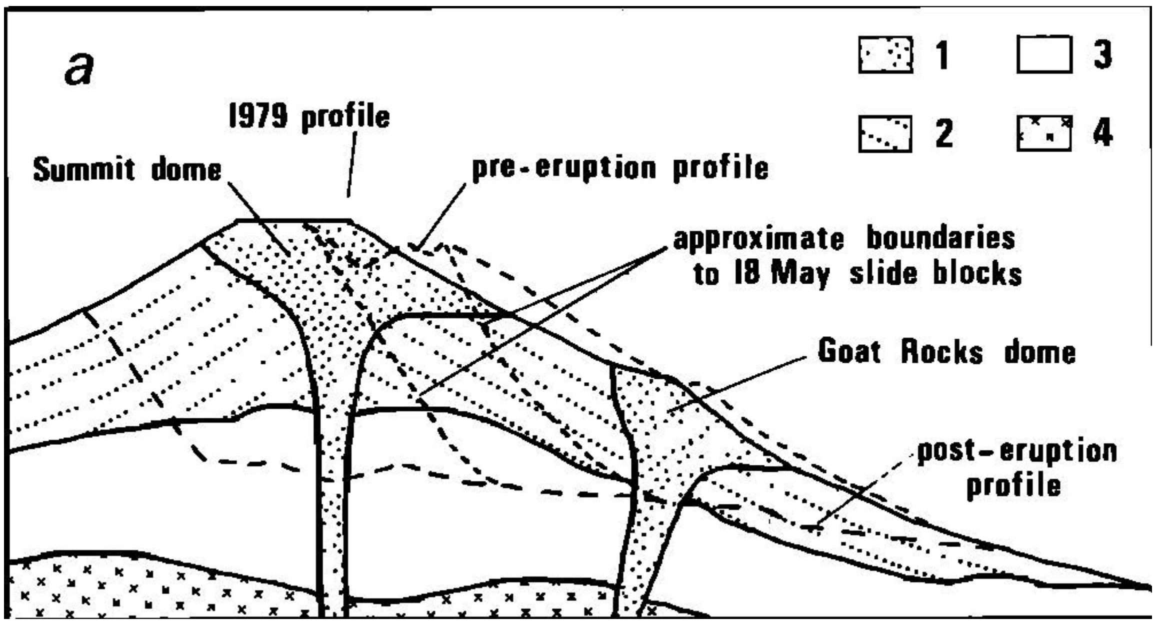

Mount St Helens before
the 18th of May 1980
(2 months)
Displacements of 1.5-2.5m/days

Voight et al., U.S. Geol. Surv. Prof. Pap., 1250,1981.

Precursor of eruption onset

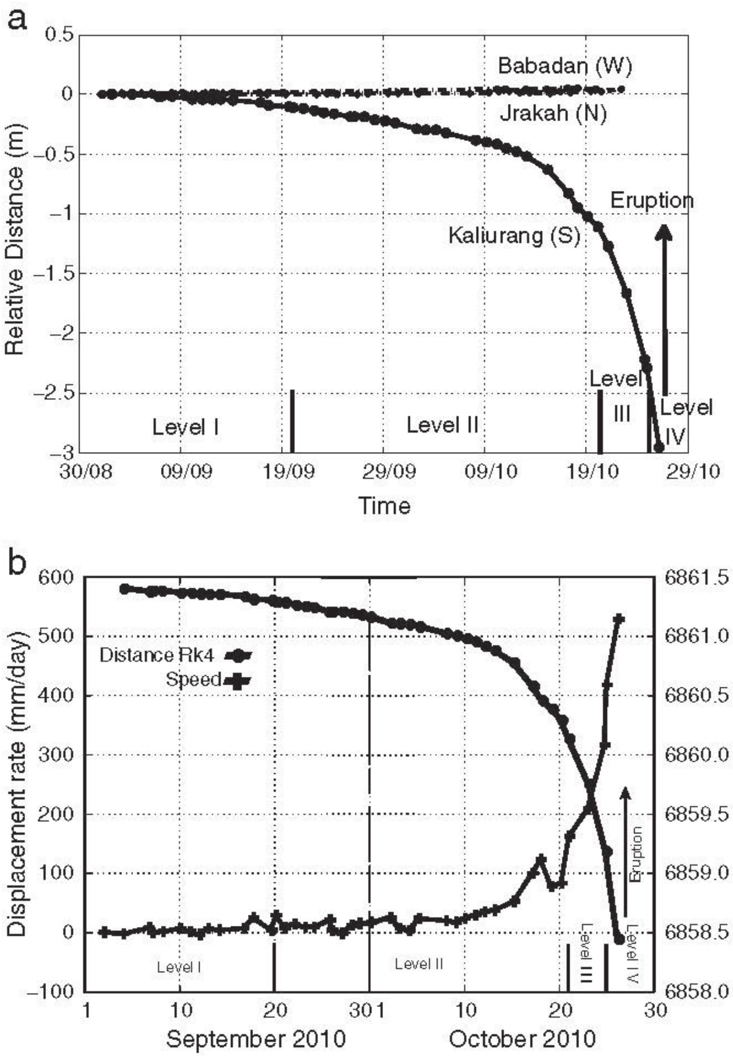

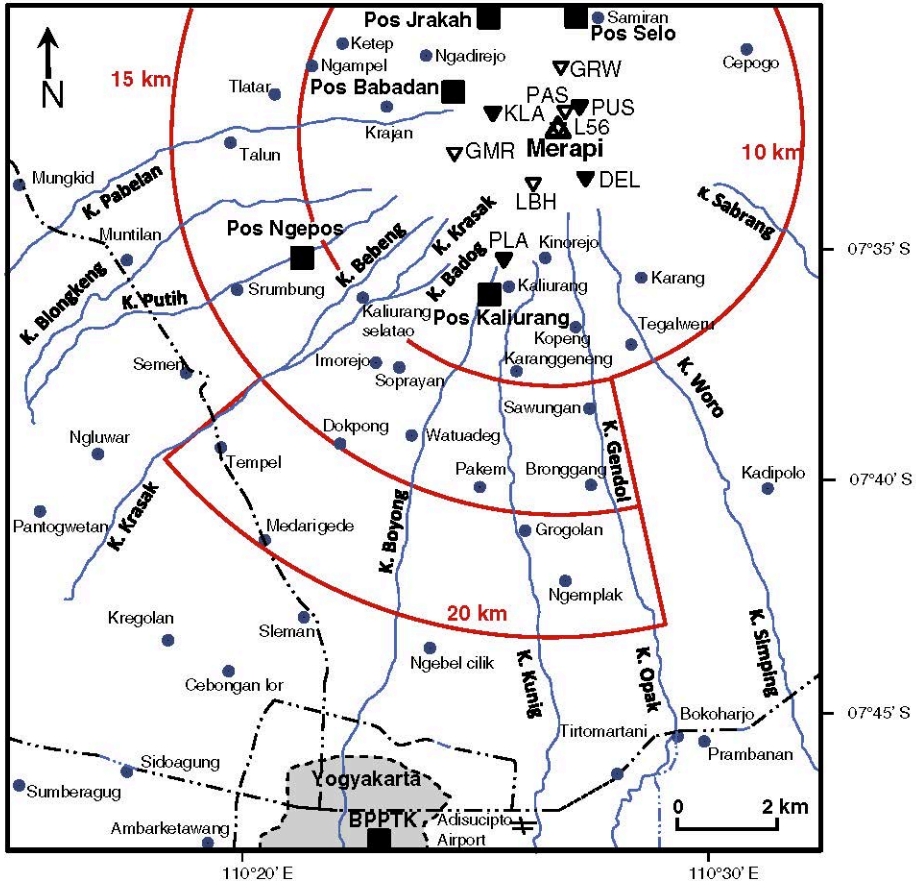

From Surono et al, 2013

Detection of magmatic intrusions emplacement

Short-term precursors:
Ex: Piton de la Fournaise, Reunion Island.

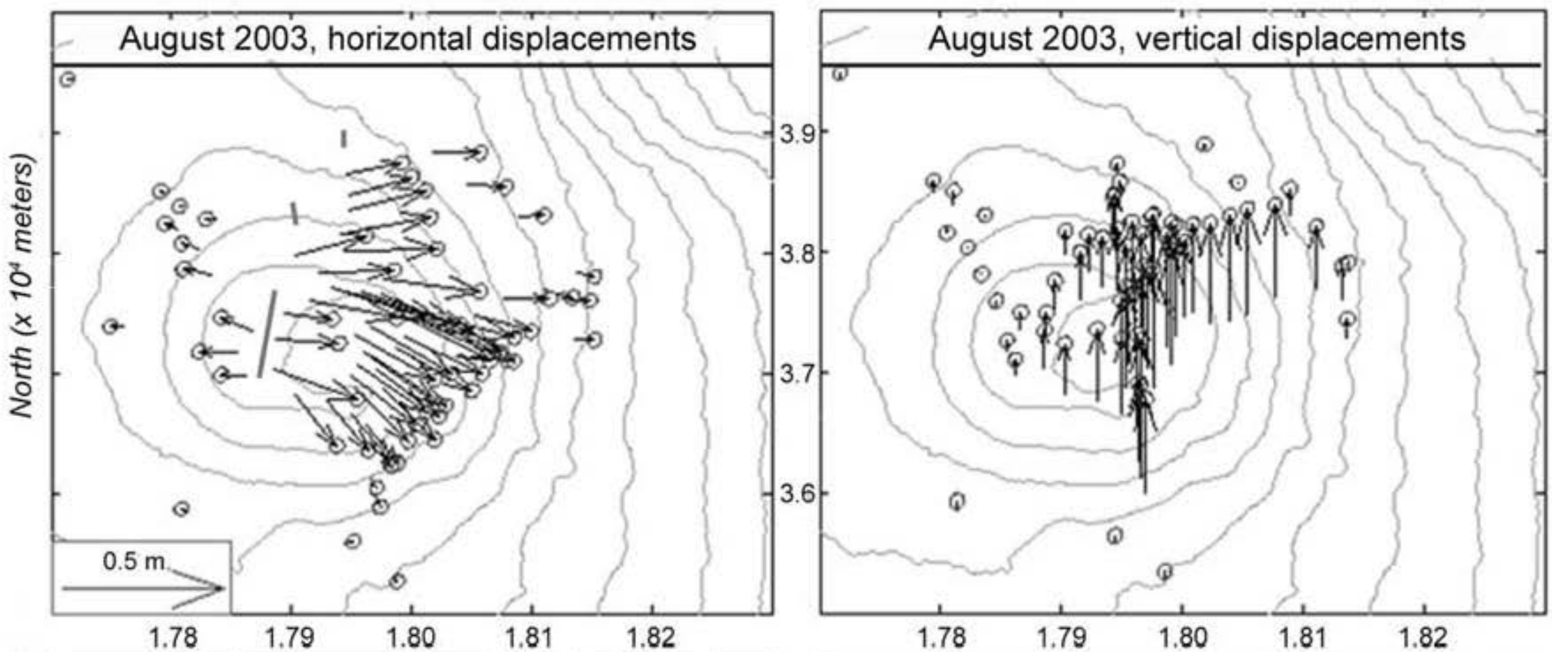

Displacements recorded during the dyke vertical propagation (20 min)
2H30 before the eruption onset *(Peltier et al, JGR, 2007)*

Understanding volcanic edifices construction.

Volcanoes growth by:
-magmatic intrusions
-eruptive deposits

The edifice growth is responsible for the present stress field.

<u>The ratio Intrusive/eruptive growth is poorly known:</u>
Global studies on plutons and eruptive products:
$V_{Intrusif}$=5-10*$V_{eruptif}$ *(Crisp 1984)*
Petrological and structural studies at La Palma, Canarian Islands:
$V_{intrusif}$=$V_{eruptif}$ (*Staudigel & Schmincke, 1984)*
Seimological data in en extensive context:
$V_{intrusif}$=2*$V_{eruptif}$ (*White et al., 2008)*
Numerical simulations, Piton de la Fournaise
$V_{intrusif}$=0.13*$V_{eruptif}$ (*Annen et al., 2001)*

Understanding volcanic edifices construction.

Deformation studies allow to quantify volume of magmatic intrusions:

$$\frac{\Delta V_{surf}}{\Delta V_{in}} = \frac{2(1-\nu)}{1+\frac{4G}{3K}},$$

Topographic variations allow to quantify volume of eruptive deposits:

Understanding volcanic edifices construction.

Edifice growth and stress field evolution.
Ex: Afar rift.

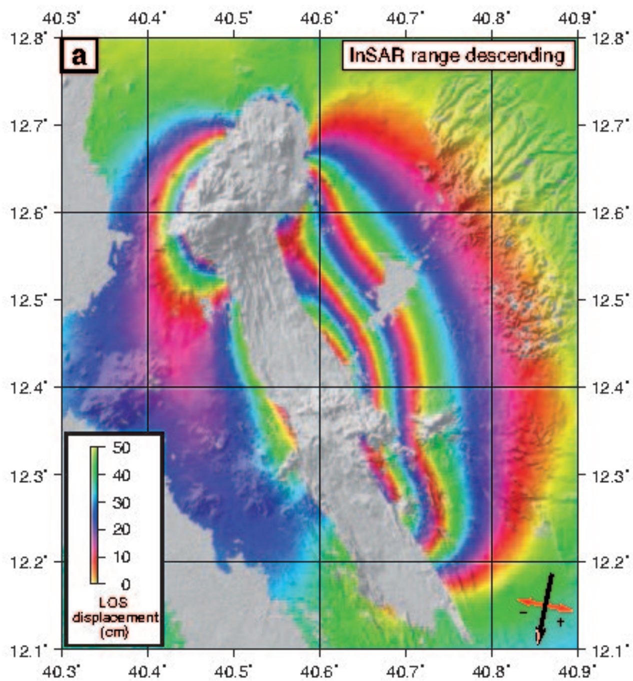

Grandin, Thèse, 2009

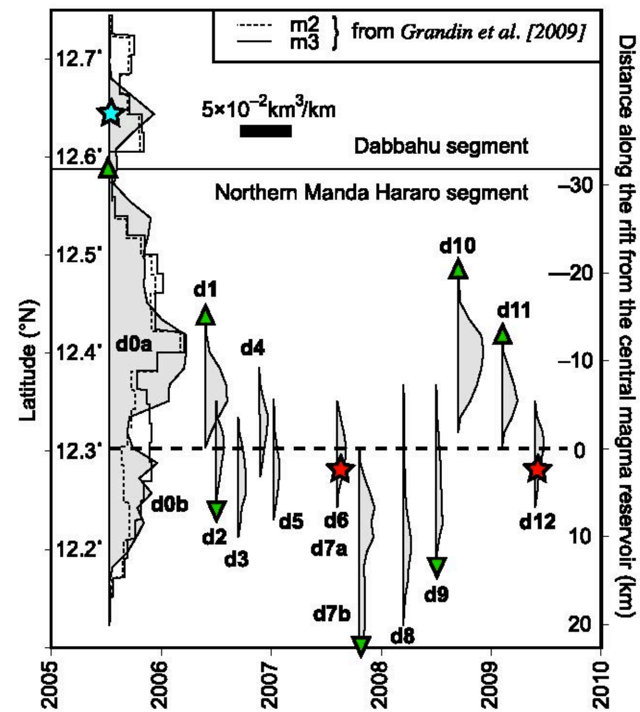

Grandin et al, 2010, JGR

Understanding volcanic edifices construction.

Edifice growth and stress field evolution.

Ex: Afar rift.

Intrusive and extrusive volumes for dyking/eruptive events since September 2005.

	Sept 2005	June 2006	July 2006	Sept 2006	Dec 2006	Jan 2007	Aug 2007	Nov 2007	April 2008	July 2008	Oct 2008	Feb 2009	June 2009	Total ($\times 10^6$ m^3)
Intruded volume ($\times 10^6$ m^3)	1750 ± 250[a]	120 ± 10[b]	47 ± 17[b]	88 ± 14[b]	58 ± 11[b]	37 ± 13[b]	48 ± 1[b]	150 ± 10[b]	90 ± 20[c]	70 ± 20[c]	170 ± 1[c]	80 ± 3[c]	50 ± 7[c]	2758 ± 227
Erupted volume ($\times 10^6$ m^3)							4.6 ± 1.5[d]						11 ± 1.8[d]	15.6 ± 3.3[d]

[a] Grandin et al., 2009.
[b] Hamling et al., 2009.
[c] I. Hamling unpublished data.
[d] Estimate from field and remote sensing observations.

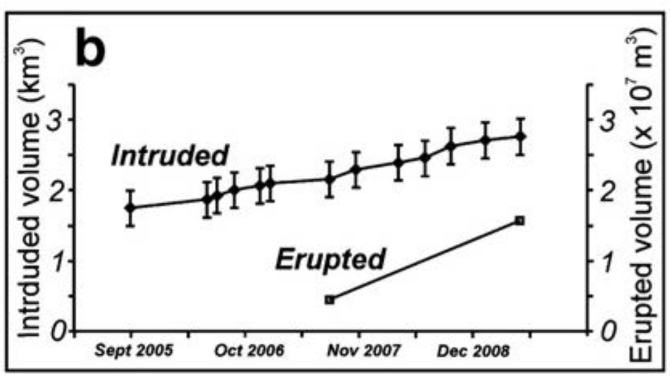

Fergusson et al., EPSL, 2010

Deformation is a useful information

In order to know the plumbing system geometry and state of pressure.

But complemetary informations are required: gravimetry, gas emissions, seismicity.

Comparison between seismicity rate and deformation

$$D(t) = A + B\left[\sigma_c - P_0 - P\left(1 - \exp\left(\frac{-t}{\tau}\right)\right)\right]^{-\gamma}$$

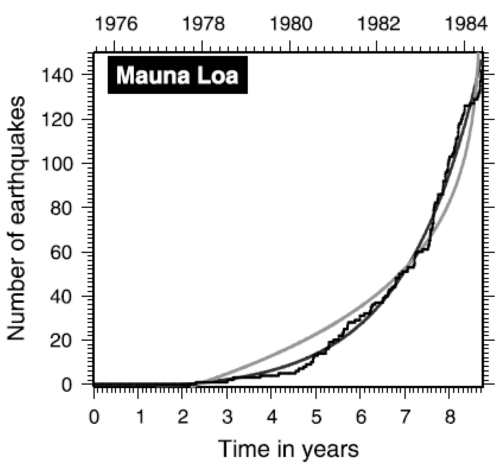

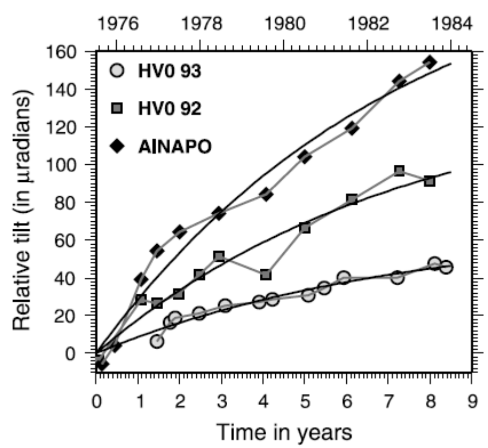

Lengliné et al, 2008

Gravimetry and deformation

Overpressure within a reservoir can be due to:

-case 1:gas exsolution due to crystallisation *(Tait et al, 89)*

→ no input of fresh magma (ΔM=0)

-case 2: a new input of magma → unrest

For case 2 (for a spherical reservoir):

$$\Delta V_{uplift} = \frac{\Delta M}{\rho} \frac{2(1-\upsilon\ \ )}{1+{}^{4G}/_{3K}}$$

Gravity measurements allows to constrain ΔM and to estimate which amount of magma is stored at depth.

Numerical modeling: first example.

• **Albino F.**, Pinel V., Massol H., Collombet M., Conditions for detection of ground deformation induced by conduit flow and evolution, *Journal of Geophysical Research, 2011*.

Coupling 2 fields :

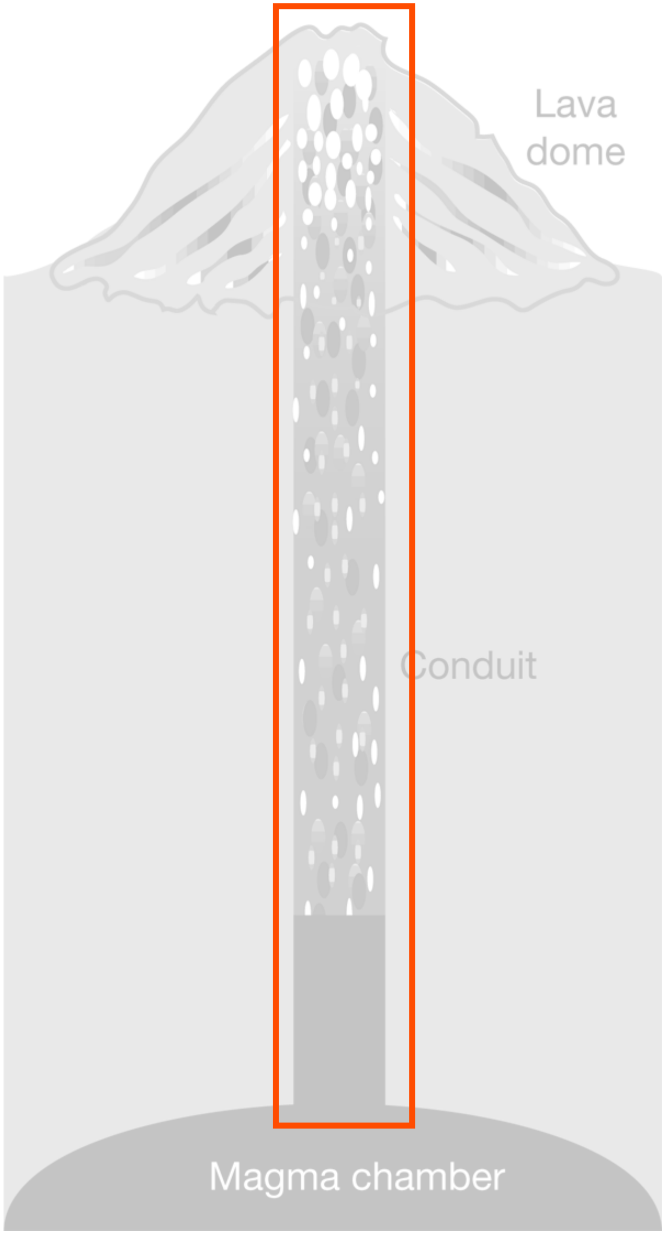

Models of fluid flow in a rigid conduit
-including crystallization, degassing…,
-aiming at understanding
effusive/explosive transitions, flux rate
variations
Sparks, 1997, Melnik & Sparks 1999,
Barmin et al., 2002

Plug formation is expected.

Not often linked to geophysical
observations

Coupling 2 fields :

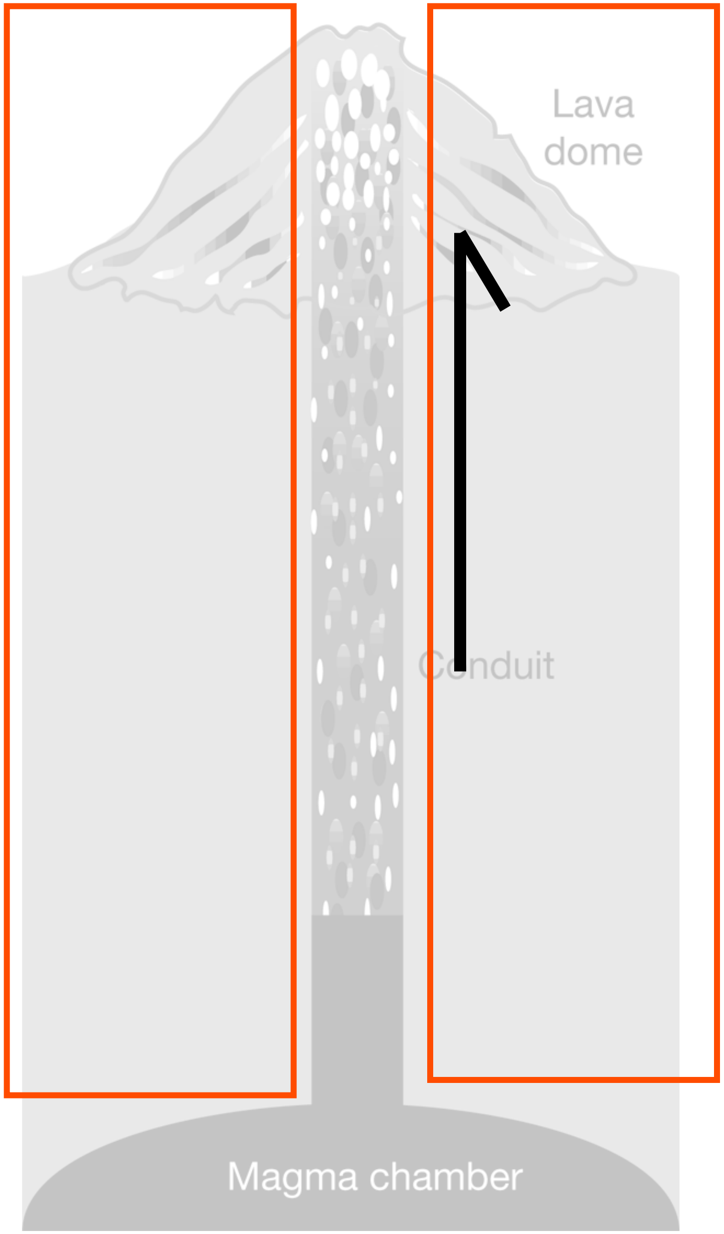

Models used to interpret geophysical observations

(Beauducel et al, 2000, Green et al, 2006, Anderson et al, 2011…)

Not often related to the physics of magma flow

Coupling 2 fields :

First attempt of one-way coupling

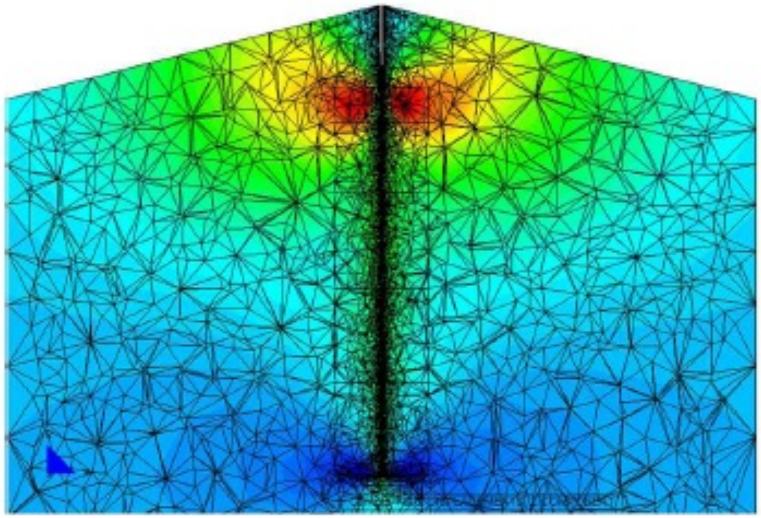

(Hautmann et al, Tectonophysics, 2009)

*Pressure applied are derived from Costa et al, 2007

*No tangential stress on the conduit wall

Model description :

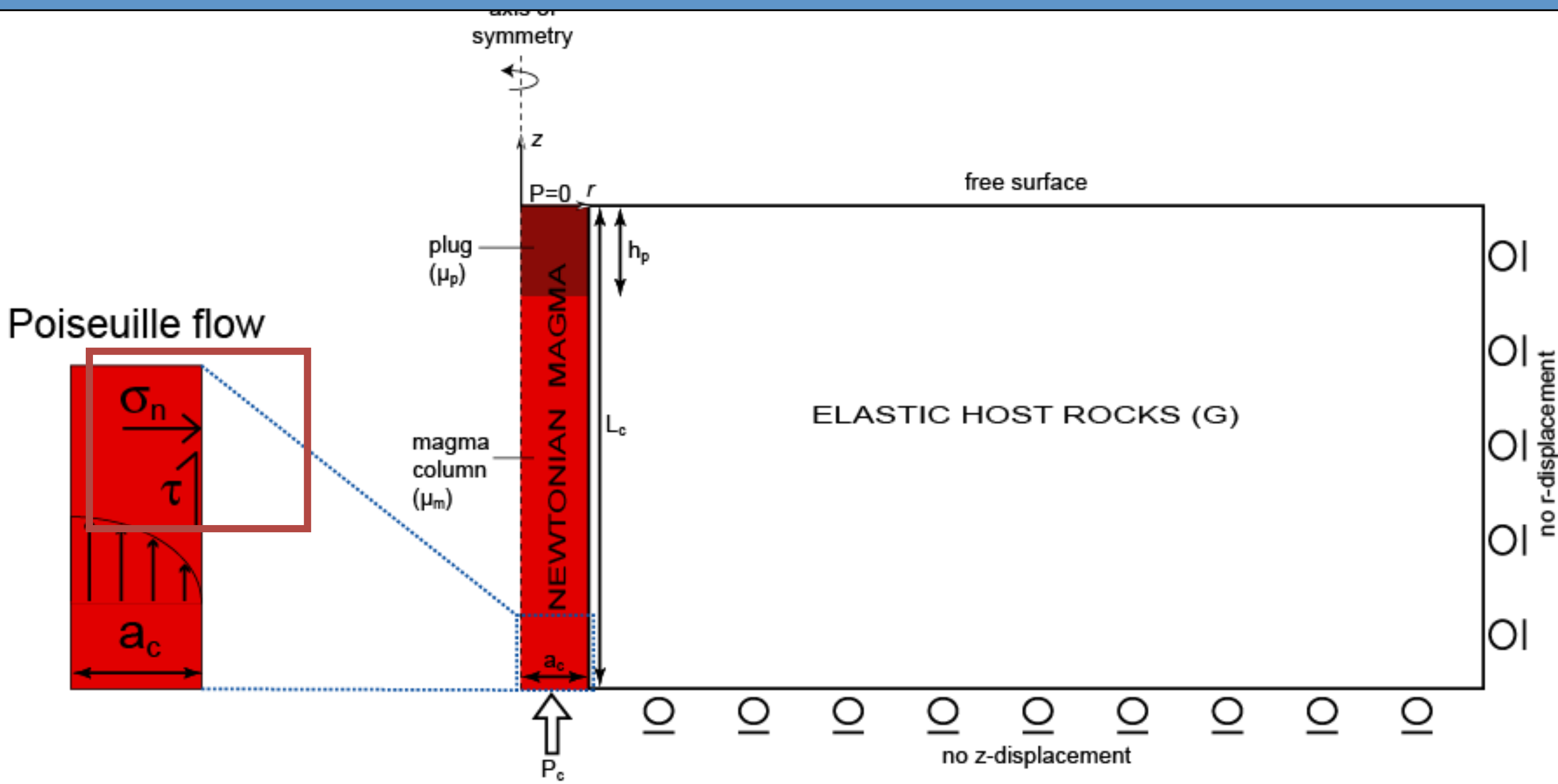

- Axial symmetry
- Stress continuity at the solid-fluid interface
- Full coupling

Effect of plug formation :

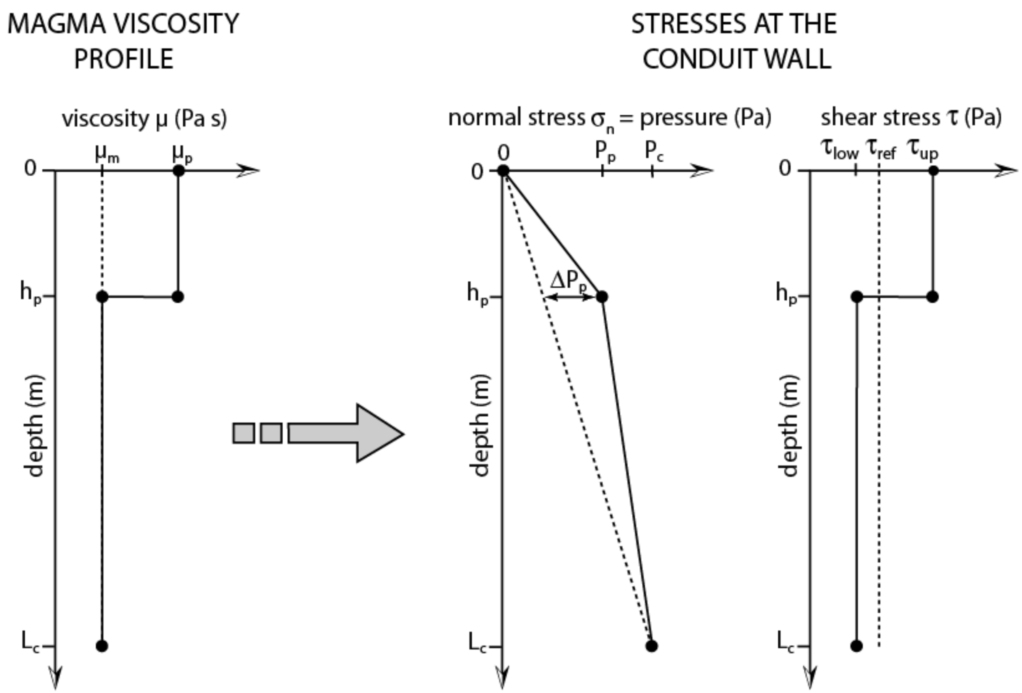

- Reference state: a constant viscosity flow
- Perturbation : increase of viscosity in the upper part of the conduit

Distance of detection

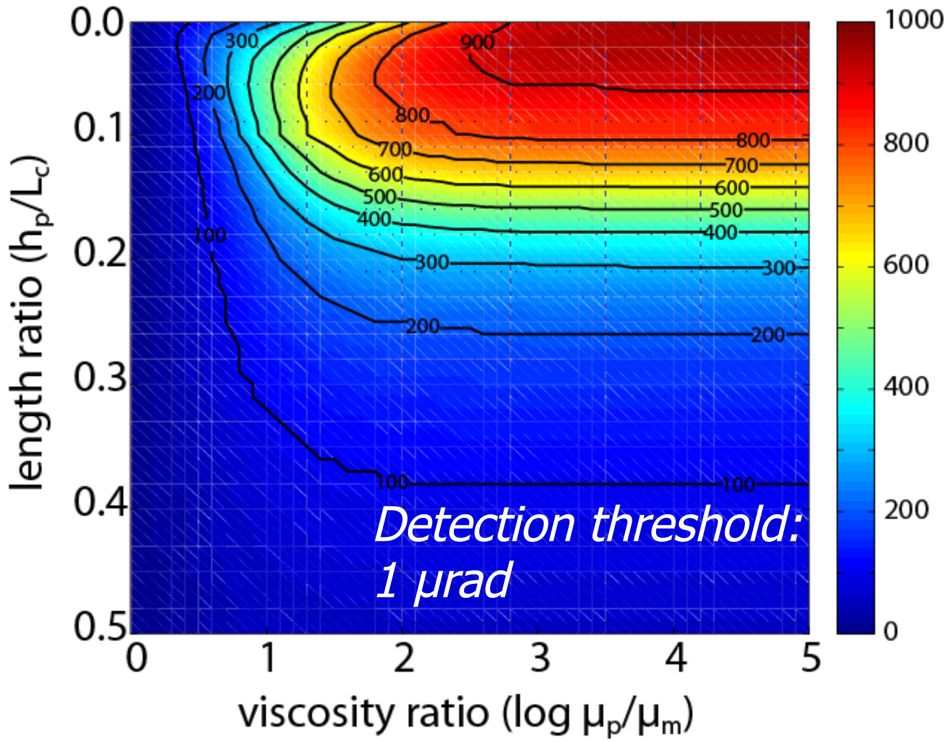

a_c = 15 m ; L_c = 5000 m ; P_c = 10 MPa ; G = 0.8 GPa

Critical distance from crater for tilt detection is < 1 km

Distance of detection

Increase with conduit radius overs conduit length a_c / L_c

Decrease with the ratio G/Pc

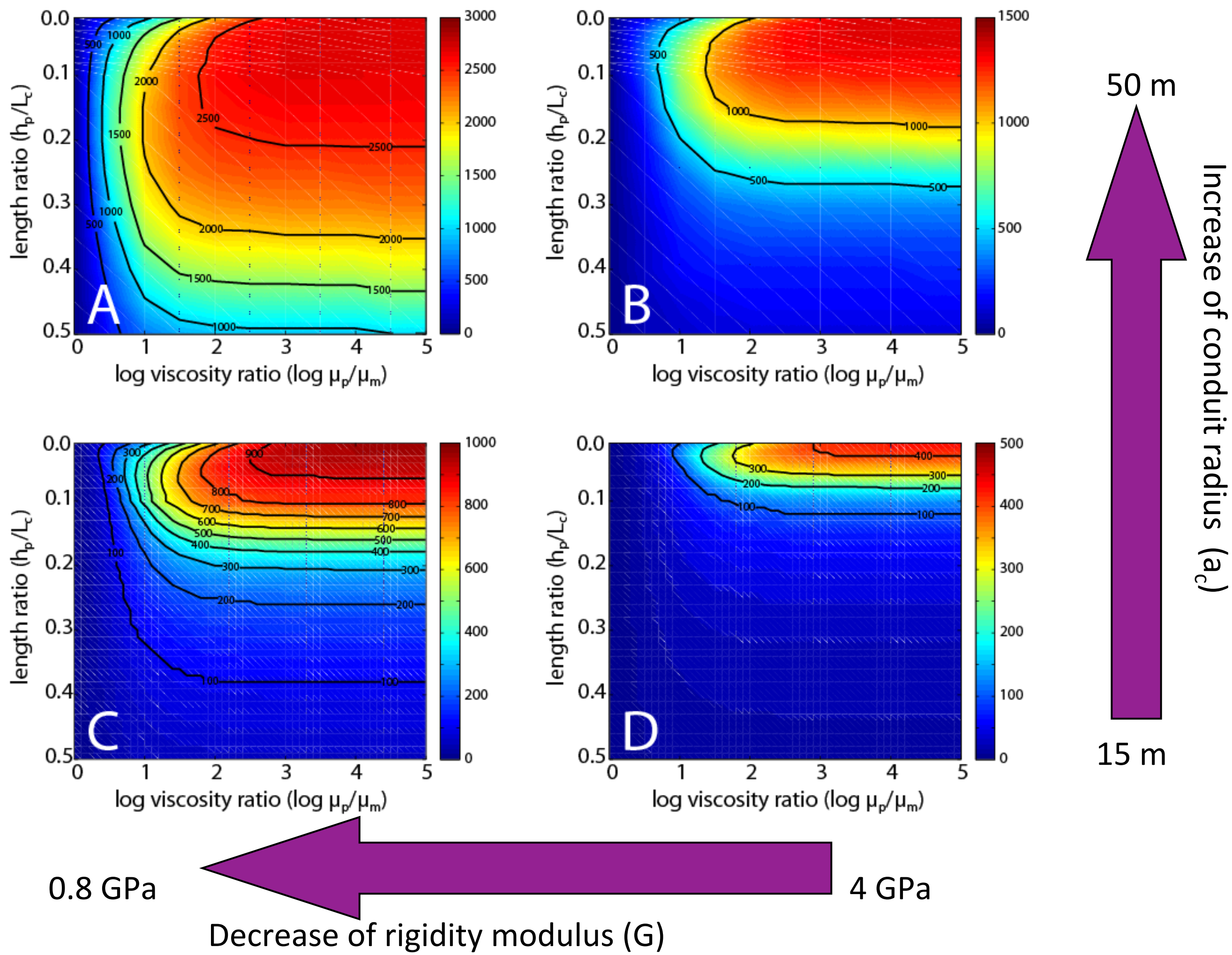

Joint interpretation of deformation and flow rate evolution

a) Upper magma viscosity increase

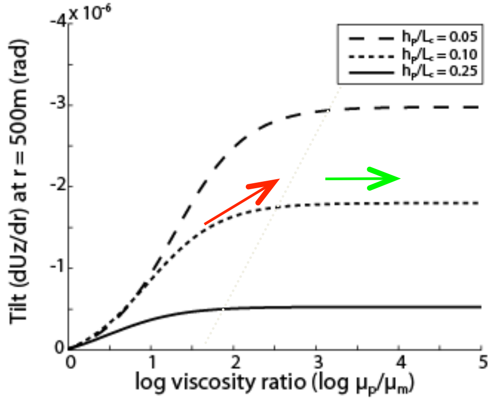

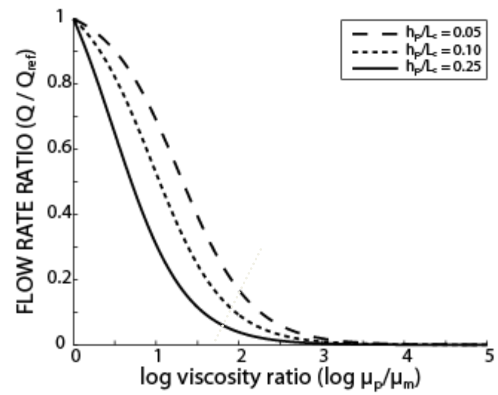

- **Increase** of tilt amplitude correlated to magma flow rate reduction
- Above a critical threshold for viscosity contrast, tilt remains **constant**.

b) Plug thickness increase

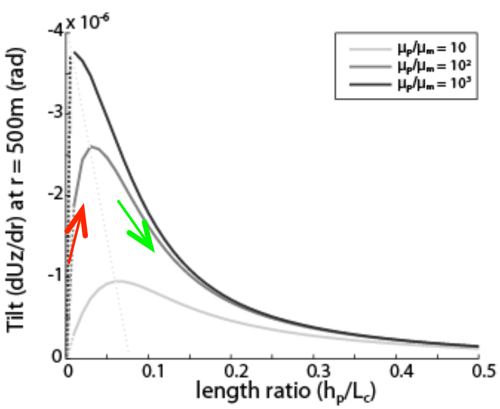

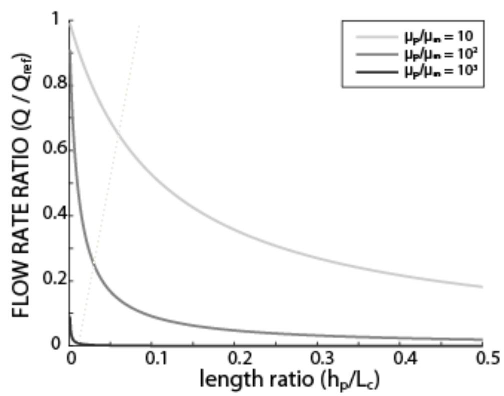

- **Decrease** of tilt amplitude correlated to magma flow rate reduction
- Rapid **increase** of tilt amplitude during the early stage of plug growth.

Joint interpretation of deformation and flow rate evolution

a)

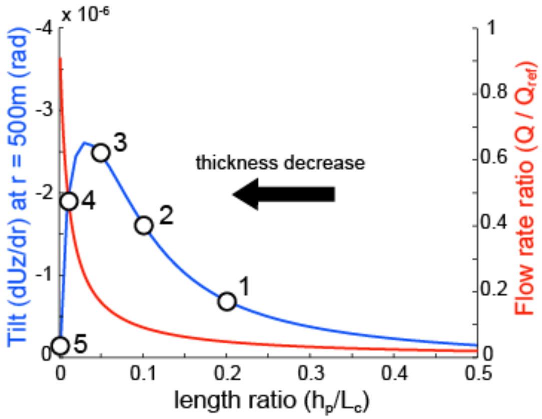

- Evolution of plug thickness around a critical size can induce a succession of inflation and deflation
- Plug reduction can explain tilt reversal observed before eruptions *(Chadwick et al, 1988)*

b)

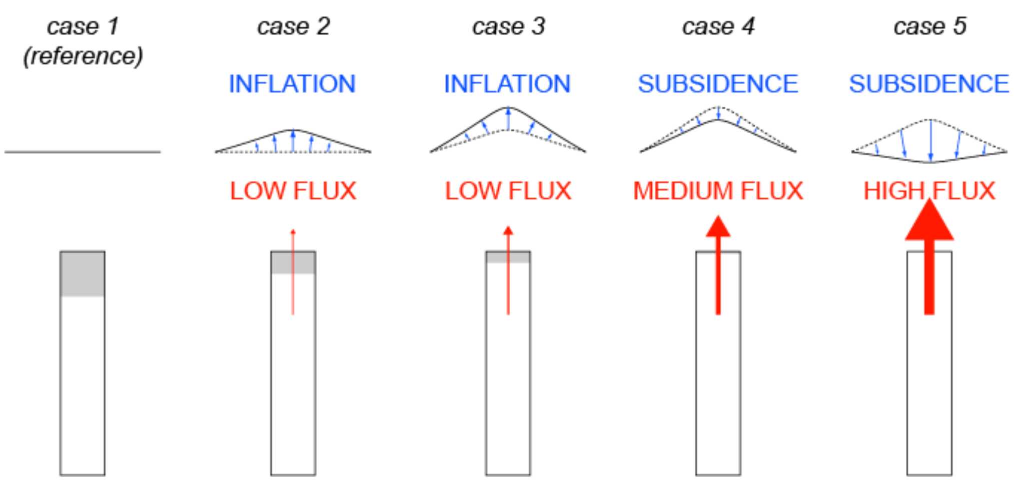

This mechanism can partly explained observations

Montserrat

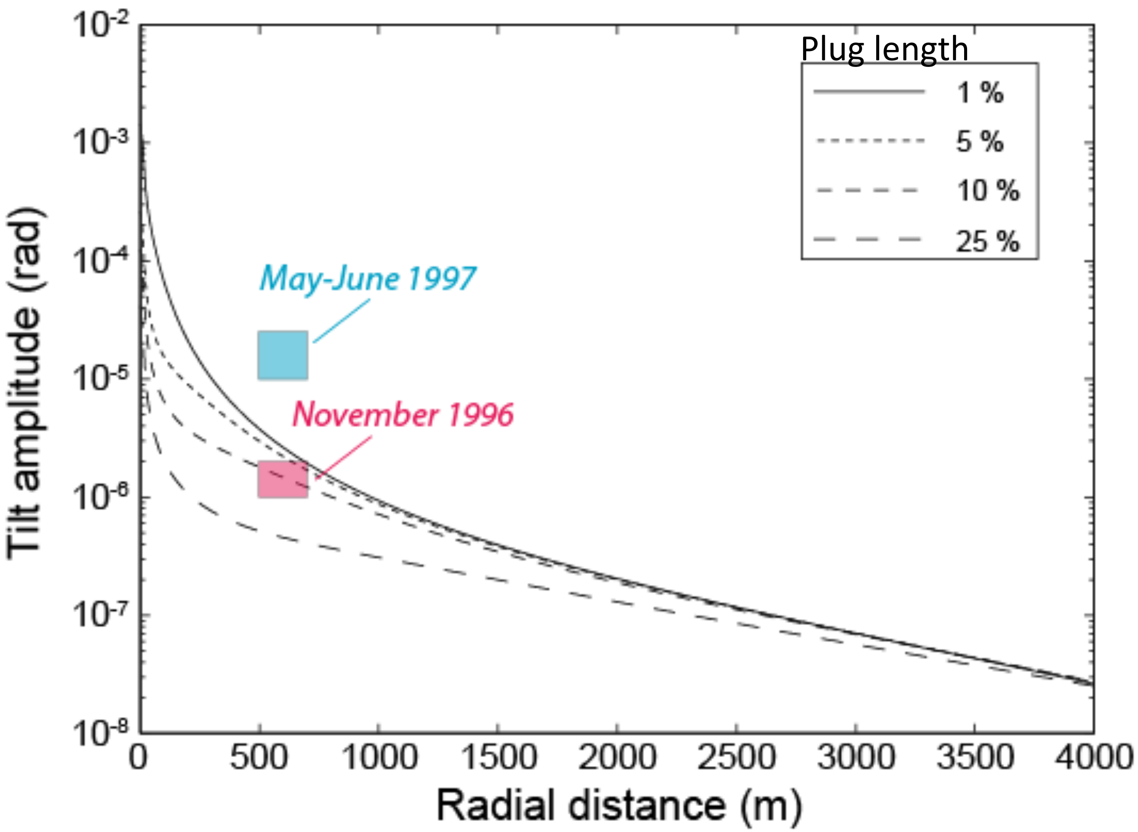

a_c = 15 m ; L_c = 5000 m
P_c = 10 MPa ; G = 0.8 GPa
$\mu_p/\mu_m = 10^5$

More realistic viscosity profiles do a better job

Previously

Step function for μ

μ profile for compressible magma

Sparks, 1997
1D gas loss

Collombet, 2009
2D gaz loss

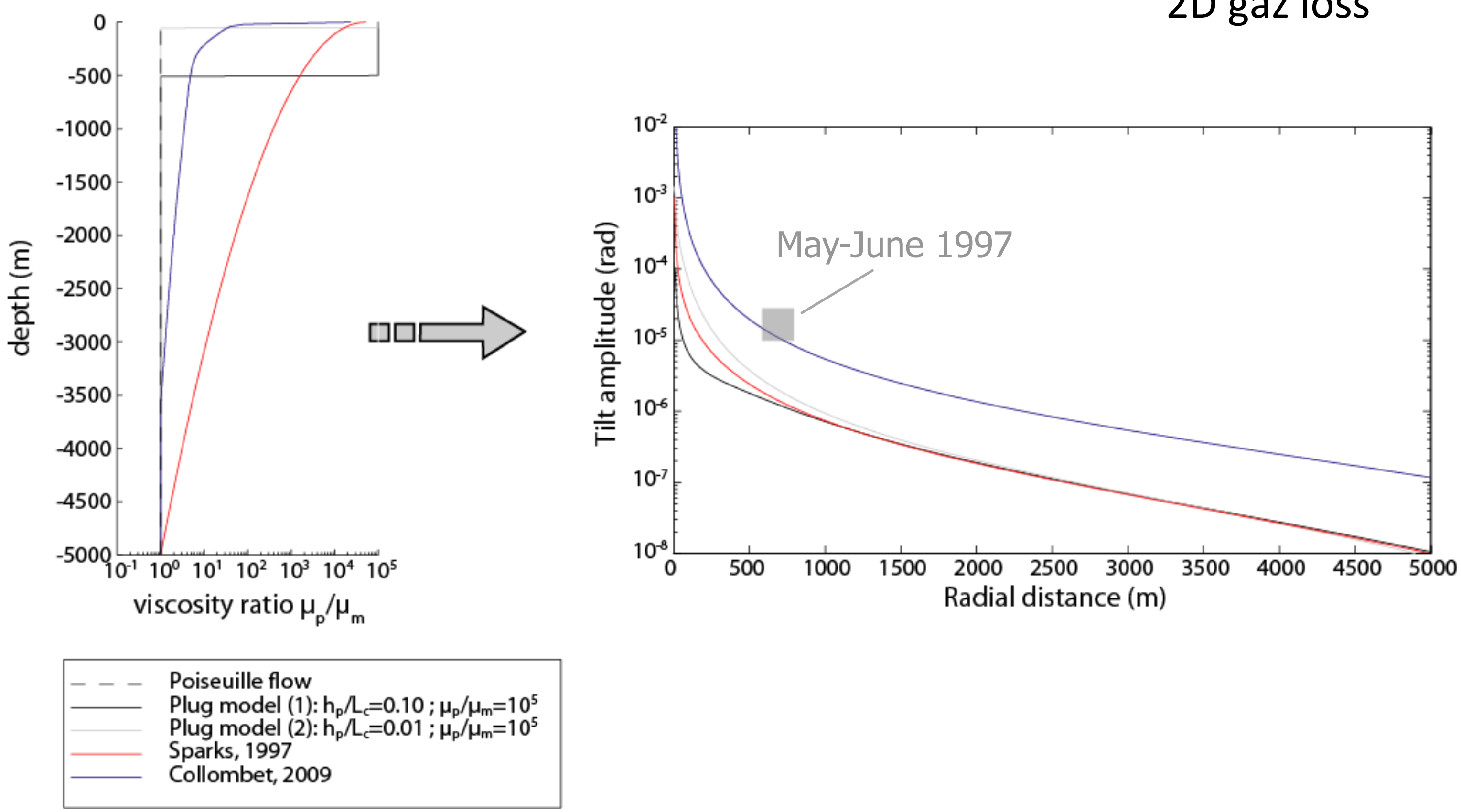

Comparing various sources of deformation

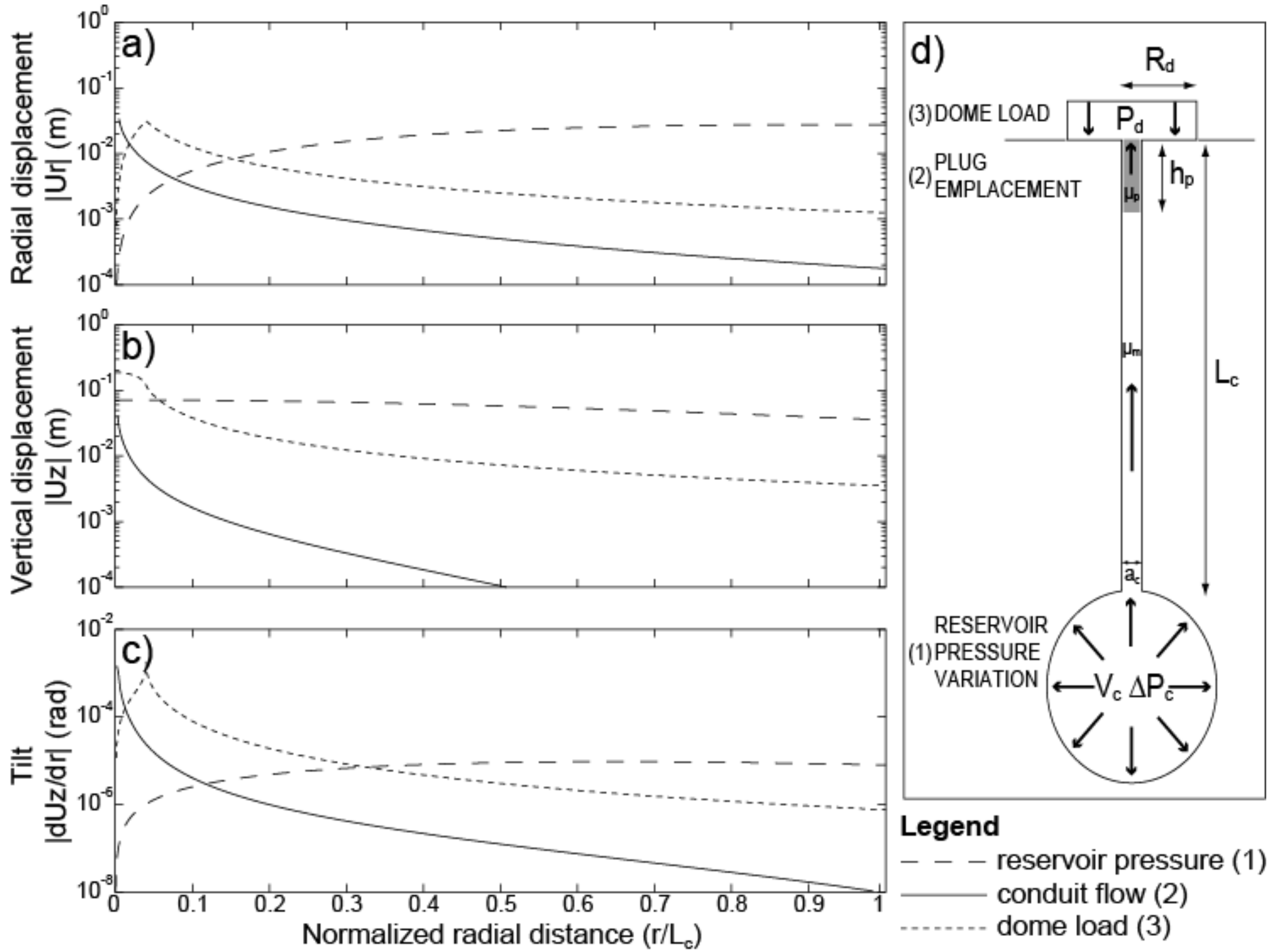

Interest of numerical modelling in this case :

*Full Coupling fluid+ solid.

*Coupling various physics: fluid dynamics + degassing
and solid mechanics

Numerical modeling: 2nd example

INFLUENCE OF SURFACE LOAD VARIATIONS ON MAGMA STORAGE ZONES

Various origine for surface load variations :

* Volcanic system evolution: edifice construction/destruction

* External causes:

  - Ice load variations above subglacial volcanoes (Katla, Iceland)

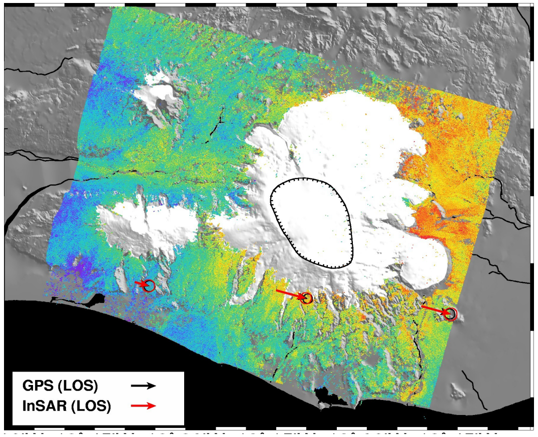

Katla: a subglacial volcano beneath Myrsdalsjökull ice cap:

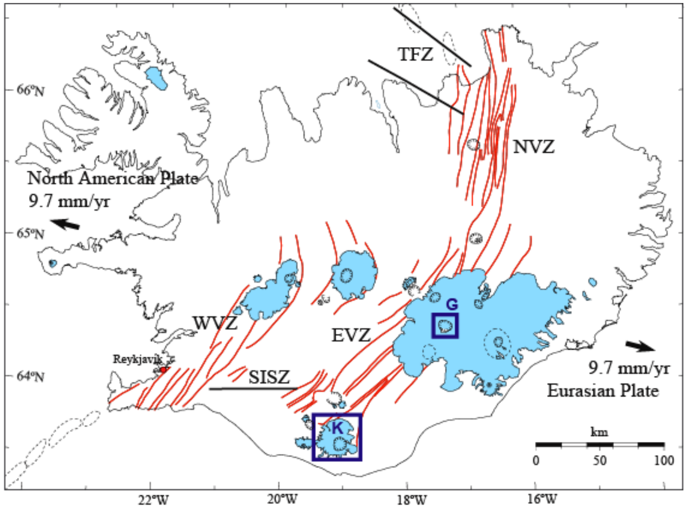

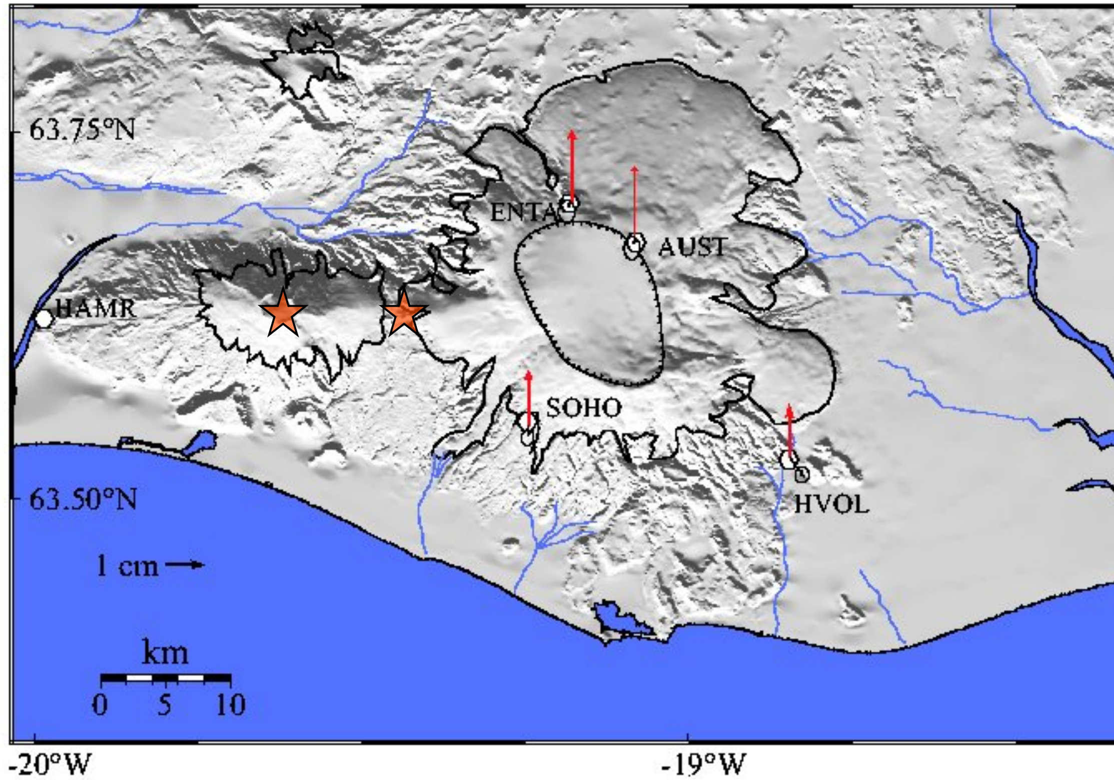

Last eruption 1918

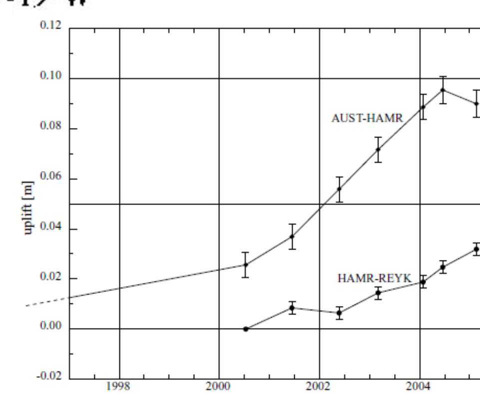

Uplift recorded by GPS campaigns
1.8 cm/y at AUST compared to the ice cap edge

Myrsdalsjökull ice load variations:

2 time scales:

(Gudmundsson et al., 2007)

Seasonal Effect

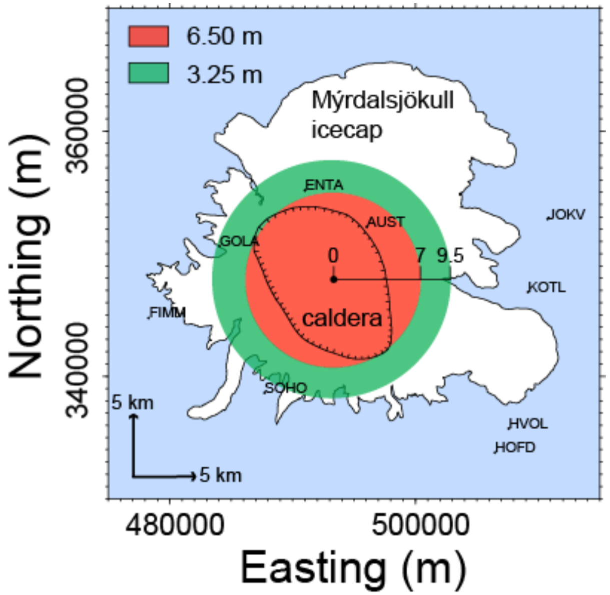

Long term effect

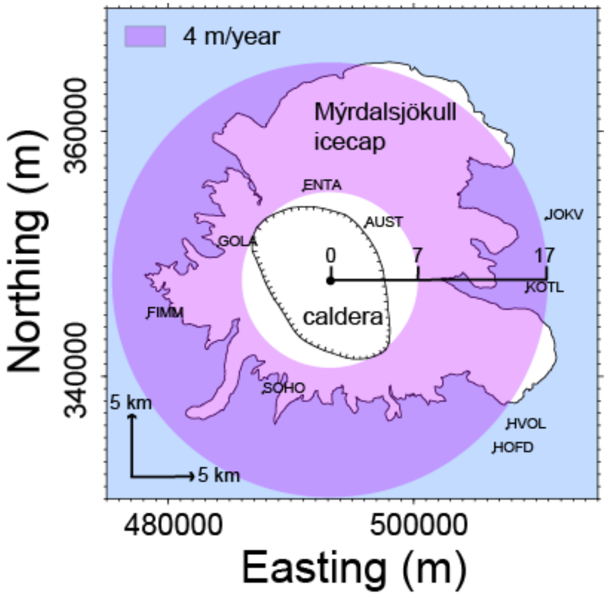

- Snow accumulation/melt during winter/summer
- Amplitude : 0.04 MPa

- Glacier retreat due to global warming since 1890.
- Amplitude: 0.035 MPa/y

Myrsdalsjökull ice load variations:

2 time scales:

(Gudmundsson et al., 2007)

Seasonal Effect

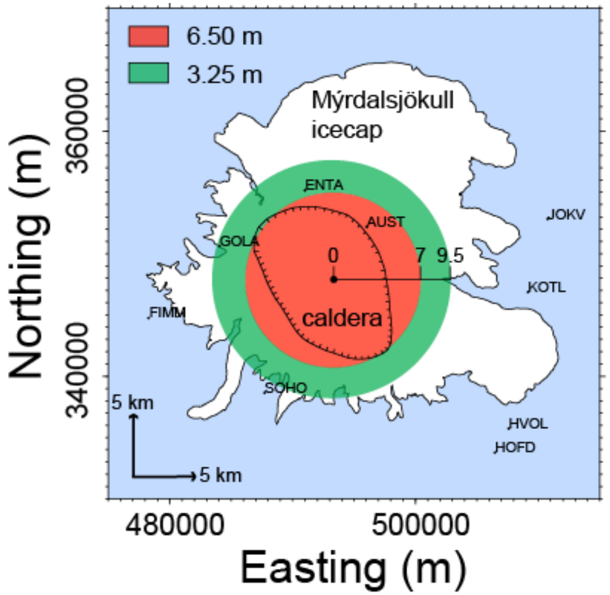

Long term effect

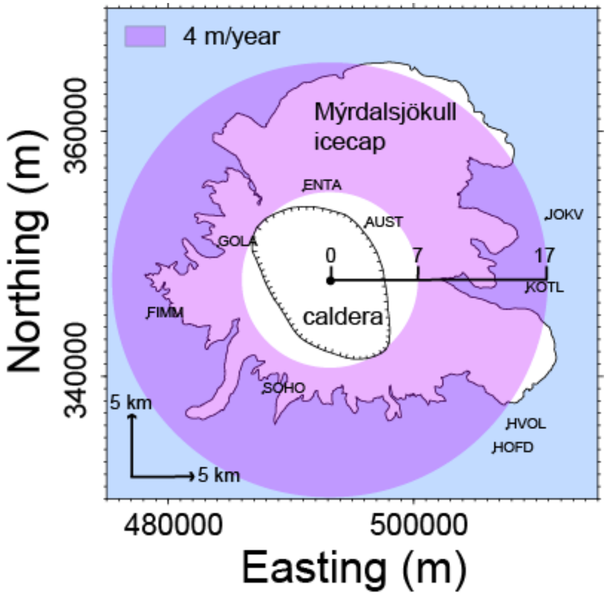

- Snow accumulation/melt during winter/ summer
- Amplitude : 0.04 MPa

- Glacier retreat due to global warming since 1890.
- Amplitude: 0.035 MPa/y

A seasonal displacement superimposed on the uplift

CGPS SOHO/REYK Up Component (mm)

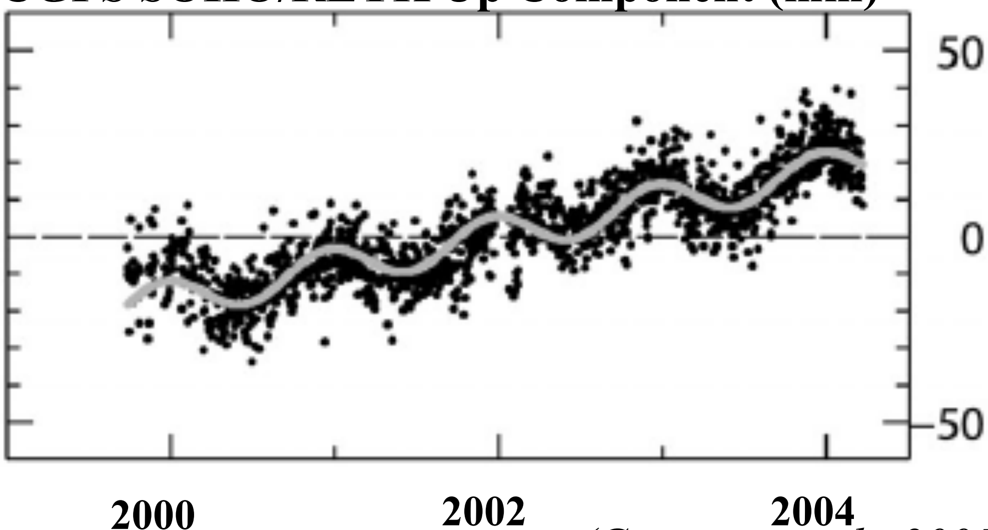

(Geirsson et al., 2005)

Seismicity seasonality

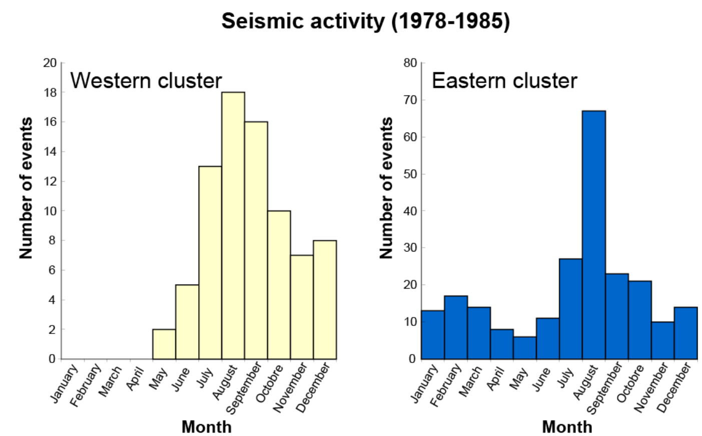

More events during the summer
(*Einarsson & Bransdottir, 2000*)

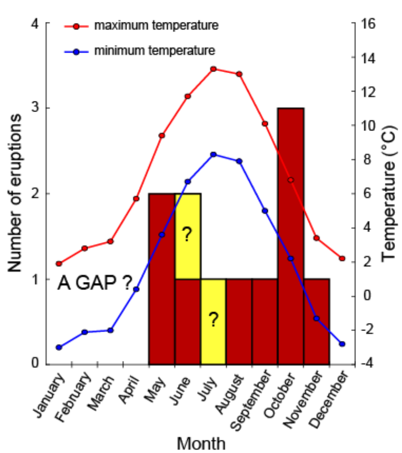

All historical eruptions during the summer

(*Eliasson & al., 2005*)

Various consequences of surface load variation :

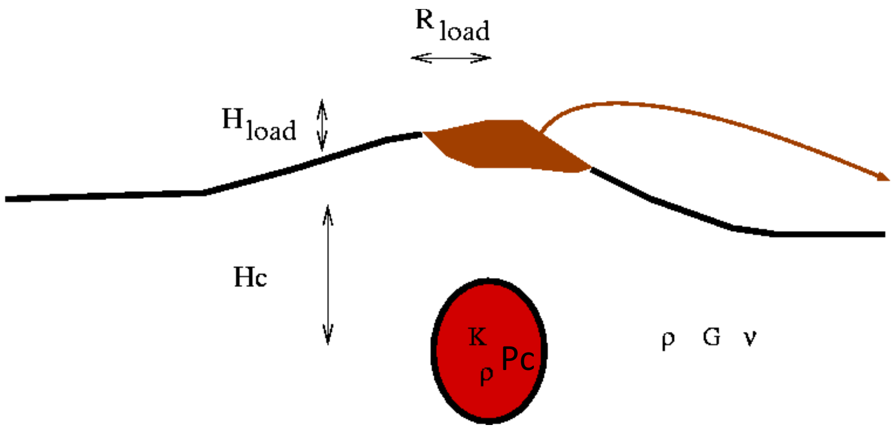

*Variation of magma pressure Pc

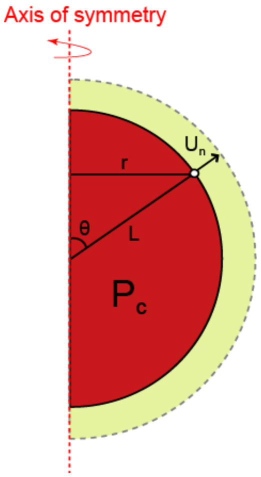

Volume variations are function of:

1) the equation of state of the fluid

$$\Delta P_c = K\frac{\boxed{\Delta V_c}}{V_c}$$

2) the boundary displacement which depends on the solid surrounding medium

$$\boxed{\Delta V_c} = \int_0^{\pi} (2\pi\, r.L.U_n)\, d\theta$$

Various consequences of surface load variation :

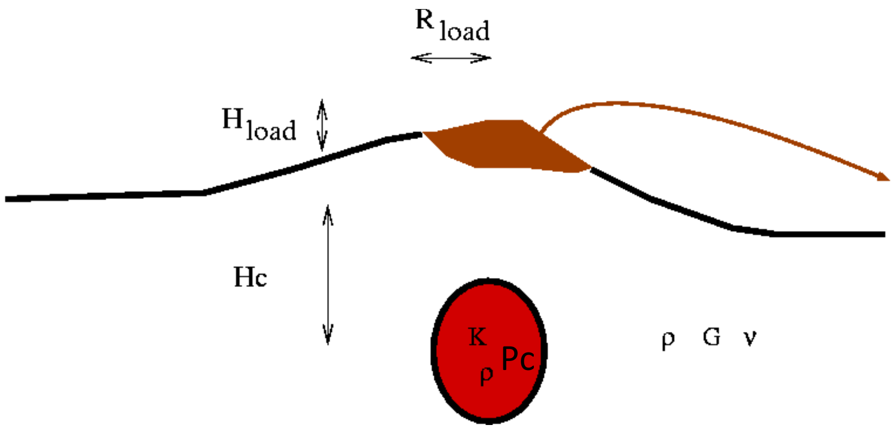

*Variation of magma pressure Pc

*Surface deformation

*Stress field variations → Modification of rupture conditions
Seismicity rate evolution

Model description:

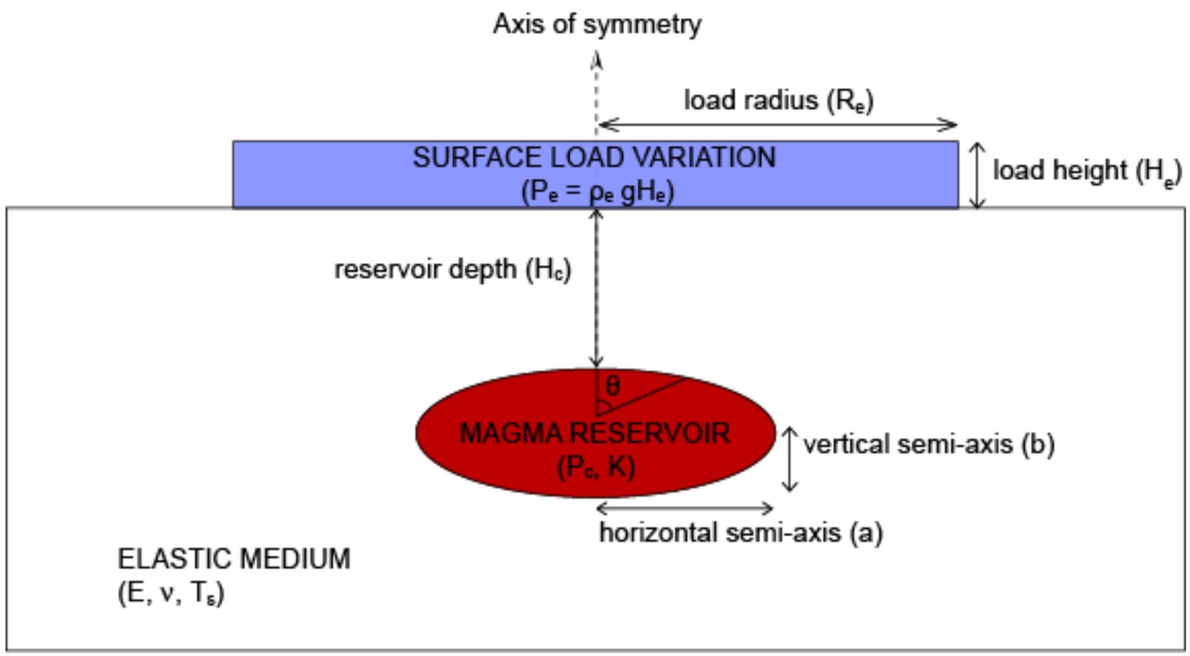

- Crust: elastic, homogene, isotropic,
- Magma fluid with bulk modulus K

- Axial geometry, Reservoir : ellipsoïde & Various load distribution

- Initial state: lithostatique $\sigma_{rr}=\sigma_{zz}=\sigma_{\theta\theta}$

Mesh and boundary conditions:

- FEM -COMSOL
- Magmatic reservoir: pressure condition applied at the wall
- Surface load: pressure applied at the surface

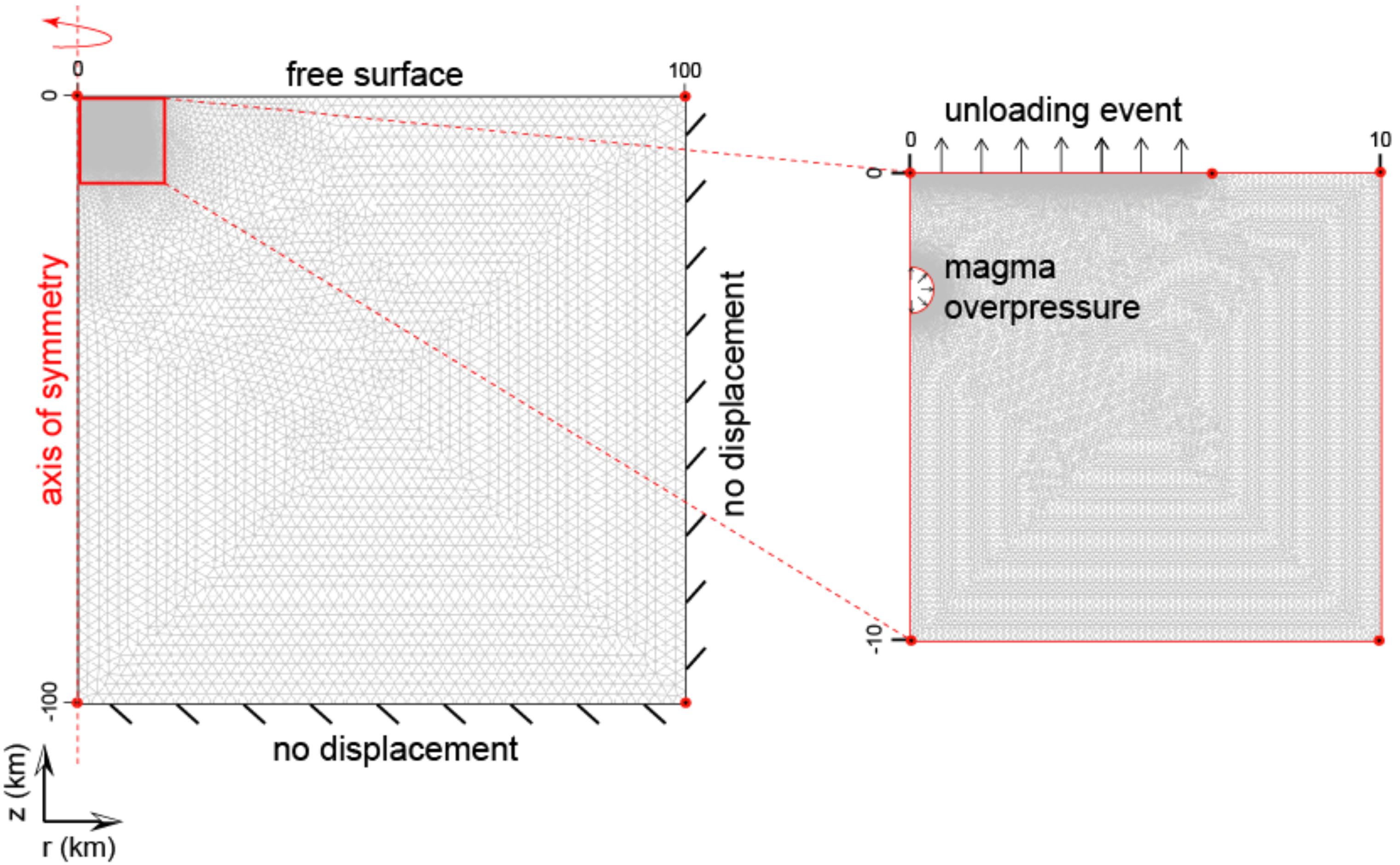

Pressure change at the axis:

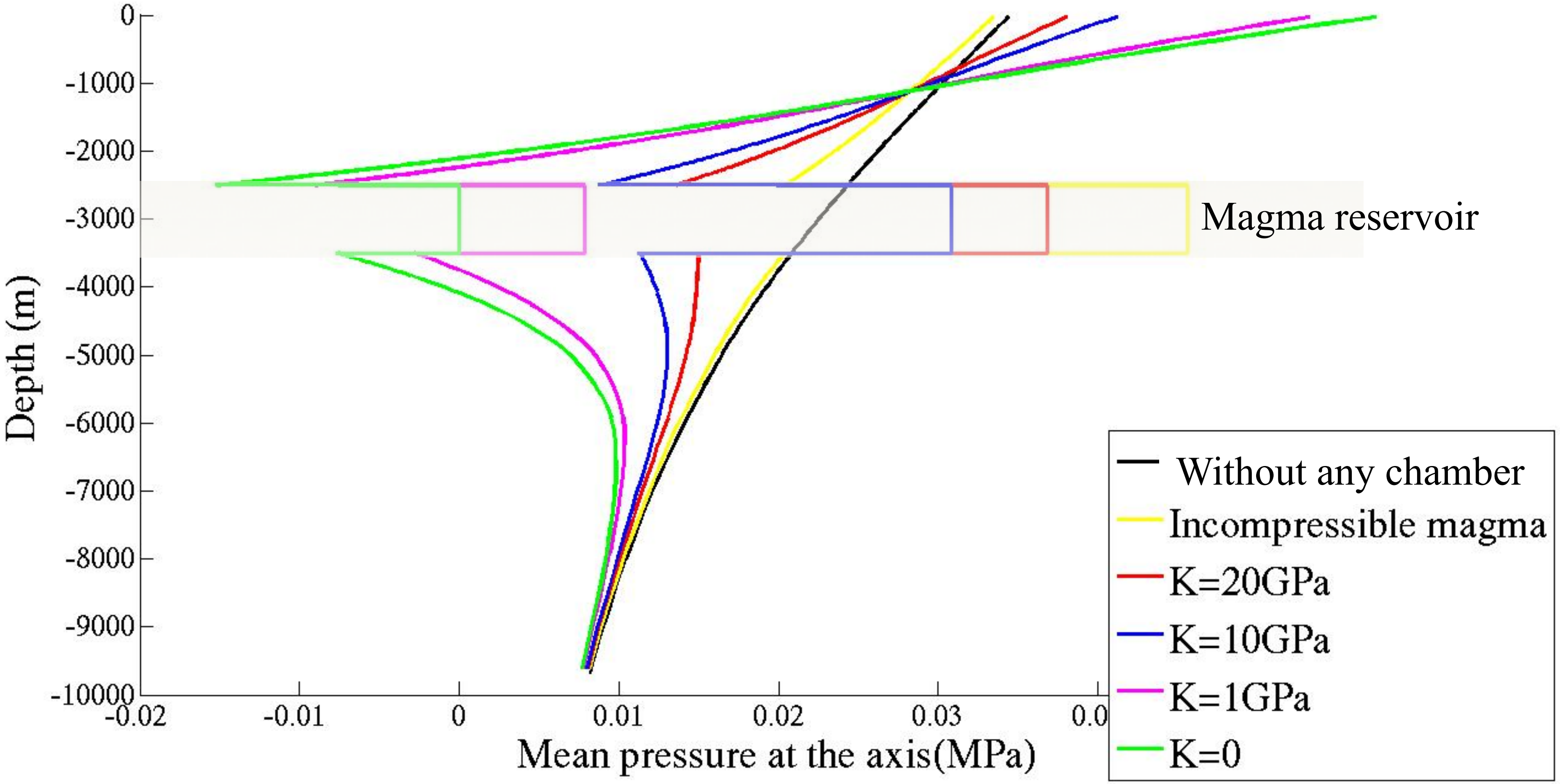

Sigmundsson et al.,Trans. Phil. Roy. Soc, 2010

Seasonal effect: influence on surface displacement:

(a 10 km^3 magma reservoir with a top at 2.5 km depth)

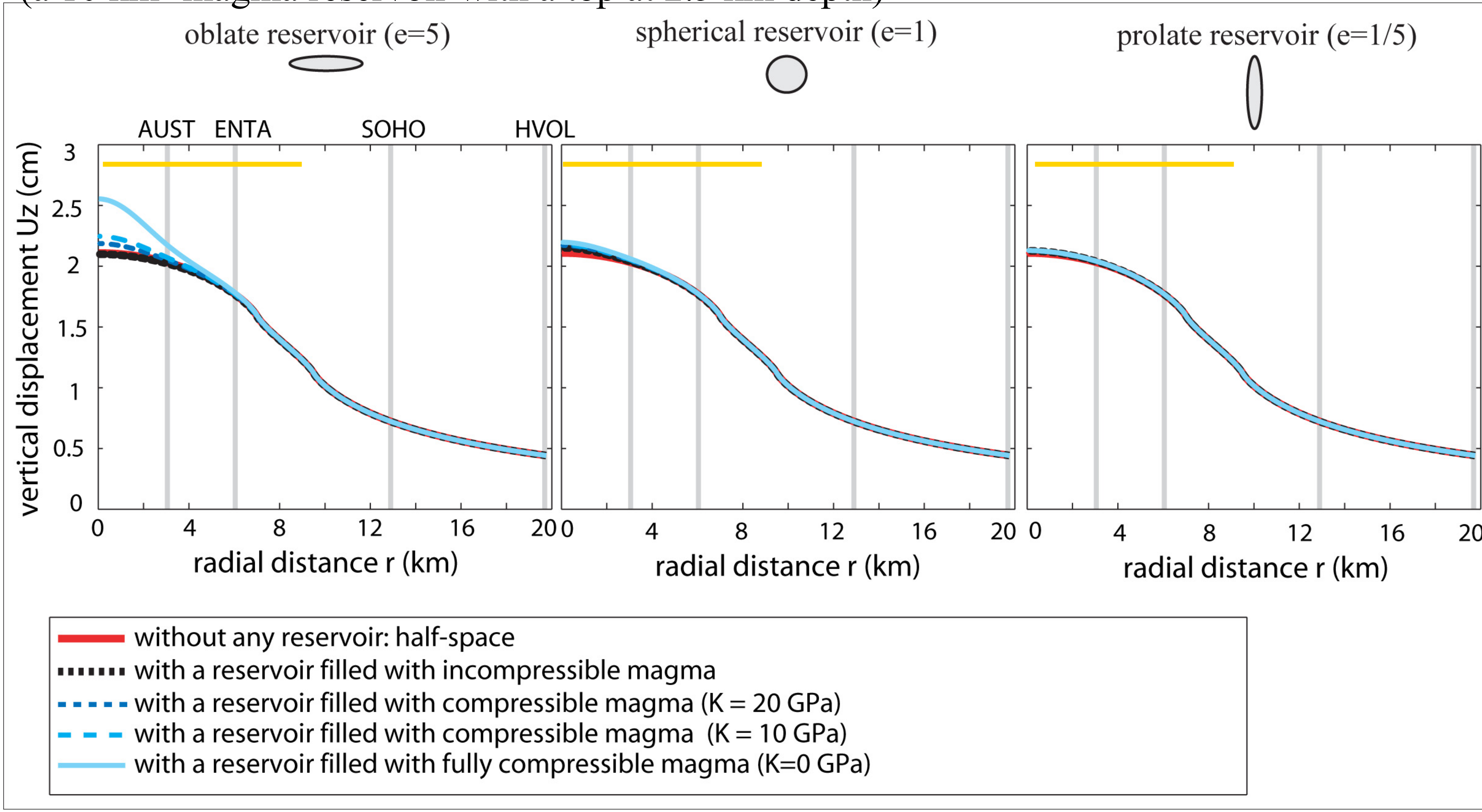

Almost no effect of the reservoir on the displacement field except directly above the reservoir for an oblate shape.

→Displacements around Myrdalsyökull can be interpret considering an homogeneous half-space to obtain Young's modulus estimation (E=29 ±5 GPa, *Pinel et al, GJInt, 2007*)

Seasonal effect: influence on seismicity rate:

Coulomb stress change ($\Delta CFF=\Delta\tau-\mu'\Delta\sigma_n$) induced by the seasonal snow melt

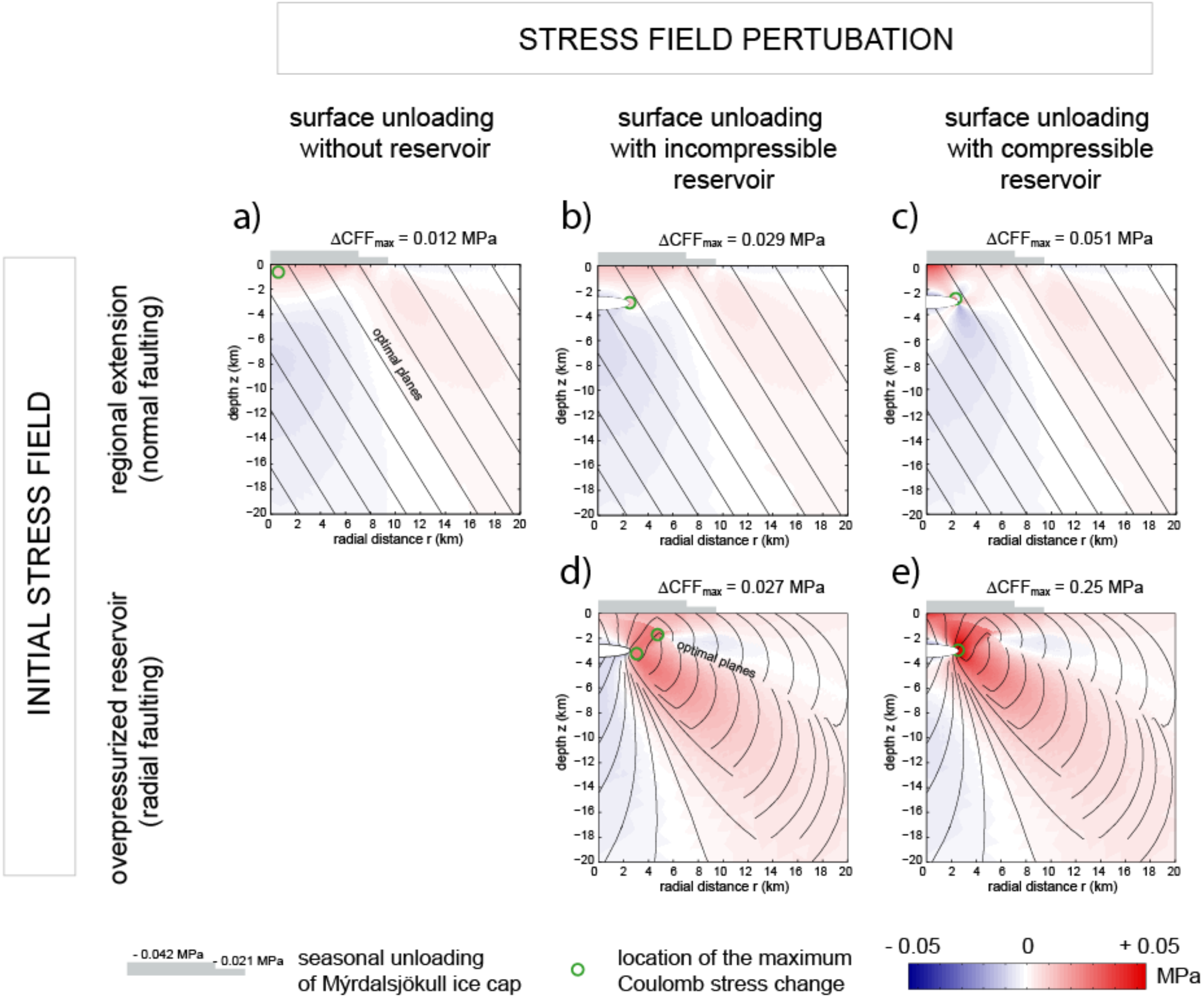

- With a reservoir, the amplitude of the ΔCFF is increased (by a factor 20) and maximum at the periphery.

Seasonal effect: influence on seismicity rate:

Earthquakes location

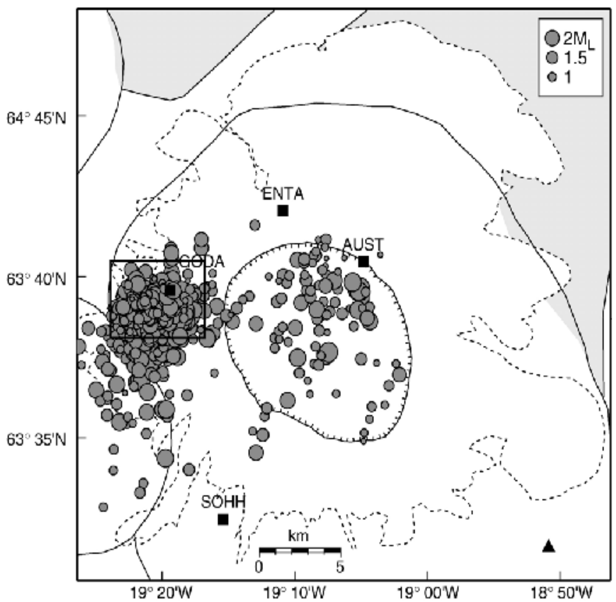

Earthquakes seasonality

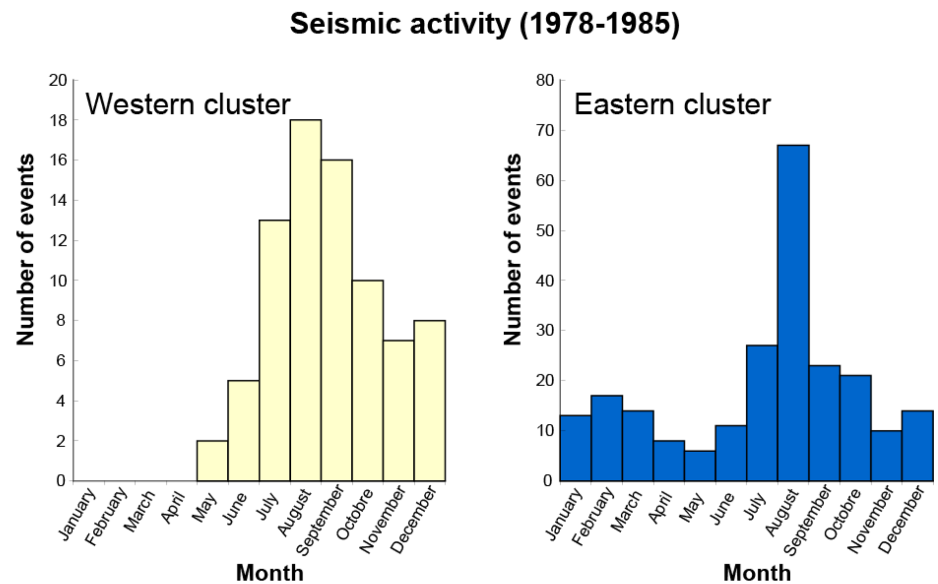

More events during the summer
(*Einarsson & Bransdottir, 2000*)

Seasonal effect: influence on eruption likelihood:

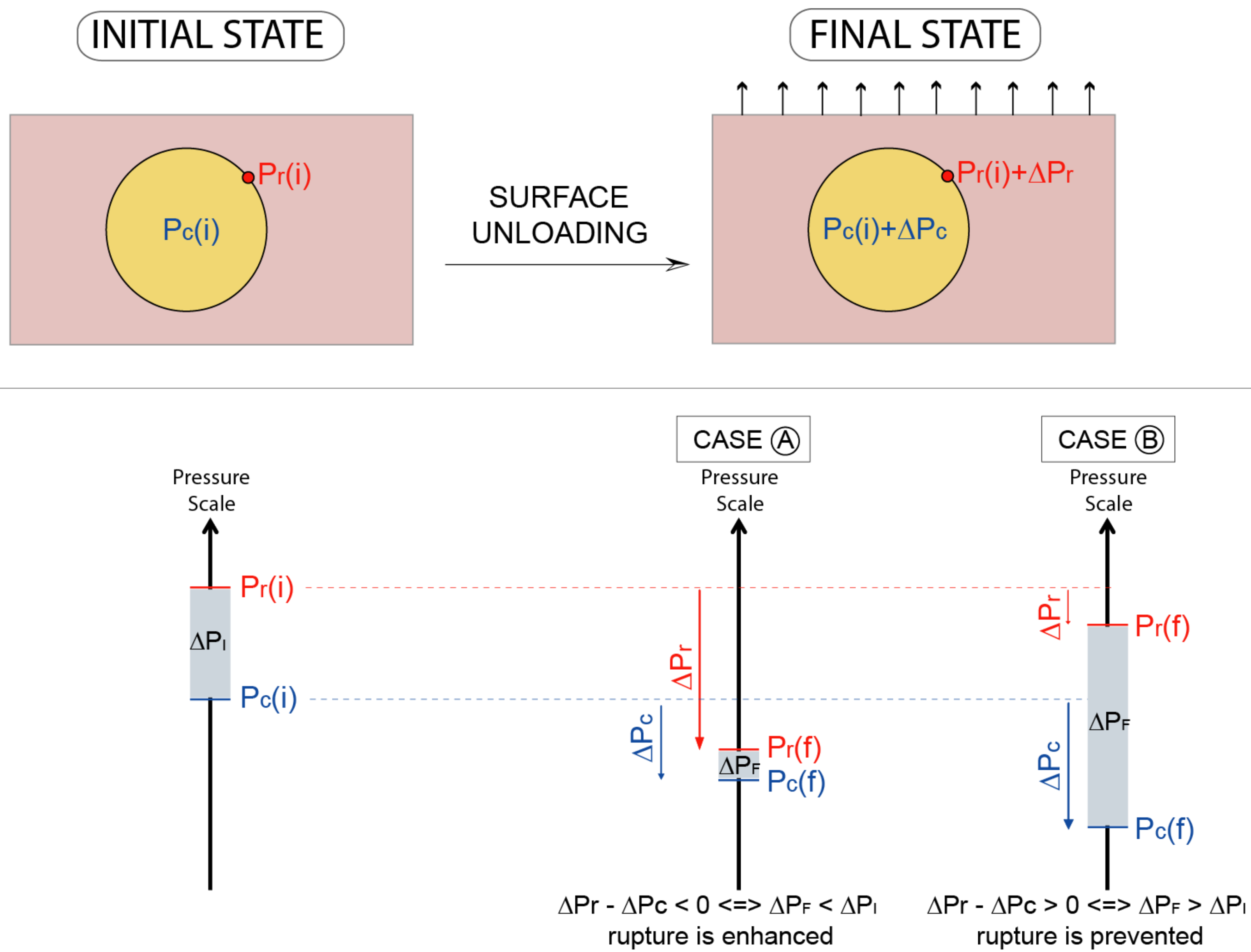

Seasonal effect: influence on eruption likelihood:

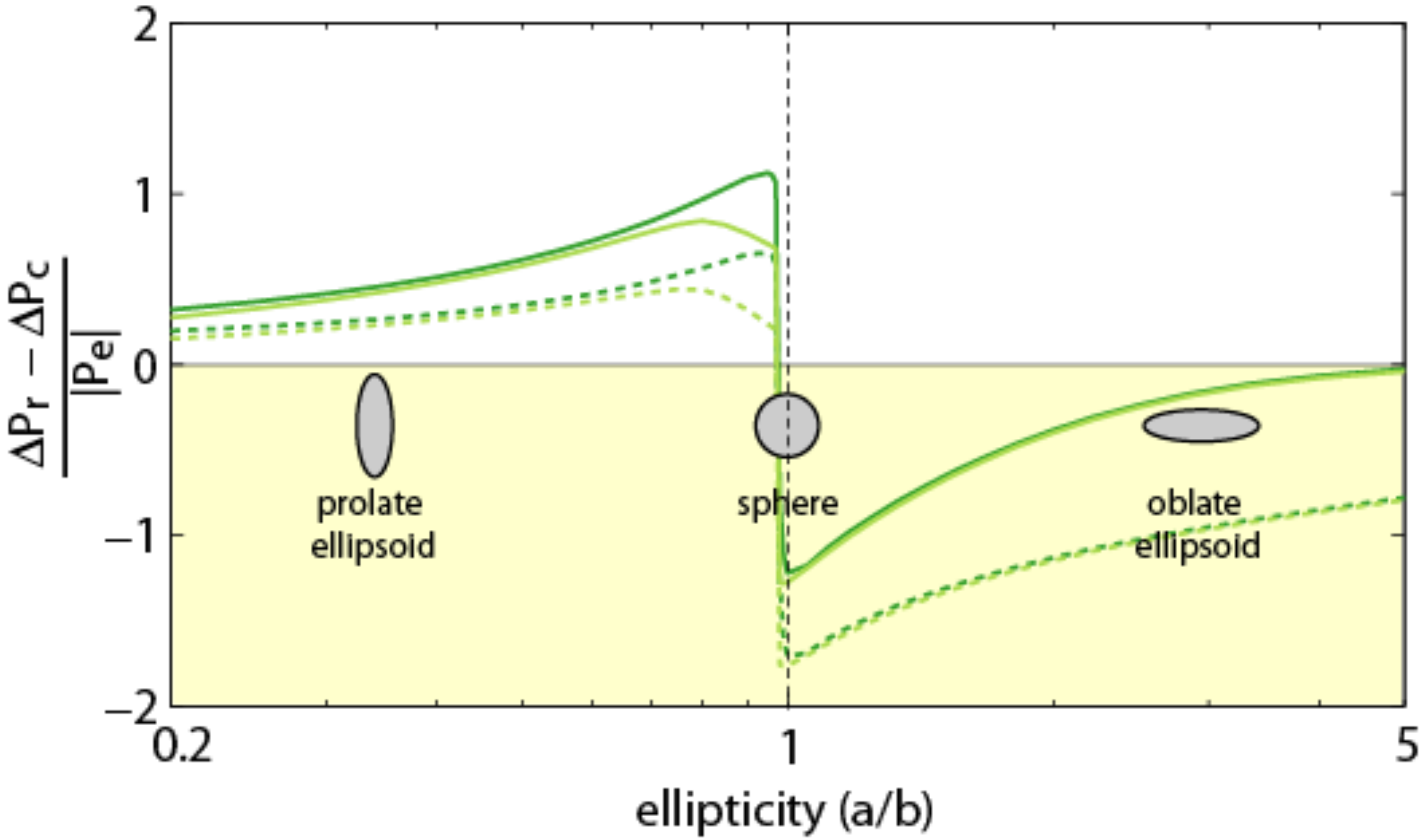

Seasonal effect: influence on eruption likelihood:

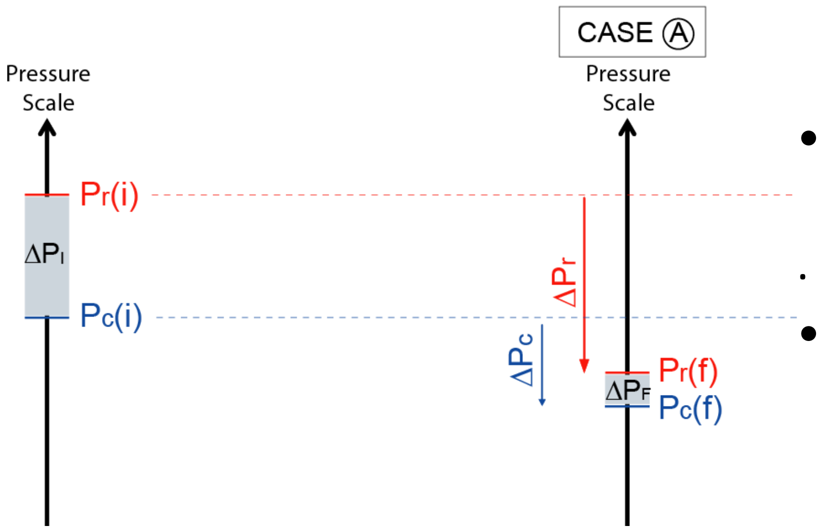

- For compressible magmas, during unloading periods eruptions are favored.

.

- Effect amplitude is around 0.01 MPa.

$\Delta P_F = \Delta\ P_I - 0.01$ MPa

- Dyke intrusions can be modulated by seasonal ice load variations.

- As the effect amplitude is small, it will be observed only if the magma input rate is low (smaller than 0.1 bars/y)

Seasonal effect: influence on eruption likelihood:

Historical eruptions

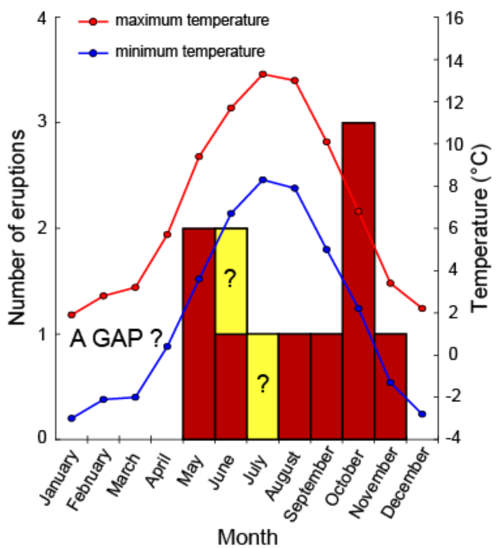

No historical eruptions during winter (*Eliasson & al., 2005*)

Myrsdalsjökull ice load variations:

2 time scales:

(Gudmundsson et al., 2007)

Seasonal Effect

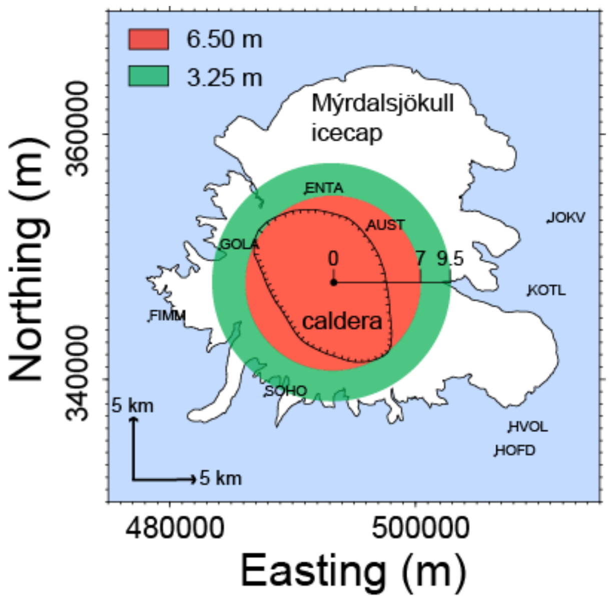

Long term effect

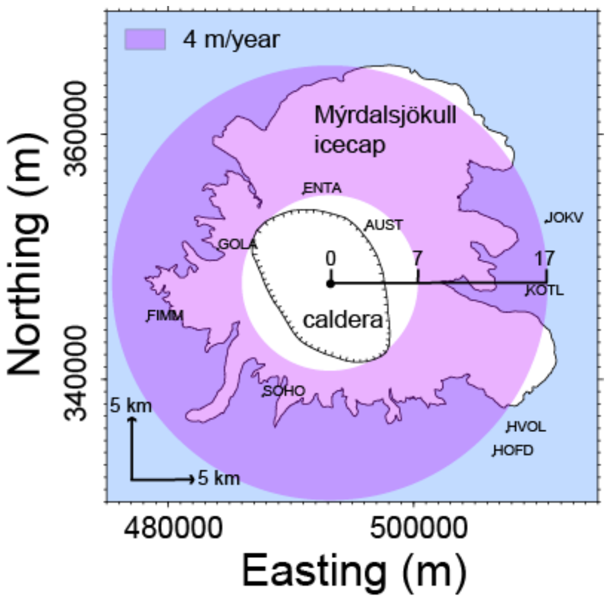

- Snow accumulation/melt during winter/ summer
- Amplitude : 0.04 MPa

- Glacier retreat due to global warming since 1890.
- Amplitude: 0.035 MPa/y

Introduction of visco-elasticity

a)

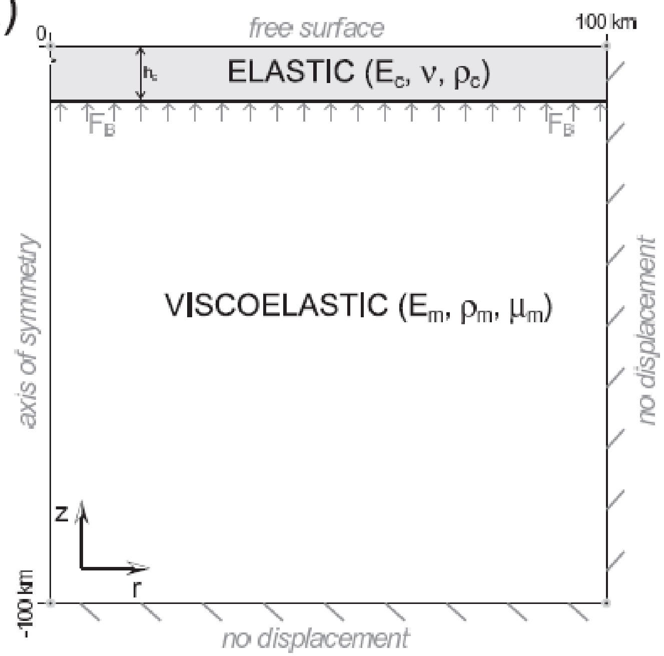

b)

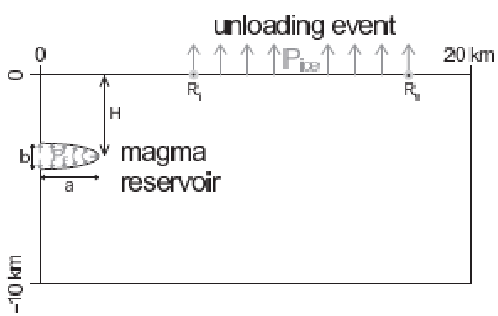

Icecap	Symbol	Value	Crust (elastic)	Symbol	Value
Internal Radius	R_i	7 km	Thickness	h_c	10 km
External Radius	R_e	17 km	Young's modulus	E_c	30 GPa
Pressure decrease	P_{ice}	-35 kPa.yr^{-1}	Poisson's ratio	ν	0.25
			Density	ρ_c	2800 kg.m^{-3}
Magma Reservoir	**Symbol**	**Value**	**Mantle (viscoelastic)**	**Symbol**	**Value**
Horizontal axis	a	2.5 km	Young's modulus	E_m	30 GPa
Vertical axis	b	0.5 km	Density	ρ_m	3100 kg.m^{-3}
Centre Depth	H	3 km	Viscosity	μ_m	3.10^{18} Pa.s

Numerical values used

KATLA : Effect of long term ice retreat.

We estimated which part of the uplift was induced by the long term ice retreat and showed that magma input has to be considered at a rate of 4 bars/y from 2001 to 2004.

KATLA : Effect of long term ice retreat on eruption likelihood:

Results:

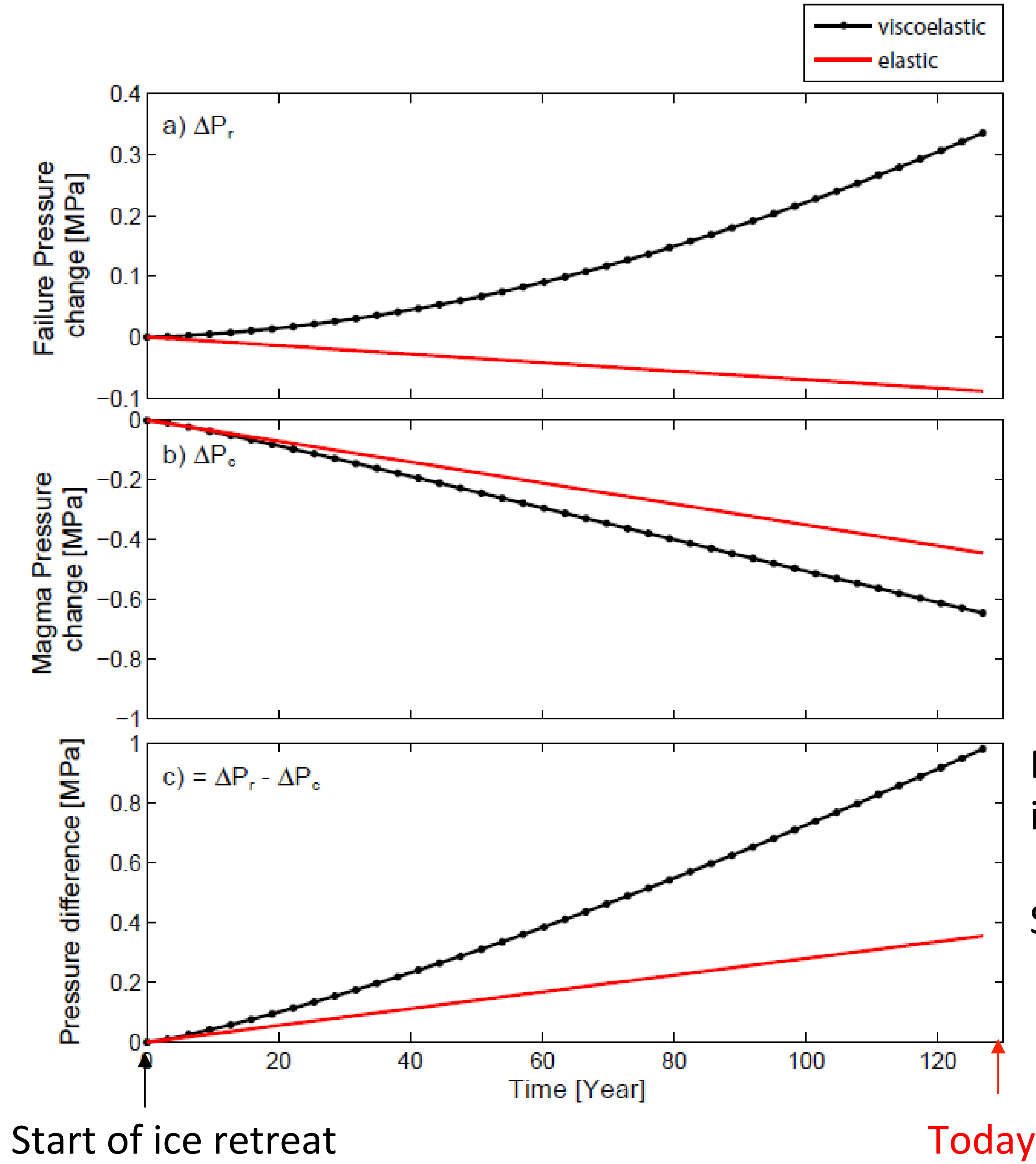

Eruption initiation is inhibited.

Storage is favored

KATLA : Effect of long term ice retreat on eruption likelihood:

Ice retreat also acts on magma production (increase of magma melting) and dykes propagation *(Hooper et al, Nature Geoscience, 2011)*

Interest of numerical modelling in this case :

*Test various reservoir shapes (parametric studies)

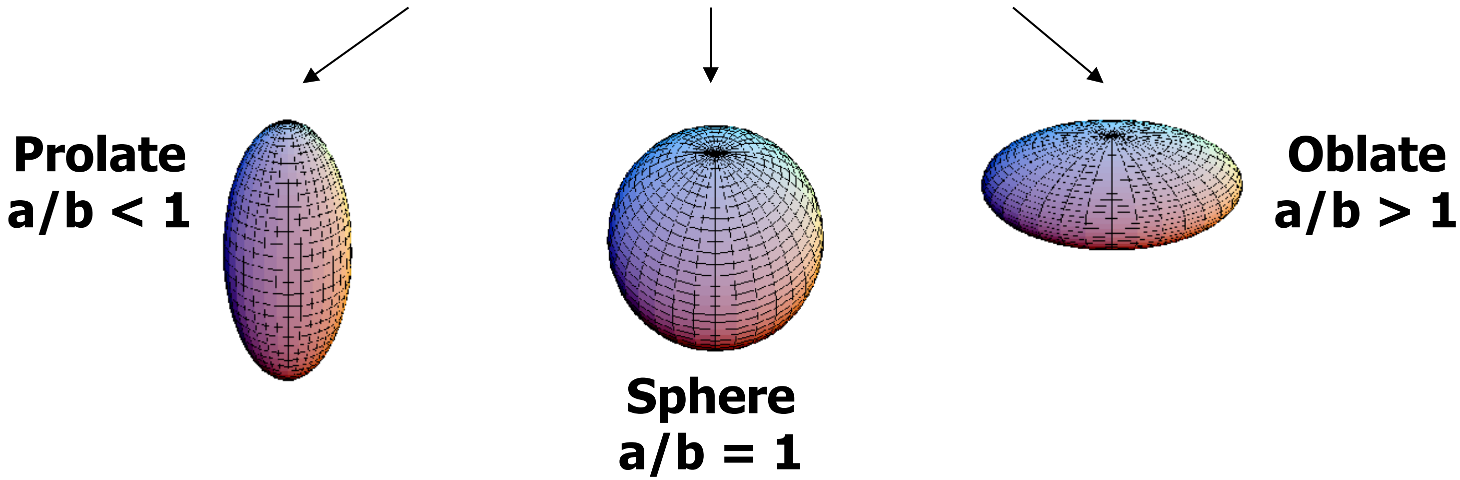

*Consider a visco-elastic rheology: temporal evolution.

Including new constrains on the local structural and physical properties or on the local state of stress, we could improve this model, using a 3D approach.

Conclusions:

Deformation data are **useful** and **not so difficult to acquire and interpret**.

Used for many years but in the last decades **major improvements in temporal and spatial resolution.**

In situ instruments have to be close enough to the source

Useful to combine with other measurements

To take home:
Deformation does not necessarily mean eruption to follow.

Bibliography:

*Earthquake and volcano deformation, P. Segall, Princeton University Press, 2010, ISBN 978-0-691-13302-7

*Volcano deformation: Geodetic monitoring techniques, D. Dzurisin, Springer-Praxis Books in Geophysical Sciences, 441p, 2007

*Imaging with synthetic aperture radar, Massonnet, D. and Souyris, J. C. 2008, EPFL-CRC Press. 280p.

*Radar interferometry - Data interpretation and error analysis(Remote Sensing and digital image processing, volume 2.), Hanssen, R. F. 2001, Kluwer Academic Publishers, 1st edition. 328 pp.

Rajout d’exercices , d’ordre de grandeur…
Presenter le cours toujours sous forme de questions….

Que doivent-ils retenir de ce cours.
Quel exam….

Il me faut une conclusion.

*Améliorer la forme du cours.
*Ameliorer lien entre origine de la deformation et modèles.